DOCTOR OF PHILOSOPHY

Structure of the LKB1-STRAD-MO25 tumour suppressor complex

Zeqiraj, Elton

Award date:
2009

DOCTOR OF PHILOSOPHY

Structure of the LKB1-STRAD-MO25 tumour suppressor complex

Elton Zeqiraj

2009

University of Dundee

Structure of the LKB1-STRAD-MO25 Tumour Suppressor Complex

By

Elton Zeqiraj

A thesis submitted for the degree of

Doctor of Philosophy

University of Dundee

September 2009

Dedikuar prindërve të mi, që gjithmonë më kanë drejtuar në kërkim të dijes.

Dedicated to my parents, that have always steered me in the persuit of knowledge.

Acknowledgements

I would like to start by thanking my supervisors Prof. Daan van Aalten and Prof. Dario Alessi for giving me the opportunity to work in their laboratories. In particular Daan for all the crystallography fundamentals and computing "tricks" and Dario for the principles of biochemistry and cell biology, that together perfectly completed my scientific preparation. Working in two labs has been a unique and excellent experience. I would also like to thank Kei and Jérôme for interesting and useful chats about LKB1, and Alex Snr. and Ramon for chats about crystallography/general biochemistry.

In addition, without the fantastic molecular biology skills of Maria Deak, I am certain that I would not have achieved nearly as much as I have over the last few years. So, a big thank you to Maria. The support staff in the unit, Aileen, Linda, Alison, Ross, Jackie and Shona were great in ensuring that things moved smoothly in the lab. Thanks also go to the unit's and divisional secretaries Judith, Alison, Naomi and Connie. The DSTT has been of invaluable help and I would like to thank Sam and Susan for always helping me in tissue culture, and James and Hillary for their readiness to contribute to my projects.

In particular I would like to thank the people that helped me through in the first few months, and paved my way forward. These were Fabrizio, a great friend that taught me how to calmly survive the pressure of two bosses and gave me excellent ideas on the LKB1 complex project, and Sunny for teaching me that you can always leave a reagent out if you "can not find it". I will not have survived the Dundee experience if it wasn't for the following people, whom I value immensely as friends: Abdallah for being in the same wavelength when it comes to complaining (especially about the bosses), Alban and Stephan for the Golf and beer sessions, Barry (for providing me with a flat and Speedwells), Anna and Piotr for being greatly entertaining and fun to be around, together with Alberto, Alex (LaTeX master) Jnr., Ciaran, David B., Eris, Fatema, Frank R., Gerta, Helge, Jacob, Juanma, Jürgen (The German), Laura (aLLora), Laura P., Louise, Mabi, Miratul, Rebecca, Silvia, Simon, Wale, Wingate and Xu Inc.

And finally, a special thank you goes to Bea for contributing greatly to this work, but also for being near me when I needed her most.

Declaration

I declare that the following thesis is based on the results of investigations conducted by myself, and that this thesis is of my own composition. Work other than my own is clearly indicated in the text by reference to the relevant researchers or to their publications. This dissertation has not in whole, or in part, been previously submitted for a higher degree.

Elton Zeqiraj

We certify that Elton Zeqiraj has spent the equivalent of at least nine terms in research work at the School of Life Sciences, University of Dundee, and that he has fulfilled the conditions of the Ordinance General No 14 of the University of Dundee and is qualified to submit the accompanying thesis in application for the degree of Doctor of Philosophy.

Prof. Daan M.F. van Aalten **Prof. Dario R. Alessi FRS FRSE**

List of publications

The work described in this thesis has been published in the following articles:

Zeqiraj E, Filippi BM, Deak M, Alessi DR and van Aalten DMF (2009) Structure of the LKB1-STRAD-MO25 complex reveals an allosteric mechanism of kinase activation. **Science** *(In press)*

Zeqiraj E, Filippi BM, Goldie S, Navratilova I, Boudeau J, Deak M, Alessi DR and van Aalten DMF (2009) ATP and MO25α regulate the conformational state of the STRADα pseudokinase and activation of the LKB1 tumour suppressor. **PLoS Biol** 7(6): e1000126.

Alessi DR and Zeqiraj E (2007) Protein phosphorylation. **The Biochemist** 29(4):20-3 *(Mini review)*

The Amino Acid Code

Amino acid	**Three letter code**	**One letter symbol**
Alanine	Ala	A
Arginine	Arg	R
Asparagine	Asn	N
Aspartic acid	Asp	D
Cysteine	Cys	C
Glutamic acid	Glu	E
Glutamine	Gln	Q
Glycine	Gly	G
Histidine	His	H
Isoleucine	Ile	I
Leucine	Leu	L
Lysine	Lys	K
Methionine	Met	M
Phenylalanine	Phe	F
Proline	Pro	P
Serine	Ser	S
Threonine	Thr	T
Tryptophan	Trp	W
Tyrosine	Tyr	Y
Valine	Val	V
Any amino acid	Xaa	X

Abbreviations

Å	Angstrom
Amp	Ampicillin
AMP	Adenosine 5'-monophosphate
AMPK	AMP regulated kinase
AMP-PNP	Adenylyl imidodiphosphate
ANP-RGC	Atrial natriuretic peptide-receptor guanylyl cyclase
aPK	atypical protein kiase
ATP	Adenosine 5'-triphosphate
BRSK	Brain specific kinase
^{o}C	Degree Celsius
C-terminal	Carboxy-terminal
CAMK	Ca^{2+}/Calmodulin-dependent protein kinase
cAMP	Cyclic AMP (adenosine 3',5'-cyclic monophosphate)
CCP4	Collaborative computational project number 4 in protein crystallography
Cdc	Cell division cycle
CDK	Cyclin-dependent protein kinase
CDK2	Cyclin dependent protein kinase 2
CFT	C-terminal flanking tail
CK1	Casein kinase 1
COSMIC	Catalogue of Somatic Mutations in Cancer
cpm	Counts per minute
Da	Dalton
ddH2O	Doubly distilled water, milli-Q water
dH2O	Distilled water
DNA	Deoxyribonucleic acid
DSTT	Division of Signal Transduction Therapy
DTT	Dithiothreitol
EDTA	Ethylenediamine tetraacetic acid
EGTA	Ethyleneglycol bis (2-aminoethylether)-N'N'tetraacetic acid
EGFR	Epidermal growth factor receptor
EphB	Ephrin B receptor tyrosine kinase
ErbB3 (Her3)	Epidermal growth factor receptor
ERK	Extracellular signal-regulated kinase
ESRF	European synchrotron radiation facility
g	Gram (or gravity)
GSH sepharose	Glutathione sepharose
GSK3	Glycogen synthase kinase-3
GST	Glutathione-S-transferase
h	hour
HEPES	N-(2-Hydroxyethyl)piperazine-N'-(2-ethanesulfonic acid)
HNSCC	Head and neck non-small cell carcinoma

Continued on next page ...

Abbreviations continued

IPTG	Isopropyl β-D-thiogalactoside
K	Degree Kelvin
kDa	Kilo Dalton
KSR	Kinase suppressor of Ras
l	Litre
LB	Luria-Bertani medium
LDS	Lithium dodecyl sulphate
m	Milli (or mouse)
M	Molar
μ	Micro
MAPK	Mitogen activated protein kinase
MARK	Microtubule affinity-regulating kinase
MEK	Map kinase kinase
MES	2-(N-morpholino) ethane sulphonic acid
min	Minute
mol	Mole
MOPS	3-Morpholinopropanesulfonic acid
MO25	Mouse protein 25
MPD	2-Methyl-2,4-petanediol
MST4	Mammalian STE20-like protein kinase 4
mTOR	mammalian target of rapamycin
n	Nano
N-terminal	Amino-terminal
NCBI	National center for biotechnology information
NSCLC	Non-small cell lung carcinoma
NUAK1(ARK5)	AMPK-related kinase 5
OD	Optical density
OMIM	Online Mendelian Inheritance in Man
OSR1	Oxidative stress responsive-1
PAGE	Polyacrylamide gel electrophoresis
PAK	p21-activated kinase
PDB	Protein database bank
PDBID	Protein database bank identifier
PDK1	3-phosphoinositide dependent protein kinase-1
PEG	Polyethylene glycol
PH	Pleckstrin homology
PhK	Phosphorylase kinase
PJS	Peutz-Jeghers syndrome
PKA	cAMP dependent protein kinase
PKB	Protein kinase B (aka Akt)
PKI	Pseudo substrate inhibitor peptide (for PKA)
PMSE	Polyhydramnios, megalencephaly and symptomatic epilepsy
PSK	Pseudokinase
PTEN	Phosphatase and tensin homologue on chromosome ten
PVDF	Polyvinylidene fluoride

Continued on next page ...

Abbreviations continued

RMSD	Root mean square deviation
rpm	Revolutions per minute
RPTPs	Receptor protein tyrosine phosphatases
SD	Standard deviation
SDS	Sodium dodecyl sulfate
sec	second
SH2	Src Homology 2
SH3	Src Homology 3
SNF1	Sucrose non-fermenting kinase-1
SNRK	SNF-related protein kinase 2
SPAK	STE20/SPS1-related Proline-Alanine-rich Kinase
SPR	Surface plasmon resonance
STK11 (LKB1)	Ser/Thr kinase 11
STRAD	STE20-related adaptor
TAO	Thousand and one kinase
TLS-refinement	Incorporation of overall anisotropic B-factors in a refinement process
TNP-ATP	2',3'-O-(2,4,6-trinitrophenyl) adenosine 5'-triphosphate
Tris	Tris (hydroxymethyl) aminomethane
U	Units
UBA	Ubiquitin-associated domain
UV	ultraviolet
V	Volts
v-src	viral-sarcoma oncogene
v/v	Volume to volume
w/v	Weight to volume
WNK	With no lysine (K)
YSK	SPS1/STE20-related protein kinase

Summary

A landmark study published over ten years ago established a link between mutations of the *LKB1* gene and the Peutz-Jeghers cancer syndrome. Since then, much effort has been devoted to understanding the functional roles of the protein encoded by the *LKB1* gene. LKB1 is a Ser/Thr kinase that is activated by binding to the pseudokinase STRAD and the scaffolding protein MO25. LKB1 activates AMPK and twelve other members of the AMPK family of kinases, thus controlling cellular energy and cell polarity. Much attention has been focused towards protein kinases activated by LKB1, although the mechanism by which STRAD and MO25 activate LKB1 remains unknown. The work described in this thesis was conducted with the aim of understanding the interactions of LKB1 with STRAD and MO25, and the mechanisms by which the latter two activate LKB1. I have tried to accomplish these aims using a structural biology approach. In chapter III of this thesis I show the structure of the regulatory STRADα/MO25α complex, and in chapter IV the structure of the heterotrimeric LKB1/STRADα/MO25α complex. The structure of STRADα reveals for the first time the determinant features of kinase inactivity, and provides an example of how pseudokinases can exert their functions through their conformation rather than phosphorylation. STRADα adopts a closed conformation typical of active protein kinases, and binds LKB1 as a pseudosubstrate. STRADα binding promotes the active conformation of LKB1, which is further stabilised by MO25α interacting with the LKB1 activation loop. This represents a previously undescribed mechanism of kinase activation that may be relevant to understanding the evolution of other pseudokinases. Finally the structure of the LKB1 heterotrimer reveals how mutations found in Peutz-Jeghers syndrome and other cancers impair LKB1 function.

Contents

List of Figures

List of Tables

Chapter I

Introduction

1 Introduction

1.1 The protein kinase family

1.1.1 Historical overview of protein phosphorylation

More than five decades ago protein phosphorylation was described as a covalent and reversible regulatory mechanism of enzyme activity. The first identified protein kinase was Casein (phospho) kinase by Kennedy and Burnett in 1954 (Kennedy and Burnett, 1954). The breakthrough however, came from laboratories studying glycogen breakdown in muscle and liver tissues, that lead to the description of the active and inactive forms of glycogen phosphorylase by Fischer and Krebs (1955) and Sutherland and Wosilait (1955). Fischer and Krebs in particular could demonstrate that the inactive *b* form of glycogen phosphorylase could be converted to the active *a* form in the presence of ATP, Mg^{2+} and a protein they named phosphorylase kinase. The process of γ-phosphryl group transfer to a serine residue of phosphorylase b was later described by Fischer et al. (1959). Subsequent findings that the opposite reaction (phosphate releasing) was carried out by protein phosphatases (Ingebritsen and Cohen, 1983) made clear phosphorylation was a dynamic process of post-translational modification. In 1981 the first example that a kinase (v-src) could phosphorylate tyrosine residues was provided by Tony Hunter (Hunter and Sefton, 1980),

thus completing the identification of the three most commonly phosphorylated amino acids to date (Fig. 1.1).

The identification of the c-AMP dependent protein kinase (PKA) (Walsh et al., 1968), that could phosphorylate and activate phosphorylase kinase, provided an example of kinase signalling cascades (also referred to as signal transduction pathways)—a process very widely used in almost all eukaryotic organisms to transmit, integrate and communicate intra/extracelluar stimuli. The later sequencing of the PKA gene (Shoji et al., 1981) had perhaps the biggest impact in kinase biology, since it allowed researchers, geneticists in particular, to understand that other proteins under investigation were indeed kinases.

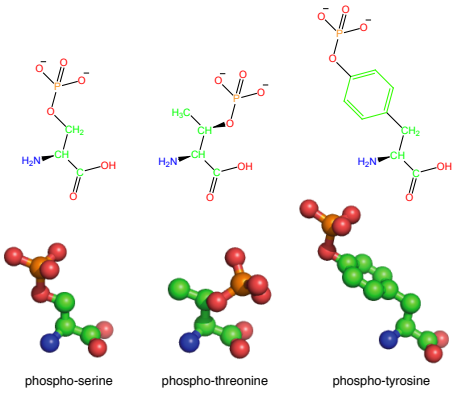

Figure 1.1: Structures of phosphorylated amino acids

1.1.2 Phylogeny of protein kinases—the human kinome

As more protein kinases were identified, it became clear in the 1980s that this was a diverse family involved in regulating many cellular processes (for more examples the reader is referred to the reviews by Hunter and Cooper, 1985 and Cohen, 2002). Despite their functional diversity, it was soon realised that kinases were related and have

evolved in part from a common origin (Barker and Dayhoff, 1982; Hanks et al., 1988). As the scientific community moved towards a genomic area in the 1990s, numerous protein kinases were identified and functions were assigned to regulating almost all aspects of cellular life. The draft release of the human genome sequence in 2001 (Lander et al., 2001; Venter et al., 2001) allowed Gerard Manning and colleagues to provide a complete catalogue of protein kinases by publishing the human kinome a year later (Manning et al., 2002) (Fig. 1.2). In this iconic diagram (Fig. 1.2), kinases are divided in eight major groups according to their sequence similarities: **AGC** (includes PKA, PKG (protein kinase G) and PKC (protein kinase C) families), **CAMK** (Ca^{2+}/calmodulin-regulated kinases), **CK1** (casein kinase 1 family), **CMGC** (includes CDKs (cyclin-dependent kinases), MAPKs (mitogen-activated protein kinases), GSK (glycogen synthase kinase) and CDK-like kinases), **STE** (related to yeast sterile kinases), **TK** (tyrosine kinases), **TKL** (tyrosine kinase-like) and **aPKs** (atypical protein kinases).

To date, there are 518 known human protein kinases (Manning et al., 2002), representing approximately 2–2.5% of the estimated total number of genes (20000–25000) in the human genome (International Human Genome Sequencing Consortium, 2004). Interestingly, ∼10% of

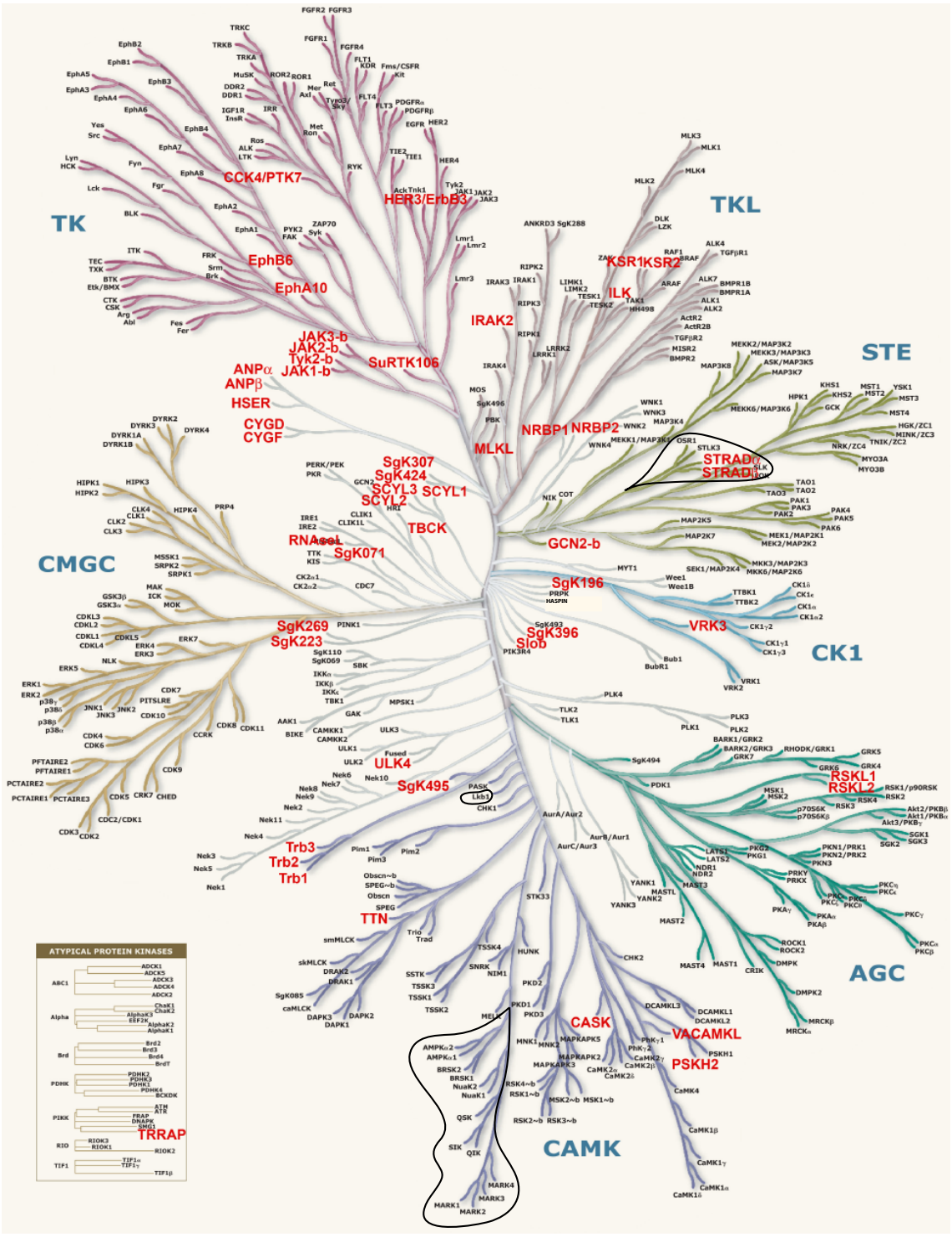

Figure 1.2: The human kinome dendogram
A catalogue of human kinases grouped according to their sequence similarities. An additional list of "atypical" kinases is also provided. In red are protein kinases that have alterations in at least one catalytic motif and predicted to be inactive—these are referred to as pseudokinases. The kinase LKB1, pseudokinases STRADα/β and the AMPK family of kinases, key subjects of this thesis, are marked with a black line. Figure adapted from Manning et al., 2002, and Boudeau et al., 2006. The human kinome is freely accessible from the following URL: http://kinase.com/human/kinome/

protein kinases lack at least one of the motifs required for catalysis—these are termed pseudokinases (Manning et al., 2002; Boudeau et al., 2006). The protein kinase family represents the third most common known functional domain in the human genome (Lander et al., 2001).

1.2 Structural features of a kinase domain

1.2.1 Overall fold of a protein kinase

The first structure of a protein kinase was the structure of protein kinase A (PKA) and was solved in 1991 by Knighton and colleagues (Knighton et al., 1991b,a). PKA also represents the most well studied kinase in terms of structure-function relationship and is presented here as a general model of protein kinase structure (Fig. 1.3). Protein kinases share a common catalytic domain, that has a bilobal structure made up of a small N-terminal lobe, and a larger, C-terminal lobe (Fig. 1.3). The two lobes are connected by a short loop (∼10 residues) referred to as the hinge region, allowing flexibility with respect to each other.

The ligand (ATP) binding pocket is highly conserved amongst all active kinases and some pseudokinases. ATP binds between the two small and large lobes with the adenine ring buried inside a large hydrophobic pocket, thus completing the so-called hydrophobic spine

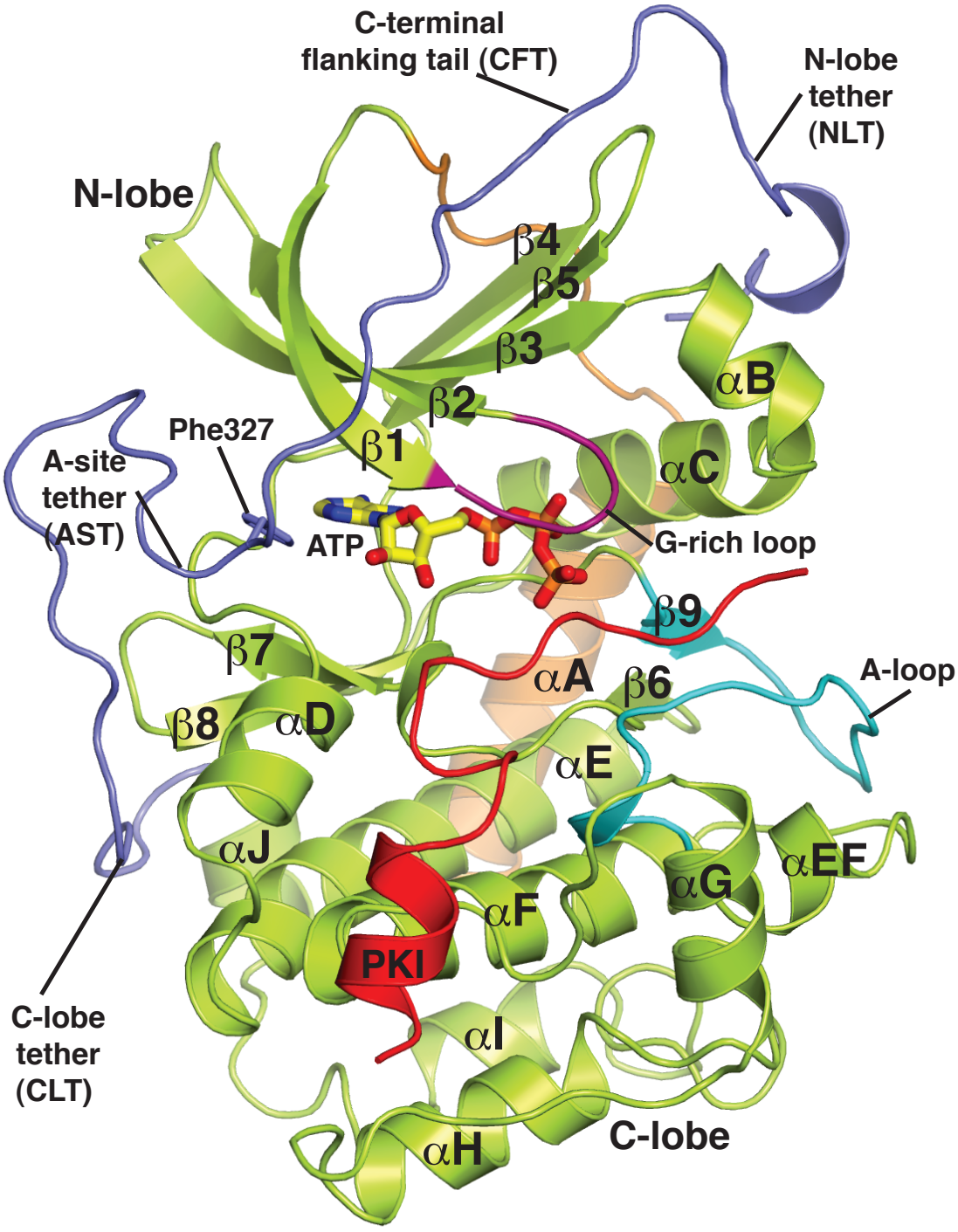

Figure 1.3: Structure of a typical protein kinase
Structure of protein kinase A (PKA; PDBID = 1ATP) determined by Knighton et al., 1991 (Knighton et al., 1991a) in complex with the PKI inhibitor peptide (red). The kinase core domain is coloured green and the secondary structure, N- and C-lobes are labelled. The N- (orange) and C-terminal (blue) flanking regions are labelled αA and CFT respectively. The activation loop (A-loop) is coloured cyan and the glycine-rich (G-rich loop) is coloured magenta. The hydrophobic residue (Phe327) present in the CFT, and is part of the active site tether (AST) is shown as sticks. A bound ATP molecule is shown as sticks with yellow carbons. The same nomenclature (Knighton et al., 1991b; Yang et al., 2009) is used throughout this thesis unless specified otherwise.

(Kornev et al., 2006) of the kinase domain (the ATP binding site is discussed in detail in section 1.2.6). Two Mg^{2+} ions, required for phosphoryl transfer, coordinate active site residues and the phosphate groups of ATP. The N-terminal lobe is comprised of a five-stranded antiparallel β-sheet with a conserved αC helix spanning the domain between β-strands β3 and β4 (Fig. 1.3). With the exception of the loop between the αC helix and the β4 strand that is anchored firmly to the C-terminal lobe, the two lobes show few further interactions.

The larger C-terminal lobe contains mostly α-helices and has a relatively rigid structure. This lobe contributes a small two-stranded β-sheet (β7/β8, Fig. 1.3) and together with residues from the loops before/after this sheet contribute to a mainly hydrophobic environment suitable for binding the adenine ring of ATP. The catalytic and metal binding motifs, together with the substrate binding site are located in the C-lobe (Fig. 1.3) (Knighton et al., 1991a). The activation segment (Fig. 1.3) is perhaps the most mobile structure of the kinase domain and its conformation is subject to post-translational modification as well as allosteric regulation. Correct positioning of the activation segment is a prerequisite for the correct alignment of substrate binding and active sites.

The kinase core domain is often surrounded by N- and C-terminal

flanking sequences, that interact with the kinase domain. These are the N-terminal αA helix and the C-terminal flanking tail (CFT) (Fig. 1.3).

1.2.2 Conserved motifs of protein kinases

In 1988, Hanks et al., provided a multiple sequence alignment of 65 protein kinases, revealing conserved features of the kinase family (Hanks et al., 1988). Analysis of sequence conservation revealed 11 (later updated to 12 (Taylor and Radzio-Andzelm, 1994)) functional motifs, and according to these revelations the protein kinase domain was divided into sub-domains (Fig. 1.4) (Hanks et al., 1988; Taylor and Radzio-Andzelm, 1994).

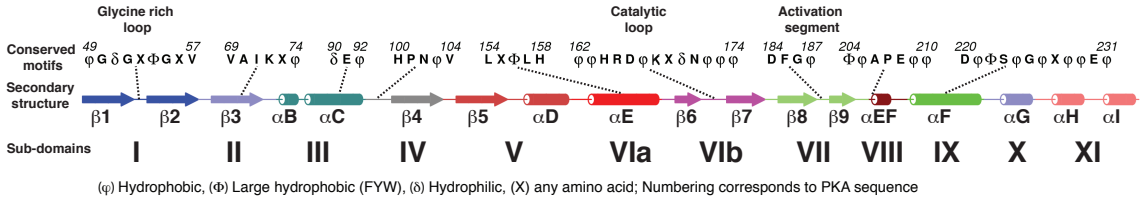

Figure 1.4: Kinase domain secondary structure, sub-domains and conservation of key motifs
The secondary structure is labelled and the consensus sequence of common motifs and key conserved loops are given. These were deduced from multiple sequence alignments of representative protein kinases from each branch of the human kinome. The sub-domain nomenclature as described by Hanks et al., 1988 and Taylor and Radzio-Andzelm, 1994 is indicated. The figure was partially adapted from Kannan et al., 2007.

After the structure of PKA (Fig. 1.3) was solved, the function of these motifs became more apparent. In sub-domain I the small glycine residues from the glycine-rich loop ensure no steric clashes occur with the β/γ phosphate groups of ATP (Fig. 1.3). In sub-domain II, a

lysine residue from the VAIK motif (Lys72 in PKA, Lys31 in CDK2), makes two important interactions—an electrostatic interaction with a conserved glutamate residue (Glu91 in PKA, Glu51 in CDK2) from helix αC (sub-domain III) and a second interaction with the α phosphate group of ATP. Because this motif is found in a β-strand, the alanine and lysine side chains in the VAIK motif, point, by definition, within the ATP binding pocket. This explains the requirement of a small, mainly hydrophobic residue (usually alanine) in this motif that avoids steric clashes with ATP.

The catalytic loop resides in sub-domain VIb, C-terminal to the β6 present in the C-lobe and contains the catalytic (HRD) motif, with the aspartate (PKA Asp166) acting as the catalytic base. The catalytic motif is followed by a conserved lysine residue (PKA Lys168) that positions the γ-phosphate of ATP and an asparagine residue (PKA Asn171) required for coordination of one of the two Mg^{2+} ions (Fig. 1.4). The second Mg^{2+} ion is coordinated mainly by the Mg^{2+} binding loop (sub-domain VII), also referred to

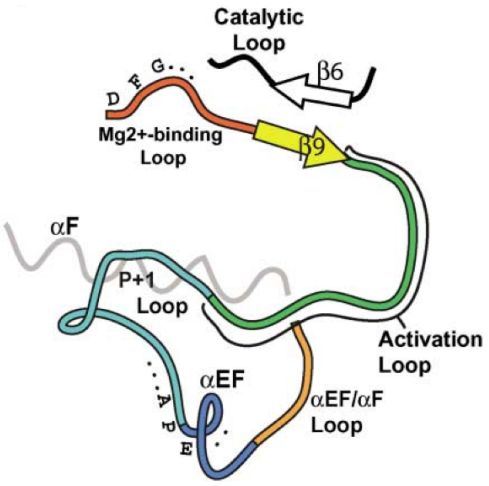

Figure 1.5: Activation segment of a protein kinase. Image was taken from Nolen et al., 2004 and the same nomenclature is used throughout this thesis.

as the DFG motif that follows immediately the β9 strand (Fig. 1.4). The aspartate residue (PKA Asp184) is pivotal for catalysis. The DFG motif located just before the β9 strand, starts the very important activation segment of the kinase domain, that ends with the APE motif prior to helix αEF (Fig. 1.5). This 20-25 amino acid region (DFG ... APE) hosts three important conserved functional motifs—the DFG Mg^{2+} binding loop, the activation loop (or "T" loop) where activatory phosphorylation takes place, and the substrate binding loop (P+1) loop (Nolen et al., 2004) (Fig. 1.5).

1.2.3 Plasticity of a kinase domain

With the determination of PKA structures (Knighton et al., 1991b,a) it became clear the position of the N-terminal to the C-terminal lobe was dependent on the presence and nature of the ligand in the ATP binding site (Prade et al., 1997; Zheng et al., 1993). Zheng et al., 1993 crystallised PKA in the presence/absence of ATP, thus revealing for the first time two states of the enzyme, an active "closed" conformation observed in complex with

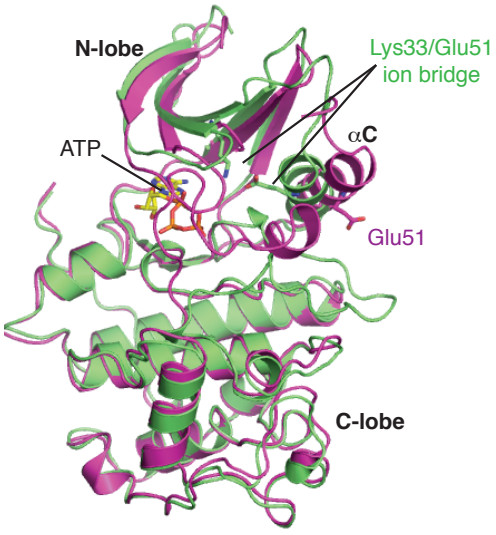

Figure 1.6: Open (magenta) and closed (green) conformations of CDK2

ATP:Mg^{2+} and an inactive "open" conformation, in the absence of Mg^{2+}ATP. This is in agreement with the observation that interactions between the two lobes are largely mediated by ATP, and that in the absence of ATP, the two lobes are relatively uncoupled. Interestingly, also "intermediate" conformations were observed in the PKA structures in complex with a broad, non-specific natural product inhibitor staurosporine (Prade et al., 1997), suggesting that protein kinase inhibitors utilised the conformational flexibility of the protein kinase domain. Thus "locking" the kinase domain in a particular intermediate conformation could be exploited for the design of more specific kinase inhibitors (discussed by Liu and Gray, 2006). Other protein kinases have been crystallised in the open/closed conformations (reviewed by Johnson et al., 1996, Huse and Kuriyan 2002 and Nolen et al., 2004) and this is illustrated in Fig. 1.6. There are two hallmark features of a typical closed conformation, that have so far been observed in all active kinases: formation of the Glu/Lys ion bridge connecting helix αC and the N-lobe β sheet (Fig. 1.6) and the formation of a short $\beta6/\beta9$ sheet between the catalytic loop ($\beta6$) and activation segment ($\beta9$) (Fig. 1.5).

1.2.4 Activity modulators of protein kinases

Protein kinases have evolved different mechanisms to properly align the catalytic machinery and the substrate binding site. In most cases, protein kinases are regulated by phosphorylation of residues in their activation loop. This can contribute to the correct positioning of helix αC, but more importantly it aligns the activation segment in a particular orientation, away from the ATP binding pocket. In some kinases the conserved catalytic Asp residue in the catalytic loop (Asp166 in PKA) is preceded by an Arg residue (Arg165 in PKA)—these are termed RD-kinases (Johnson et al., 1996) and the basic pocket surrounding the site of T-loop phosphorylation has been termed the "RD pocket" (Johnson et al., 1996; Nolen et al., 2004). The RD pocket is formed by residues contributed by helix αC (PKA His87) and basic residues from the activation segment (PKA Lys189) (Knighton et al., 1991b), thus the activatory phosphate can be seen as an interconnecting module of activation segment and the catalytic loop, while at the same time influencing inter-lobe conformational changes.

Many inactive protein kinases lack a proper alignment of the Glu residue due to rotation, disorder or twisting of the regulatory helix αC. For instance, in the inactive cyclin dependent protein kinase 2 (CDK2) structure, Glu51 (from helix αC) points away from the ATP

binding site (De Bondt et al., 1993) and assumes an "open" conformation (Fig. 1.6). After binding of CDK2 to activatory cyclins, rotation of the αC helix aligns Glu51 to interact with Lys33, which is now perfectly aligned to interact with ATP (Jeffrey et al., 1995) (Fig. 1.6). The formation of this Lys/Glu ion bridge represents one of the hallmarks of the "closed" active conformation (Johnson et al., 1996; Huse and Kuriyan, 2002; Nolen et al., 2004). In addition, protein kinases unrelated to CDK2 are regulated by an induced alignment of the helix αC, such as AGC kinases (Bayliss et al., 2003) and tyrosine kinases (Filippakopoulos et al., 2008). Interestingly, in the case of CDK2 mentioned above, both phosphorylation by upstream CDK kinases as well as binding of activity modulators such as cyclins, are required to assume a "closed" active conformation and a proper alignment of the activation segment, that is optimal for substrate binding and phosphoryl transfer (Jeffrey et al., 1995; Russo et al., 1996). In addition, protein kinases unrelated to CDK2 are regulated by an induced alignment of helix αC and activation loop phosphorylation. Examples include Aurora-A/B (AGC kinases) regulated by the TXP2/INCEP binding modules respectively (Bayliss et al., 2003; Sessa et al., 2005) and tyrosine kinases such as the proto-oncogene Fes/Fps that is regulated by an SH2 domain present in the same polypeptide chain (Filippakopou-

los et al., 2008).

While activation loop phosphorylation either by auto-phosphorylation or phosphorylation by other kinases is a common mechanism of regulating kinase activity, regulatory mechanisms other than the ones described above exist. For instance, phosphorylase kinase (PhK) does not require T-loop phosphorylation for activity, but contains a glutamine residue in its activation loop that substitutes for the negative charge usually provided by the phosphate group (Owen et al., 1995). The assumed position of the activation segment via regulatory/activity modulators is one of the main subjects of this thesis.

1.2.5 N- and C-terminal flanking regions

Interesting features of a kinase domain are interacting flanking sequences at its N- and C-termini (Fig. 1.3), that in some cases modulate protein kinase activity. The C-terminal flanking tail (CFT) is a conserved feature of AGC kinases and wraps around both lobes of the kinase domain (Fig. 1.3) (Kannan et al., 2007b). Kannan et al., defined three sites that tether the CFT to the kinase domain: C-lobe tether (CLT), active site tether (AST) and N-lobe tether (NLT) (Kannan et al., 2007b). The latter contains the conserved hydrophobic motif that binds to a hydrophobic pocket present in the N-lobe and regulates (AGC) kinase activity (reviewed by Biondi and Nebreda,

2002 and Gold et al., 2006). The C-lobe tethers the initial residues of the CFT and the most dynamic part of the CFT is the active site tether (AST). An important feature of the AST is the interaction of a large hydrophobic residue (Trp/Phe) with ATP (Kannan et al., 2007b; Yang et al., 2009), that closes the hydrophobic ATP binding pocket (Fig. 1.3). Interestingly, yeast genetic screens identified a loss-of-function mutant that corresponds to the equivalent residue (Phe327) in PKA (Yang et al., 2009). Yang et al., have provided an explanation for this phenotype, and have demonstrated the Phe327Ala exhibits significant reduction in catalytic efficiency (Yang et al., 2009).

N- and C-terminal regions have been documented to (up/down)-regulate kinase activity in many different ways. There are well known examples of SH2 and SH3 domains, present in the same polypeptide of tyrosine kinases that contribute to inactive kinase conformations (Sicheri and Kuriyan, 1997). Other examples include the microtubule affinity-regulating (MARK1-4) isoforms, that contain a ubiquitin associated (UBA) domain at their C-terminus that interacts with the N-lobe of the kinase domain (Panneerselvam et al., 2006) and is required for activation by the upstream kinase LKB1 (Jaleel et al., 2006).

1.2.6 The ATP binding site

Understanding the molecular interactions of ATP binding to a protein kinase domain is important for unveiling details of the reaction mechanism. In addition, most available protein kinase inhibitors are ATP competitive and utilise the same binding pocket to inhibit kinase activity and function. The adenine base of ATP is bound by all kinases in an analogous fashion, sandwiched by hydrophobic residues from the N- terminal and C-terminal lobes (Fig. 1.7A) Two hydrogen bonding interactions can be observed between the polar adenine nitrogen groups and the protein backbone of the kinases hinge-region (Fig. 1.7B). The adenine N1 accepts a hydrogen from the backbone amide, whereas the adenine amino group donates a hydrogen to the backbone carbonyl. Interestingly, almost all known protein kinase inhibitors have been found to mimic the adenine N1 interaction with the protein, and many protein kinase inhibitors mimic both interactions (Komander et al., 2003, 2004; Liu and Gray, 2006). In addition, the ribose ring of ATP interacts via hydrogen bonds with (generally) acidic amino acids (Fig. 1.7B).

While the adenine ring of ATP is held via hydrophobic forces, the phosphate groups on the other hand, are coordinated mainly via hydrogen bonding interactions with active site residues as well as two

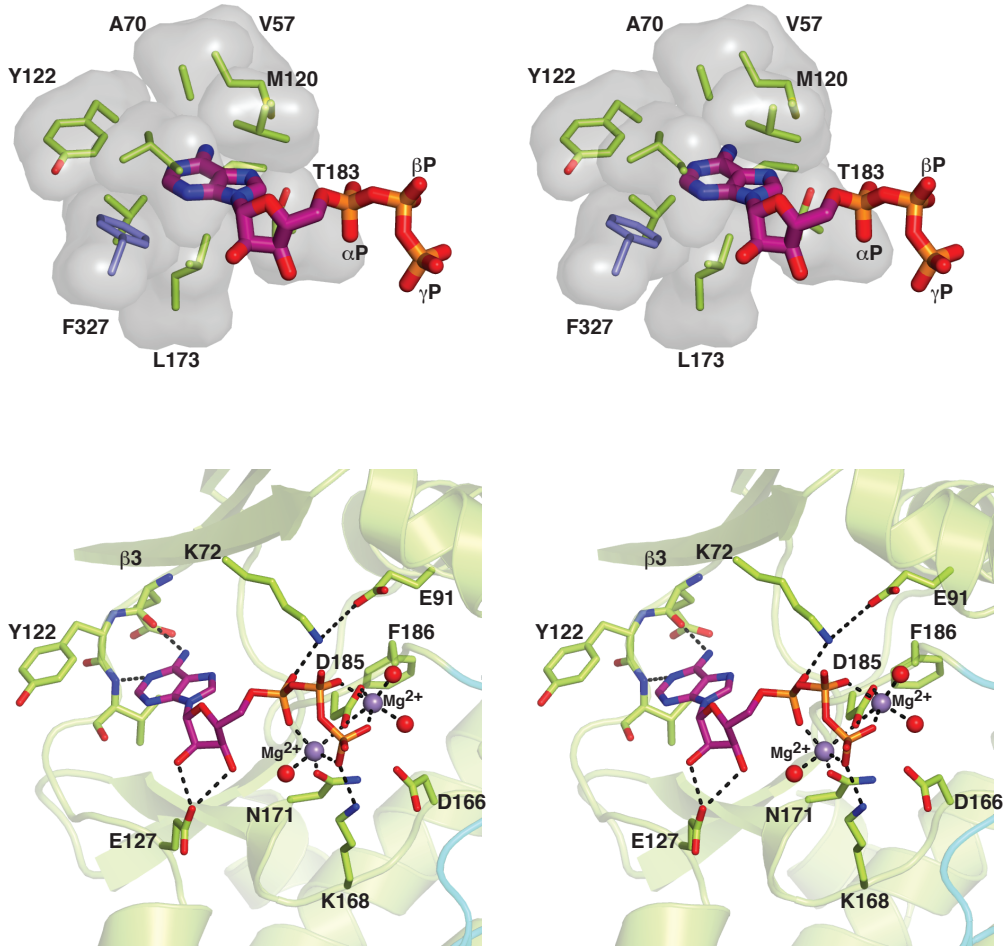

Figure 1.7: Conserved interactions in the ATP binding pocket
A) Stereo view of hydrophobic interactions between ATP (represented as sticks) and residues from the ATP binding pocket of PKA (represented as sticks and transparent surface). Phe327 (from the C-terminal flanking tail) is the only residue not part of the kinase domain and coloured blue.
B) Stereo view of conserved interactions between the ATP phosphate moiety (represented as sticks), residues from the ATP binding pocket (represented as sticks), Mg^{2+} ions (blue spheres) and nearby water molecules (red spheres). Dashes represent hydrogen bonds. The structure of PKA/ATP:Mg^{2+} (PDBID 1ATP (Knighton et al., 1991b)) is shown in both (A) and (B).

Mg^{2+} ions (Fig. 1.7B). As mentioned above, of particular importance is the lysine residue from the VAIK motif that coordinates the α-phosphate, thus linking the ligand binding to the regulatory αC helix. The β/γ-phosphate groups are tethered by Mg^{2+} ions that are held in place by the conserved apartate residue from the DFG motif, aided by a conserved asparagine (catalytic loop) and surrounding

water molecules (Fig. 1.7B). The presence of Mg^{2+} is required for correct positioning of the γ-phosphate and its transfer, and mutation of the Mg^{2+} binding residue (PKA Asp185) leads to (near) complete loss of activity. Another residue (PKA Lys168), in hydrogen bonding distance to the γ-phosphate (Fig. 1.7B), plays a key role in γ-phosphate/substrate binding, at least for Ser/Thr kinases (Johnson et al., 2001).

1.2.7 Substrate binding to Protein Kinase A

The first protein kinase structure reported by Knighton et al., (Knighton et al., 1991b) provided significant insights into substrate binding and recognition (Knighton et al., 1991a). The structure of PKA was determined in complex with a 24 residue pseudo-substrate inhibitor peptide (termed PKI), which has an alanine instead of a phosphorylatable Ser/Thr residue (Knighton et al., 1991a). The residues determining substrate specificity were identified, and a nomenclature was devised applicable to all kinases. The phosphorylated residue of the peptide occupies the P-site, and the neighbouring sites were accordingly numbered p+1, p+2 and p-1, p-2, etc, depending if they were C- or N-terminal to the site of phosphorylation, respectively (Fig. 1.8A). As mentioned above, the peptide binding region lies almost entirely in the larger lobe of the kinase domain (Fig. 1.8). The N-terminal part of

the peptide folds into a short α-helix, which is required for high affinity binding, and also forms multiple contacts with exposed aromatic residues of the C-terminal lobe.

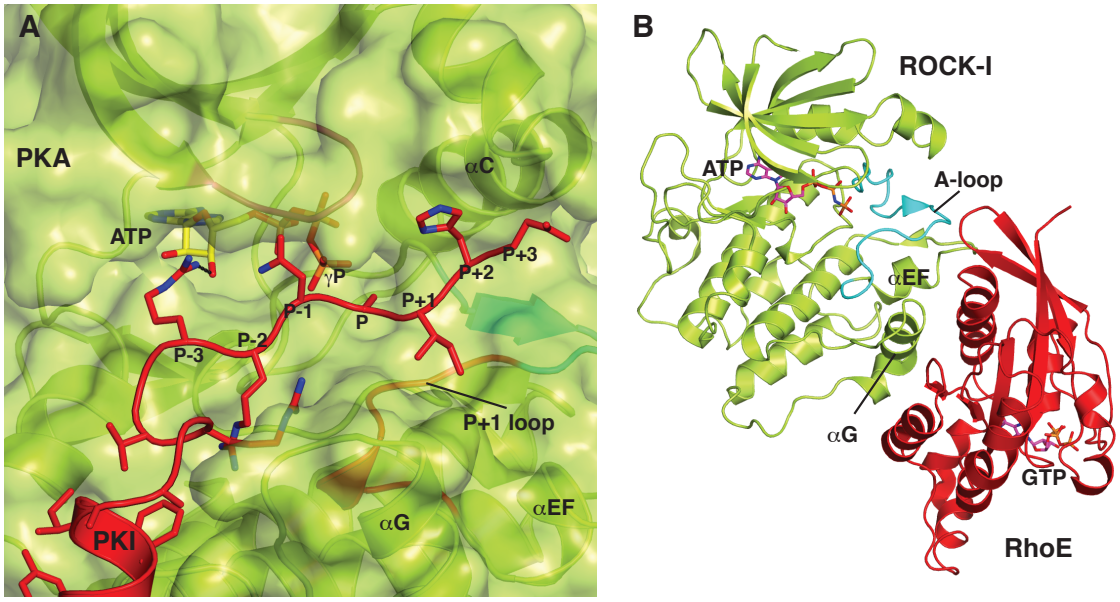

Figure 1.8: Substrate binding to protein kinases
A) Structure of PKA (coloured green and represented as cartoons with transparent surface) and bound PKI inhibitor peptide (red cartoon) (PDBID 1ATP) Knighton et al. (1991a). P = position of the phosphorylatable residue. In this case this is an alanine residue since PKI is a pseudosubstrate. The activation and p+1 loops are coloured cyan and red respectively.
B) Complex structure of ROCK-I kinase with its substrate RhoE (PDBID = 2V55) determined by Komander et al., 2008.

Recently, complexes between protein kinases and protein substrates have been solved. In 2005, Dar et al., reported the structure of the RNA-dependent protein kinase (PKR) complexed to the translation initiation factor α-2 subunit (eIF2α) (Dar et al., 2005). Another example is the structure of the Rho-associated protein kinase (ROCK-I) in complex with the Rho-related GTP-binding protein (RhoE) (Komander et al., 2008) (Fig. 1.8B). Interestingly, in both cases helix αG (C-lobe) was involved in substrate interaction, suggesting a role

for this helix in substrate binding, additional to the p+1 loop (Fig. 1.8B).

1.2.8 Mechanism of phosphate transfer

For the phosphoryl transfer in protein kinases, two mechanisms are possible: the associative, concerted mechanism (S_N2) in which the γ-phosphate is transferred to the substrate hydroxyl-group under inversion of its stereochemistry via a single step. The transition state for this mechanism consists of a penta-covalent phosphorane moiety with three negative charges (Fig. 1.9). The second possible mechanism is a dissociative two-step mechanism (S_N1), in which a trigonal-planar metaphosphate (PO_3^-) is formed by breaking the P-O bond (Fig. 1.9).

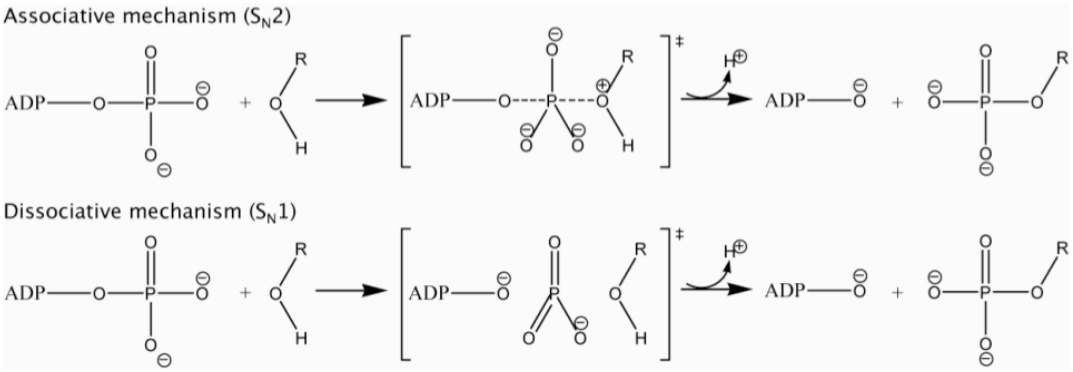

Figure 1.9: Possible reaction mechanisms of phosphate transfer
Schematic representations of the associative (S_N2) and dissociative (S_N1) mechanism discussed by Knowles., 1980. Adapted from Cook et al., 2002..

Evidence for both reaction mechanisms are available from studies with transitions state analogues such as nitrate (NO_3^-) and aluminium fluoride (AlF_3), both planar compounds assumed to resemble the transition state of a phosphoryl reaction. Structures are available, for a

quaternary complex of CDK2 with a substrate peptide, ADP, Mg^{2+}, and nitrate (Cook et al., 2002), supporting a mainly dissociative mechanism. Similarly, the structure of PKA in complex with a substrate peptide, ADP, Mg^{2+} and aluminium fluoride (AlF_3) has been determined and supports a mainly associative mechanism (Madhusudan et al., 2002). The mechanisms are not mutually exclusive and can partially co-exist.

1.3 Protein kinases in disease

Given the key roles protein kinases play in orchestrating almost all aspects of cellular life, it is no surprise that a large number of these genes are mutated in disease. Because of the diverse functionality, these include both gain- and loss-of-function mutations. A list of protein kinases and phosphatases that are mutated in various human diseases is given in Table 1.1, with the aim of illustrating the crucial importance of protein phosphorylation as one of the key post-translational modifications. In more complex human disorders such as cancer, both germline and somatic mutations in genes coding for kinases can lead to the breakdown of protein kinase signalling networks and progress to severe malignant conditions. Another classic example of a multifactorial disease where signalling by kinases is of crucial importance, is type II diabetes that is caused by a combination of normal ageing

processes and genetic factors, coupled with the side effects of obesity and lack of exercise. Altogether these lead to a breakdown of protein phosphorylation signalling cascades controlled by insulin.

Disease causing mutations in protein kinases continue to be found at high frequencies. For instance, in a recent enterprise by the Wellcome Trust Sanger Institute for the Cancer Genome Project, the protein kinase family represents the highest number of genes with somatic mutations in 339481 human tumour samples and 4775 genes analysed (statistics from the Catalogue of Somatic Mutations in Cancer (COSMIC) database accessible online at http://www.sanger.ac.uk/genetics/CGP/cosmic/ (Forbes et al., 2008). In some types of cancers (e.g. lung cancer), mutations in as many as 141 protein kineses (out of the total 518) were found (Davies et al., 2005). It is worth noting however, not all of the found mutations were cancer driving mutations. Finally, mutated and activated protein kinases have proved to be possible targets for the development of new anticancer therapies, and the first Abl tyrosine kinase inhibitor (Imatinib) was approved as a drug for the treatment of chronic myeloid leukaemia (CML) in 2001. It is thought that over 25% of all drug targets currently under investigation by the pharmaceutical companies comprise protein kinases, a figure likely to be significantly higher in oncology (Cohen, 2002b).

Table 1.1: Some of the inherited human diseases caused by mutations in protein kinases and phosphatases. Table adapted from Alessi and Zeqiraj, 2007. Data can be retrieved from the Online Mendelian Inheritance in Man (OMIM) database (http://www.ncbi.nlm.nih.gov/omim/). STRADα and LKB1 entries are highlighted.

Disease	Kinase
Myotonic muscular dystrophy	Myotonin protein kinase
X-linked agammaglobulinaemia	Bruton's tyrosine kinase
Hirschsprung's disease, men	RET2
Autosomal recessive severe combined immunodeficiency (SCID)	ZAP70
Polycythaemia vera	JAK2
X-linked SCID	JAK3
Polyhydramnios, megalencephaly and symptomatic epilepsy (PMSE)	STRADα
Craniosynostosis	FGF receptor kinase
Papillary renal cancer	Met receptor kinase
Chronic myelogenous leukaemia	TEL/PDGF receptor kinase
Myelogenous leukaemia	Abelson tyrosine kinase
Non-Hodgkin's lymphoma	ALK
Peutz-Jeghers syndrome	LKB1
Coffin-Lowry syndrome	RSK2
Ataxia telangiectasia	ATM
Li-Fraumeni syndrome	CHK2
Williams syndrome	LIMK1
Leprechaunism, diabetes	Insulin receptor kinase
Wolff-Parkinson-White syndrome	AMPK
Gordon hypertension syndrome	WNK1 and WNK4
Wolcott-Rallison syndrome	EIF2AK3
Melanoma and other sporadic cancers	B-Raf and CDKN2A
Hereditary early-onset Parkinson's disease	PINK1 and LRRK2
Pulmonary hypertension	TGFβ receptor BMPR-II
Neuronal development disorders	CDKL5
Familial advanced sleep phase syndrome	CK1δ
5-10% non-small-cell lung cancers	EGF receptor kinase
Hyporesponsiveness to bacterial infection	IRAK4
Colon, breast and other sporadic cancers	PI3K (p110α subunit)

Disease	Phosphatase
X-linked myotubular myopathy	MTM1 tyrosine phosphatase
Cowden's disease	PTEN phosphatase

1.4 The *LKB1* gene—disease implications

1.4.1 Discovery of the LKB1 gene

The LKB1 gene was first identified in 1996 by Jun-ichi Nezu from Chugai Pharmaceuticals, Tokio, Japan, in a screen aimed at identifying new kinases. The sequence was given the pseudo-acronym LKB1 (not standing for a specific name), and was deposited in the NCBI public database (NCBI accession code = NM 000455; GenBank ID U63333.1) without the publication of a research paper. A single *LKB1* gene (also referred to as serine/threonine kinase 11, *STK11*), is present in the human genome. The *LKB1* gene is composed of 11 exons (23 kb) and is located in chromosome 19 (gene locus 19p13.3). The human LKB1 protein comprises 433 residues (mouse 436 residues) with the catalytic kinase domain encompassing residues 43–309 (Fig. 1.10). Interestingly, the catalytic domain shares less homology to other protein kinases, explaining why LKB1 is localised within the centre of the human kinome dendogram and does not belong to any of the seven groups classified by Manning et al. 2002 (Fig. 1.2). A sequence similarity search of eukaryotic genomic databases using the BLAST tools (http://blast.ncbi.nlm.nih.gov/Blast.cgi) with sequences of the N- and C-terminal regions of LKB1 reveals no similarities to known functional domains. LKB1 is widely expressed at varying levels in

all foetal and adult tissues examined (Hemminki et al., 1998; Jenne et al., 1998). An additional isoform of LKB1 (denoted LKB1 short) is found in testis and this is a result of alternative mRNA splicing after exon VIII (Towler et al., 2008; Denison et al., 2009). The two isoforms share 100% sequence identity between residues 1–370 (Fig. 1.10) (Towler et al., 2008; Denison et al., 2009).

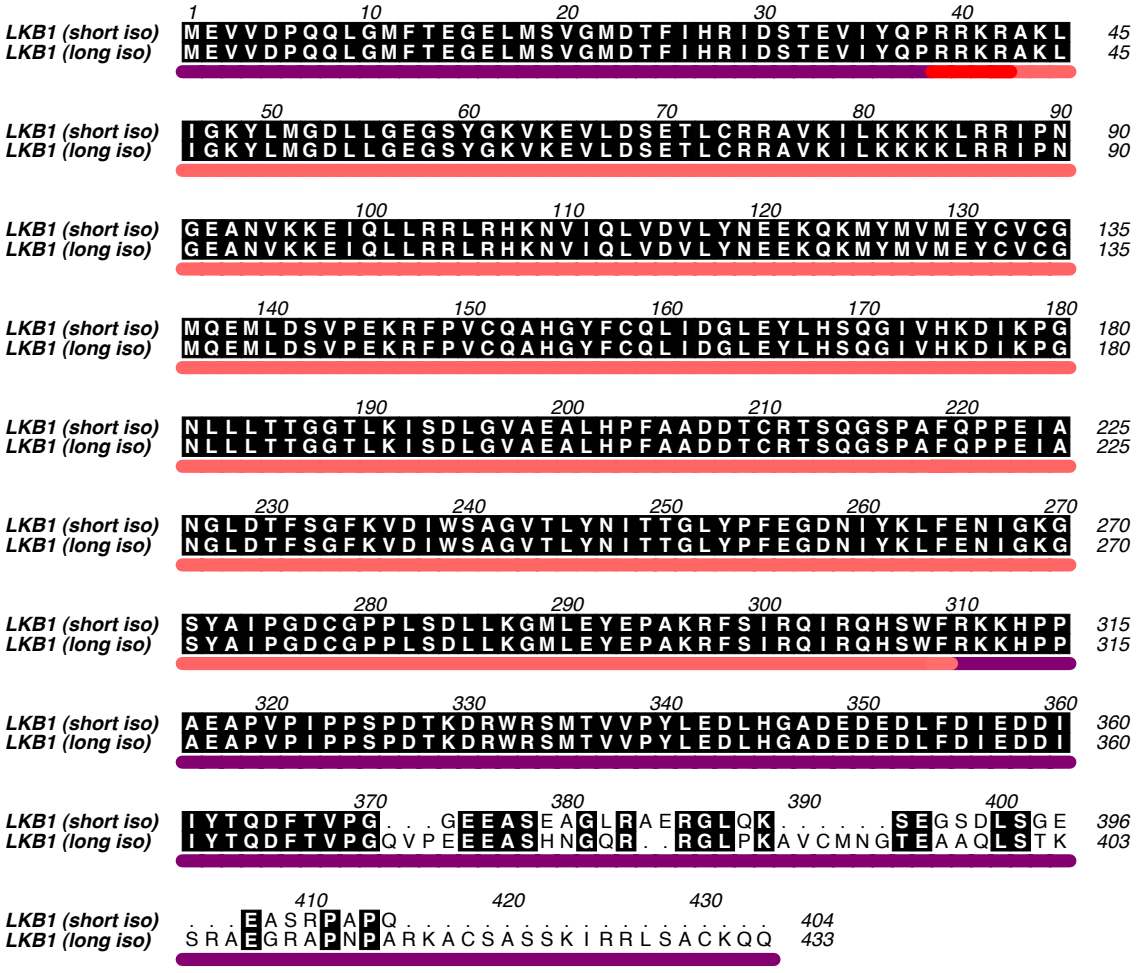

Figure 1.10: Sequence alignment of the LKB1 splice isoforms
Sequences of the LKB1 short isoform found predominantly in testis and LKB1 long found in all tissues (Towler et al., 2008; Denison et al., 2009). The kinase domain is underlined in pink, whereas the N- and C-terminal regulatory domains (NRD and CRD) are underlined in purple. The sequence of the nuclear localisation signal (NLS) is underlined in red.

1.4.2 LKB1 is the causative gene for PJS

Peutz-Jeghers syndrome (PJS) is a rare genetic disorder inherited in an autosomal dominant fashion and is discussed in section 1.4.3 below. The first genetic link between PJS and LKB1 was provided in 1997 when three studies reported the gene locus (19p13.3) responsible for the condition (Amos et al., 1997; Hemminki et al., 1997; Mehenni et al., 1997). Intensive sequencing of all genes present in that locus (29 in total), from samples derived from PJS patients, demonstrated that 11 out of the 12 PJS families studied had mutations in the gene coding for LKB1. The findings were described in the landmark paper of Akseli Hemminki (a graduate student in Lauri Aaltonen's laboratory) and collegues (Hemminki et al., 1998). In the same year, a second group, which had originally collaborated with the Aaltonen laboratory, also reported mutations of the *LKB1* gene in PJS subjects (Jenne et al., 1998). Moreover, point mutations that alter key catalytic residues, (e.g. Asp174Asn (Mehenni et al., 1998)) suggested a strong link between LKB1 kinase activity and PJS. In the last decade, a large number of studies have reported mutations of the *LKB1* gene in PJS patients as well as sporadic cancers with the largest number of genetic alterations occurring in the kinase domain. Thus far, 62 missense mutations, 77 frameshift mutations, 36 nonsense mutations

and 19 in-frame deletions of the LKB1 gene have been identified from samples of PJS and other cancer patients (these are summarised in Fig. 1.11).

Early studies of PJS patients have reported that only about half of the individuals carry LKB1 germline mutations, suggestive that other tumour suppressor genes are responsible for causing PJS in the remaining patients (Alhopuro et al., 2005; Wang et al., 1999). However, with recently improved methods the detection of LKB1 alterations in PJS patients has soared by up to 80% (Hearle et al., 2006; Volikos et al., 2006; Sanchez-Cespedes, 2007), thus lessening the probability of a second PJS locus. Interestingly, a recent study has reported an activating germline mutation in the smooth muscle myosin gene (*MYH11*) in a patient with PJS-like features (Alhopuro et al., 2008). Two missense and two frmeshift functionally evaluated MYH11 mutations were found to possess increased actin-activated ATPase activity (Wallace et al., 2005; Alhopuro et al., 2008), as well as unregulated (phosphorylation dependent) motor activity (Alhopuro et al., 2008). Mutations in the *MYH11* may therefore be responsible for causing polyposis in the remaining PJS patients, although more work is necessary to conclude that *MYH11* is indeed the missing PJS gene.

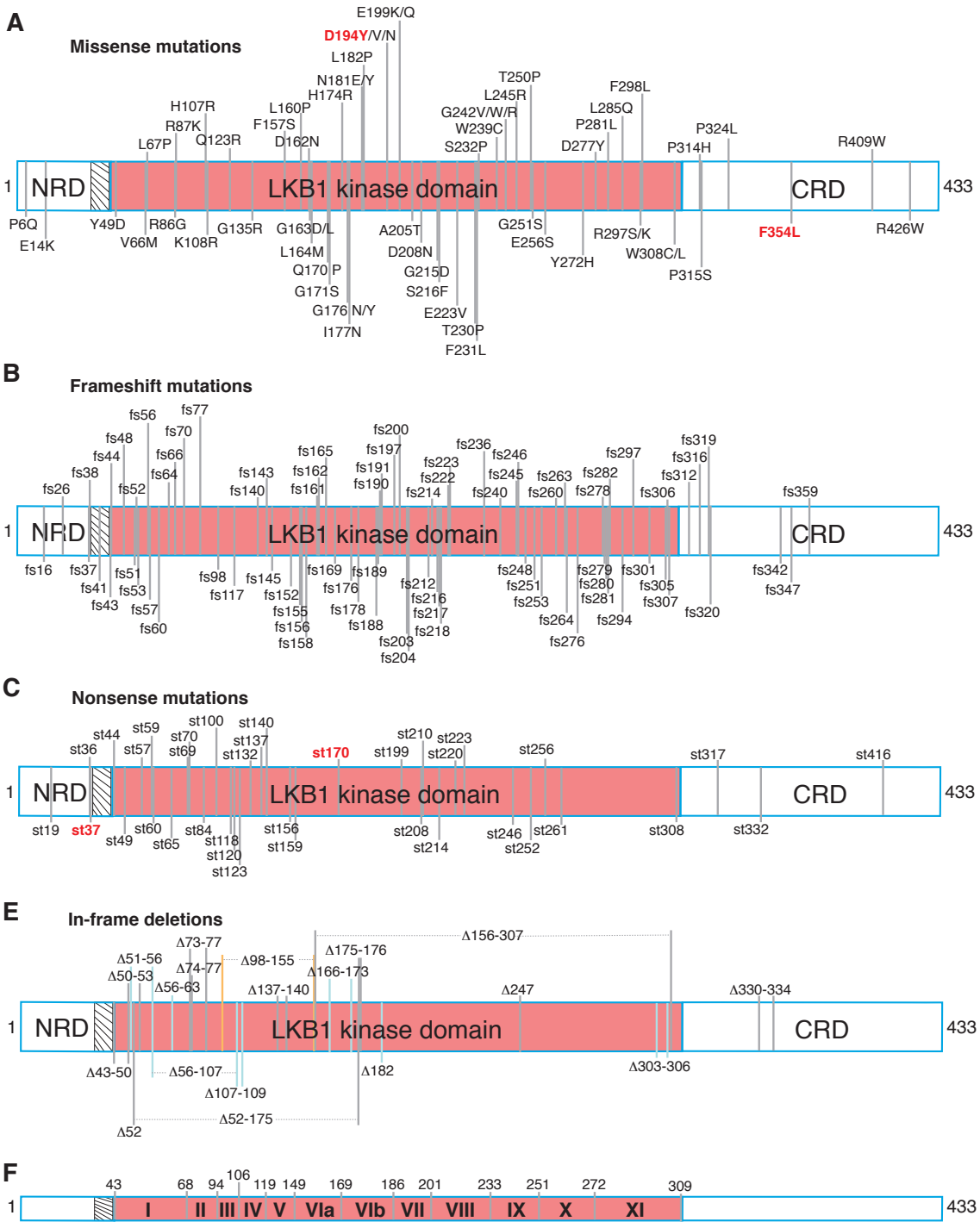

Figure 1.11: List of disease causing mutations in the *LKB1* gene
Mutations identified in the human *LKB1* gene in patients with PJS and sporadic cancers are represented schematically on the primary structure of the LKB1 protein: (A) missense mutations, (B) frameshift mutations, (C) nonsense mutations and (D) in-frame deletions. Silent mutations, splicing mutations and large exonic deletions are not listed. Data were acquired from the published literature, the Catalogue of Somatic Mutations in Cancer (COSMIC) database (Forbes et al., 2008), (Boudeau et al., 2003b),(Alessi et al., 2006) and references therein. The nuclear localisation signal (residues 38–42) is shown as a hatched rectangle and the kinase domain of LKB1 (residues 43–309) is coloured pink. The most frequently found somatic mutations to date ("hot-spots") are coloured red. NRD, N-terminal regulatory domain; CRD, C-terminal regulatory domain; fs, frameshift; st, stop.
E) To aid representation of the LKB1 kinase domain, an annotation of all the standard subdomains (Hanks et al., 1988) is provided.

1.4.3 Peutz-Jeghers syndrome

PJS is an autosomal dominant inherited disease characterised by hamartomatous polyposis of the Gastro-Intestinal (GI) tract and "soft"/mucosal tissue pigmentation. PJS symptoms were first observed in twin sisters with unique "ink-black pigmentation of the lips and mouth" and reports date back to the late 19th century (reviewed by Hemminki, 1999). However, the relationship between mucocutaneous pigmentation and polyposis was first described by Dr Johannes Peutz in a Dutch family in 1921 (Peutz, 1921) and further characterised in the 1940s by Dr Harold Jeghers and co-workers (Jeghers et al., 1949).

The presenting features of PJS are melanin pigmentation primarily around the mouth, eyes and nostrils, but also around the anus, buccal mucosa, vulva fingers and toes (Peutz, 1921; Jeghers et al., 1949). The major clinical symptoms however, are polyp formation in the GI tract that cause intussusception, obstruction, abdominal pain, GI bleeding and polyp extrusion (Buck et al., 1992; Harned et al., 1995). PJS patients require close monitoring of polyp growth by enteroscopies and the only treatment available is the surgical removal of polyps, although this is accompanied by a very high recurrence rate (Katajisto et al., 2007). Interestingly, recent studies have reported that rapamycin (inhibitor of the mTOR kinase) reduces polyp burden as well as polyp

size in mouse models of PJS (Wei et al., 2008, 2009; Robinson et al., 2009; Shackelford et al., 2009), suggesting this type of treatment may be beneficial to PJS patients.

While the occurrence of polyps does not constitute a life threatening condition, patients with PJS are more predisposed to developing malignant tumours in multiple tissues (Tomlinson and Houlston, 1997; Hemminki, 1999; Westerman et al., 1999a). PJS is a relatively rare condition with a current estimated rate of 1 in ∼10000–120000 live births (Hemminki, 1999).

1.4.4 Somatic LKB1 mutations

Unexpectedly, LKB1 somatic mutations are increasingly being found in tumour samples of non-PJS patients and an estimated 6% of samples from a variety of cancers analysed so far, have somatic LKB1 mutations (Table 1.2). As expected, the frequency of LKB1 mutations in the GI tract is relatively high, 25% (number of samples n = 21; Table 1.2). Interestingly, cervical and skin cancers display higher than average frequency rates (16% and 10% respectively; Table 1.2). From the 205 mutated samples catalogued thus far by the COSMIC database, Asp194Tyr (Mg^{2+} binding residue) and Phe354Leu (positioned C-terminal to the kinase domain) amino acid substitutions appear to be more frequent than others, together with nonsense muta-

tions at position 37 and 170 (Fig. 1.11). This could however, represent a finding that is skewed towards the lung cancer samples since these represent 58% of the total number of mutated samples (Table 1.2).

Table 1.2: LKB1 somatic mutations found in tissue samples and cell lines derived from cancer patients. Numbers were acquired from the Catalogue of Somatic Mutations in Cancer (COSMIC) database* accessible online at http://www.sanger.ac.uk/genetics/CGP/cosmic/ (Forbes et al., 2008).

Primary tissue	Number of samples	Mutated samples	Frequency
Biliary tract	29	1	3%
Cervix	203	32	16%
GI tract**	21	5	24%
Kidney	71	1	1%
Large intestine	438	12	3%
Liver	10	1	1%
Lung	1132	120	11%
Oesophagus	24	1	4%
Ovary	162	4	2%
Pancreas	151	6	4%
Prostate	5	1	§20%
Skin	146	15	10%
Small intestine	29	1	3%
Stomach	184	3	2%
Testis	45	1	2%
Upper aerodigestive tract	57	1	2%
Totals	3311	205	6%

*The latest update for the *STK11* gene was 28^{th} of May 2009
**Gastrointestinal tract (site unknown)

§ Insufficient number of samples

A well established link between LKB1 inactivation and non-small-cell lung carcinoma (NSCLC) is now evident (Sanchez-Cespedes et al., 2002; Sanchez-Cespedes, 2007; Ji et al., 2007), with some studies claiming that mutations in the *LKB1* gene occur in 30% of NSCLC cases. The frequency of LKB1 mutations found in all lung cancers however, is likely to be $\sim$ 10% (Table 1.2). It must be noted that

a large number of LKB1 mutations found in NSCLC co-occur with v-Kirs2 Kirsten rat sarcoma (K-Ras) viral oncogene homologue mutations (Ji et al., 2007). Therefore, it can be expected that a large number of these LKB1 mutations will be passenger rather than driving mutations.

1.4.5 Cellular and animal models of the LKB1 tumour suppressor

Given the large number of inactivating mutations (Fig. 1.11) of the LKB1 kinase associated with PJS and other types of cancers, it is clear the *LKB1* gene represents a key tumour suppressor. Cellular and animal models generated in various laboratories have also demonstrated this. LKB1 is capable of inducing a G1 cell cycle arrest when over expressed in HeLa and G361 cells, which lack endogenous LKB1 (Tiainen et al., 1999). In addition, mouse knockout studies have shown that heterozygous $LKB1^{+/-}$ mice develop polyps similar to those observed in PJS patients (Rossi et al., 2002; Bardeesy et al., 2002). Moreover, conditional bi-allelic LKB1 inactivation in mice, results in tumour transformation in a number of tissues including: lung (Ji et al., 2007), skin (Gurumurthy et al., 2008) pancreas (Hezel et al., 2008), endometrial lining (Contreras et al., 2008), prostate (Pearson et al., 2008) and more recently mammary gland (McCarthy et al., 2009). This is consistent with the types of human cancers where LKB1 inactivating

mutations have been reported (Table 1.2). Finally, studies with crosses of *LKB1*$^{+/-}$ mice and mice models of well known tumour suppressors such as *PTEN*$^{+/-}$, *PTEN*$^{-/-}$ (Huang et al., 2008) and *p53*$^{+/-}$, *p53*$^{-/-}$ (Takeda et al., 2006; Wei et al., 2005), show tumour susceptibility and accelerated tumourigenesis.

1.5 The LKB1 signalling pathway

1.5.1 LKB1 forms complexes with STRAD and MO25

The genetic link between the *LKB1* gene and PJS syndrome prompted investigation by many laboratories aimed at understanding the function/regulation of this kinase. The breakthrough came with the discovery that Ste20 related adaptor (STRAD) and the scaffolding mouse protein 25 (MO25; also known as calcium binding protein 39 (CAB39)) bind to LKB1 (Baas et al., 2003; Boudeau et al., 2003a). The formation of this heterotrimeric complex leads to stabilisation and full activation of LKB1 (Baas et al., 2003; Boudeau et al., 2003a). In humans, there are two closely related isoforms of STRAD (STRADα and STRADβ) and MO25 (MO25α and MO25β) that similarly interact with LKB1 (Boudeau et al., 2004). Interestingly, binding of STRAD and MO25 causes complete exclusion of LKB1 from the nucleus to the cytoplasm, suggesting LKB1 may be carrying out its chief

functions outside the nucleus (Baas et al., 2003; Boudeau et al., 2003a, 2004).

Although it is clear that STRADα/β and MO25α/β form highly stable complexes with LKB1, the details of these interaction sites remain unknown. In 2003, Baas et al., reported the non-kinase N- and C-terminal domains are not required for LKB1/STRADα interaction, suggesting a prominent role of the LKB1 kinase domain in complex formation (Baas et al., 2003). STRADα forms a stable complex with MO25 in the absence of LKB1 (Baas et al., 2003), although the physiological role of this binary complex alone is unclear. The last three residues (Trp-Glu-Phe, termed the WEF motif) of STRADα bind to MO25α with high ($\sim$0.5–1.0 μM) affinity (Milburn et al., 2004). Interestingly, the presence of STRADα is required in order to detect MO25α binding to LKB1 in a HEK 293 co-expression assay (Boudeau et al., 2003a). A study carried out by Boudeau et al., demonstrated through mutagenesis studies an arginine residue (Arg240) present on MO25 is involved in LKB1 binding (Boudeau et al., 2004).

The discovery of STRAD and MO25 as the two subunits of the LKB1 complex played a significant role in subsequent studies that resulted in the identification of LKB1 substrates (discussed in sections 1.5.7 and 1.5.8), previously hindered by the difficulties in detecting LKB1

kinase activity.

1.5.2 The STRAD isoforms are pseudokinases

Both STRADα and STRADβ, together with 46 other members of the human kinome (Manning et al., 2002) are classified as pseudokinases, because they lack key residues required for catalysis (Manning et al., 2002; Boudeau et al., 2006). The subject of pseudokinases remains controversial, since for some proteins that lack catalytic residues and hence are classified as pseudokinases, protein kinase activity has been observed. In the case of WNK (With No (K) Lys) protein kinases, protein kinase activity has been measured, and their role in activating SPAK and OSR1 kinases by phosphorylation (Vitari et al., 2005), contributes to the regulation of ion transport and blood pressure (reviewed by Richardson and Alessi, 2006). Interestingly, the WNK1 crystal structure revealed that the function of the initially missing Lys residue from the VAIK motif (subdomain II) is replaced by a Lys residue present in the neighbouring subdomain I (Min et al., 2004). Thus, it is possible the initial prediction ($\sim$10%) of the number of kinases classified as pseudokinases, is likely to be an overestimate as more examples of pseudokinses displaying kinase activity are being reported (e.g. IRAK2 (Kawagoe et al., 2008), CASK (Mukherjee et al., 2008)). However, the exact mechanism of activity for IRAK2 and

CASK remains unexplained. In the case of the latter which lacks the Mg^{2+} binding motif, phosphoryl transfer was reportedly catalysed in a Mg^{2+} independent manner (Mukherjee et al., 2008).

STRADα is predicted to lack residues in four catalytic motifs (three are missing in STRADβ), and is classified in the severely substituted group (group G) by Boudeau et al., together with 13 other pseudokinases (Boudeau et al., 2006). STRADα can bind ATP and MgATP although no kinase activity has been detected so far, despite numerous attempts ((Boudeau et al., 2004) and Dr J. Boudeau unpublished results). Therefore, the functional significance of STRADα nucleotide binding remains unclear.

Beside the two STRADα/β isoforms that share 41% sequence identity (54% sequence similarity), there are 4 different splice isoforms of STRADα and 3 different splice isoforms of STRADβ deposited in the NCBI (http://www.ncbi.nlm.nih.gov/) and Uniprot (http://www.uniprot.org/) sequence databases (Fig. 1.12A). All STRADα isoforms share the same pseudokinase domain, and differ mainly in the N- and C-terminal regions (Fig. 1.12A). Similarly, STRADβ isoform differences are found in the non-pseudokinase regions, with the exception of STRADβ isoform 3 that lacks the first 138 residues (Fig.1.12B). It is not clear whether STRADβ3 is present at the protein level, as this

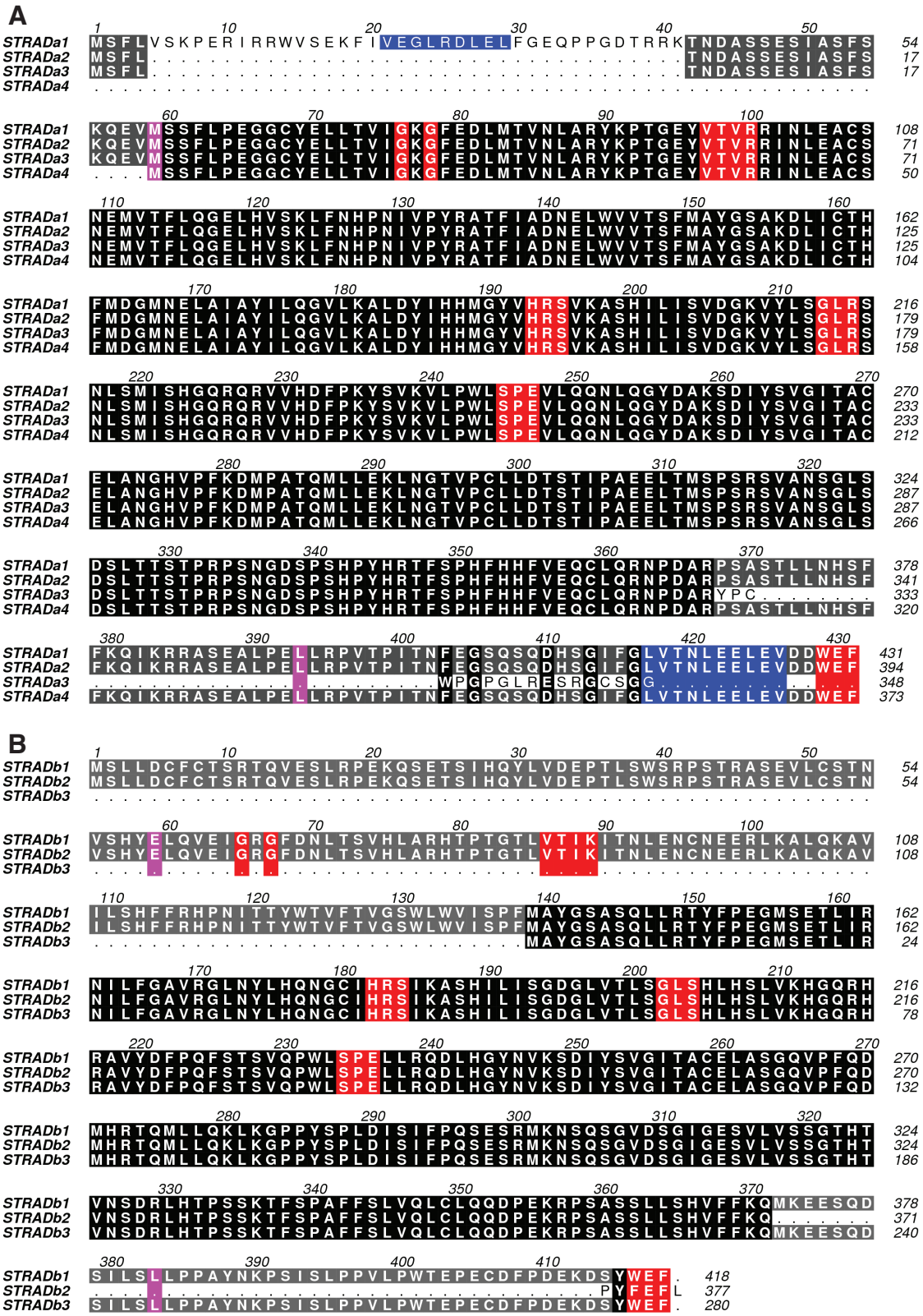

Figure 1.12: STRADα/β splice isoforms
Sequences of the STRADα (A) and STRADβ (B) splice isoforms. The start and finish of the pseudokinase domains are indicated in magenta. Common motifs of a typical kinase domain (in order of appearance for STRADα: glycine-rich loop, VAIK (VTVR) motif, HRD (HRS) motif, DFG (GLR) motif, APE (SPE) motif and the WEF motif), are coloured red. Two STRADα export signal sequences (residues 21–29 and 417–426) are coloured blue (Dorfman and Macara, 2008).

fragment is predicted to lack part of the N-lobe of the kinase domain (Fig.1.12B) and may be unstable.

At present, the function of the different splice isoforms of STRADα/β are unclear. One study found that some STRADα isoforms (9 reported in total) affected LKB1 localisation and stimulated LKB1 activity at different levels (Marignani et al., 2007). However, it is dificult to study these further, since only 4 sequences have been deposited and are publicly available (Fig.1.12A). It is possible that the different N- and C-termini contribute to changes in the localisation patterns of LKB1, given that two export signal sequences (STRADα residues 21-29 and 417-426) have been recently identified in these regions (Fig. 1.12) (Dorfman and Macara, 2008).

Interestingly, STRADα3 and STRADβ2 lack the WEF motif, previously shown to be required for MO25α binding (Boudeau et al., 2003a; Milburn et al., 2004; Boudeau et al., 2004). LKB1 activity should remain unaffected in the presence of these isoforms, since deletion of the WEF motif from STRADα1 does not alter LKB1 activity (Boudeau et al., 2003a, 2004). The majority of studies thus far (including the ones presented in this thesis) have been carried out using STRADα1 and STRADβ1. These are referred to here as simply STRADα and STRADβ unless specified otherwise.

1.5.3 Deletion of the *STRADA/LYK5* gene causes PMSE syndrome

Recently, it was reported that a severe human developmental and epileptic syndrome termed Polyhydramnios-Megalencephaly- Symptomatic Epilepsy (PMSE), was caused by a homozygous partial deletion in the STRADα gene (*LYK5*), truncating 180 C-terminal residues of the protein (Puffenberger et al., 2007). Individuals affected by this condition suffer from severe mental retardation, gross movement disorders and childhood mortality (Puffenberger et al., 2007). Histological staining of neuronal tissues of PMSE patients has suggested elevated mTOR pathway activity (Puffenberger et al., 2007) that could potentially result from loss of LKB1 kinase activity (see section 1.5.9). The exact molecular mechanisms of how this mutation affects STRADα structure/function or its ability to activate LKB1 has not been studied.

1.5.4 MO25—a multifunctional protein that is evolutionary conserved

MO25α and MO25β are two highly similar proteins that share 79% sequence identity (88% sequence similarity). MO25α was first identified as a gene expressed at the early cleav-

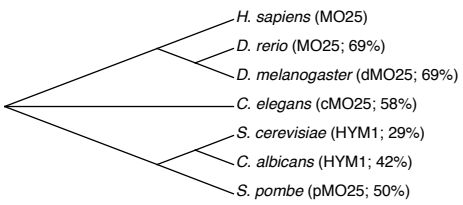

Figure 1.13: Conservation of MO25. Names and the percentage identity to the human sequence are given in brackets.

age stage of mouse embryogenesis and

predicted, incorrectly, to bind Ca^{2+} ions (Miyamoto et al., 1993). In the late 1990s it was noticed as a protein with unusually high degree of evolutionary conservation (Karos and Fischer, 1996; Nozaki et al., 1996; Karos and Fischer, 1999). Sequences of the *D. rerio* (MO25), *D. melanogaster* (dMO25), *C. elegans* (cMO25), *S. pombe* (pMO25), *C. albicans* (HYMA) and *S. cerevisiae* (HYM1) genes are 69%, 69%, 58%, 50%, 42% and 29% identical to human MO25α respectively (Fig. 1.13). In 1996, Karos and Fischer reported a mutant filamentous fungi (*Aspergillus nidulans*) where conidiospore development was affected at the metula stage. The gene responsible was sequenced and named HymA (hypha-like metulae) to describe the hypha-like phenotype of these undifferentiated metulae (Karos and Fischer, 1996). In follow up studies, the same authors demonstrated that the *S. cerevisiae* Hym1 is an essential gene suggesting it carried out important functions that were evolutionary conserved (Karos and Fischer, 1999).

Recent studies have described interesting genetic interactions of MO25 with other kinases—intriguingly, like STRADα/β, these belong to the STE group of kinases (Fig. 1.2). One of these is the germinal centre (GC) kinase Fray, that together with dMO25 regulate *Drosophila* asymmetric division (Yamamoto et al., 2008). The human Fray orth-

logue is the oxidative stress response (OSR1) kinase, one of the closest kinases to STRADα/β (Fig. 1.2). In fission yeast pMO25 is part of a signalling network (NAK1-Orb6-Mob2p), important for cell morphogenesis, polarity control and cell separation (Kanai et al., 2005). pMO25 has been shown to form a complex with NAK1, homologue of MST1-4 and YSK kinases in humans, and this interaction is important for NAK1 localisation and activity (Kanai et al., 2005). Together pMO25 and NAK1 are important for the kinase activity of Orb6p, a kinase homologous to Warts/Lats (*Drosophila*) and NDR human (AGC group) kinases (Kanai et al., 2005).

Similar genetic interactions have been demonstrated in *S. cerevisiae*, between Hym1 and Cbk1 that is similar to the Warts/Lats/NDR kinases (Bidlingmaier et al., 2001). In budding yeast this constitutes a large signalling network, designated Regulation of Ace2p activity and cellular Morphogenesis (RAM), and includes Hym1, Cbk1, Kic1, Tao3, Mob2 and Sog2 (Jorgensen et al., 2002; Nelson et al., 2003). Interestingly, Kic1 is related to the STE20 kinases and may well represent an active STRADα orthologue in yeast.

Recently, ten Kloster and collegues have demonstrated through a yeast two hybrid screen that MO25α interacts with human MST4, and together MO25 and LKB1 are responsible for localisation of MST4

to the apical membrane (ten Klooster et al., 2009). This leads to MST4 phosphorylation of Ezrin and cellular brush border formation (ten Klooster et al., 2009). However, given the multitude of MO25 interactions with other kinases in lower organisms, it is possible that MO25 regulates these kinases independently of LKB1. Future studies in higher eukaryotes may indeed establish additional roles for MO25 in activating/regulating kinases other than LKB1.

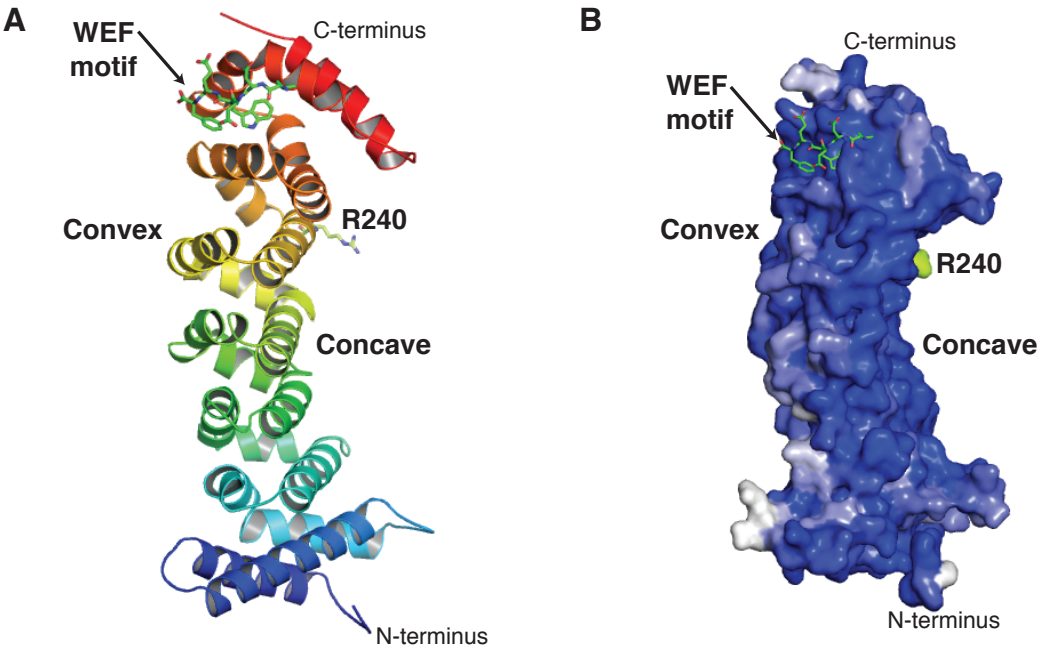

Figure 1.14: Structure of MO25α—an α-helical repeat protein
A) Ribbon diagram of the MO25 structure determined by Milburn et al., 2004. STRADα C-terminal WEF motif (residues 428-431) are shown as sticks with green carbons.
B) Surface representations of the MO25 structure coloured by sequence conservation (dark blue = invariant, white = non conserved) from *C. elegans* to *H. sapiens*.

1.5.5 Structure of MO25α—an α-helical repeat protein

The discovery that MO25α/β isoforms form complexes with STRADα/β and LKB1 and required for the activation of the later (Baas et al., 2003; Boudeau et al., 2003a), provided more functional insights and

suggested a scaffolding role for MO25. The crystal structure of MO25α (Milburn et al., 2004) revealed an α-helical repeat protein (Fig. 1.14A), that at a superficial topological level resembles other scaffolding proteins such as Pum1, β-catenin and importin-α (Graham et al., 2000; Conti and Kuriyan, 2000; Wang et al., 2001). A common structural feature for this class of scaffolding proteins (not related by sequence), is their distinctive horse-shoe shape with a concave and convex side (Fig. 1.14). Interestingly, these proteins bind their macromolecular partners through their concave surface (Graham et al., 2000; Conti and Kuriyan, 2000; Wang et al., 2001). Milburn et al., were able to crystallise MO25 in the presence of a C-terminal peptide of STRADα previously known to interact with MO25 (Baas et al., 2003), and showed the last three residues (termed the WEF motif) bind to a conserved, hydrophobic pocket present in the MO25 convex surface (Fig. 1.14) (Milburn et al., 2004). Therefore, the structure suggested, the unoccupied and highly conserved concave surface of MO25 (Fig. 1.14B) could harbour binding sites for STRAD and LKB1 (Milburn et al., 2004). Further structural and biochemical analysis identified a residue present in the concave surface of MO25α (Arg240; Fig. 1.14), that could be involved in interacting with LKB1 (Boudeau et al., 2004; Milburn et al., 2004).

1.5.6 LKB1 regulation by post-translational modification

Most protein kinases are phosphorylated in their activation loop, leading to their activation. Alessi and collegues identified Thr212 present in the LKB1 activation loop, as a putative target for transfer of the activatory phosphate (Boudeau et al., 2004). Interestingly, no phosphorylation of Thr212 could be detected and mutation of this residue to an unphosphorylatable residue (alanine) and phospho-mimicking (glutamine) residue had little/no effect to LKB1 activity (Boudeau et al., 2004). Thus, these results supported the notion that LKB1 is activated allosterically by binding to STRAD and MO25 rather than phosphorylation of the activation loop. The molecular mechanisms by which this is achieved has not been described thus far and is one of the main subject of this thesis.

LKB1 can auto-phosphorylate on residues Ser185, Thr336 and Ser402 (Sapkota et al., 2002a; Alessi et al., 2006) and is phosphorylated by other kinases at residues Ser31, Ser307, Ser325, Thr363 and Ser428 (Sapkota et al., 2001, 2002b; Alessi et al., 2006; Xie et al., 2009) (Fig. 1.15). In addition, LKB1 contains a prenylation site, Cys431, that was shown to be modified by a farnesyl group (Collins et al., 2000; Sapkota et al., 2001) (Fig. 1.15). Individual mutations of these sites either to alanine or aspartate/glutamate residues (to mimic phosphorylation of

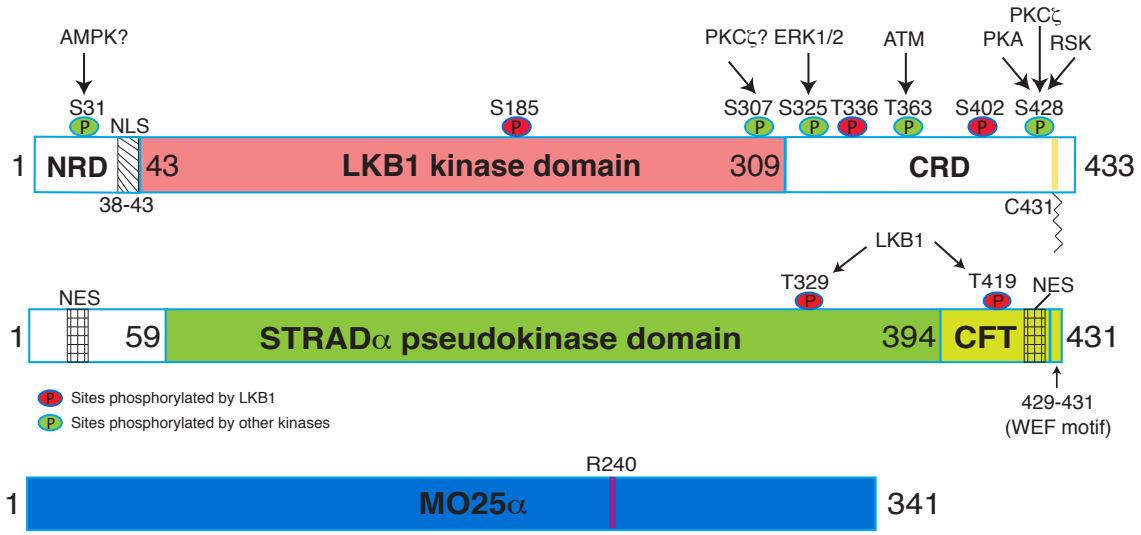

Figure 1.15: LKB1 complex domain architecture and post-translational modifications Domain architecture of the components of the LKB1 complex. Post translational modifications of LKB1 and STRADα are shown (references are provided in section 1.5.6). NRD = N-terminal regulatory region, CRD = C-terminal regulatory region, NLS = Nuclear localisation signal, NES = Nuclear export signal.

Ser/Thr residues respectively) do not significantly affect LKB1 activity. Some phosphorylation sites however, have been shown to respond to specific cellular stresses such as phosphorylation by ATM of Thr363 in response to DNA damage (Sapkota et al., 2002b).

Recently, Zheng et al., and Esteve-Puig et al., reported that ERK MAP kinase could phosphorylate Ser325 (Zheng et al., 2009; Esteve-Puig et al., 2009). The authors show that in melanoma cells expressing oncogenic (V600E) B-Raf, phosphorylation of Ser325 (by ERK) and Ser428 (by p90RSK) resulted in lower activation of AMPK (Zheng et al., 2009; Esteve-Puig et al., 2009). These findings could be the beginning of an interesting avenue of LKB1 signalling—the ultimate aim being explaining how cancer cells continue to grow in energy-deprived conditions that could lead to new cancer treatment therapies

(Martin et al., 2009b).

1.5.7 LKB1 activates the AMP-activated protein kinase

Activation of AMPK requires phosphorylation of Thr172 within the activation segment of the catalytic subunit (Hawley et al., 1996). The identification of the long sought-after upstream kinase that phosphorylates and activates AMPK, came about from elegant work in yeast genetics. In yeast, there are three protein kinases Elm1, Pak1/Sak1, and Tos3 that phosphorylate and activate the yeast AMPK homologue (SNF1) (Hong et al., 2003; Sutherland et al., 2003). It was quickly realised that members of the Ca^{2+}/calmodulin-dependent protein kinase kinase (CaMKK) family and LKB1 kinases could be mammalian orthologues to these yeast kinases (Hong et al., 2003; Sutherland et al., 2003). Before the discovery of STRAD and MO25 as activatory components of the LKB1 complex (Baas et al., 2003; Boudeau et al., 2003a), no appreciable phosphorylation and activation of AMPK by LKB1 was detected due to poor LKB1 activity (Dr G. Sapkota and Dr S. Hawley, unpublished results). Soon after the discovery of the LKB1/STRAD/MO25 complex, AMPK was identified as the first physiological substrate of LKB1 (Hawley et al., 2003; Woods et al., 2003; Shaw et al., 2004). More importantly, LKB1 could phosphorylate the activatory threonine residue (Thr172) present in AMPK

activation loop (Hawley et al., 2003; Woods et al., 2003; Shaw et al., 2004), phosphorylation of which is also observed at low levels of cellular energy, that is accompanied by activation of AMPK (Hawley et al., 1996). These findings were subsequently confirmed in animal studies, whereby in LKB1 conditional mouse knockouts in muscle (Sakamoto et al., 2005) and liver tissues (Shaw et al., 2005), the activity of AMPK was severely reduced, thus demonstrating that LKB1 was the major upstream kinase of AMPK *in vivo* in these tissues (Sakamoto et al., 2005; Shaw et al., 2005).

Two other protein kinases, CaMKKβ (Hawley et al., 2005; Woods et al., 2005) and the transforming growth factor-β-activated kinase (TAK1) (Momcilovic et al., 2006; Xie et al., 2006) have been reported as upstream kinases for AMPK activation. While there is compelling evidence for CaMKKβ as an alternative AMPK activating kinase to LKB1, mainly in response to elevated Ca^{2+} levels, the implication of TAK1 requires further investigation. Interestingly, LKB1 rather than CaMKKβ is thought to be the upstream kinase for AMPK in conditions of energy stress. Because LKB1 is believed to be constitutively active, other means of regulation involving dephosphorylation of Thr172 by protein phosphatase 2C (PP2C) (Sanders et al., 2007) and regulation via glycogen binding to the AMPKβ subunit (McBride

et al., 2009) have been described for AMPK.

1.5.8 LKB1 is a master kinase

Closer examination of the kinome tree, reveals the AMPKα1/2 isoforms are clustered with other related protein kinases within the CAMK group (Fig. 1.2), suggesting these too may be LKB1 substrates. Subsequent work carried out in the Alessi group, showed that

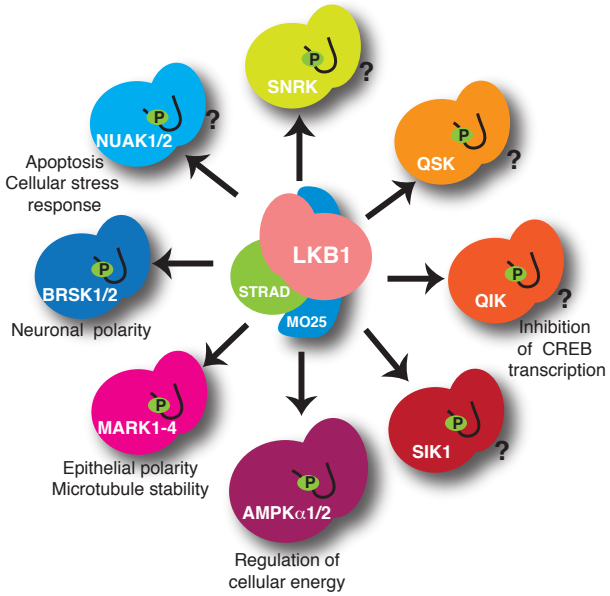

Figure 1.16: LKB1 activates the AMPK family of kinases by phosphorylating their activation loop

the LKB1 complex efficiently phosphorylated 12 of these AMPK-related kinases (Lizcano et al., 2004; Jaleel et al., 2005) (Fig. 1.16), named: BRSK1/2 (brain specific kinase 1/2) isoforms, MARK1-4 (microtubule affinity regulating kinase) isoforms, NUAK1 also referred to as ARK5 (AMPK-related kinase 5), NUAK2, also referred to as SNARK (sucrose-non-fermenting AMP-activated protein kinase related protein kinase), QIK (qin induced kinase), QSK, SIK (salt inducible kinase), SNRK (sucrose non-fermenting related kinase). These findings are suggestive of LKB1 having the role of a master kinase ca-

pable of activating many members of the AMPK-related protein kinase family. Thus, LKB1 can influence a variety of cellular processes (Fig. 1.16) and some of these functions are presented below. For recent reviews the reader is directed to articles by Shackelford and Shaw, 2009 and Jansen et al., 2009.

1.5.9 The LKB1-AMPK axis in regulating cellular energy

The name AMP-activated protein kinase (AMPK) was adopted in 1989 after it was discovered by Grahame Hardie and colleagues as the (same) kinase that phosphorylated acetyl-CoA Carboxylase (ACC) (Munday et al., 1988) and HMG reductase (HMGR) (Carling et al., 1989), both rate limiting enzymes in the fatty acid and cholesterol synthesis respectively. This shed light on earlier reports that the ACC and HMGR phosphorylation events respond to changes in the levels of adenylate nucleotides, first reported by Yeh et al., 1980.

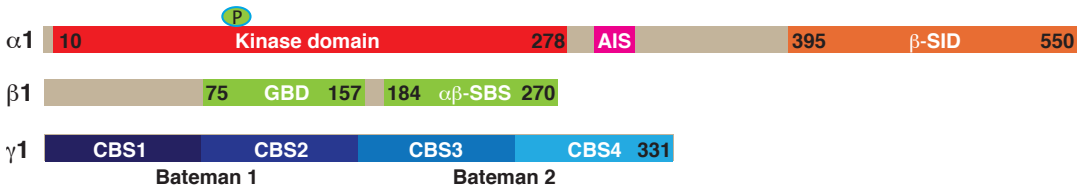

Figure 1.17: AMPK complex domain architecture
Domain architecture of the components of the AMPK complex ($\alpha1/\beta1/\gamma1$). Phosphorylation of residue Thr172 by upstream kinases on the $\alpha1$ subunit is indicated. AIS = Autoinhibitory sequence (residues 312-335), β-SID = β subunit interacting domain, GBD = glycogen binding domain, α/β-SBS = α/β subunit binding sequence, CBS = Cystathione-β-Synthase motifs.

AMPK is a holoenzyme composed of three subunits—a catalytic α (protein kinase) subunit, a β subunit that contains a glycogen binding

domain (GBD) and a third γ subunit, that contains four cystathione-β-synthase (CBS) domains responsible for binding ATP/AMP (Fig. 1.17). Although the domain architecture (Fig. 1.17) is similar across eukaryotes, multiple subunit isoforms with different patterns of tissue distributions exist (reviewed by Hardie, 2007 and Stienberg and Kemp, 2009). Recently, studies by Xiao and collegues (Xiao et al., 2007), Amodeo et al., (Amodeo et al., 2007) and Townley and Shapiro (Townley and Shapiro, 2007), have provided valuable information of how the heterotrimeric $\alpha/\beta/\gamma$ subunits of human, and yeast AMPK core complexes assemble. In addition, crystal structures in complex with AMP and ATP nucleotides have described the molecular basis of AMPK regulation by adenylate nucleotides (Xiao et al., 2007; Amodeo et al., 2007; Townley and Shapiro, 2007). In particular, the AMPK core structure reported by Xiao et al., 2007, in complex with both ATP and AMP revealed that two of the CBS motifs of the γ subunit were able to bind ATP under normal physiological conditions—these could be exchanged with AMP, whereas one of the CBS domains contained an nonexchangeable AMP binding site (Xiao et al., 2007). More recently, the crystal structure of the *S. pombe* kinase domain together with the autoinhibitory sequence (AIS, Fig. 1.17) C-terminal to AMPK was reported by Chen et al., 2009. The AIS (residues 312-

335) binds to both N- and C-lobes of the kinase domain and possibly by constraining the movement of helix αC contributes to an overall inactive conformation Chen et al. (2009).

At present, almost weekly scientific reports continue to implicate AMPK in a variety of functions. To date, there is compelling evidence that AMPK is involved in controlling cellular and tissue metabolism, regulation of glucose uptake, transcription, cell growth and proliferation and recently the establishment and maintenance of cell polarity (Fig. 1.18; reviewed by (Hardie, 2007b; Steinberg and Kemp, 2009; Shackelford and Shaw, 2009)). In addition, AMPK plays important physiological roles at the whole body level by integrating stress responses such as exercise, nutrient and hormonal signals to control food intake and energy expenditure (reviewed by (Hardie and Sakamoto, 2006; Steinberg and Kemp, 2009). Unsurprisingly, AMPK is a key emerging drug target for the treatment of diabetes and other metabolic syndromes (for recent reviews see (Hardie, 2007a) and (Zhang et al., 2009)). Ultimately, the end result of AMPK activation by LKB1 is to switch on catabolic pathways that generate ATP, while switching off biosynthetic pathways and other processes that consume ATP, in response to cellular energy stress (Fig. 1.18). This energy switch is in response to ATP consuming metabolic reactions producing ADP that

is converted to AMP by the enzyme adenylate kinase, contributing to a higher AMP:ATP ratio. It is the AMP:ATP ratio that serves as the main sensor mechanism detected by AMPK regulating the cellular and whole tissue metabolism (Fig. 1.18).

A prominent role of LKB1 is the inhibition of the mammalian target of rapamycin (mTor) kinase via AMPK, leading to inhibition of protein synthesis (Fig. 1.18). Thus, the LKB1-AMPK axis ensures that cell growth and proliferation is coupled to the availability of cellular energy by feeding regulatory input to the mTor kinase. This is done by directly phosphorylating raptor (component of mTor complex 2) (Gwinn et al., 2008), as well as inactivating the tuberous sclerosis complex (TSC) that lies upstream of the mTor pathway (reviewed by (Alessi et al., 2006; Shaw, 2009)).

1.5.10 The role of LKB1 in polarity

Another key role of LKB1 is to control cell polarity (Hezel et al., 2008; Martin and St Johnston, 2003; Baas et al., 2004a), which may be mediated by AMPK (Zheng and Cantley, 2007) as well as some of the AMPK related kinases (Fig. 1.18). The MARK1-4 kinases that are activated by LKB1 (Lizcano et al., 2004), are perhaps the most studied of the AMPK-related kinases (Baas et al., 2004b). Important physiological roles for these kinases were first demonstrated in orthol-

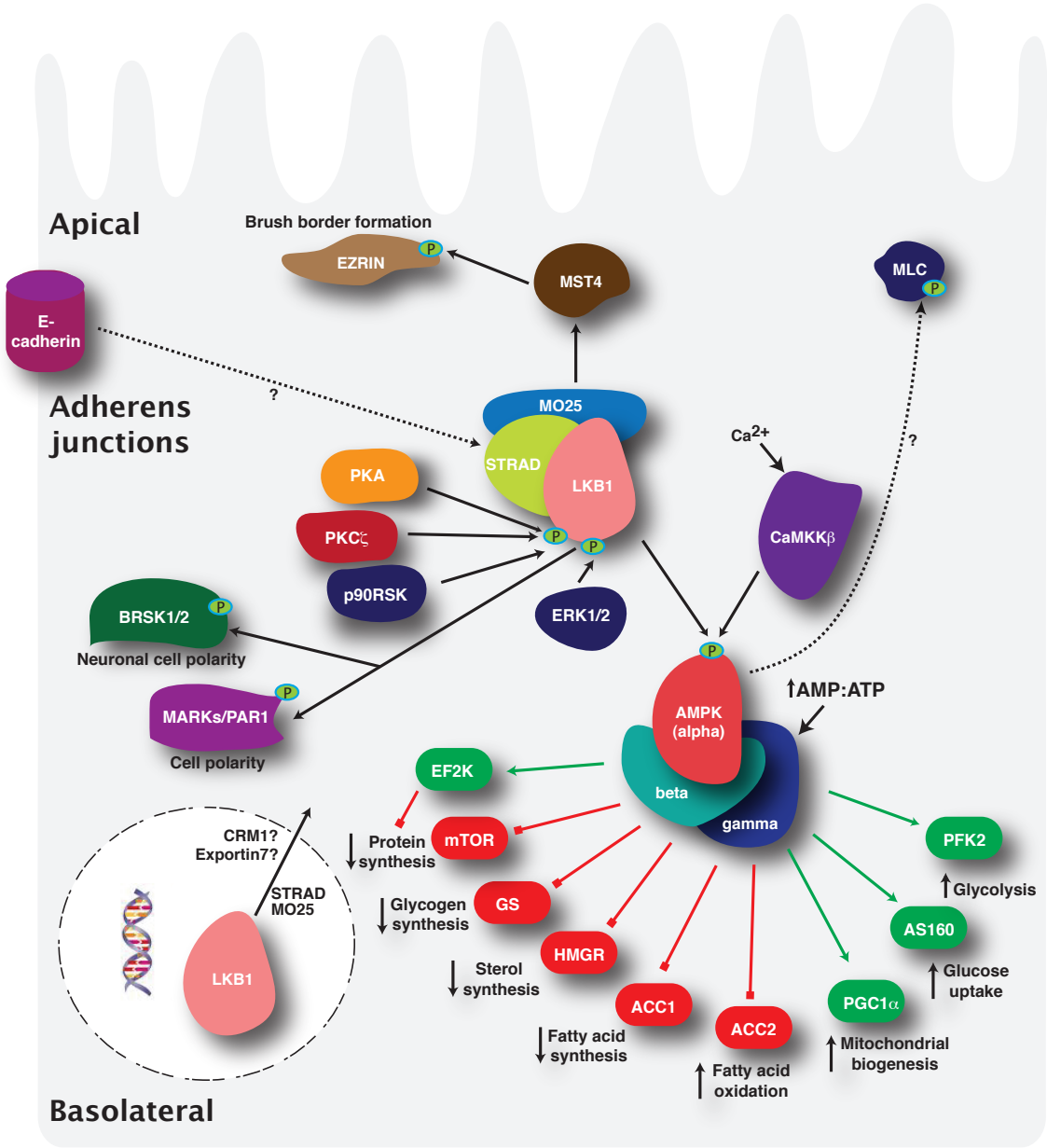

Figure 1.18: LKB1 dependent signalling pathways
LKB1 is re-localised to the cytoplasm by STRAD and MO25. The LKB1 complex phosphorylates and activates AMPK in response to raises in the AMP:ATP ratio. AMPK controls a series of metabolic reactions, (green arrow = target activation, red blunt-headed arrow = target inactivation). A brief description of the effect in the respective metabolic reactions is noted. LKB1 can also phosphorylate and activate the AMPK related kinases (BRSK1/2 and MARK1-4) that control cell polarity. MO25 interacts with MST4 and in an LKB1 dependent manner can regulate Ezrin phosphorylation and brush border formation. An interaction between STRAD and E-catherin has been established and thought to control AMPK phosphorylation in adherens junctions. Other kinases that phosphorylate LKB1 and AMPK are indicated. The figure was adapted and redrawn from Alessi et al., 2006, Hardie, 2007b and Shackelford and Shaw, 2009. References are provided in their respective sections.

ogous genes from yeast, worms and flies. The MARK orthologues of *C. elegans* and *D. melanogaster* are members of the partition-defective kinase family and are called Par-1. The nematode Par-1 orthologue controls the partitioning of the *C. elegans* zygote (Kemphues et al., 1988), whereas the *D. melanogaster* Par-1 regulates cell polarity (Shulman et al., 2000; Martin and St Johnston, 2003). In higher eukaryotes, the MARK2 isoform is reportedly important for maintaining polarity in neuronal (Biernat et al., 2002) and epithelial cells (Mandelkow et al., 2004), as well as the organisation of the microtubule network (Cohen et al., 2004).

More recently, a role for the BRSK1/2 (SAD-B/A) in neuronal cell polarity has been described (Barnes et al., 2007; Shelly et al., 2007). According to these reports, BRSK1/2 control neuronal polarisation and axon guidance via a pathway that is dependent on LKB1 Ser428 phosphorylation by PKA (Barnes et al., 2007; Shelly et al., 2007). It is important to note that this is unlikely to depend on LKB1 direct activation of the BRSK isoforms, since LKB1 Ser428 phosphorylation does not alter LKB1 kinase activity (Fogarty and Hardie, 2009). It is possible the phosphorylation of this site alters the sub-cellular localisation and/or association of LKB1 with other regulatory components.

1.6 Project aims

At the start of this project (September 2005), little was known of how the tumour suppressor kinase LKB1, interacted with its regulatory partners, STRAD and MO25. Neither was the mechanism of LKB1 activation clear—LKB1 unlike other kinases requires no phosphorylation. Thus, the central aim of this work was to express, purify, crystallise and solve the structure of the LKB1/STRAD/MO25 heterotrimeric complex.

Through a structural and biochemical approach, the results of which are covered by Chapters III, IV and V of this thesis, I have sought to answer the following questions:

- How do STRAD/MO25 bind LKB1?
- What is the mechanism by which a pseudokinase (STRAD) activates a kinase (LKB1)?
- What is the mechanism by which the scaffolding protein MO25 activates LKB1?
- How do oncogenic mutations affect LKB1 activity, and/or complex formation?
- Why/how did pseudokinases evolve?

Chapter II

Materials and Methods

2 Materials and methods

2.1 Reagents

Listed are standard chemicals and enzymes used for protein cloning, expression, purification, analysis, crystallisation and enzyme activity measurments.

2.1.1 Cloning

Solid agarose was purchased from BDH (VWR, UK), TAE-buffer was kindly prepared by the media kitchen (University of Dundee). HiFi Taq polymerase was purchased from Roche Diagnostics (Lewes, UK). DNA 1kb ladder was supplied from Promega. QIAGEN Mini-Prep Plasmid and Gel-extraction kits were obtained from Qiagen Ltd. (Crawley, UK).

2.1.2 Gene expression, protein production and purification

Bovine serum albumin (BSA), DNase I, bicine, trizma base, *N*-(2-hydroxyethyl)-piperazine-*N*'-2-ethane-sulfonic acid (HEPES), sodium chloride (NaCl), sucrose and glycerol were purchased from Sigma-Aldrich Co. Ltd. (Dorset, UK). Complete protease inhibitors cocktail tablets were purchased from Roche Molecular Biochemicals (Lewes, UK) or alternatively a protease inhibitor mix was kindly made by

Helge Dorfmüller (section 2.3.2) and contained benzamidine, phenylmethanesulfonyl fluoride (PMSF) (Sigma) and Leupeptin (Peptide Institute Inc.). Ethylenediamine-tetraacetic acid (EDTA), ethyleneglycol-tetraacetic acid (EGTA) and hydrochloric acid (HCl) were purchased from BDH Chemicals Ltd. Dioxin-free Isopropyl thio-β-D-galactoside (IPTG), dithiothreitol (DTT) and 2-mercaptoethanol were obtained from Melford Laboratories (Ipswich, UK). Tris(2-carboxyethyl)phosphine hydrochloride (TCEP) was from Calbiochem-Merck Chemicals Ltd, (Nottingham, UK). Bradford reagent was from Pierce (Chester, UK). Glutathione sepharose 4B (GSH sepharose) was from GE Healthcare (Buckinghamshire, UK) and Ni-NTA agarose was from Qiagen Ltd. (Crawley, UK). PreScission and Tobacco Etch Virus (TEV) proteases were kindly produced as recombinant proteins with an N-terminal GST and 6-His tag respectively by Sharon Shepherd (University of Dundee).

2.1.3 Protein analysis

40% (w/v) 29 : 1 acrylamide was from Flowgen Bioscience (Nottingham, UK). *N,N,N',N'*-tetramethylethylenediamine (TEMED), β-mercaptoethanol (BME) and sodium dodecyl sulphate (SDS) were bought from BDH (Poole, UK). Ammonium persulphate (APS) was from Sigma-Aldrich (UK). NuPAGE sample reducing agent and Nu-

PAGE LDS sample buffer (5×) were purchased from Invitrogen or made up as 6× concentrated stocks (section 2.3.6). PageRuler unstained protein ladder was from Fermentas (Paisley, UK). Precision protein standards (pre-stained, broad range) were purchased from Bio-Rad (Herts, UK). SuperSignal(R)West Pico Chemiluminescent Substrate (ECL) was from Thermo Fisher and X-ray (medical) film from Konika/Minolta.

2.1.4 Protein crystallisation

Crystallistion screens Crystal Screen I & II, Index, MembFac and Peg Ion were purhcased from Hampton Research (California, USA), Wizard I & II were from Emerald BioSystems (Washington, USA), Protein Complex was from Sigma-Aldrich Co. Ltd. (Dorset, UK) and ProPlex was from Molecular Dimensions Ltd. (Suffolk, UK).

2.1.5 Phosphonucleotide binding assays

Adenosine-5'-triphosphate (ATP) and adenosine-5'-diphosphate (ADP) were bought from Melford Laboratories (Ipswich, UK), and 2',3'-O-(2,4,6-trinitrophenyl) adenosine 5'-triphosphate (TNP-ATP) was from Invitrogen Ltd. (Paisley, UK).

2.1.6 Protein lysine methylation

Dimethylamine-borane complex (DMB; Fluka product 15584) and a formaldehyde solution (37% stock; Fluka product 33220) were purchased from Sigma-Aldrich (Dorset, UK).

2.2 Equipment

Two in-house diffractometers were used throughout this thesis to test crystals. These were Rigaku Micromax 007 rotating anode generator equipped with an R-AXIS IV++ image plate detector and a Rigaku XStream nitrogen cryostream. 24-well hanging drop VDX Plates and 18 mm siliconised circle cover slips, goniometer heads, additional X-ray equipment and tools were from Hampton Research (CA, USA). Sitting drop MRC 96 well plates and Crystal Clear sealing tape were from Jena Bioscience GmbH (Germany). The ÄKTA purifier/ÄKTA prime purification systems and size exclusion chromatography columns were from GE Healthcare (Buckinghamshire, UK). Centrifuge tubes, rotors and centrifuges were from Beckmann (California, USA). Fluorescence measurements of the ATP analogue 2',3'-O-2,4,6-trinitrophenyl-ATP (TNP-ATP) were carried out with a Varian Cary Eclipse fluorescence spectrophotometer equipped with a thermostatic cuvette holder equilibrated at 25 °C (Varian Inc. California, USA). Disposable (Kartell, 4-

sided) cuvettes were ordered from VWR (Jencons, West Sussex, UK). 20 ml and 2 ml spin concentrators with a 10000 molecular weight (MW) cut-off were bought from Viva Science (Hannover, Germany). Disposable 10 ml and 25 ml EconoPac Chromatography Columns were from BioRad (Herts, UK) and disposable desalting columns (product nr. 17-0851-01) were from GE Healthcare. Syringe filter units (GF-prefilter, 0.2 and 0.45 μm pore size) and buffer filtration devices were from Sartorius (Goettingen, Germany). Slide-A-Lyzer dialysis cassettes and Snake Skin dialysis tubing (MW cut-off 10000-50000 Da) were purchased from Pierce (Chester, UK). Transfer for western blotting was performed in a wet-system using the X-Cell SureLock MiniCell electrophoresis system and X-Cell II Blot Module were from Invitrogen (Groningen, The Netherlands). X-ray films were developed using an automatic film processor Konica Corporation (Japan). Cell culture dishes (10 cm radius), six well plates and cell scrapers were from Costar (Cambridge, MA, U.S.A.). SPR measurements were carried out using a BIAcore T100 instrument (GE Healthcare, Buckinghamshire, UK).

2.3 General solutions and buffers

2.3.1 Bacterial media

Luria Bertani broth (LB) media and LB-plates were kindly supplied by the media kitchen (University of Dundee). The media contain 10.0 g bacto-tryptone, 5.0 g bacto-yeast extract, 10.0 g NaCl, 950 ml ddH_2O and were adjusted to pH 7.0 with NaOH. The media was adjusted to 1 l using ddH_2O after autoclaving for 20 minutes at 2 bar. For media containing the antibiotic Ampicillin (Amp) a stock was added to a final concentration of 50 μg/ml (LB + Amp). LB + Amp-plates contained 100 μg/ml Amp (LB + 2× Amp) and an additional 15 g/l bacto-agar.

2.3.2 Protease inhibitor mix

A 20 mM stock of PMSF was dissolved in MeOH. Benzamidine (200 mM) and leupeptin (1 mM) were dissolved in ddH_2O. The following protocol is for making 50 ml of 100× concentrated stocks divided in 100 aliquots. Stock solutions were mixed in a 50 ml Falcon tube as follows: 1 ml of PMSF, 10 ml benzamidine, 238 μl leupeptin plus 13.4 ml of MeOH. 250 μl of water were pipetted into an Eppendorf tube, to which 250 μl of protease inhibitors were added, thus giving a protease inhibitor with final concentrations: 0.1 muM PMSF, 5 mu leupeptin

and 1 mM benzamidine. The aliquots were snap frozen in liquid N_2 and frozen until further use at -80 ^oC.

2.3.3 Agarose gel electrophoresis buffer and DNA sample buffer

TAE (Tris-acetate-EDTA) buffer was supplied as 10× concentrated stock by the media kitchen (University of Dundee) and contained the following chemicals dissolved in 1 l of ddH_2O water: 48.4 g tris base, 11.4 ml of glacial acetic acid, 100 ml of 0.1 M EDTA (pH 8.0). To obtain 10 ml of 6× concentrated DNA sample buffer, 25 g bromophenol blue, 25 g of xylene cyanol FF and 4 g glycerol were dissolved in ddH_2O.

2.3.4 SDS-PAGE stock solutions

SDS-polyacrylamide fels for electrophoresis were made using the following stock solutions: 1.5 M Tris-HCl (pH 8.6), 2 M Tris-HCl (pH 6.8), 10% (w/v) SDS and 40% acrylamide solution containing bis-acrylamide at 29:1 from Flowgen Bioscience and TEMED. A 10% (w/v) APS solution was made fresh from solid APS on the day of usage.

2.3.5 Electrophoresis buffer

A 10× stock solution of tris-glycine SDS-polyacrylamide gel running buffer was made by dissolving 30.3 g of tris-base, 144 g glycine and 10 g of SDS in a total volume of 1 l ddH_20.

2.3.6 SDS sample buffer

SDS sample buffer (5× concentrated) contained 250 mM Tris-HCl pH 6.8, 10% (w/v) SDS, 50% (v/v) glycerol, 0.025% (w/v) bromophenol blue, and 5% (v/v) 2-mercaptoethanol.

2.3.7 SDS-PAGE visualisation buffer

Proteins analysed by SDS-PAGE were stained using a Coomassie staining solution prepared by dissolving 2.5 g of Coomassie blue in 400 ml of ddH_2O, 100 ml of glacial acetic acid and 500 ml of MeOH and mixed by stirring overnight. For destaining an identical solution without Coomassie blue dye was used.

2.3.8 Transfer and wash buffer for western blotting

Tris-glycine transfer buffer (containing 20% methanol) was used to transfer the proteins from SDS-PAGE gels onto a nitrocellulose membrane. A 25× stock was made of 18.2 g tris and 90 g of glycine dissolved in 500 ml of ddH_20. Stripping buffer (1 liter) was prepared

using 15 g glycine, 1 g SDS and 10 ml Tween-20 (final concentration 1.0%) and was adjusted using concentrated HCl to pH 2.2. TBS-T wash buffer buffer was Tris-HCl pH 7.5, 0.15 M NaCl, and 2.5% (v/v) Tween-20.

Table 2.1: Solutions for pouring five separation gels.

	Acrylamide concentration				
Stock solution	6%	8%	10%	12%	15%
40% acrylamide	5.3 ml	7.0 ml	8.8 ml	10.5 ml	13.1ml
1.5 M Tris-HCl, pH 8.6	8.8 ml	8.8 ml	8.8 ml	8.8 ml	8.8 ml
ddH_20	20.5 ml	18.8 ml	17.0 ml	15.3 ml	12.6 ml
10% SDS	350 μl	350 μl	350 μl	350 μl	350 μl
TEMED	31 μl	31 μl	31 μl	31 μl	31 μl
10% APS	118 μl	118 μl	118 μl	118 μl	118 μl
Total volume	35 ml	35 ml	35 ml	35 ml	35 ml

Table 2.2: Solutions for pouring five stacking gels.

Stock Solution	Volume
40% acrylamide	1419 μl
2 M Tris-HCl, pH 6.8	930 μl
ddH_20	12 ml
10% SDS	150 μl
TEMED	15 μl
10% APS	128 μl
Total volume	15 ml

2.4 Pouring of gels for SDS-PAGE

SDS-PAGE gels were manually poured in 10% and 12% acrylamide concentrations as required. Glass plates were assembled with rubber gaskets and clamps according to the manufacturer's protocol. Gels were poured in two steps: First the solution for the separation gels was prepared according to Table 2.1. The reagents were mixed gently but thoroughly and poured into glass plates without delay. This was then

covered with a thin layer of isopropanol to obtain a smooth surface and left to polymerise for 15 minutes at room temperature (RT). The isopropanol was carefully removed and the surface of the separating gel was washed with water. For the second step, ingredients of the stacking gel (Table 2.2) were mixed together, and after gentle mixing this was poured on the top of the separating gel. To obtain the wells for sample loading a 12 well comb was immediately inserted and the gels were left for a further 15 minutes to polymerise. Gels were stored in SDS-running buffer (see section 2.3.5) at 4 ^{o}C.

2.5 Lysis and purification buffers

2.5.1 Buffers for GST affinity chromatography and further purification of proteins produced in *Escherichia coli (E. coli)*

The following buffers were prepared (and kept at 4 ^{o}C) for the purification of wild type and mutant forms of GST tagged STRADα and MO25α.

Buffer A (lysis buffer): 50 mM Tris-HCl pH 7.8, 150 mM NaCl, 270 mM Sucrose, 20 mM imidazole, 1 mM benzamidine, 1.0 mM EGTA, 1.0 mM EDTA, 0.1% (v/v) β-mercaptoethanol, supplemented with 0.1 mM PMSF, 0.5 mg/ml lysozyme and 0.3 mg/ml DNAse-I.

Buffer B (low salt purification buffer): 50 mM Tris-HCl pH 7.8, 150 mM NaCl, 270 mM Sucrose, 1 mM benzamidine, 1.0 mM EGTA,

1.0 mM EDTA, 0.1% (v/v) β-mercaptoethanol.

Buffer C (high salt purification buffer): 50 mM Tris-HCl pH 7.8, 500 mM NaCl, 270 mM Sucrose, 1 mM benzamidine, 1.0 mM EGTA, 1.0 mM EDTA, 0.1% (v/v) β-mercaptoethanol

Buffer D (ion exchange buffer): 50 mM Tris-HCl pH 7.8, 270 mM Sucrose, 1 mM benzamidine and filtered using a cellulose filter with a 0.2 μm pore size.

Buffer E (ion exchange buffer): 50 mM Tris-HCl pH 7.8, 500 mM NaCl, 270 mM Sucrose, 1 mM benzamidine and filtered using a cellulose filter with a 0.2 μm pore size.

Buffer F (gel filtration buffer): 25 mM Tris-HCl pH 7.8, 150 mM NaCl 1 mM DTT and filtered using a cellulose filter with a 0.2 μm pore size.

2.5.2 Buffers for Ni^{2+} metal affinity chromatography and further purification of proteins produced in *E. coli*

The following buffers were prepared (and kept at 4 ^{o}C) for the purification of the STRADα/MO25α complex.

Buffer A (lysis buffer): 50 mM Tris-HCl (pH 7.8), 50 mM NaCl, 5% glycerol, 20 mM imidazole, 1 mM benzamidine, 0.2 mM EGTA, 0.2 mM EDTA 0.075% (v/v) β-mercaptoethanol, supplemented with 0.1 mM PMSF, 0.5 mg/ml lysozyme and 0.3 mg/ml DNAse-I.

Buffer B (purification buffer): Buffer A without supplements.

Buffer C (crystallisation buffer): 25 mM Tris-HCl pH 7.8, 1 mM DTT and filtered using a cellulose filter with a 0.2 μm pore size.

2.5.3 Buffers for Ni^{2+} metal affinity chromatography and further purification of proteins produced in *Spodoptera frugiperda* 21 (Sf21) cells

The following buffers were prepared (and kept at 4 ^{o}C) for the purification of the LKB1/STRADα/MO25α complex.

Buffer A (MBS cell wash buffer) 20 mM Mes/NaOH pH 6.3, 140 mM NaCl, 40 mM KCl.

Buffer B (lysis buffer) 50 mM Tris-HCl pH 7.8, 150 mM NaCl, 5% glycerol, 0.2 mM EDTA, 0.2 mM EGTA, 1 mM benzamidine, 0.1 mM PMSF, 5 μM leupeptin, 20 mM imidazole and 0.075% (v/v) β-mercaptoethanol.

Buffer C (low salt purification buffer) 50 mM Tris-HCl pH 7.8, 150 mM NaCl, 5% glycerol, 0.2 mM EDTA, 0.2 mM EGTA, 1 mM benzamidine, 20 mM imidazole and 0.075% (v/v) β-mercaptoethanol.

Buffer D (high salt purification buffer) 50 mM Tris-HCl pH 7.8, 500 mM NaCl, 5% glycerol, 0.2 mM EDTA, 0.2 mM EGTA, 1 mM benzamidine, 20 mM imidazole and 0.075% (v/v) β-mercaptoethanol.

Buffer E (loading buffer): 50 mM Tris-HCl pH 7.8, 5% glycerol, 0.2 mM EDTA, 0.2 mM EGTA, 1 mM benzamidine and 1 mM DTT.

Buffer F (ion exchange buffer): 50 mM Tris-HCl pH 7.8, 5% glycerol, 0.2 mM EDTA, 0.2 mM EGTA, 1 mM benzamidine, 1 mM DTT and filtered using a cellulose filter with a 0.2 μm pore size.

Buffer G (ion exchange buffer): 50 mM Tris-HCl pH 7.8, 500 mM NaCl, 5% glycerol, 0.2 mM EDTA, 0.2 mM EGTA, 1 mM benzamidine and 1 mM DTT and filtered using a cellulose filter with a 0.2 μm pore size.

Buffer H (gel filtration buffer): 25 mM Tris-HCl pH 7.8, 350 mM NaCl, 2 mM TCEP and filtered using a cellulose filter with a 0.2 μm pore size.

2.5.4 Buffers for GST affinity chromatography of proteins produced in HEK293 cells

The following buffers were prepared (and kept at 4 ^{o}C) for the purification of GST-LKB1/Flag-STRADα/Myc-MO25α and GST-STRADα/Myc-MO25α complexes.

Buffer A (lysis buffer): 50 mM Tris-HCl pH 7.5, 1 mM EGTA, 1 mM EDTA, 1% (w/v) Nonidet P-40 (substitute), 1 mM sodium orthovanadate, 50 mM sodium fluoride, 5 mM sodium pyrophosphate, 0.27 M sucrose, 1 mM DTT, 1 mM benzamidine and 0.1 mM PMSF.

Buffer B (wash buffer): 50 mM Tris-HCl pH 7.5, 150 mM NaCl, 1 mM EGTA/EDTA and 1mM DTT.

2.6 General cell culture and DNA transformation

2.6.1 Culturing of Sf9 and Sf21 cells

Sf9 and Sf21 cells (Invitrogen) were cultured in Sf-900 II media supplemented with 1 mM L-glutamine and 100 μ/ml antibiotic/antimycotic solution (Invitrogen). Stocks were grown in suspension using 2 l Erlenmeyer flasks (VWR (Corning), UK) and their growth was monitored every 36-48 h to ensure cultures did not exceed confluence levels of 6-7 $\times$ 10^6 cells/ml. When confluent, cells were diluted (on average every 3 days) in fresh media to a density of 1.5-2.0 $\times$ 10^6 cells/ml.

2.6.2 Bacterial strains

E. coli strains used in this thesis were DH5α (for cloning) and BL21(DE3)pLysS (for recombinant protein expression). Stocks were obtained from Novagen Promega (Southampton, UK) and Novagen Promega (Darmstadt, Germany) respectively. DH10Bac^{TM} competent cells were used for MultiBac virus recombination and obtained from Invitrogen Ltd. (Paisley, UK).

2.6.3 Preparation of competent *E. coli* cells

To grow a new batch of chemically competent *E. coli* cells (DH5α or BL21(DE3)pLysS), frozen commercial stocks were streaked onto an LB plate and incubated overnight at 37 °C. A single colony from this

plate was inoculated in 5 ml of LB media in a 50 ml Falcon tube overnight in a 37 °C shaking incubator (220 rpm). This culture was transferred into 200 ml of LB-medium and grown until OD_{600} = 0.6-0.8 was reached. Cells were then harvested in a sterile and pre-cooled centrifuge bottle and centrifuged at 3400 *g* for 15 min at 4 °C. The supernatant was removed and the cells were washed 4 times in ice cold and sterile filtered 0.1 M $CaCl_2$. The cell pellet was re-suspended in 12 ml of sterile filtered 0.1 M $CaCl_2$ and 7 ml of autoclaved glycerol. The re-suspended cells were transferred in 250 μl aliquots into sterile microfuge tubes, snap frozen in liquid nitrogen and stored at −80 °C.

2.6.4 DNA transformation into competent *E. coli* cells

This protocol was used for plasmid DNA transformation into competent *E. coli* strains DH5α and BL21(DE3)pLysS (see section 2.6.3). Competent cells were thawed on ice and aliquoted (30-50 μl) into sterile 1.5 ml Eppendorf tubes. To these, approximately 100-200 ng of plasmid DNA (around 1 μl of typical miniprep plasmid DNA, general concentration between 100-300 ng/μl) were added. Cells were incubated on ice for a further 15 minutes prior to heat-shocking at 42 ^{o}C for 60-90 seconds in a water bath. The cells were recovered on ice for an additional 5 minutes and plated onto LB + Ampicillin agar plates (see section **??**). The plates were incubated upside down overnight at

37 ^{o}C to allow for colony growth.f

For transformation of DH10Bac^{TM} cells, 20 μl of cells were transferred into sterile 1.5 ml Eppendorf tubes, mixed with 2 μl of miniprep plasmid DNA as above and incubated on ice for 15 min. Cells were then heat-shocked for 45 s at 42 ^{o}C and transferred briefly on ice. 1 ml of SOCII media was added and the cells were transferred to a 14 ml round-bottom (loose-cap) Falcon tube, and incubated for 4 h at 37 ^{o}C to allow recovery of cells. 50 μl of recovered cells and serial dilutions with SOCII media (1:10, 1:100 and 1:250) were then plated in LB-agar plates supplemented with 50 μg/ml kanamycin, 10 μg/ml tetracycline, 7 μg/ml gentamycin, 40 μg/ml IPTG, and 200 μg/ml X-gal. Plates were wrapped in tin foil and incubated at 37 ^{o}C for 48 h and a further 48 h at 4 ^{o}C to allow colour formation, thus aiding blue/white colony selection (section 2.6.6).

2.6.5 Glycerol stocks of bacterial expression cells

A single colony of transformed BL21(DE3)pLysS expression bacterial cells was inoculated into 5 ml of LB + Amp medium and grown overnight at 220 rpm at 37 °C. Overnight cultures were stored as 50% glycerol stocks at −80 °C.

2.6.6 Isolation of recombinant bacmid DNA

LB media was supplemented with 50 μg/ml kanamycin, 10 μg/ml tetracycline and 7 μg/ml gentamycin and transferred into 4 ml aliquots to round-bottom (loose-cap) Falcon tubes. Using a sterile loop, three (definite) white colonies were individually picked and transferred into each of the LB aliquots. Overnight cultures were grown at 37 ^{o}C in a shaking (220 rpm) incubator and centrifuged for 10 min at 3500 *g*. Supernatants were gently discarded and the pellets resuspended in 250 μl of Qiagen (resolubilisation) Buffer P1 (15 mM Tris-HCl, pH 8.0, 10 mM EDTA, 100 μg/ml RNase A), transferred to sterile Eppendorf tubes and 250 μl of Qiagen (lysis) Buffer P2 (0.2 M NaOH, 1% SDS) was added. Tubes were gently inverted 5-6 times and left on ice for 4 min. At room temperature (RT), 350 μl of Qiagen (neutralisation) Buffer P3 (3 M potassium acetate, pH 5.5) was added, the tubes were inverted gently as above and centrifuged at 13000 rpm for 10 min at 20 ^{o}C. The supernatants were transferred to sterile Eppendorfs and 400 μl of (lower phase) phenol:chloroform was added. Tubes were inverted gently for 2 min and centrifuged again at 13000 rpm for 3 min. The upper phase supernatant (450–500 μl) was then transferred to sterile Eppendorfs and the remaining material was disposed in an appropriate phenol waste bottle. Finally 1 ml of absolute ethanol (HPLC grade)

was added and the tubes were stored at -20 ^{o}C overnight.

On the second day, the precipitated DNA was pelleted by centrifugation at 4 ^{o}C for 10 min at 13000 rpm. The supernatant was decanted and the pellet was washed twice by adding 1 ml of 70% ethanol and centrifugation for 2 min at 13000 rpm at 4 ^{o}C and removal of as much as possible supernatant on the second step. The pellet was air-dryed for 0.5–2 h at RT, resolubilised in 40 μl of sterile ddH_2O and stored at -20 ^{o}C.

2.7 Molecular cloning (completed by Dr Maria Deak)

2.7.1 General molecular biology and vectors

Dr Maria Deak performed the molecular cloning and mutagenesis for all the constructs used in this thesis. The TOPO technology (Invitrogen) was used for general subcloning procedures and the QuikChange method (Stratagene) was used for site directed mutagenesis. The sequences of all constructs were verified by the DNA sequencing service (School of Life Science, University of Dundee). Bacterial expression monocistronic vectors used in this thesis were pGEX6 (Pharmacia Amersham) with a PreScission cleavage site after the GST affinity tag, pOPT (no affinity tag) and pOPTH (6-His affinity tag). The pOPCH (6-His affinity tag) polycistronic vector (Tan, 2001) was

used for co-expression of STRADα/MO25α, and together with the pOPT series were kindly provided by Dr Roger Williams and Dr Olga Perisic, University of Cambridge, UK. The pFBDM vectors used for the MultiBac technology (Berger et al., 2004) and co-expression of LKB1/STRADα/MO25α were kindly provided by Dr Imre Berger and Prof Timothy J. Richmond, ETH Zürich, Switzerland.

2.7.2 Cloning of STRADα

STRADα (residues 54-431) was cloned as a GST (N-terminally) fused gene in a pGEX vector containing an engineered PreScission protease site between GST and STRADα. Alternatively, STRADα and STRADα mutants (residues 58-431) were cloned in a pOPH (Tan, 2001) vector fused to an N-terminal 6-His tag followed by a TEV protease recognition site with sequence MAHHHHHHMENLYFQG.

2.7.3 Cloning of STRADα/MO25α

A bi-cistronic expression system was used to co-express and purify the STRADα/MO25α complex in *E. coli*. The cloning procedure was followed as described by Tan (2001). Both STRADα and MO25α genes were subcloned as separate cassettes from the pOPT single vectors into a pOPCH polycistronic vector. Full length MO25α (residues 1-341) was subcloned from a pOPT (no tag) vector as an *Nde*I/*Bam*H1

insert. STRADα (residues 59-431) with an N-terminal 6-His tag followed by a TEV protease site (sequence MAHHHHHHMENLYFQG) was subcloned from a pOPTH vector as a *Bsp*E1/*Mlu*1 insert.

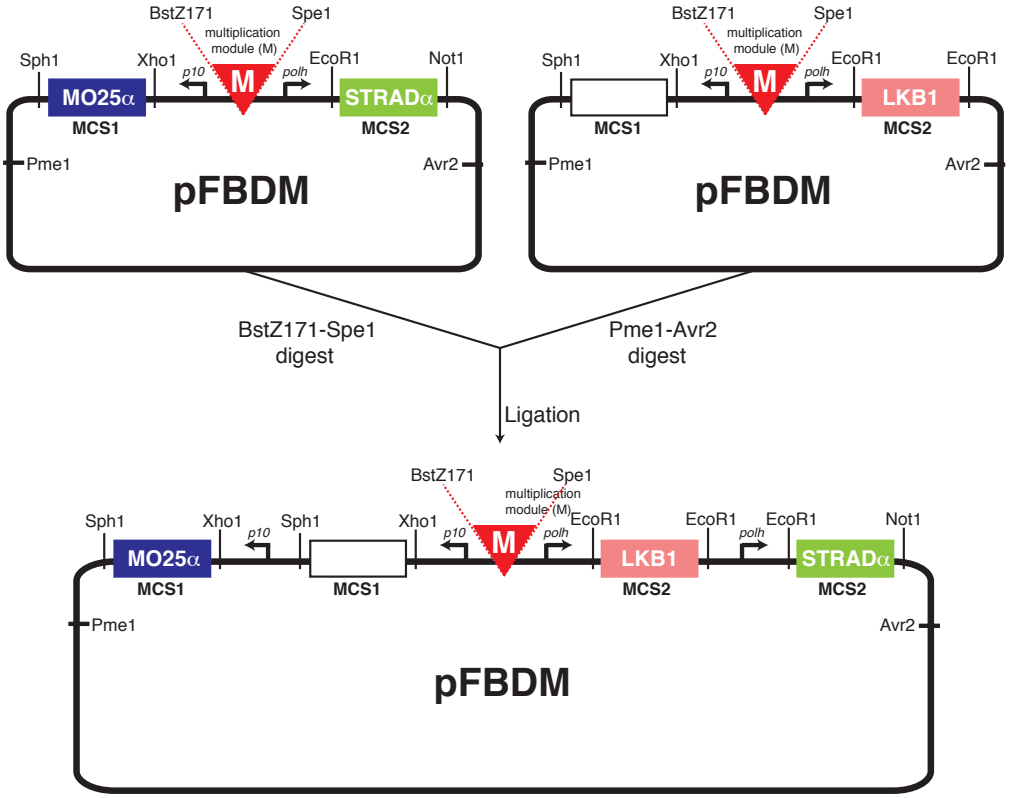

Figure 2.1: Strategy for cloning LKB1/STRADα/MO25α in a polycistronic vector
A) STRADα and MO25α were subcloned in separate multiple cloning sites (MCS) in a pFBDM vector (Berger et al., 2004) using the indicated restriction enzymes. The vector was subsequently digested using BstZ171/Spe1 enzymes and "opening" the multiplication module (M).
B) Similarly LKB1 was subcloned in separate vector and both MCS1 and MCS2 (containing LKB1) were digested using Pme1/Avr2 enzymes.
C) The digested LKB1 insert was ligated in the already "opened" multiplication module of the pFBDM vector from (A), thus generating a final vector containing all three genes with their individual promoters and an empty MCS.

2.7.4 Cloning of LKB1/STRADα/MO25α

The cloning procedure as described previously by Berger et al. (2004) was followed. MO25α (residues 1-341) and STRADα (residues 59-431) clones were inserted into the multiple cloning site (MCS) 1 and MSC2

of a pFBDM$^{STRAD\alpha/MO25\alpha}$ vector respectively, using EcoR1/Not1 (STRADα) and Xho1/Sph1 (MO25α) restriction sites. LKB1 (residues 43-346) preceded by an N-terminal 6-His tag and a TEV protease site (sequence MAHHHHHHENLYFQG) was inserted separately into MSC2 of a different pFBDM^{LKB1} vector using EcoRI/EcoRI sites. Both MSC1 and MSC2 (containg the LKB1 insert) were then cut using Pme1/Avr2 restriction enzymes and ligated into the BstZ171/Spe1 digested dual (STRADα/MO25α containing) pFBDM$^{STRAD\alpha/MO25\alpha}$ vector, thus generating a hybrid pFBDM vector containing all three genes. A diagram sumarising this section is provided in Fig. 2.1.

2.8 Production of recombinant proteins and purification

2.8.1 Expression conditions of GST-STRADα and GST-MO25α

Wild type and mutant forms of STRADα (residues 54-431) and MO25α (residues 1-341) were expressed individually as GST fusion proteins in *E. coli*. Cells were grown in LB medium (section 2.3.1) to $A_{600} = 0.7$ at 37 ^{o}C, and protein expression was induced by the addition of 250 μM IPTG and incubated for a further 16 h at 26 ^{o}C.

2.8.2 Cell lysis and purification of GST-STRADα and GST-MO25α

Cells were harvested by centrifugation for 30 min at 3500 g and re-suspended in ice-cold Buffer A (section 2.5.1). Cells were lysed by

sonication (10 × 10 s pulses) and lysates were clarified (by centrifugation at 26000 *g*) and incubated for 1 h on a rotating platform with glutathione-Sepharose (0.5 ml/l of culture), pre-equilibrated in Buffer B (section 2.5.1). Beads were then washed with 10 column volumes (CV) of Buffer B and a further 50 column volumes of high salt Buffer C containing 500 mM NaCl (section 2.5.1). Beads were re-equilibrated in 10 CV of Buffer B and the proteins were eluted by incubating with PreScission protease for 16 h. For nucleotide binding (section 2.12) and SPR experiments (section 2.13), protein eluates were dialysed for 16 h against 5 l of assay buffer containing 50 mM Tris-HCl pH 7.8, 50 mM NaCl, 270 mM sucrose and 1 mM DTT, concentrated to 7 mg/ml, divided into aliquots and stored at −80 ^{o}C. For crystallography studies, STRADα preperations were further purified by anion exchange and size exclusion chromatography. A 5 ml HiTrapQ column was used for anion exchange and STRADα (diluted 1:3 with no salt Buffer D, section 2.5.1), was allowed to bind to the column at a flow rate of 5 ml/min and eluted using a salt gradient (0-500 mM NaCl, adjusted with Buffer E, section 2.5.1) over 30 column volumes. The STRADα peak was pooled, concentrated to 2-3 ml and loaded onto a Superdex S75 26/60 gel filtration column (equilibrated in Buffer F, section 2.5.1). The purity of the eluting peak from each purifi-

cation step was analysed by SDS-PAGE and (prior to crystallisaton) MALDI-TOF analysis. A gel showing a typical STRADα preparation for crystallisation is provided in chapter III (Fig. 3.4).

2.8.3 Co-expression conditions of His-STRADα/MO25α

N-terminally 6-His-tagged STRADα was co-expressed with untagged full length MO25α in *E. coli* BL21(DE3)pLysS cells. Cells were grown in LB medium (section 2.3.1) to A_{600} = 0.7 at 37 ^{o}C, before protein expression was induced by the addition of 250 μM IPTG and incubated for a further 16 h at 26 ^{o}C.

2.8.4 Cell lysis and purification of His-STRADα/MO25α

Cells were harvested by centrifugation for 30 min at 3500 *g* and re-suspended in ice cold lysis Buffer A (section 2.5.2. Cells were lysed using a French Press cell disrupter (18000 psi) and the lysate was cleared by centrifugation at 26000 *g* for 30 min. The supernatant was then passed through a pre-filter and a 0.2 μm filter before loading onto a 5 ml HiTrap IMAC HP column (GE Healthcare) previously charged with Ni^{2+}. The column was then washed with 10 volumes of wash Buffer B (section 2.5.2), and the STRADα/MO25α complex was eluted by applying a gradient of 20-300 mM imidazole in wash Buffer B. The eluted sample was analysed by SDS-PAGE, concentrated to 3

ml and loaded onto a Superdex 75 26/60 gel filtration column, pre-equilibrated in crystallisation Buffer C (section 2.5.2). A Coomassie stained gel from a typical His-STRADα/MO25α complex purification is provided in Chapter 3 of this thesis (Fig. 3.2).

2.8.5 Isolation of His-tagged and untagged STRADα for SPR measurements

His-STRADα and untagged STRADα (residues 59-431) used for SPR measurements in section 2.13, were first isolated in complex with MO25α as described in sections 2.8.3 and 2.8.4. After gel filtration in buffer containing 50 mM Tris-HCl pH 7.8, 50 mM NaCl, 270 mM sucrose and 0.075% (v/v) β-mercaptoethanol, the STRADα/MO25α complex (20 mg) was resuspended in 20 ml of the same buffer with increased (300 mM) NaCl concentration (resuspending buffer). This was then passed through 2 ml of Ni^{2+}-agarose beads, equilibrated in the same resuspending buffer and the beads were washed with 50 column volumes of resuspending buffer containing 500 mM NaCl and were re-equilibrated with 10 column volumes of resuspending buffer. His-STRADα was eluted in resuspending buffer supplemented with 150 mM imidazole. The eluted His-STRADα sample was equaly divided and dialyzed against 5 l of assay buffer containing 50 mM Tris-HCl pH 7.8, 50 mM NaCl, 270 mM sucrose and 1 mM DTT. Untagged STRADα was obtained by incubation with TEV protease (1:30) for

16 h at 4 ^{o}C. Uncleaved STRADα and the TEV protease were removed by passing the post-cleavage sample through Ni^{2+}-agarose beads. A summary and SDS-PAGE analyis of the fore-mentioned procedure is provided in Fig. 2.2. His-STRADα and untagged STRADα were finally dialyzed in assay buffer concentrated to 7 mg/ml, divided into aliquots and stored at -80 ^{o}C. Protein concentrations were determined by measuring the absorbance of the purified proteins at 280 nm (section 2.10.1) in assay buffer.

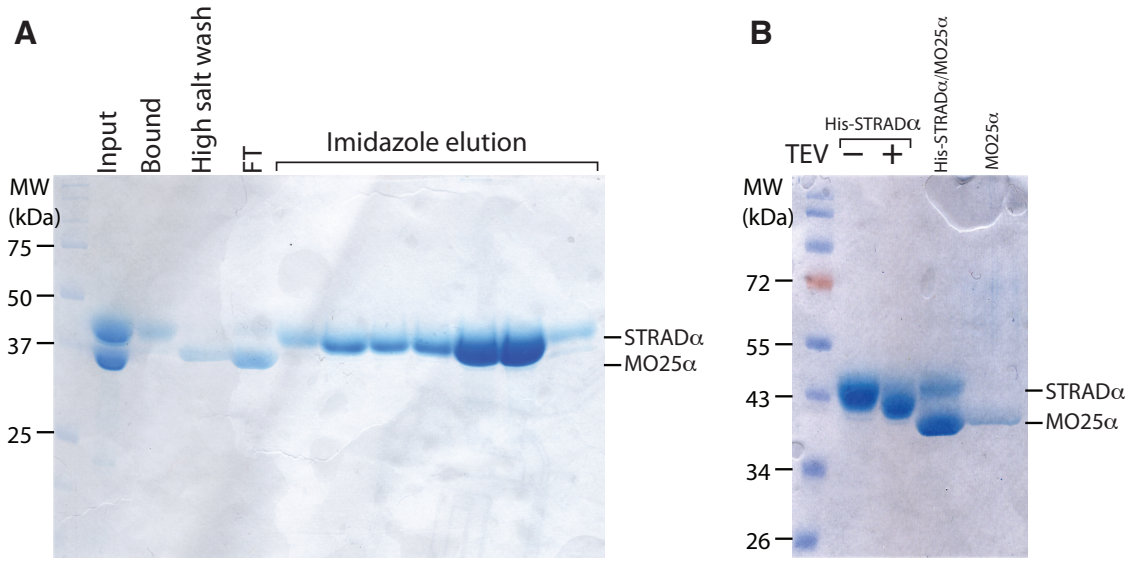

Figure 2.2: Isolation of His-STRADα and untagged STRADα for SPR experiments
A) Purified His-STRADα/MO25α complex (input lane) was passed through NiNTA agarose beads as described in section 2.8.5. The flowthrough was collected and shown in the lane labelled FT. The bound His-STRADα (bound lane) was washed with high salt buffer containing 500 mM NaCl to remove any remaining MO25α, prior to imidazole elution. The eluted fractions (labelled) were run on a gel and their purity was assessed by Coomassie blue staining/visualisation.
B) Eluted fractions were incubated overnight with TEV protease and electrophorised on a 12% acrylamide gel. His-STRADα/MO25α complex and MO25α were run side-by-side as controls.

2.8.6 Conditions and virus amplification for co-expression of the LKB1/STRADα/MO25α complex

The MultiBac expression system (Berger et al., 2004) was used to co-produce the LKB1/STRADα/MO25α complex in Sf21 insect cells. Sf9 and Sf21 cells (Invitrogen) were cultured as described in section 2.6.1. Recombinant bacmid was generated in DH10Bac^{TM} cells and extracted using the phenol:chloroform method described in section 2.6.6. Recombinant progeny 1 (P1) baculovirus was produced by transfecting recombinant bacmid into Sf9 cells. The cells were washed three times in media containing no antibiotics/antimycotics and 5 ml of cells were seeded in 25 cm^3 flasks at a density of 0.9 $\times$ 10 ^{6} cells/ml and allowed to attach for 30-45 min. Meanwhile, in a 12 well plate, 12 μl of Cellfectin reagent (Invitrogen) and 10 μl of bacmid DNA (section 2.6.6) were added to 500 μl of SF900II media and left at RT for 45 min. A further 2 ml of SF900II media was added to the DNA/Cellfectin mix and this was transferred to the attached cells from which the present media had been aspirated. The attached cells, together with the 2.5 ml of added DNA/Cellfectin/media were incubated overnight at 27 ^{o}C in an incubater with appropriate humidity. The media was then aspirated, cells were washed once with SF900II fresh media containing antibiotic/antimycotic and 5 ml of this fresh media was finally added.

The P1 virus was harvested after 6 days by centrifugation at 800 rpm for 10 min. Aliquots (400 μl) of the decanted supernatant were made and stored at -80 ^{o}C.

A P2 virus was generated by infecting Sf21 cells (1.0×10^6 cells/ml) using the P1 virus (400 μl/100 ml cells). The supernatant from this culture (P2 virus) was harvested 72 h post-infection, and 3 ml were used to infect 600 ml of Sf21 cells (1.5×10^6 cells/ml), thus generating a P3 virus 48 h post-infection. This culture was used (1:10) to infect 6 l of Sf21 cells for protein production.

2.8.7 Cell lysis and purification of the LKB1 heterotrimeric complex

Cells were grown in suspension 48 h post-infection, were washed once in Buffer A (section 2.5.3) and harvested in ice-cold lysis Buffer B (section 2.5.3). Cells were lysed using a continuous flow cell disruptor at 35000 psi, and the lysate was clarified by centrifugation at 26000 g for 30 min. The supernatant was incubated on a rolling platform for 1 h at 4 ^{o}C with 8 ml of NiNTA agarose beads, pre-equilibrated in low salt Buffer C (section 2.5.3). The beads were washed with 10 CV of low salt Buffer C and 60 CV of high salt Buffer D (section 2.5.3), followed by a re-equilibrating step with 10 CV of low salt Buffer C. The protein was eluted from a disposable column with 10 CV of low salt Buffer C supplemented with 100 mM imidazole. Fractions were combined ($\sim$60

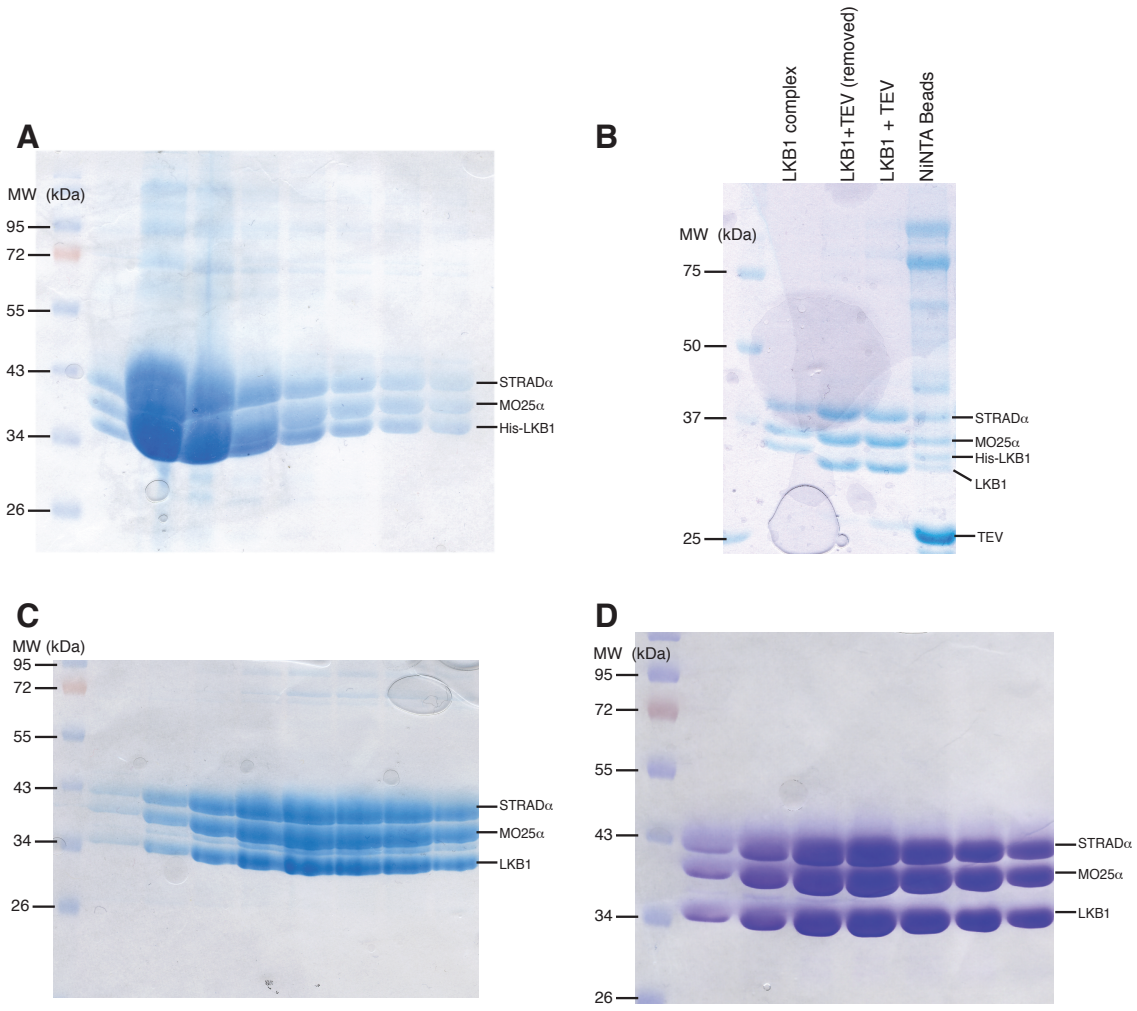

Figure 2.3: Purification of the LKB1/STRADα/MO25α complex
A) Elution of the LKB1 heterotrimeric comlplex from NiNTA beads using 120 mM imidazole. B) Fractions from (A) were combined (first lane) and His-TEV protease was added (1:20) and incubated for 48 h at 4 ^{o}C (third lane). His-TEV and uncleaved His-LKB1 complex were removed using NiNTA beads (fourth lane) leaving cleaved LKB1 complex free of His-TEV protease (second lane).
C) Eluted fractions from an anion exchange chromatography column. The LKB1 heterotrimeric complex eluted at ∼250 NaCl. If trace amounts of uncleaved LKB1 were evident, the fractions were pulled and passed through fresh NiNTA beads for a second time before loading on a gel filtration column.
D) Peak fractions of eluted LKB1 heterotrimeric complex run on a Superdex-S200 26/60 gel filtration column.

mg of protein) and 3 mg of His-tagged TEV protease was added prior to dialysis against 5 l of loading Buffer E (section 2.5.3) for 48 h. The TEV protease and uncleaved LKB1 were removed by passing through 2 ml of NiNTA beads prior to loading the sample on a 5 ml HiTrap-Q column (GE Healthcare). Bound proteins were eluted over 30 CV

using a salt gradient of 0-500 mM NaCl, generated with Buffers F and G (section 2.5.3). The LKB1/STRADα/MO25α complex eluted as a single peak at ∼250 mM NaCl. Peak fractions were analysed by SDS-PAGE, pulled together and if neccessary passed through fresh NiNTA beads for a second time to remove any remaining uncleaved His-LKB1 2.3. The sample was divided in half, concentrated to 3 ml and loaded on a Superdex-S200 26/60 column (GE Healthcare), pre-equilibrated in crystallisation Buffer H (section 2.5.3). Alternatively the protein sample was methylated using the protocol described in section 2.9 before loading on a gel filtration column as described above. In both cases the LKB1/STRADα/MO25α complex eluted as a single peak and its purity was assessed by SDS-PAGE and MALDI-TOF linear mass spectrometry. The purification procedure is summarised in Fig. 2.3. Additional analyses of LKB1 complex preparations are provided in Chapter 4 of this thesis.

2.8.8 HEK293 cell culture, transfections and lysis (completed by Dr Beatrice M. Filippi)

HEK293 cells were cultured on 10 cm diameter dishes in 10 ml DMEM supplemented with 10% (v/v) fetal bovine serum, 2 mM L-glutamine, 100 U/ml penicillin, and 0.1 mg/ml streptomycin. For transfection experiments, 3 to 9 μg of DNA was mixed with 20 μl of 1 mg/ml

polyethylenimine (Polysciences) in 1 ml of plain DMEM for each dish, and the mixture was left to stand for 30 min and added to the cells. Cells were lysed 36 hours post-transfection in 1 ml of ice-cold lysis Buffer A (section 2.5.4) per dish. The cell lysates were clarified by centrifugation at 20000 *g* for 15 min at 4 ^{o}C, and the supernatants divided into aliquots, frozen in liquid nitrogen and stored at -20 ^{o}C.

2.8.9 Expression of fusion proteins in HEK293 cells and affinity purification (completed by Dr Beatrice M. Filippi)

10 cm diameter dishes of HEK293 cells were transiently transfected with 3 μg of the pEBG-2T constructs (GST-LKB1) together with 3 μg of the indicated pCMV5 constructs (Flag-STRADα and Myc-MO25α). Cells were harvested and lysed (section 2.8.8), 36 h post-transfection. The clarified lysates were incubated for 1 h on a rotating platform with glutathione-Sepharose (20 μl/dish of lysate) that was previously equilibrated in lysis Buffer A (section 2.5.4). Beads were then washed twice with wash Buffer B (section 2.5.4) and twice with 50 mM Tris-HCl, pH 7.5 For immunoblotting analysis, the beads were resuspended in SDS sample buffer after this step and the samples were immunoblotted as described in section 2.10.2. For protein kinase assays and gel electrophoresis, the beads were washed twice with wash Buffer B (section 2.5.4), and proteins were eluted from the resin by

incubation with the same buffer containing 20 mM reduced glutathione (pH re-adjusted to 7.5) and 270 mM sucrose. The beads were then removed by filtration using a SpinX column with a 0.44 μm filter, and the eluate was divided into aliquots and stored at -80 ^{o}C.

2.9 Lysine methylation protocol

Prior to lysine methylation the His-STRADα/MO25α samples were dialyzed overnight against 5 l of buffer containing 25 mM Tris-HCl pH 7.5, 50 mM NaCl, 10% glycerol, 1 mM benzamidine and 0.075% (v/v) β-mercaptoethanol. The LKB1/STRADα/MO25α complex was methylated after elution from the anion exchange column (described in section 2.8.7 and the same elution buffer (containg 250 mM NaCl) was used. STRADα was methylated in Buffer B (section 2.5.1).

The lysine methylation method previously described by Walter et al. (2006) using dimethylamine-borane complex (DMB) and formaldehyde (section 2.1.6), was followed with minor modifications. The following protocol (carried out at 4 ^{o}C) is described for 1 ml of protein solution. The methylation reaction was performed overnight at protein concentrations of 1 mg/ml or less in a 50 ml falcon tube. Twenty microliters of freshly prepared 1 M dimethylamine-borane complex (DMB) and 40 μl of 1 M formaldehyde were added to the protein solution, and the reactions were gently mixed and incubated at 4 ^{o}C for

2 h. A further 20 μl DMB and 40 μl formaldehyde were added and the incubation continued for another 2 h. Following a final addition of 10 μl DMB, the reactions were incubated overnight at 4 ^{o}C.

Th methylation reaction lead to significant amount of precipitated protein, which was removed by centrifugation for 30 min at 3500 rpm in a benchtop centrifuge. The supernatant was then concentrated down to 2 ml and buffer exchanged in a disposable desalting column (section 2.2). The eluates (containing the methylated protein, as determined by a Bradford assay) were pulled together, concentrated and buffer exchanged further in a Vivaspin concentrator. Finally the sample was concentrated again to 2.5-3.0 ml before loading on a gel filtration column as described in sections 2.8.2 (STRADα), 2.8.4 (His-STRADα/MO25α complex) and 2.8.7 (LKB1/STRADα/MO25α complex).

2.10 Analysis and storage of protein preparations

2.10.1 Determination of protein concentrations

Protein and whole cell-lysate concentrations were determined using the Bradford method. A standard curve was constrcuted according to the manufacturers protocol, using 1 ml of the Bradford reagent thoroughly mixed with increasing amounts of known BSA concentrations

(0-5 mg/ml). The absorbance at wavelength 595 nm (A_{595}) was measured for a series of increasing protein concentrations and the values were used to constrcut a calibration-curve for subsequent protein measurements. A cuvette containing the same volume of water/buffer was used as blank and subtracted from each measurement. Protein solutions of highly concentrated samples were diluted to display an A_{595} reading within the linear range of Bradford measurements, generally between 0.1-0.7 arbitrary absorbance units (AU).

Alternatively, protein concentrations were calculated using Beer-Lambert's law (Stryer et al., 2002, p69) by measuring the absorbance of the purified proteins in assay buffer at 280 nm. Theoretical extinction coefficients (ε) were calculated using the ExPASy proteomics server (http://www.expasy.org) and were: His-STRADα = 37735 M^{-1} cm^{-1}, STRADα = 36245 M^{-1} cm^{-1} and MO25α = 22015 M^{-1} cm^{-1}. A cuvette (1 cm pathlength) containing buffer or ddH_2O only was used as blank. Highly concentrated protein solution were diluted accordingly to give an A_{280} reading between 0.1-0.6 AU (assumed linear range; measured in a 1 cm pathlength cuvette) and the following formula was used for calculating the final protein concentration.

$$Concentration(mg/ml) = (\frac{A_{280}}{\varepsilon}) \times MW(Da) \times Dilution factor \quad (1)$$

2.10.2 Immunoblotting (completed by Dr Beatrice M. Filippi)

Cell lysates or purified proteins were subjected to SDS-PAGE and transferred to nitrocellulose membranes over 2 h at 40 V. The membranes were blocked for 1 hour in TBS-T buffer (section 2.3.8 containing 10% (w/v) skimmed milk. The anti-GST (DSTT), anti-Flag (Sigma) and anti-Myc antibodies (Roche) were diluted 1000-fold before the membranes were immunoblotted in the same buffer containing the forementioned antibodies, for 16 h at 4 ^{o}C. Membranes were then washed six times with TBS-T buffer and incubated with the appropriate horseradish peroxidase-conjugated secondary antibodies (Pierce) in TBS-T buffer containing 10% (w/v) skimmed milk. After repeating the washing steps, detection was performed using the enhanced chemiluminescence reagent (ECL) and the films were developed using a film automatic processor (SRX-101; Konica Minolta Medical).

2.10.3 MALDI-TOF analysis

Matrix-assisted laser desorption/ionisation and time-of-flight (MALDI-TOF) analysis were carried out in the Fingerprints and Proteomics Facility, University of Dundee, UK, by Dr Kenny Beattie and Dr David Campell.

2.10.4 Analytical ultracentrifugation (AUC)

Sedimentation-equilibrium determinations were carried out by Dr Mark Agacan, AUC facility, University of Dundee, UK. An Optima XL-1 analytical ultracentrifuge (Beckman Coulter) with absorbance optics was used. The sedimentation-velocity experiments were run at 45000 rpm at 293 K and the data were analysed with the program SEDFIT (Schuck, 2000). Samples were prepared in 25 mM Tris-HCl pH 7.8, 150 mM NaCl, 2 mM DTT and centrifuged at 14000 rpm in a benchtop centrifuge at 4 ^{o}C for 30 min prior to AUC analysis. Various concentrations (0.75-3.0 mg/ml) of the unmethylated and methylated LKB1/STRADα/MO25α purified for crystallisation (section 2.8.7) were analysed in the absence/presence of 0.1 mM ATP and 1 mM $MgCl_2$.

2.10.5 Dynamic light scattering

Dynamic light scattering (DLS) analysis were carried out at 293 K using a Proterion DynaPro-LSR DLS instrument coupled with a microsampler and analysed using DLS Proterion's Dynamics V6 software (both from Proterion, Piscataway, NJ, USA). 12 or 45 μl quartz sample cells (cuvettes) were used, and samples were prepared in 25 mM Tris-HCl pH 7.8, 150 mM NaCl, 2 mM DTT. Prior to DLS analysis

samples were centrifuged at 14000 rpm in a benchtop centrifuge at 4 ^{o}C for 30 min.

2.10.6 Storage of purified protein preparations

Recombinantly expressed and purified protein preparations were "snap" frozen in liquid nitrogen (generally at concentrations 1-3 mg/ml), and the aliquots were stored at −80 °C in buffers containing 270 mM Sucrose. In the absence os sucrose, 10% (v/v final concentration) of glycerol was added. Aliquots were thawed at 4 °C when required.

2.11 Enzyme assays

2.11.1 Assaying LKB1 by measuring phosphorylation of the LKBtide peptide (completed by Dr Beatrice M. Filippi)

The activity of recombinant LKB1/STRADα/MO25α complexes was assayed towards the LKBtide peptide substrate (SNLYHQGKFLQTFCGSPLYRRR) (Lizcano et al., 2004). All assays were performed by using 0.35 μg of recombinant proteins expressed and purified from HEK293 cells as described in section 2.8.9. Phosphotransferase activity towards the LKBtide peptide was measured in a total assay volume of 50 μl consisting of 50 mM Tris-HCl pH 7.5, 0.1 mM EGTA, 0.1% (v/v) 2-mercaptoethanol, 10 mM magnesium acetate, 0.1 mM [γ-^{32}P]ATP (200 cpm/pmol) and 0.2 mM LKBtide peptide. The assays

were carried out at 30 ^{o}C and were terminated after 15 minutes by applying 40 μl of the reaction mixture onto P81 membranes. These were washed in phosphoric acid, and the incorporated radioactivity was measured by scintillation counting as described previously for MAP kinase by Alessi et al. (1995). One Unit (U) of activity represents the incorporation to the substrate of 1 nmol of γ-^{32}P per minute.

2.11.2 Assaying LKB1 by measuring activation of the heterotrimeric AMPK kinase (Completed by Dr Beatrice M. Filippi)

The rat AMPK heterotrimeric complex ($\alpha_1\beta_2\gamma_1$ subunits) was purified from *E. coli* (Neumann et al., 2003) and provided by the Division of Signal Transduction Thereapy, University of Dundee (Fig. 2.4). The AMPK activity was measured following its phosphorylation with LKB1 as reported by Lizcano et al. (2004). 0.3 μg of AMPK complex, were incubated with or without 10 ng of wild type or mutant LKB1/STRADα/MO25α complex in an assay buffer containing 50 mM Tris-HCl pH 7.5, 0.1 mM EGTA, 0.1% (v/v) 2-mercaptoethanol with the addition of 5 mM magnesium acetate and 0.1 mM cold ATP, in a final volume of 20 μl. After incubation at 30 ^{o}C for 30 min-

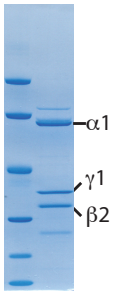

Figure 2.4: Typical AMPK purification

utes the AMPK kinase activity was determined by adding 30 μl of the same assay buffer containing 5 mM magnesium acetate, 0.1 mM [γ-^{32}P]ATP (300 cpm/pmol) and 0.2 mM AMARA peptide (AMARAASAAALARRR) (Dale et al., 1995) as substrate. After incubation for 20 min at 30 ^{o}C, incorporation of γ-^{32}P into the peptide substrate was determined by applying the reaction mixture onto P81 phosphocellulose paper and scintillation counting as described in section 2.11.1. Similarly, one Unit (U) of activity represents the incorporation to the substrate of 1 nmol of γ-^{32}P per minute.

2.11.3 Purification and kinase activity assays of STRADα

STRADα residues 59-431 (wild type and mutant forms) preceded by a 6-His purification tag, were expressed in *E. coli* BL21(DE3)pLysS cells. The expression and purification procedure was followed as described in sections 2.8.3 and 2.8.4 for the STRADα/MO25α complex. After the imidazole elution step 2.8.3, STRADα was assayed for activity. Approximately 3-5 μg of PKA, wild type or mutant His-STRADα were assayed in a 25 μl reaction mixture containing 50 mM Tris-HCl pH 7.5, 0.1% (v/v) 2-mercaptoethanol, 0.1 mM EGTA, 10 mM magnesium acetate, and 0.2 mM [γ-^{32}P]ATP (5000 cpm/pmol) in the presence of 5 μg of bovine MBP. In assays where 3 μg of bacterially expressed MO25α (Milburn et al., 2004) was present, this was incubated

with STRADα for 30 minutes at 4 ^{o}C before the reaction was started. In assays where magnesium acetate was omitted, 2 mM EDTA was added instead. After incubation for 60 min at 30 ^{o}C, reactions were terminated by the addition of 6 μl of LDS sample buffer (5 times concentrated) and reaction mixtures (30 μl) were electrophoresed on SDS-polyacrylamide gels. These were dried and analyzed by autoradiography to quantify STRADα autophosphorylation or MBP phosphorylation.

2.12 Measurement of STRADα binding to phosphonucleotides

2.12.1 Nucleotide binding experiments

Fluorescent measurements of bound TNP-ATP were obtained at 25 ^{o}C in assay buffer and with the addition of 0.5-1.0 mM $MgCl_2$ where indicated, using 1 cm pathlength cuvettes in a VARIAN Cary Eclipse Fluorescence spectrophotometer. Fluorescence was recorded from 500-600 nm (slit width = 20 nm; PMT = 800 V) after excitation at 410 nm (slit width = 10 nm). In all cases, signal from the TNP-ATP buffer control was subtracted as background. For binding studies, STRADα and STRADα mutants were assayed at 2 μM. In cases where STRADα/MO25α complexes were assayed, wild type or mutant MO25α (2 μM) were pre-incubated for at least 2 h at 4 ^{o}C prior

to a fluorescence binding experiment. For saturation binding experiments, concentrated stocks of TNP-ATP were added stepwise, covering a range of concentrations from 0.05-30 μM. For displacement experiments, the concentration of TNP-ATP was fixed at 5 μM, and ATP or ADP was titrated in, covering a range of concentrations from 0.05-500 μM. In all assays, concentrated stocks of nucleotides were added in steps of 0.5-1.0 μl to 1 ml of reaction mixture, ensuring that the total added volume did not exceed 1% of the total volume of the reaction.

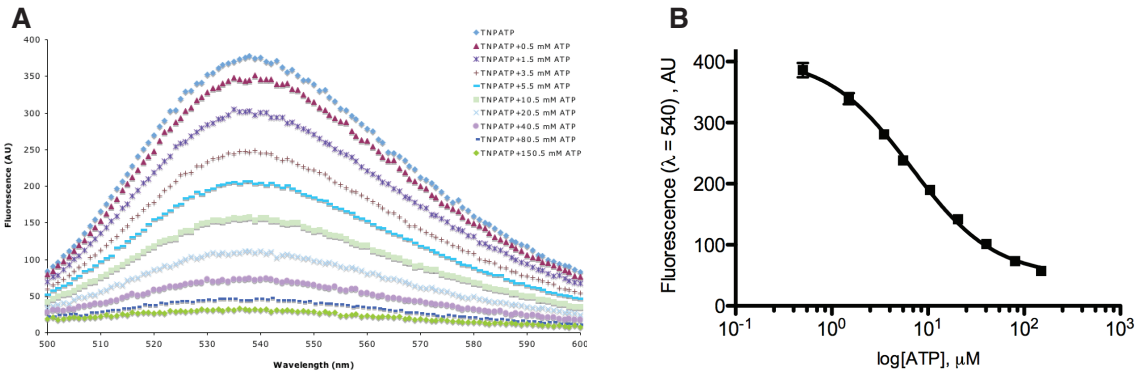

Figure 2.5: Typical TNP-ATP displacement experiment
A) Fluorescence emission spectra (excitation 410 nm) of TNP-ATP (5 μM) bound to STRADα (4 μM) with/without stepwise addition of unlabelled ATP as described in section 2.12.1.
B) Emisson at $\lambda = 540$ nm was plotted as a function of added ATP. A dose response curve, fitted using equation 3 (section 2.12.2) gave an inhibitory concentration (IC_{50}) = 6.6 $\pm$ 0.5 μM. Data are presented as the mean $\pm$ SEM of three separate measurements.

Data collected form a typical experiment for constructing a dose response curve of TNP-ATP displacement by ATP is provided in Fig. 2.5.

2.12.2 Data analysis for the nucleotide binding experiments

Data were analysed using the GraphPad-PRISM software, and to calculate the K_d values for TNP-ATP, data from saturation binding experiments were fitted to the following quadratic equation suitable for tight binding interactions with ligand depletion (Copeland, 2000, p.92).

$$[RL] = \frac{([R] + [L] + K_d) - \sqrt{([R] + [L] + K_d)^2 - 4[R][L]}}{2} \qquad (2)$$

Where [RL] equals the concentration of receptor/ligand complex, calculated as the fractional occupancy (F_x/F_{max}) $\times$ [R]. [R] equals the total binding capacity, fixed at 1.5 μM. [L] equals the concentration of added TNP-ATP. In the displacement studies, equilibrium constant values for ATP and ADP were calculated by first determining the $\log IC_{50}$ value, using a standard dose response equation:

$$F_x/F_{max} = minimum + \frac{maximum - minimum}{1 + 10^{([N] - logIC_{50})}} \qquad (3)$$

where [N] equals the concentration of added nucleotide and F_x/F_{max} represents the fractional occupancy. Equilibrium constants for the competing ATP and ADP (K_d^N), were fitted using the rearranged

Cheng-Prusov equation (Cheng and Prusoff, 1973) below:

$$logIC_{50} = log(10^{logK_d^N} \times \frac{1 + [TNP - ATP]}{K_d^{TNP-ATP}}) \quad (4)$$

2.13 Surface Plasmon Resonance (SPR) measurements

2.13.1 BIAcore assays of STRADα/MO25α interaction (completed by Dr Iva Navratilova)

SPR measurements were performed using a BIAcore T100 instrument. Wild type and mutant forms of MO25α (Fig. 2.6) were immobilized on a CM5 sensor chip using standard amine-coupling chemistry and 10 mM HBS, pH 7.4 was used as the running buffer. The carboxymethyl dextran surface was activated with a 7 min injection of a 1:1 ratio of 0.4 M 1-ethyl-3-(3-dimethylaminopropyl) carbodiimide hydrochloride (EDC)/0.1 M N-hydroxy succinimide (NHS). MO25α (5-7 μM) was coupled to the surface with a 1 min injection of protein diluted in 10 mM sodium acetate (pH 5.5). Re-

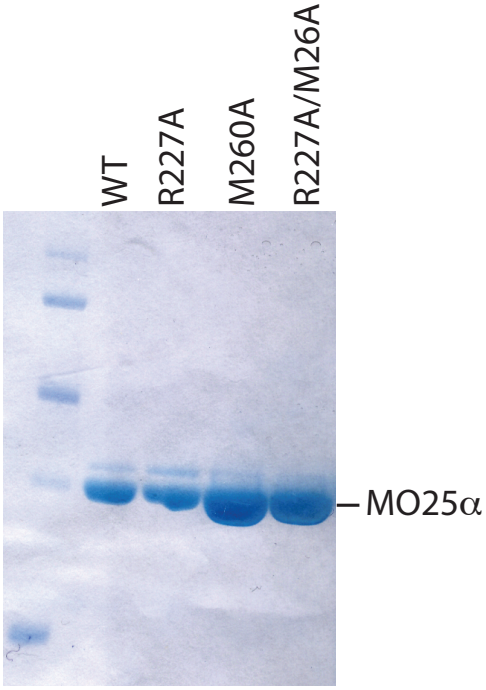

Figure 2.6: Purification of MO25α for assays

maining activated groups were blocked with a 7 min injection of 1 M ethanolamine (pH 8.5). MO25α was immobilised on three flow-cells of a CM5 chip at densities 1700-2500 response units (RU) performed at 25 ^{o}C, leaving one flow cell as a reference to subtract any possible non-specific binding.

STRADα was prepared in running buffer containing 50 mM Tris, pH 7.8, 50 mM NaCl, 270 mM sucrose, 1 mM DTT (section 2.8.5 and Fig. 2.2) with added 0.005% P20 and 0.1 mg/ml BSA in the presence/absence of 100 μM ATP and 1 mM $MgCl_2$, and injected over all four surfaces at nine concentrations of a 3-fold concentration series (5 μM - 0.3 nM). Each concentration was injected in duplicate over all surfaces. Association was measured for 60 s at a flow rate of 50 μl/min and dissociation was measured for 3 minutes. STRADα dissociated completely from the MO25α surfaces, thus eliminating the need for a regeneration step. Sensograms from BIAcore experiments are provided in Fig. A.3.

2.13.2 Data analysis for the SPR measurements

Data were analysed using Scrubber 2 (BioLogic Software, Campbell, Australia) and CLAMP (Myszka and Morton, 1998) software (carried out by Dr Iva Navratilova). Data were double referenced to the reference surface to subtract any possible non-specific binding and to the

blank buffer injections to subtract drift of the target from surface. Data were fitted to a 1:1 or 2:1 binding site model where appropriate. Kinetic association (k_a) and dissociation rate (k_d) constants were separately determined from the BIAcore sensograms and equilibrium dissociation constants (K_d) were calculated using the equation below that describes the law of mass action at quilibrium.

$$K_{d1} = \frac{k_{d1}}{k_{a1}} \qquad and \qquad K_{d2} = \frac{k_{d2}}{k_{a2}} \tag{5}$$

Equlibrium constants were also independently calculated by fitting the measured response (R) from specific binding to a saturation binding isotherm (Lungmuir isotherm). At first, dose response curves for calculating the Hill slope (H) of the data were fitted with the following equation:

$$R = minimum + \frac{maximum - minimum}{1 + 10^{((logEC_{50} - [STRAD]) \times H)}} \tag{6}$$

For those datasets with a Hill slope H = 1 ± 0.1 the isotherm was fitted to the equation below describing binding to one interacting site:

$$R = \frac{R_{max} \times [STRAD]}{[STRAD] + K_d} \tag{7}$$

For those datasets displaying a Hill slope H < 1, the isotherm was

fitted to the equation below describing binding to two interacting sites:

$$R = (\frac{R_{max1} \times [STRAD]}{[STRAD] + K_{d1}}) + (\frac{R_{max2} \times [STRAD]}{[STRAD] + K_{d2}}) \quad (8)$$

Where R_{max1} and R_{max2} are the relative maximal changes in response for sites 1 and 2 respectively and K_{d1} and K_{d2} are the equilibrium dissociation constants for sites 1 and 2 respectively.

2.14 Protein crystallography

2.14.1 General theory

This Materials and Methods section does not include the theory behind the applied crystallographic techniques, as this would go beyond the scope of this chapter. Therefore, the reader referred to the relevant literature on this topic. For deeper insights into the process of crystallisation, please refer to the following titles: "Crystallisation of Biological Macromolecules" (McPherson, 1999), and "Crystallisation of Nucleic Acids and Proteins" (Ducruix et al., 1999). "Crystallography Made Crystal Clear" (Rhodes, 2006) is recommended as a general reference for the underlying theory of diffraction experiments. A more comprehensive and advanced account is provided by the text of the International Union of Crystallography (IUCr) "Fundamentals of Crystallography" (Giacovazzo et al., 2002).

2.14.2 Crystallisation methods

The crystal structures described in this thesis were obtained from crystals grown using the vapour diffusion method in the sitting drop and the hanging drop setup (Fig. 2.7). The sitting drop method consisted of a reservoir with added 70–80 μl of mother liquor. On the platform, 0.5-1 μl of protein solutions were pipetted and mixed with an equivalent amount of mother liquor, and if required, 0.2-0.3 μl of additive solutions. The wells were sealed using Crystal Clear sealing tape, thus allowing easy visualisation of the drops. The hanging drop setup was used mainly for crystal optimization after initial crystallisation hits were established by the sitting drop method. Pre-greased (24-well) VDX plates were filled with 0.5-0.7 ml of mother liquor solutions. 1.0–1.5 μl of the protein solution and an equivalent volume of the mother liquor were pipetted onto a siliconised glass cover slip, which was mounted upside down onto the well. A closed system for vapour diffusion was created by distributing the vacuum grease between the cover slip and the top of the well. All crystal visualisation and screening was done manually using an inverted-lens light microscope.

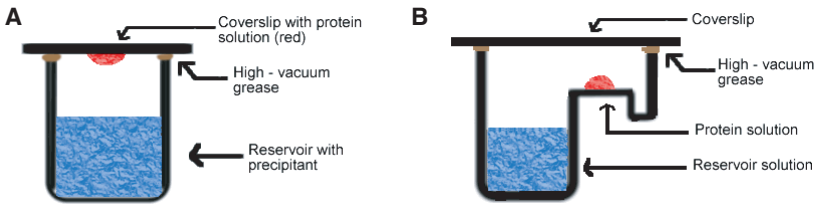

Figure 2.7: Schematic diagram of the crystallisation setup used in this thesis
Hanging drop (A) and sitting drop (B) method. The reservoir, mother liquor solution (blue) contains precipitant. The protein solution (red) is a mixture of protein (in buffer) and diluted mother liquor. The sealed closed system ensures an equilibrium is reached over time, through vapour diffusion from the red to the blue solutions. Pictures are courtesy of Davidson College, Davidson, NC 28035.

2.14.3 Crystal screening

Screening for initial crystallisation conditions was performed using a wide range (∼500 conditions) of commercially available crystallisation screens (2.1.4). The screens used, were designed by the sparse matrix screening technique (Jancarik and Kim, 1991) were non-redundant, and varied in pH as well as in utilising different salts, buffers and precipitants over a broad range. Additionally, screens designed specifically for protein-protein complexes (Radaev and Sun, 2002) were also used (2.1.4).

The protein concentration used for crystallisation condition screening (stated in the experimental sections of the relevant chapters) was assessed by concentrating the respective protein to near the solubility limit, and subsequently diluting this concentration to an extent in which the protein precipitates in 50–70% of the conditions of Hampton Crystal Screens 1 & 2. If more than 50% of the screens showed

clear drops, the protein solution was further concentrated by a factor of 1.5 If the number of conditions leading to amorphous precipitation exceeded 70%, the protein was diluted by a factor of 0.7

For crystal optimisation, the sparse matrix conditions were reproduced using chemicals of the highest available purity. Generally, crystals were reproduced in grid screens of the initial condition, and sometimes further optimized by additive screens. For grid screening, a simple matrix was used based on the initial crystallisation hit, in which the pH of the buffer molecule, and the concentrations of both the salt and the precipitant (the three common constituents of the commercially available screens) were altered by 10-20%. The protein concentration was also changed in parallel screens. Following this optimisation step, additive screening was performed using the comercially available additive screen from Hampton Research. These contained a wide array of biological co-factors, ions, organic molecules and solvents, and various precipitants such as polymers and detergents. Using a grid-optimised condition, 1 μl of protein solution was mixed with 1 μl of mother liquor, and 0.25 μl of the additive was added to each drop. Because of the higher dilution in the drop from adding the additive, the precipitant and salt concentrations were increased accordingly. Screening was performed at 20 ^{o}C, with the exception of STRADα trials where

screening was also performed at 4 and 30 ^{o}C.

2.14.4 Crystallisation of His-STRADα/MO25α complex

The STRADα/MO25α complex was concentrated to 7.5 mg/ml, followed by addition of ATP to a final concentration of 10 mM and $MgCl_2$ (final concentration of 1 mM). The sitting drop vapor diffusion method (section 2.14.2) was used to grow crystals by mixing 1 μl of protein solution with 1 μl of mother liquor. For the unmethylated complex, the optimised mother liquor consisted of 20 mM Li_2SO_4, 50 mM sodium citrate pH 5.6 and 6% (v/v) PEG4000. For the methylated complex, the mother liquor was composed of 0.1 M MES pH 6.4 and 10% (v/v) PEG8000. For both conditions, 0.25 μl of 1 M NDSB-256 was added to the crystallisation drop. Rod-shaped crystals of the unmethylated complex appeared after 3 h and grew to 0.05 mm (maximum dimension) after 24 h. The methylated sample yielded bigger crystals that appeared after 24 h and grew to a maximum length of 0.5 mm after three days. Crystals were flash frozen in liquid nitrogen after cryoprotection with mother liquor containing 20% (v/v) glycerol (unmethylated) and 25% (v/v) PEG8000 and 10% (v/v) PEG300 (methylated).

2.14.5 Crystallisation of the LKB1/STRADα/MO25α complex

Both methylated and unmethylated LKB1/STRADα/MO25α complex were concentrated to 8.0 mg/ml followed by the addition of AMP-PNP and $MgCl_2$ to a final concentration of 5 mM. Crystals were grown at 20 ^{o}C using the hanging drop vapour diffusion method (section 2.14.2). Crystals of the unmethylated sample were obtained by mixing 1.5 μl of protein and 1.2 μl of mother liquor (1.8 M $(NH_4)_2SO_4$, 0.1 M Tris-HCl pH 9.0) and 0.3 μl of 2 mM NaCl. For the methylated protein sample, crystals were grown by mixing 1.5 μl of protein with 1.5 μl of mother liquor (1.6 M $(NH_4)_2SO_4$, 0.1 M Tris-HCl pH 8.25). In both cases crystals appeared after 36-48 h and reached maximal size after 4 days. For cryoprotection, 23% (v/v) glycerol was added to the mother liquor solution.

2.15 Crystal handling

All diffraction experiments were performed using frozen crystals cryoprotected in an appropriate solution containing the mother liquor and a suitable cryo-protectant. These were handled using a small nylon loop mounted on a metal pin. General cryo-protectants such as glycerol, low molecular weight (200-300 MW) polyethylene glycols (PEGs), ethylene-glycol, 2-methyl-2,4-pentanediol (MPD), isopropanol, satu-

rated NaCl and Li_2SO_4 were routinely tested. Crystals were then frozen in a gas stream set to 100 K or directly in liquid nitrogen and stored in a suitable storage/transport dewar.

2.16 General data collection and processing strategies

Data were collected at the European Synchrotron Radiation Facility (ESRF), indexed and proccessed using software from the CCP4 package (Collaborative Computational Project, 1994) and HKL2000 (Otwinowski and Minor, 1997). The data collection strategy was calculated using PREDICT (M.E.M. Noble, University of Oxford, UK) and BEST (Popov and Bourenkov, 2003) to collect data with full completeness and approximate levels of redundancy. During individual data collections, images were processed and scaled to verify the correctness of the assumed data collection strategy and this was altered where necessary. Scaling of a complete data-set was performed, and the statistics in the highest resolution shell were used to determine a reasonable resolution cut-off ($I/\sigma I > 2$ and R_{merge} for the highest resolution shell $< 60\%$). Radiation damage was monitored carefully, and generally 3-4 fold data redundancy and 90-100% completeness was aimed for each dataset. Typical X-ray diffraction images for HisSTRADα/MO25α and LKB1/STRADα/MO25α complex crystals are shown in Fig. 2.8. Summaries of data collection paramaters are given

in the rescpective chapters, where these structures are discussed.

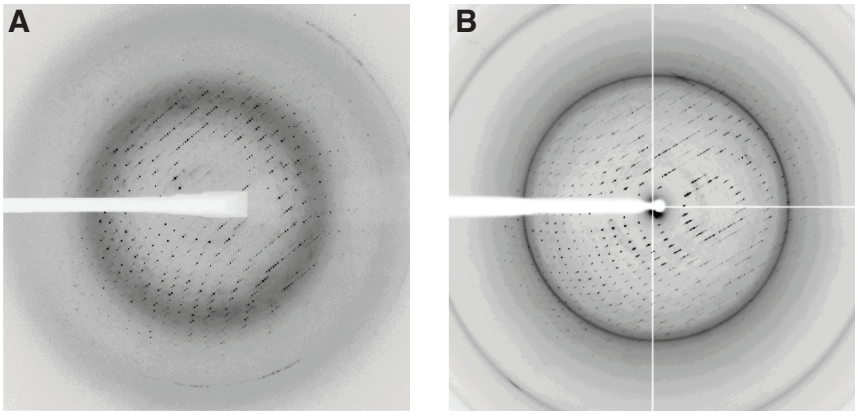

Figure 2.8: Images from diffraction experiments
X-ray diffraction images acquired during data collection of (A) His-STRADα/MO25α complex crystals, diffracting to 2.35 Å and (B) LKB1/STRADα/MO25α complex crystals, diffracting to 2.65 Å.

2.16.1 Determination of the His-STRADα/MO25α complex structure

Data were collected at 100 K on stations ID14-3, ID14-4 and ID23-2 at the European Synchrotron Radiation Facility (ESRF) and processed using the MOSFLM and SCALA programs from the CCP4 package (Collaborative Computational Project, 1994). The structures of the unmethylated/methylated complexes were solved by a combination of molecular replacement with MOLREP (Vagin and Teplyakov, 1997) and real-space searches with FFFEAR (Cowtan, 1998). An initial molecular replacement run was carried out with MOLREP using the 1.85 Å structure (PDBID 1UPK) of MO25α (Milburn et al., 2004) as a search model. Using the resulting phases, the STRADα molecule was then located by performing a real-space search with FFFEAR (Cowtan, 1998) using the 2.1 Å structure (PDBID 1U5R) of TAO2 (Zhou

et al., 2004). Thus, a solution with one complex in the asymmetric unit was found and the structure was refined by alternating rounds of refinement with REFMAC5 (Murshudov et al., 1997) (including TLS refinement (Winn et al., 2001) during the last macrocycles) and manual model building with the program COOT (Emsley and Cowtan, 2004). For the methylated complex, this resulted in a final model with an R-factor of 0.206 (R_{free} = 0.254) that was validated using PROCHECK (Laskowski et al., 1993) and MOLPROBITY (Lovell et al., 2003). STRADα residues 292-347, 383-385, 402-424 and MO25α residues 337-341 were not associated with clear electron density and were not included in the model. A summary of diffraction data parameters, the relevant details of refinement and statistics are provided in chapter 3, Table 3.1 of this thesis. Coordinates and observed structure factor amplitudes have been deposited at the Worldwide Protein Data Bank (wwPDB, http://www.wwpdb.org/), with accession code 3GNI.

2.16.2 Determination of the LKB1/STRADα/MO25α complex structure

Data were collected at 100 K on station ID14-3 at the European Synchrotron Radiation Facility (ESRF) and processed using the DENZO and SCALEPACK programs from the HKL2000 suite (Otwinowski and Minor, 1997).

Structures of the unmethylated/methylated complexes were solved by a combination of molecular replacement with PHASER (McCoy, 2007) and averaging/automatic model building using RESOLVE (Terwilliger, 2003). A molecular replacement run was carried out using the structures of MO25α (PDBID 1UPK (Milburn et al., 2004)) and the STRADα structure determined in this thesis (PDBID 3GNI) as search models. This gave a solution with two copies of each model in the asymmetric unit (asu). The resulting model phases were then further improved by solvent flattening and two-fold averaging using RESOLVE (Terwilliger, 2003), which also built four LKB1 fragments as Cα trace. Using the partially built LKB1 model, the structure of the AUR2 protein kinase (PDBID 1OL7 (Bayliss et al., 2003), 24.5% sequence identity to LKB1) was superimposed using the secondary structure matching function in COOT (Emsley and Cowtan, 2004). Regions of this initial LKB1 model that did not have any associated electron density were removed. The structure was further refined by alternating rounds of refinement with PHENIX (Adams et al., 2002) and REFMAC (Murshudov et al., 1997) (using strict NCS during the first macrocycles and TLS refinement (Winn et al., 2001) during the last macrocycles) and manual model building with the program COOT (Emsley and Cowtan, 2004). For the methylated complex, this re-

sulted in a final model consisting of 1835 ordered residues out of 2080 possible residues, with an R-factor of 0.239 (R_{free} = 0.290), that was validated using PROCHECK (Laskowski et al., 1993) and MOLPROBITY (Lovell et al., 2003). A summary of diffraction data parameters, the relevant details of refinement and statistics are provided in chapter IV, Table 4.1 of this thesis. Coordinates and observed structure factor amplitudes have been deposited at the Worldwide Protein Data Bank (wwPDB, http://www.wwpdb.org/), with accession code 2WTK.

2.17 Data analysis and figure preparations

2.17.1 Structure visualisation, representation and analysis

All structural representations and figures were prepared with the PyMOL molecular graphics system available at http://www.pymol.org (DeLano, 2004). Secondary structure was analysed using DSSP (Kabsch and Sander, 1983) and sequence alignments were performed using MUSCLE (Edgar, 2004), which were edited and displayed using the program ALINE (Bond and Schüttelkopf, 2009). Structure superpositions were completed using the program LSQKAB or the program coot (Emsley and Cowtan, 2004). Electron density maps were generated using the programs FFT, MAPMASK and MAPMAN, all part of the CCP4 package (Collaborative Computational Project, 1994).

2.17.2 Data analysis and statistics

Statistics and non-linear regression analysis were carried out using GraphPad-PRISM® 5 software, CA, USA (www.graphpad.com) and Microsoft Excel® from the Microsoft Office 2004 package (www.office.microsoft.com).

2.17.3 Image annotation and writting

All images shown in this thesis were annotated using Adobe Illustrator (Adobe System Inc.). This document was prepared using the LaTeX typesetting system available at http://www.latex-project.org/. Referencing was done in conjuncion with BibTeX available at http://www.bibtex.org/.

Chapter III

Structure of the STRADα pseudokinase complexed to ATP and MO25α

3 Structure of the STRADα pseudokinase complexed to ATP and MO25α

3.1 Foreword

In the work described below, mutagenesis studies involving expression of LKB1, STRADα and MO25α in HEK293 cells, pulldown and LKB1 activity assays were a collaborative effort involving Dr Beatrice Maria Filippi, University of Dundee, who helped with these experiments. Details of the experimental work are provided in chapter II Materials and Methods section of this thesis.

3.2 Aims

At the start of this project no structures of pseudokinases were known. Thus, the aim of this work was to determine the structure of STRADα pseudokinase and understand the characteristics, functions and evolution of this subset of the protein kinase family. Particularly, the aim was to elucidate how STRADα interacts and cooperates with MO25α to regulate LKB1 activity. To achieve this, the structure of STRADα was determined in complex with ATP and MO25α, and structural and biochemical analyses of these findings are described in this chapter.

3.3 Overview of experimental procedures

3.3.1 Expression and purification of STRADα/MO25α complex

STRADα comprises a pseudokinase domain (residues 58-394), two nuclear export sequences (residues 21–29 and 417–426) (Dorfman and Macara, 2008) and a C-terminal WEF motif (residues 429–431) previously shown to interact with MO25α (Boudeau et al., 2003a; Milburn et al., 2004) (Fig. 3.1A). The STRADα pseudokinase domain (residues 59–431, preceded by a 6-His purification tag) and full length MO25α (residues 1–341) were cloned in a polycistronic vector (Fig. 3.1B) and co-expressed in *E. coli*.

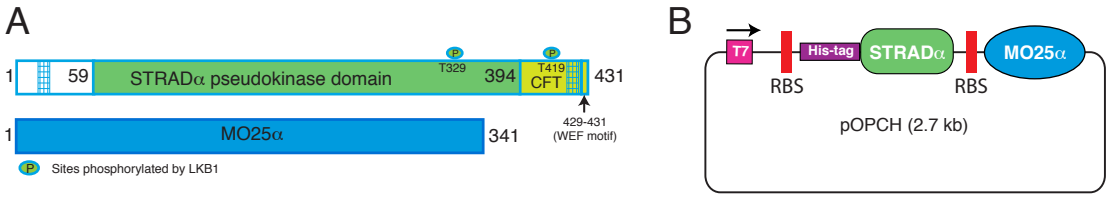

Figure 3.1: Domain architecture of STRADα and MO25α
A) Boundaries of the STRADα pseudokinase domain and the C-terminal flanking tail (CFT). Sequence motifs and phosphorylation sites are labelled. Nuclear export signal sequences (residues 21–29 and 417–426 (Dorfman and Macara, 2008)) are shown as grids. Sites phosphorylated by LKB1 (Baas et al., 2003) are labelled. Coloured regions were used for crystallisation. B) Architecture of the pOPCH vector (Tan, 2001) used to recombinantly co-express the *STRADA/MO25A* genes. RBS = Ribosomal binding site.

The His-STRADα/MO25α complex eluted as a heterodimer of the expected size from a gel filtration column, yielding approximately 60 mg of the complex from 4 l of culture (Fig. 3.2). During purification, a minor low molecular weight eluting shoulder to the main peak was found to consist of mainly uncomplexed His-STRADα (Fig.

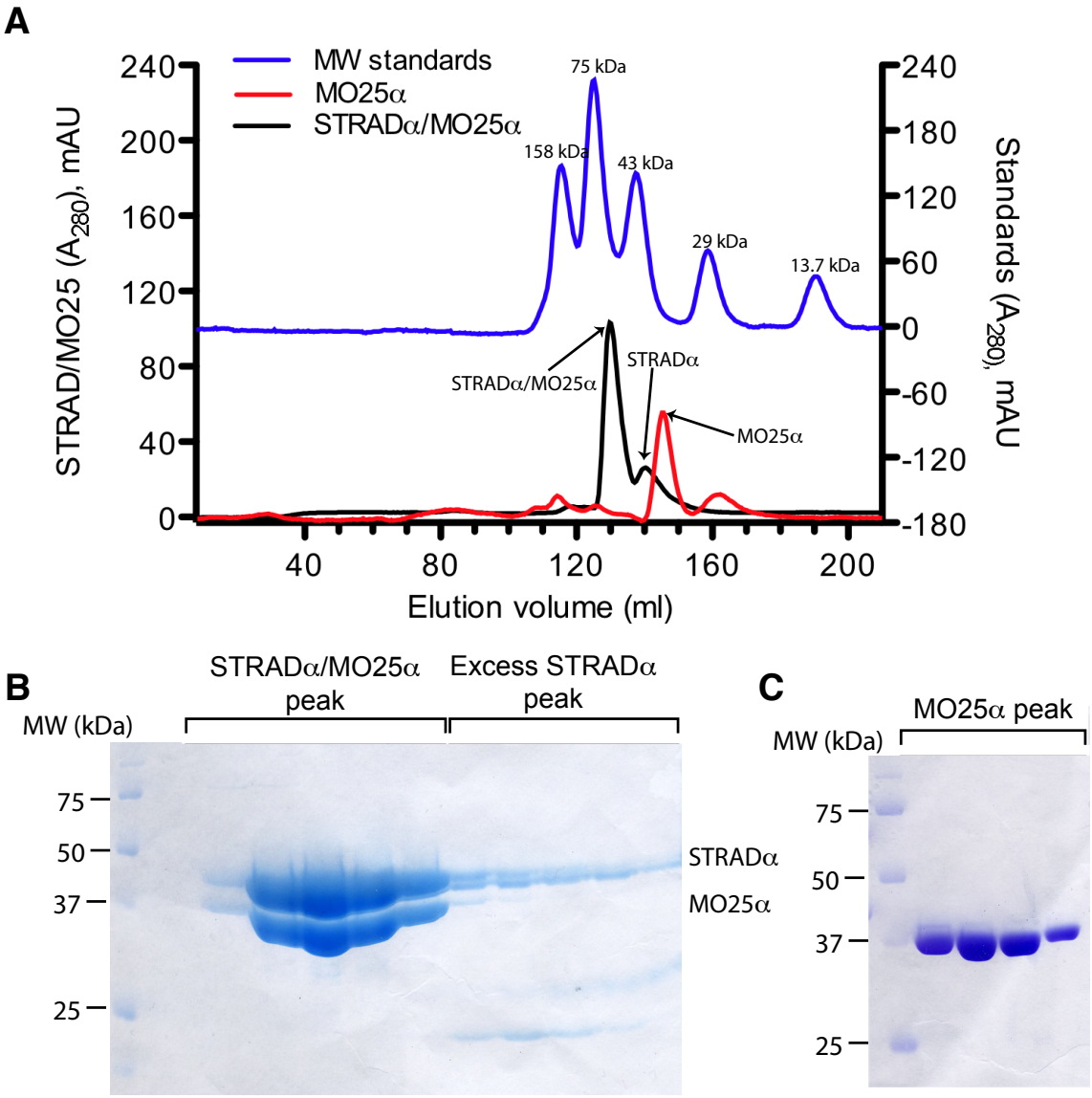

Figure 3.2: Isolation of the heterodimeric STRADα/MO25α complex
A) Gel filtration profiles of His-STRADα/MO25α co-expressed in *E. coli* and crystallised in this thesis. The elution profile of separately expressed MO25α monomer as well as the molecular mass standards Aldolase (158 kDa), Conalbumin (75 kDa), Ovalbumin (43 kDa) Carbonic anhydrase (29 kDa) and Ribonuclease A (13.7 kDa) are also shown.
B & C) Fractions in which His-STRADα/MO25α dimer and MO25α monomer eluted, were analysed by SDS-PAGE and stained with Coomassie blue dye. In the His-STRADα/MO25α purification, a minor low molecular weight eluting shoulder to the main peak was found to consist of mainly uncomplexed His-STRADα.

3.2B). As His-STRADα was the subunit used for nickel affinity purification of the complex, it will be expected to be present in excess. There was no evidence for large molecular weight aggregates of His-STRADα/MO25α (Fig. 3.2A).

3.3.2 Crystallisation and structure solution of STRADα/MO25α complex

Initial crystals of the STRADα/MO25α complex in space group $P2_12_12_1$ diffracted only to 4.8 Å resolution (Table 3.1 and Fig. 3.3A). With the help of chemical lysine methylation (Walter et al., 2006), diffraction of these crystals (retaining the same space group and unit cell dimensions) improved to 2.35 Å (Table 3.1 and Fig. 3.3B).

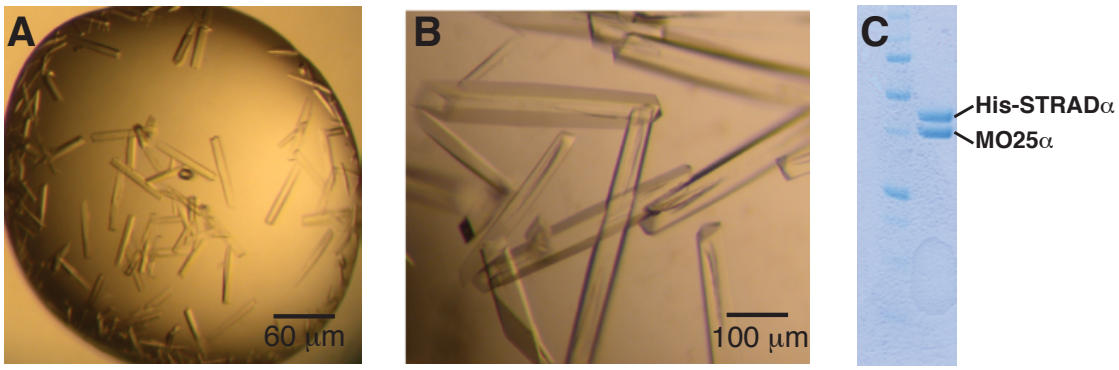

Figure 3.3: Crystals of the STRADα/MO25α complex
Crystals of the native His-STRADα/MO25α complex (A), and methylated His-STRADα/MO25α complex (B).
C) SDS-PAGE gel (Coomassie stained) of LKB1 complex crystals after three subsequent washes in mother liquor.

From mass shift calculations between methylated and non-methylated complex using MALDI-TOF analysis (Appendix Fig. A.1), 9 out of 14 lysines in STRADα and 21/43 lysines in MO25α appeared to be di-methylated. The structures of both methylated and unmethylated

crystals were solved by molecular replacement and revealed the same packing/ intermolecular interactions (Table 3.1). The high resolution, methylated form of the complex was refined to a final model with good statistics (R_{free}/R_{work} of 0.254/0.206, Table 3.1).

3.3.3 Crystallisation attempts of the STRADα pseudokinase domain

Initially, STRADα (residues 54-431) was expressed in *E. coli* as a gene fused to GST and purified for crystallisation (Fig. 3.4). Despite testing several commercial crystallisation screens and buffer conditions including addition of ATP and ADP, these trials were unsuccessful. A second attempt was made when the His-STRADα/MO25α was successfully expressed and crystallised. The STRADα monomer was isolated from the STRADα/MO25α preparations by washing away MO25α with buffer containing high salt concentration, as described in chapter II section 2.8.5 of this thesis. This was then further purified by size exclusion chromatography. Crystallisation screens were set up for STRADα (residues 58–431) with and without the 6-His purification tag and in the presence and absence of ATP. The same procedure was repeated with the methylated sample without success in crystallisation. Notably, STRADα formed heavy precipitates in approximately 90% of the screening conditions. This could be a consequence of the high protein concentrations (8–10 mg/ml) that are

Table 3.1: Summary of data collection, structure refinement and analysis. Values for the highest resolution shell are given in brackets.

	Native	**Methylated**
Space Group	$P2_12_12_1$	$P2_12_12_1$
Unit cell (Å)		
a	73.3	73.7
b	83.5	82.9
c	134.3	134.3
Molecules/asu		
STRADα	1	1
MO25α	1	1
Resolution (Å)	20-4.8 (4.97-4.80)	20-2.35 (2.48-2.35)
Observed reflections	13019	190928
Unique reflections	4229 (409)	34668 (4988)
Redundancy	3.0 (3.0)	5.5 (5.6)
$I/\sigma I$	13.6 (1.9)	13.4 (2.9)
Completeness (%)	98.9 (97.1)	99.6 (99.9)
R_{merge}	0.094 (0.487)	0.100 (0.617)
R_{work}, R_{free}	-	0.206, 0.254
RMSD from ideal geometry		
bonds (Å)	-	0.011
angles (^{o})	-	1.277
B-factor RMSD (Å^2)		
(backbone bonds)	-	1.063
Average B-factor (Å^2)		
protein	-	28.59
ligand (ATP)	-	34.46
water	-	28.36
Ramachandran plot statistics (%)		
Most favoured region	-	92.4
Addittional allowed region	-	6.7
Generously allowed region	-	0.7
Disallowed region	-	0.2

typically used in setting up crystallisation conditions. However, lower protein concentrations (2 mg/ml) did not improve the crystallisation of STRADα. It is possible that in the absence of MO25α, STRADα is unstable and/or prone to forming large molecular aggregates that disfavour crystallisation. In the absence of a STRADα alone crystal structure, the structure of STRADα determined in complex with MO25α and ATP is discussed in this chapter.

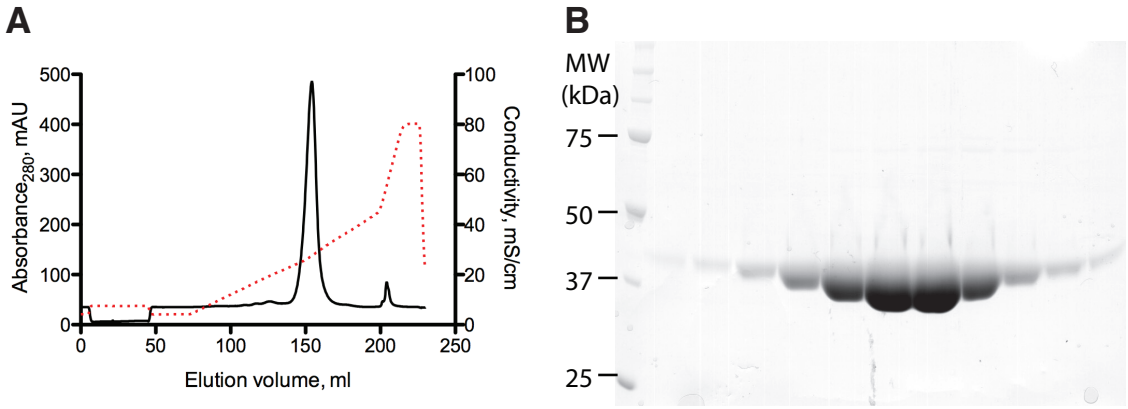

Figure 3.4: Purification of the STRADα pseudokinase domain
A) UV absorbance (λ = 280 nm; black line) of a typical STRADα (residues 54-431) purification using anion exchange chromatography. The red graph is the measured conductivity representing the ionic strength gradient used to elute STRADα bound to the anion column. STRADα eluted at approximately 250 mM NaCl concentration.
B) Fractions in which STRADα eluted were analysed by SDS-PAGE and stained with Coomassie blue dye.

3.4 Structure of the STRADα pseudokinase

3.4.1 STRADα adopts the canonical kinase fold

In the STRADα/MO25α complex structure, STRADα exhibits the classical bilobal protein kinase fold, with the N-terminal lobe (residues 59–152) organised around a central β-sheet, and a C-terminal lobe

(residues 153–394) that is largely α-helical (Fig. 3.5A). Residues 402–424 were not well defined by electron density and thus were not included in the final model. These make up the C-terminal flanking tail (CFT) that terminates with the WEF motif (Fig. 3.1), for which electron density is present. A well-resolved molecule of ATP was observed in the cleft between the small and large lobe of the pseudokinase (Figs. 3.5A and 3.6). The ATP molecule displays the canonical binding mode and retains a similar conformation to that of ATP molecules bound to active kinases (RMSD = 0.9 Å on all atoms compared to ATP bound to PKA (Knighton et al., 1991b)).

3.4.2 STRADα adopts an active conformation

Although the activation loop of STRADα (residues 212–245) is not phosphorylated, it is well ordered, a feature normally observed only in structures of activated protein kinases that are phosphorylated on their activation loop (Fig. 3.5A and B). Remarkably, Asp232 in the activation loop occupies a position similar to the activating phosphorylated residue found in active kinases, e.g. (phospho)Ser181 in TAO2 (Fig. 3.7). Asp232 appears to play the same structural role as the activating phosphate group, coordinating the conserved arginine from the catalytic HRD motif (Arg194 in the STRADα HRS motif) (Fig. 3.7). Further evidence that STRADα adopts the canonical active conforma-

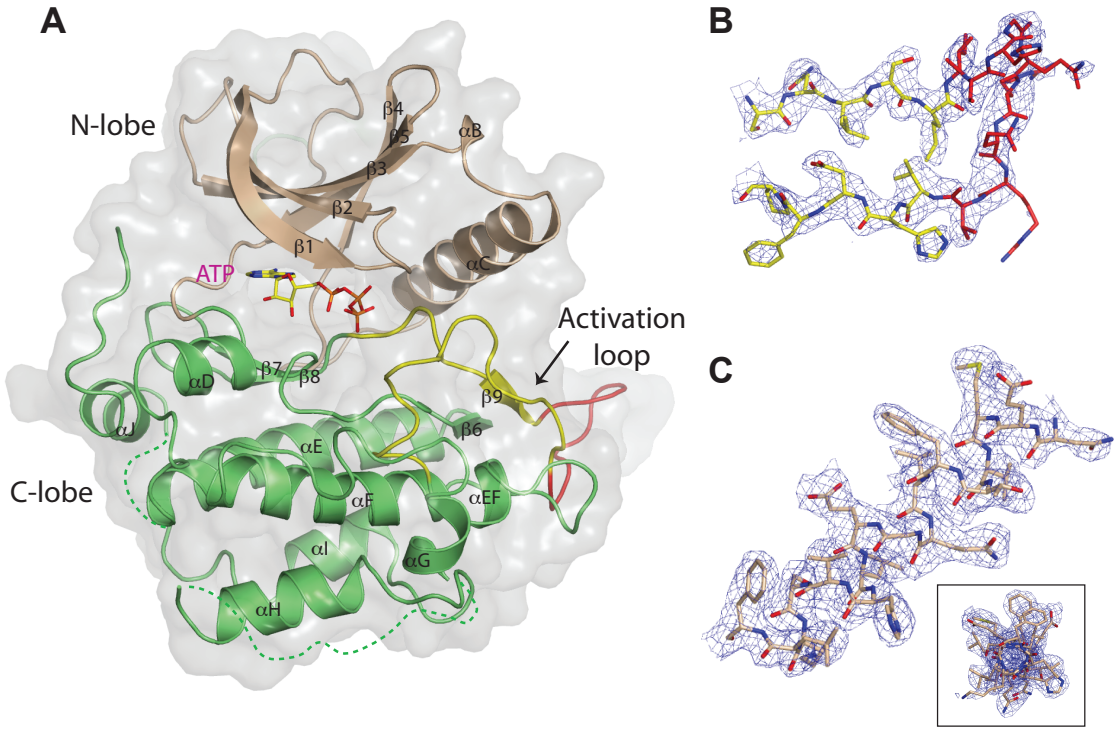

Figure 3.5: Overall structure of the STRADα pseudokinase domain
A) Overall structure of STRADα shown in cartoon representation (N-terminal lobe coloured brown, C-terminal lobe coloured green) with transparent molecular surface. For clarity the WEF motif has been omitted. Secondary structure elements are labelled according to the structure of PKA (Knighton et al., 1991b). The activation segment is coloured yellow, with the section that appears to be unique to STRADα/β (residues 221–229) coloured red. The ATP molecule is shown in sticks representation with yellow carbons. Dotted lines represent regions that were not well defined by electron density and are not included in the refined model.
B) Final $2F_o$-F_c electron density map (coloured blue and contoured at 1.0σ) for part of the activation segment of STRADα (residues 216–234). The stick model is coloured as described in (A).
C) Final $2F_o$-F_c electron density map (coloured blue and contoured at 1.0σ) for the αC helix of STRADα (residues 109–125). An alternative view, looking from the C-terminus of αC is boxed.

tion stems from the presence of a short anti-parallel β-sheet between the β6 and β9-strands, which is a characteristic feature of the active state of kinases (Fig. 3.5A) (Nolen et al., 2004). Furthermore, the STRADα αC helix is rotated into the "closed" conformation found in active kinases (Johnson et al., 1996; Huse and Kuriyan, 2002), with the conserved ion pair between the Glu118 on the αC-helix and Arg100 in subdomain-II formed via two water molecules (Fig. 3.7).

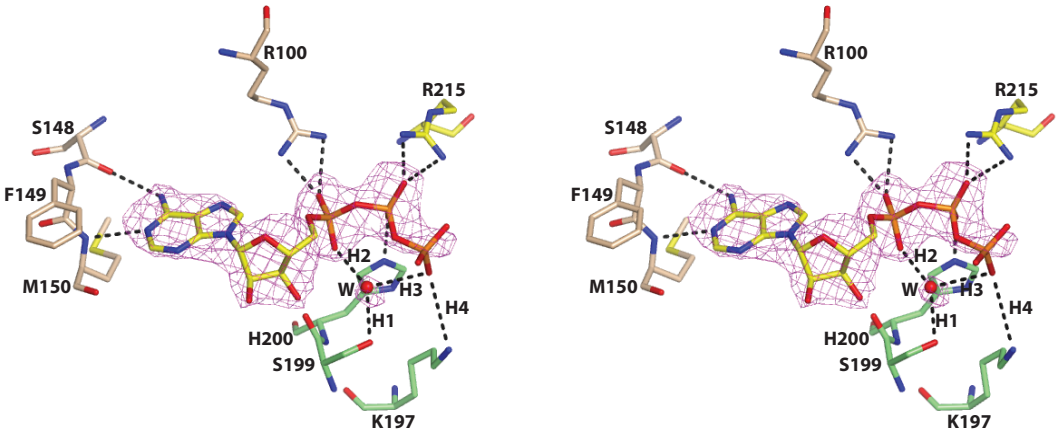

Figure 3.6: STRADα ATP coordination
Stereo figure of ATP (modeled as sticks with yellow carbons) and STRADα residues that contribute to ATP binding (coloured according to Fig. 3.5; N-lobe = brown, C-lobe = green, activation segment = yellow). Unbiased F_o-F_c electron density map for the ATP molecule is coloured magenta and contoured at 2.5σ. The same map for a water molecule (represented as a red sphere and labelled W) is contoured at 2.5σ. Hydrogen bonds are shown as dashed lines. The distances of hydrogen bonds labelled H1-H4 were measured as: H1 = 2.7 Å, H2 = 2.5 Å, H3 = 3.0 Å and H4 = 3.7 Å.

3.4.3 STRADα binds ATP using a Mg^{2+}-independent mechanism

Sequence comparison reveals that STRADα lacks numerous essential catalytic residues found in active protein kinases, namely a conserved Gly residue in the glycine rich-loop (subdomain-I), the Lys residue of

VAIK motif (subdomain-II), the catalytic Asp residue of the HRD motif (subdomain-VIb), a conserved Asn residue (subdomain-VIb) as well as the entire DFG motif in subdomain-VII (Fig. 3.8). Despite missing these key residues, STRADα adopts a similar overall conformation to that of TAO2, (sharing 25% sequence identity and 37% sequence similarity), an active protein kinase of known structure (Zhou et al., 2004) (RMSD = 1.4 Å on 197 Cα atoms). Comparison of the STRADα and TAO2 structures reveals that a number of substitutions of key catalytic residues are found in STRADα (Fig. 3.7). Met83 replaces one of the conserved Gly residues in the glycine rich loop, Arg100 substitutes the catalytic Lys residue in the VAIK motif, Ser195 replaces the Asp residue in the HRD motif, His200 substitutes for the conserved Asn in subdomain-VIb and the entire DFG motif is replaced by GLR (residues 213–215) (Fig. 3.7).

In active protein kinases, the DFG motif plays a pivotal role in coordinating two Mg^{2+} ions—one that orients the γ-phosphate into the position required for phosphoryl transfer and the other that controls ATP conformation by interacting with the β/γ phosphates. Consistent with the lack of the DFG motif in STRADα, no Mg^{2+} ions were observed in the STRADα-ATP complex, despite 1 mM $MgCl_2$ being present in the crystallization mother liquor. However, despite the absence of Mg^{2+}

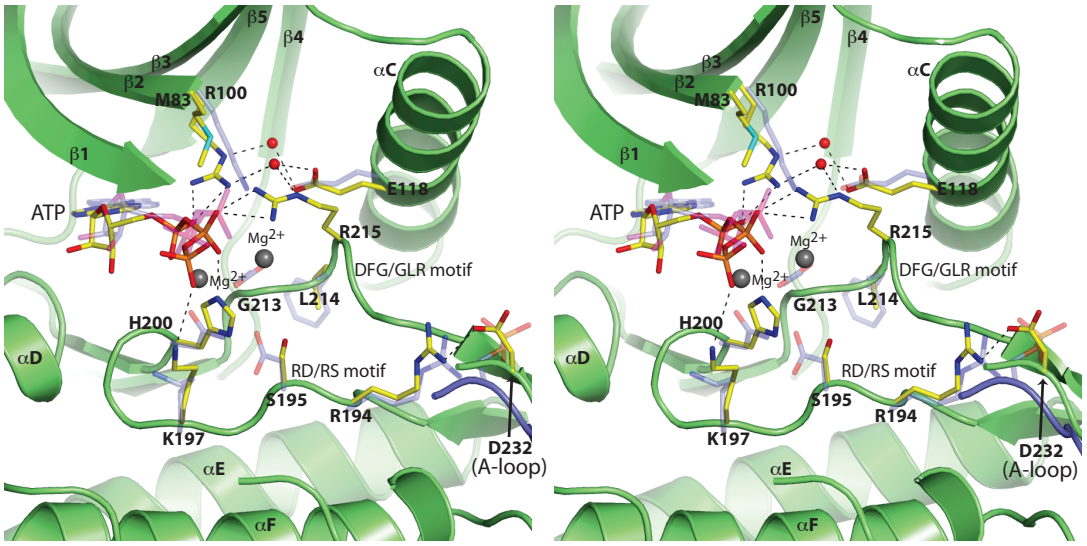

Figure 3.7: STRADα "active" site
Stereo view of superposed STRADα and TAO2 (PDBID 1U5R, (Zhou et al., 2004)) active sites, highlighting key residues required for activity. STRADα residues (labelled) are shown as stick models with yellow carbon atoms, whereas the corresponding TAO2 residues are shown with blue, transparent carbon atoms. Water molecules are represented by red spheres and gray spheres represent Mg^{2+} ions from the TAO2 structure. The glycine-rich loop and part of the activation loop have been omitted for clarity.

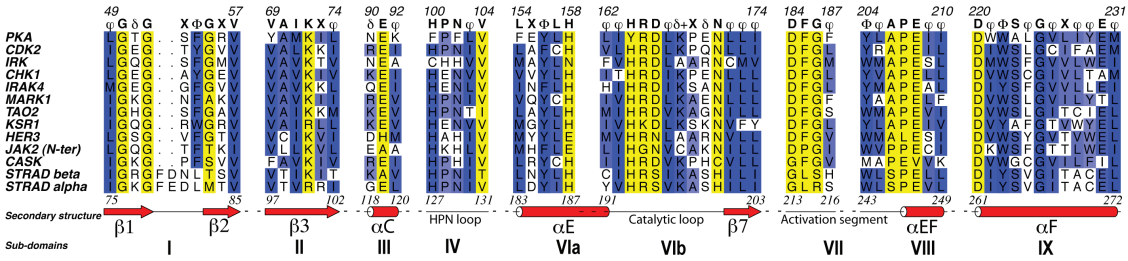

(φ) Hydrophobic, (Φ) large hydrophobic (FYW), (δ) hydrophilic, (X) any amino acid, (- -) sequence break; numbering to PKA sequence (top) and STRADα (bottom).

Figure 3.8: Comparison of STRADα sequence motifs with active protein kinases
Multiple sequence alignment of STRADα and other pseudokinases, highlighting (in yellow) key motifs that are normally essential in active eukaryotic protein kinases.

ions, the positioning of the β/γ phosphates in STRADα was similar to that of active TAO2 kinase complexed to MgATP (Fig. 3.7). The β-phosphate is tethered through interactions with Arg215 from the GLR (DFG) motif, and His200 (subdomain-VIb), basic residues that may substitute for one of the positively charged Mg^{2+} ions (Fig. 3.6). The second Mg^{2+} ion and its coordinating residues are also miss-

ing; instead the γ-phosphate is poorly coordinated and only interacts (weakly; d = 3.7 Å) with a conserved lysine (Lys197) in the catalytic loop and a nearby water molecule (Fig. 3.6). Thus, STRADα appears to have evolved a novel, Mg^{2+}-independent, mechanism to bind the phosphate groups of ATP. The presence of the two hydrogen bonds between N1 and N6 atoms of the ATP adenine ring and the protein backbone (hinge region, residues 148–150) observed in all active protein kinase structures, further illustrates the conservation of the ATP binding pocket (Fig. 3.6). Thus, the STRADα structure explains previous observations that STRADα can bind ATP in the absence of Mg^{2+}, and its similar affinity for ADP and ATP (Boudeau et al., 2004).

3.4.4 Attemtps to detect STRADα activity

Despite STRADα binding ATP in the correct orientation for activity and folding into an active conformation, STRADα (residues 59–431) expressed in *E. coli* did not autophosphorylate or phosphorylate myelin basic protein (MBP, Fig. 3.9). Attempts to detect activity in the presence and absence of MO25α and/or 10 mM $MgCl_2$ were unsuccessful. Mutations converting all the missing catalytic residues on the STRADα pseudokinase discussed above, to the equivalent residues found in the active kinase TAO2 were also generated (Fig. 3.9). How-

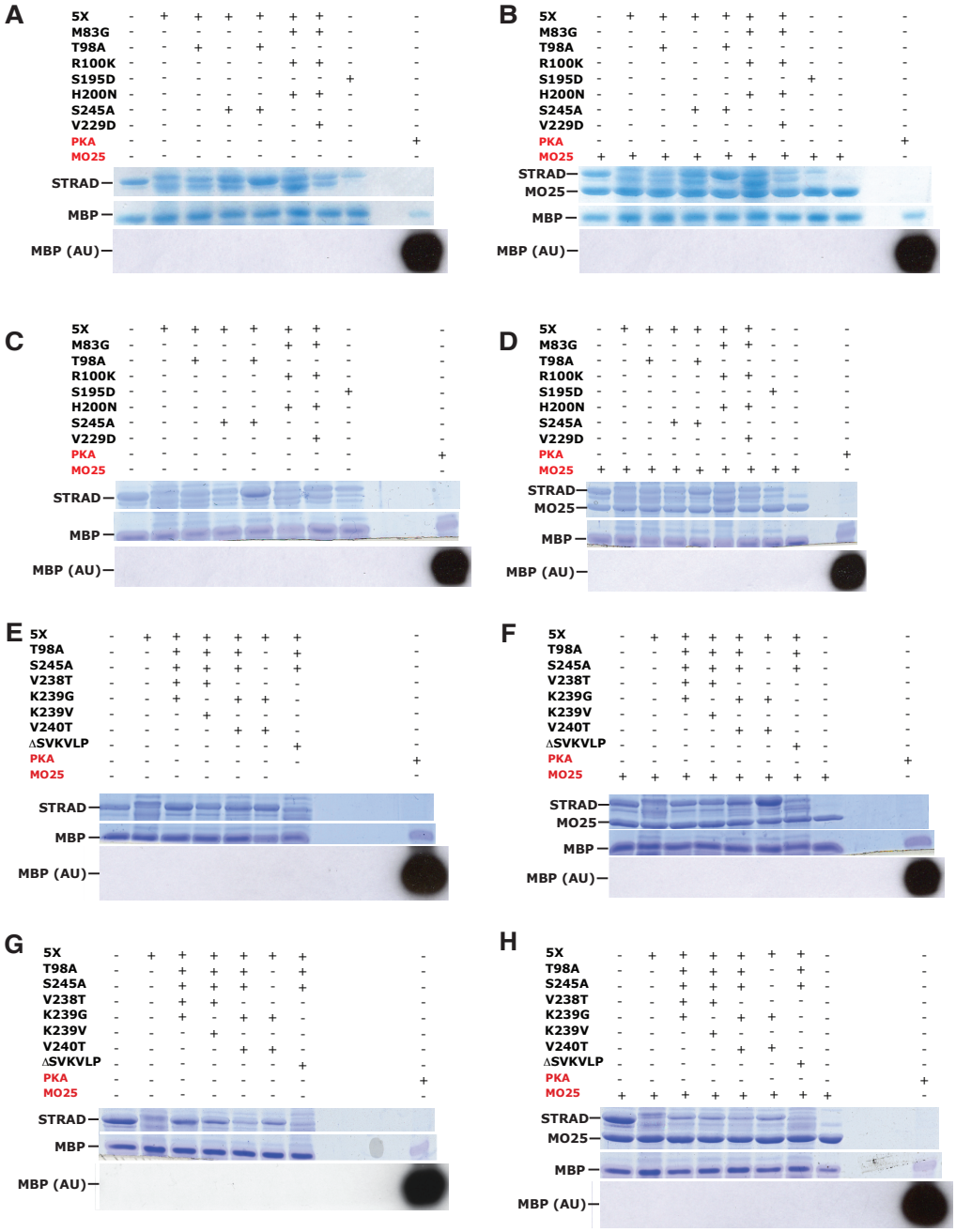

Figure 3.9: Attempts at reactivating the STRADα pseudokinase
The indicated STRADα (residues 59–431) active site mutants (A, B, C & D) and those combined with mutations/deletions from the p+1 site of the kinase (E, F, G & H) were expressed in *E. coli* and tested for kinase activity towards the generic substrate MBP. Panels A, B, E & F were tested in the presence of 0.2 mM γ-^{32}P-ATP and 10 mM magnesium acetate, whereas panels C, D, G, and H were tested in the absence of Mg^{2+} and presence of 2 mM EDTA. Where indicated, wild-type MO25α was included in the assay. In all cases, PKA assayed in the presence of Mg^{2+} was included as a positive control. *(5X = T98A + R100K + G213D + L214F + R215G)*

ever, none of these mutants showed autophosphorylation or phosphorylated myelin basic protein in the presence or absence of Mg^{2+}ATP and/or MO25α (Fig. 3.9). Similarly, mutations in the putative (protein) substrate binding site of STRADα were generated either separately, or in combination with other potential catalytic residue mutations. None of these mutations restored catalytic activity of STRADα (Fig. 3.9). Recent reports have suggested that some pseudokinases (e.g CASK) may be inhibited by the presence of Mg^{2+} ions (Mukherjee et al., 2008). Repeating the kinase assays mentioned above in the absence of $MgCl_2$, did not result in detectable STRADα kinase activity (Fig. 3.9).

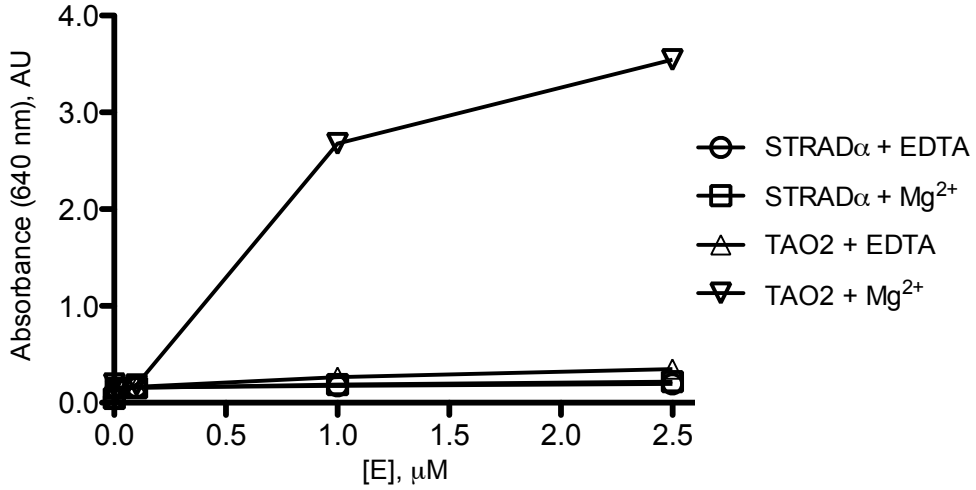

Figure 3.10: STRADα ATPase assay
Crystallisation grade purified STRADα (residues 59-431) was assayed for the ability to hydrolise ATP. A range of protein (E) concentrations (0.01-2.5 μM) were tested over 4 h at 20 ^oC. Bacterially purified TAO2 was used as control.

In order to test wheather STRADα possessed ATPase activity, a sensitive ATPase assay kit (Innova Biosciences, UK), was employed.

However, no activity for STRADα was observed, even at longer time points (up to 4 hours, Fig. 3.10). Nevertheless, it is impossible to categorically rule out that STRADα will not, highly specifically, phosphorylate an as yet unidentified substrate, or need an additional activatory factor/modification.

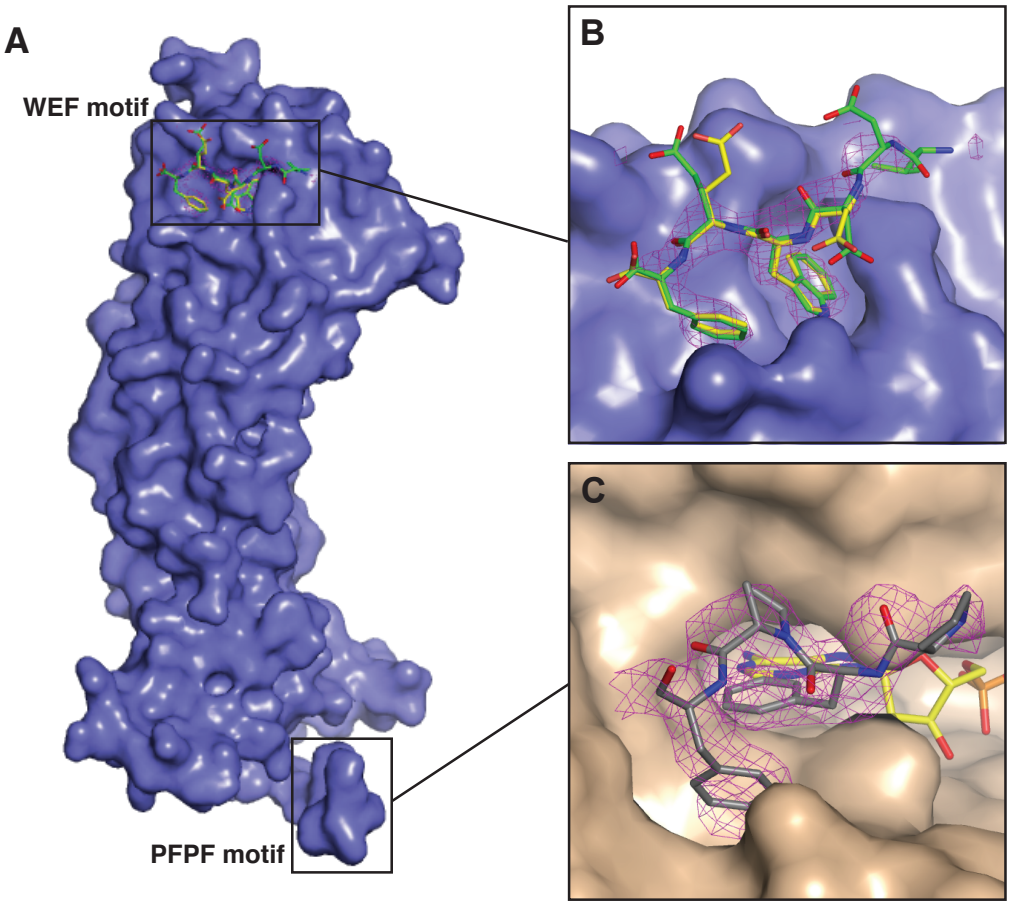

Figure 3.11: Previously described and new intermolecular interactions between STRADα and MO25α
A & B) Molecular surface of MO25α and comparison of STRADα WEF motif, binding to the MO25α WEF pocket. WEF motifs from the STRADα/MO25α complex structure and MO25α/peptide complex determined previously by Milburn *et al.*, (Milburn et al., 2004), are superimposed and shown as stick models with green and yellow carbon atoms respectively. Unbiased electron density maps (F_o-F_c are shown for the WEF motif determined in this thesis and contoured at 2.5σ).
C) The PFPF motif of MO25α that binds to a STRADα hydrophobic pocket (molecular surface coloured wheat), near the ATP binding site is shown as sticks with gray carbons. Electron density maps are displayed as described above. Part of the ATP molecule is also shown with yellow coloured carbons.

3.5 Analysis of the STRADα/MO25α complex

3.5.1 Identification of the biological STRADα/MO25α complex

The asymmetric unit of the STRADα/MO25α complex crystals contains one molecule of MO25α, with a conformation similar to the previously published MO25α/WEF peptide complex structure (Milburn et al., 2004) (RMSD = 0.6 Å on 292 Cα atoms), and one molecule of STRADα (Table 3.1). The position and conformation of the WEF motif is similar to that in the previously described MO25α/WEF complex (Milburn et al., 2004) (RMSD = 0.3 Å on 35 atoms and Fig. 3.11A and B). A second, intermolecular interaction was observed between residues 2-5 of MO25α (Pro-Phe-Pro-Phe, termed the PFPF motif here) and a hydrophobic pocket adjacent to the ATP binding groove of STRADα (Fig. 3.11A and C).

Table 3.2: Summary of buried surface areas in STRADα/MO25α crystal packing and straight line distances from the last visible STRADα residue to the first visible WEF motif residue. Entries of the total column do not include the surface area buried by the WEF motif (1050 Å^2), identical for all five possible complexes.

		Buried surface area (Å^2)		
Complex	Distance (Å)	His-tag	PSK domain	Total
A	49.6	720	2250	2970
B	82.5	0	1450	1450
C	72.4	0	420	420
D	56.0	1170	380	1550
E	31.4	0	50	50

PSK domain = pseudokinase domain

Due to tight crystal contacts (total buried surface on MO25α by

STRADα and its symmetry mates = 3550 Å^2) it was not immediately apparent which contacts represented biologically relevant interactions and which were crystallographic packing artefacts. While clear electron density is present for the last six amino acids of STRADα (residues 425–431, including the WEF motif that interacts with MO25α, Fig. 3.11B), residues 402-424 of STRADα were not visible in the electron density maps, and it was thus not possible to directly identify the appropriate symmetry mates of STRADα and MO25α that make up the biologically relevant binary complex. Analysis of the crystal contacts between symmetry related molecules suggested that there were five possible ways in which STRADα could interact with MO25α (Fig. 3.12). The five possible STRADα/MO25α complexes were studied and these were ranked in terms of total buried surface area, a possible method for distinguishing crystallographic from biological contacts (Nooren and Thornton, 2003). Discounting the WEF motif interaction (1050 Å^2 buried surface area), identical in all five possible complexes, the buried surface area in each of the possible complexes is 2970 Å^2, 1450 Å^2, 420 Å^2, 1150 Å^2 and 50 for complexes A, B, C, D and E respectively (Table 3.2 and Fig. 3.13). In addition, the distances between the last well-defined residue of the STRADα C-terminal lobe and the first well-defined residue of the WEF motif at the extreme C-

terminus of STRADα were measured for the five possible complexes. This yielded direct distances of 50, 82, 72, 56 and 31 Å for complexes A, B, C, D and E respectively (Table 3.2 and Fig. 3.12). Taken together, it appears that complex A (Fig. **??**A) is the most likely biological interaction, since STRADα binds to the (highly conserved) concave surface of MO25α and has the largest buried surface area, while also possessing a distance connectable by the missing residues (23 amino acids) from the C-terminal lobe to the WEF motif (Table 3.2 and Fig. 3.12). Similarly, analysis of the possible complexes with PISA (Krissinel and Henrick, 2007) yields the highest (1.0) Complexation Significance Score (CSS) for complex A, while predicting that complexes B, C, D and E will not be stable in solution.

The 6-His purification tag that extends from the N-terminus of STRADα (720 Å^2 and 1170 Å^2 buried surface area in complex A and D respectively) forms additional contacts between MO25α and STRADα (Table 3.2 and Figs. 3.12 and 3.13D). Surface plasmon resonance (SPR) studies demonstrate that His-tagged STRADα binds MO25α *in vitro* with the same affinity as STRADα lacking the His tag (Fig. A.2 and Table 3.3). Furthermore, MO25α residues 2-5 (PFPF motif) make hydrophobic contacts in a pocket of a symmetry related copy of STRADα (Figs. 3.11C and 3.13B). This is unlikely to constitute

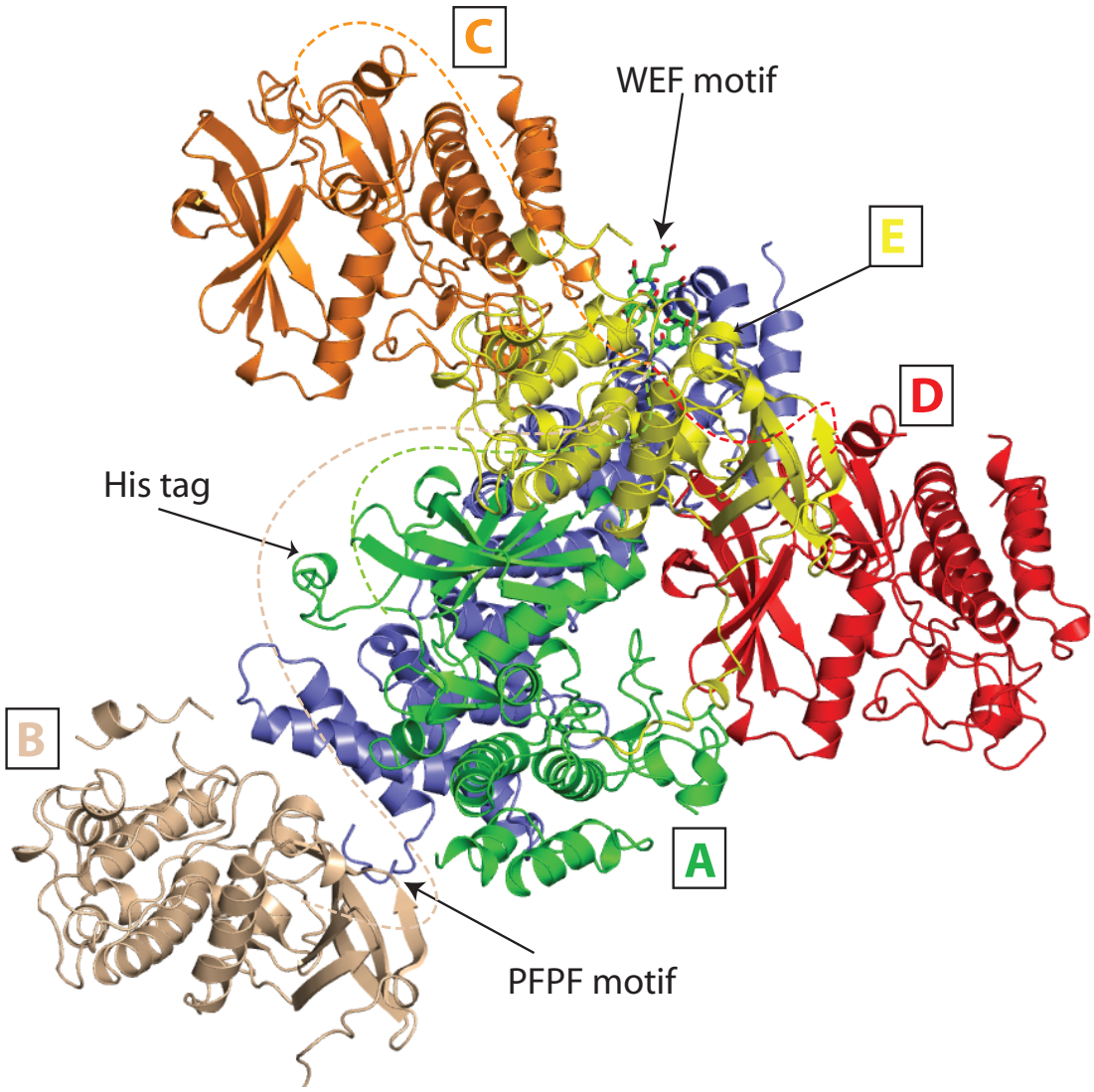

Figure 3.12: Crystallographic contacts and possible STRADα/MO25α interactions
Cartoon representations of MO25α (blue) and symmetry related STRADα molecules. The STRADα WEF motif bound to MO25α is shown as sticks with green carbons. Dashed lines represent the distance from the last residue of the C-terminal lobe of each STRADα molecule able to donate the WEF motif, corresponding to 50, 82, 72, 56 and 31 Å (straight-line distances) for molecules A, B, C, D and E respectively. An additional tight crystallographic contact, through the MO25α N-terminus ("PFPF motif") is also indicated and further discussed in section 3.5.1.

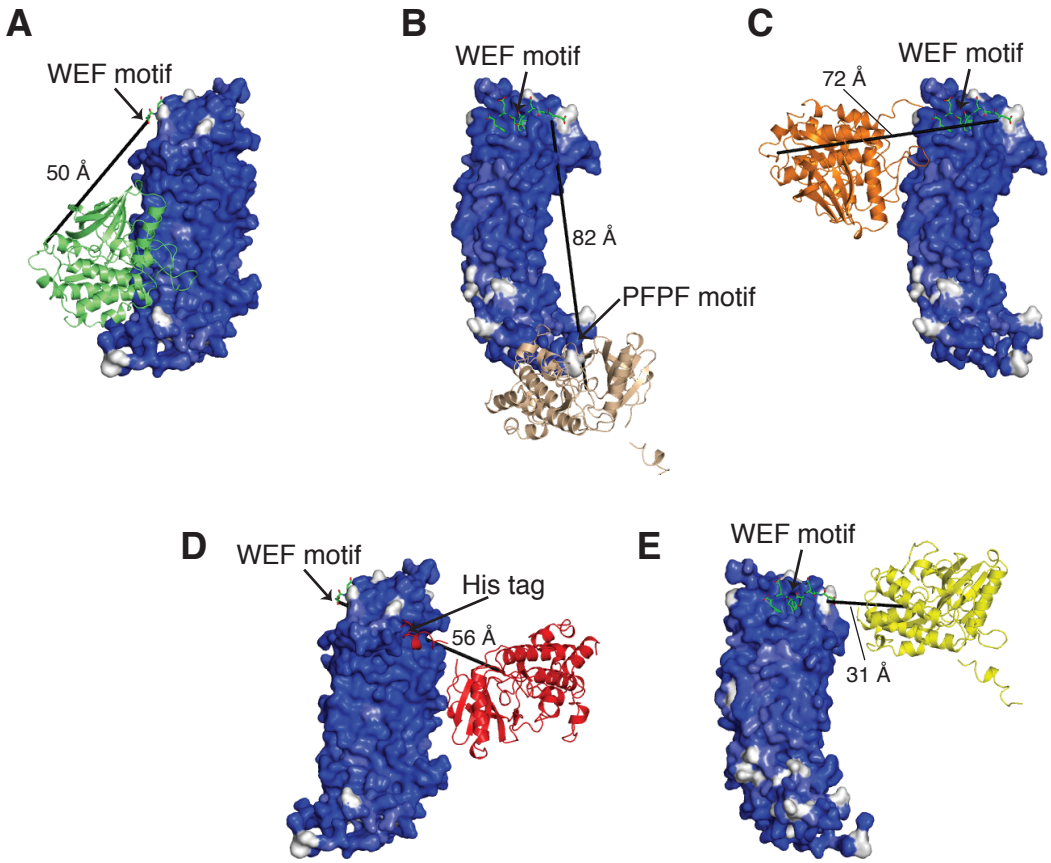

Figure 3.13: Possible STRADα/MO25α complexes
The molecular surface of MO25α is shown and coloured by sequence conservation (dark blue = conserved, white = not conserved; multiple sequence alignment provided in Fig. 3.20). The WEF motif bound to MO25α is shown as sticks with green carbons. The five possible STRADα/MO25α interactions are shown (A-E), with STRADα represented as different coloured cartoons. Direct distances from the last residue of the C-terminal lobe of each STRADα molecule able to donate the WEF motif are represented by a line and labelled. Distances and buried surface areas for each possible complex are sumarised in Table 3.2.

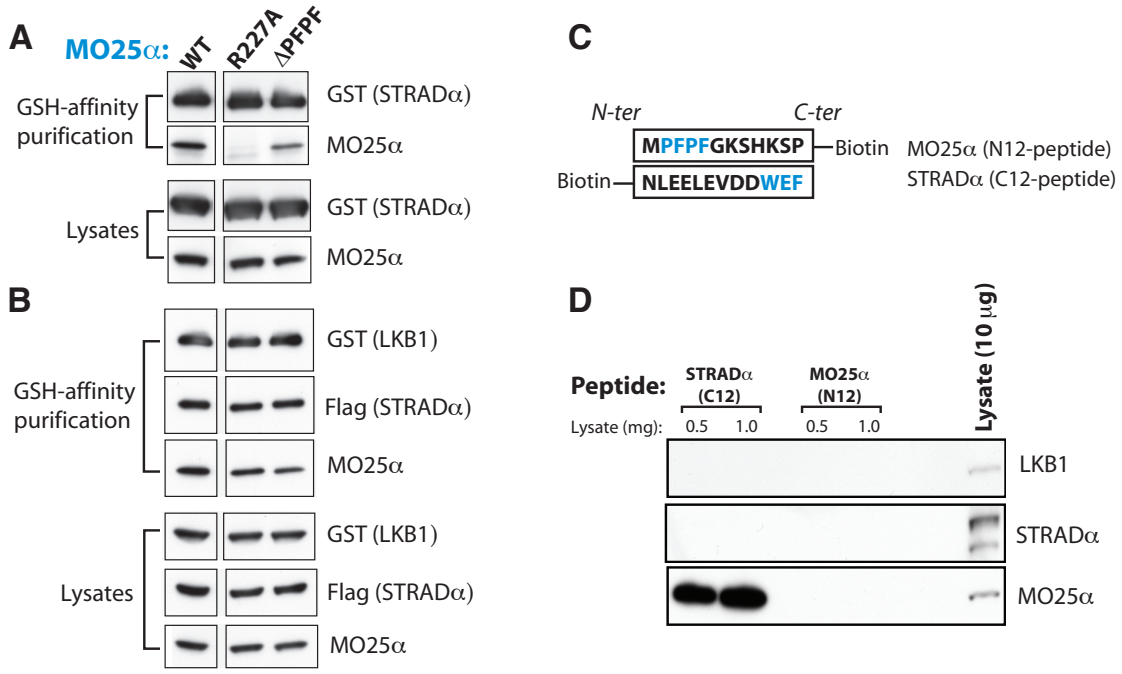

Figure 3.14: The PFPF motif is not required for MO25α interaction with STRADα or LKB1

A) The indicated constructs of GST-STRADα and untagged MO25α were expressed in 293 cells. Cells were lysed 36 h post-transfection and GST-STRADα was affinity purified on glutathione-Sepharose. The purified GST-STRADα preparation (upper panels) as well as the cell extracts (lower panel), were immunoblotted with the indicated antibodies. STRADα R227A mutant unable to bind MO25α was used as a control (this is discussed in detail in sections 3.5.2 and 3.5.3)

B) Wild type GST-LKB1 and indicated forms of Flag-STRADα and untagged MO25α were co-transfected in 293 cells. Cells 36 h post-transfection were lysed and GST-LKB1 was affinity purified on glutathione-Sepharose. The purified GST-LKB1 preparations (upper panels) as well as the cell extracts (lower panel) were immunoblotted with the indicated antibodies.

C & D) 0.5 or 1.0 mg of 293 cell lysates were incubated with 5 μg of the indicated biotinylated peptides conjugated to Streptavidin-Sepharose. Following isolation and washing of the beads, the samples were subjected to SDS-polyacrylamide gel electrophoresis and immunoblotted with the indicated antibodies to detect endogenous STRADα and MO25α.

(Experiment was carried out by Dr Jérôme Boudeau)

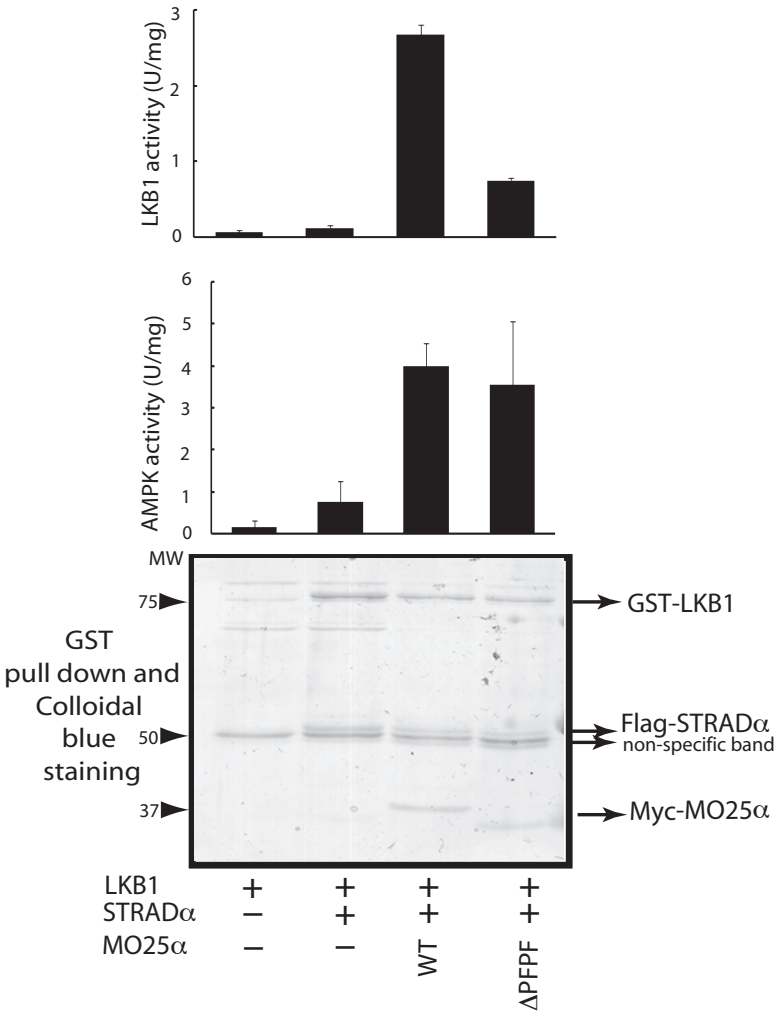

Figure 3.15: Deletion of the MO25α PFPF motif does not impair LKB1 activity Activation of the bacterially expressed AMPK complex using wild type or mutant (ΔPFPF) LKB1/STRADα/MO25α complex. The purity of LKB1 complexes was analysed by SDS-PAGE and colloidal blue-staining.

a physiological STRADα/MO25α interaction, as deleting this motif did not impair the *in vivo* interaction of MO25α with either STRADα alone or a complex of STRADα and LKB1 (Fig. 3.14A and B). Moreover, it was not possible to affinity purify STRADα or LKB1 from a cell extract employing a PFPF motif containing biotinylated peptide (Fig. 3.14C and D). A complex of LKB1/STRADα/MO25α(ΔPFPF) still activated the heterotrimeric AMPK complex expressed in *E. coli* with similar efficiency as wild type LKB1/STRADα/MO25α (Fig.

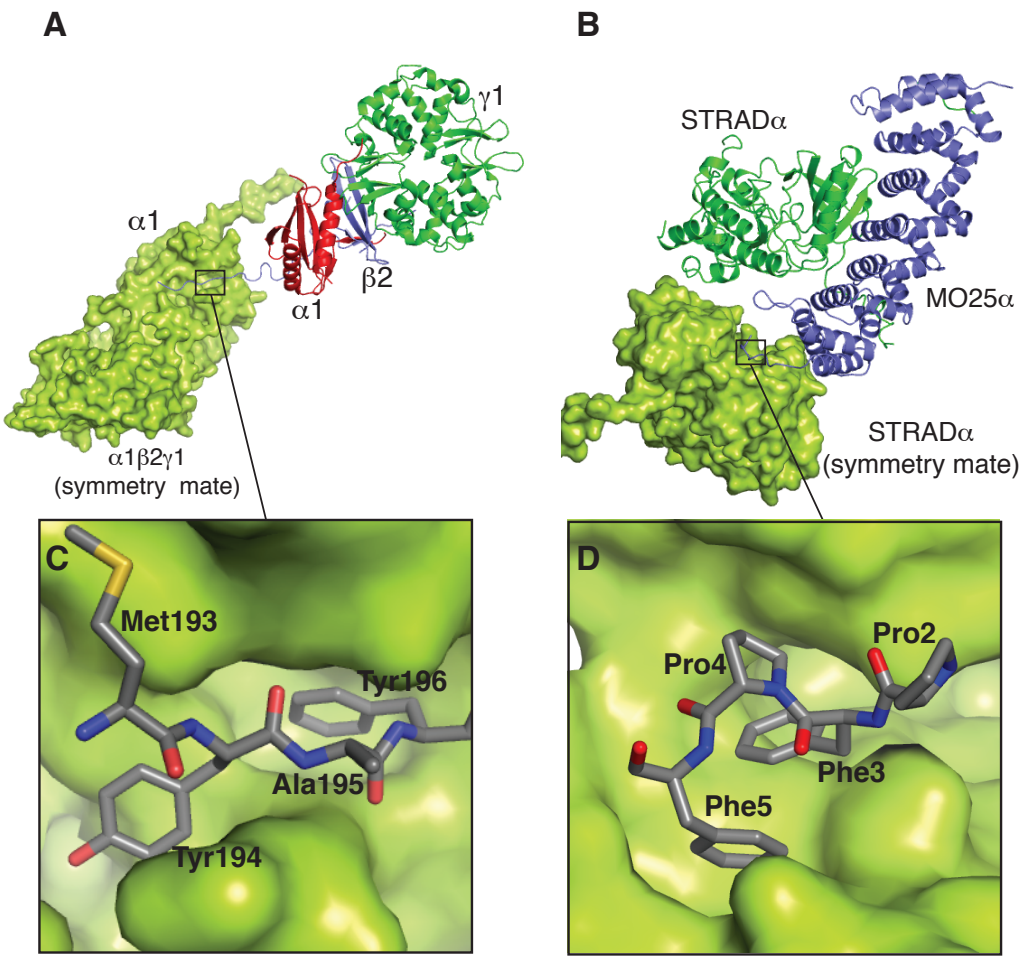

Figure 3.16: Similarities between crystallographic contacts of the AMPK subunits and the STRADα/MO25α comlpex
A) Structure of the AMPK core complex ($\alpha1/\beta2/\gamma1$ subunits) determined by Xiao et al. (2007) is shown as cartoon model. The molecular surface of a symmetry related $\alpha1/\beta2/\gamma1$ comlpex is also shown and coloured green. Part of the interchanging loop from the $\beta2$ subunit is boxed.
B) STRADα/MO25α complex (cartoon model) and a symetry related STRADα is shown with the molecular surface coloured green. The PFPF motif is boxed.

3.15). Nevertheless, it is possible that the PFPF docking site on STRADα does play a role in enabling STRADα to interact with other regulators or substrates of the LKB1 complex. Intriguingly, a similar crystallographic interaction can be observed in the structure of the mammalian AMPK heterotrimeric complex (Fig. 3.16, (Xiao et al., 2007)). In this case, a similar hydrophobic N-terminal motif "MYAF" from the $\beta2$ domain interacts with the kinase domain from the neigh-

bouring molecule in the crystal lattice, albeit not near the phosphonucleotide binding site.

3.5.2 STRADα interacts with the MO25α concave surface

MO25α is composed of seven structurally similar α-helical repeats (named R0-R6) that form a horseshoe-shaped molecule with a concave and convex surface (Milburn et al., 2004). MO25α helical repeats R1-R6 consist of three α-helices (H1-H3) each, while repeat R0 consists of only two helices (Milburn et al., 2004). Helices H3 from repeat R1-R5 are arranged in an almost parallel fashion and make up the concave surface of MO25α (Fig. 3.17). Other helical repeat adaptor proteins, such as PUM1, β-catenin and importin-α, make use of a similar concave surface to interact with macromolecular partners (Wang et al., 2001; Graham et al., 2000; Conti and Kuriyan, 2000). Strikingly, the crystal structure of the STRADα/MO25α complex reveals that, in addition to the interaction through the WEF motif, a major additional binding interface involves the STRADα N-terminal kinase lobe and the MO25α concave surface (Figs. 3.17 and 3.18). Part of the interaction surface on STRADα is N-terminal to the αC helix and comprises the loop between the αB/αC helices (residues 104-109), termed the "αB site" here (Figs. 3.17B and 3.18A). This region forms an extensive hydrogen-bonding network centered on Arg227 from the R5-H3 of

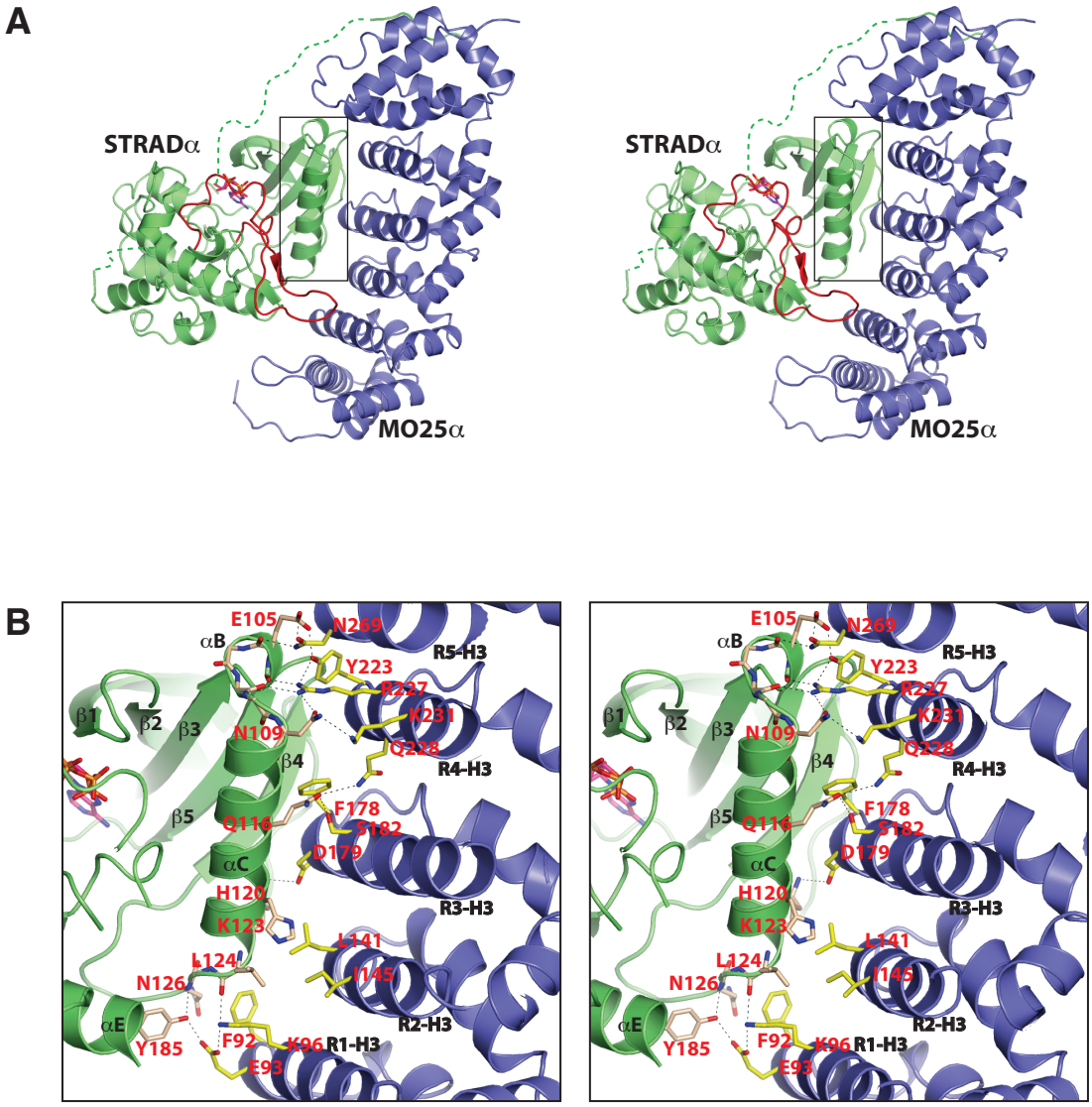

Figure 3.17: STRADα binds to MO25α concave surface of MO25α
A) Stereo view of the structure of complex A where STRADα and MO25α are coloured green and blue respectively. ATP bound to STRADα is shown as sticks with magenta carbons. The STRADα activaton segment is coloured red and the regulatory αC helix is boxed.
B) Stereo view of the main STRADα/MO25α interactions centered around helix αC. Residues that make direct contact are shown as sticks, with hydrogen bonds shown as dotted black lines.

MO25α (Fig. 3.17B), burying a total of 245 Å^2 surface area. Residues Tyr223, Arg227, Lys231 and Asn269 of MO25α engage the side chains of residues Glu105 and Asn109 of STRADα, while Leu104, Ala106, Cys107 and Ser108 contribute to the interaction via their backbone atoms (Fig. 3.17B).

The αC helix of STRADα runs along the concave surface of MO25α facing the H3 helixes of the MO25α repeats R4, R3 and R2 (Figs. 3.17 and 3.18A, termed the "αC site" here). Tethered by hydrophobic and hydrogen bonding interactions Fig. 3.17B, the αC helix forms the major interaction surface, contributing a total of 405 Å^2 buried surface area on the MO25α concave surface.

C-terminal to the αC helix, a second hydrogen-bonding network with comparable buried surface area (270 Å^2) to the "αB site" is present, and involves residues Leu124, Asn126 and Tyr185 from the STRADα helix αE (Figs. 3.17B and 3.18A, termed the "αE site" here). This region interacts with Glu93, Lys96 and Phe92 from the R1-H3 helix of MO25α (Fig. 3.17B). Together, the "αB site" and the "αE site" appear to act as anchor regions, positioning the αC helix to run along the H3 helices of R1-R5 of MO25α.

Additional interactions are found between Phe178 of MO25α, forming hydrophobic stacking interactions with residues from the N-terminal

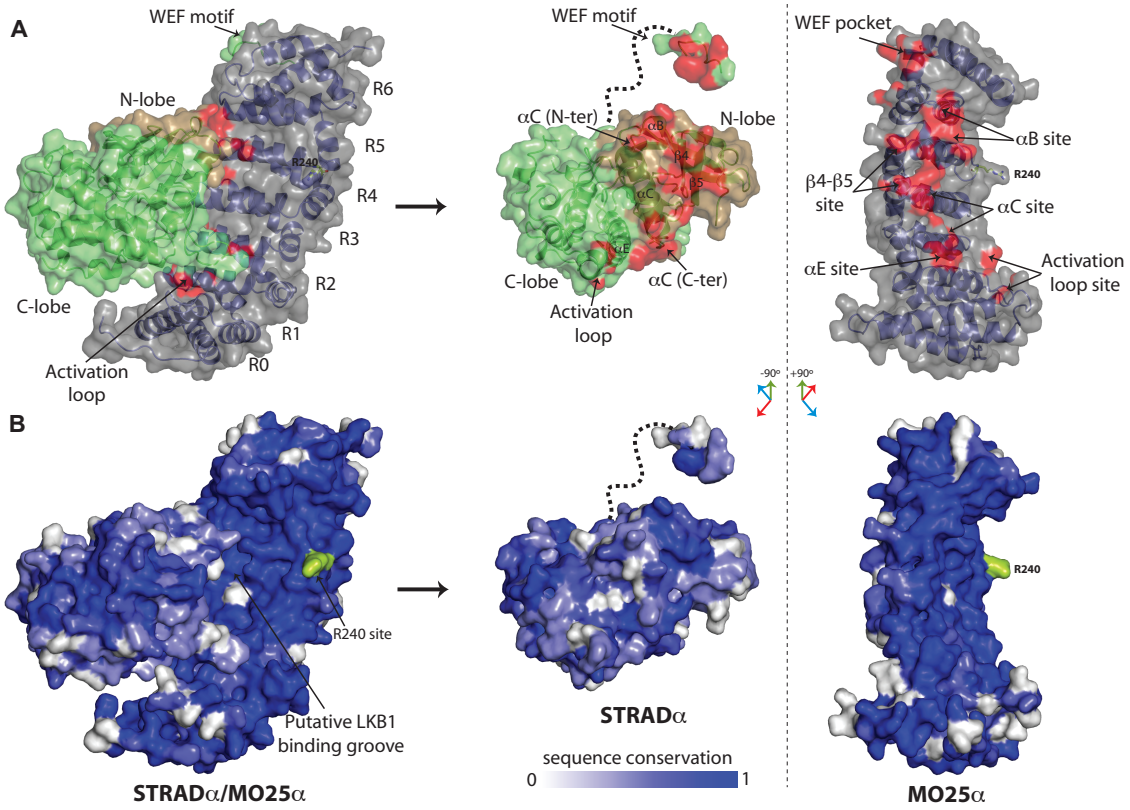

Figure 3.18: Sites of the STRADα/MO25α interaction and sequence conservation
A) STRADα/MO25α complex and the interaction surface, as defined with the program CONTACT from the CCP4 package (Collaborative Computational Project, 1994). Surfaces of atom pairs closer than 3.9 Å are coloured red. The MO25α surface is coloured grey and the N-and C-lobes of STRADα are coloured brown and lime green, respectively. Arg240 is shown as sticks. To aid visualization, on the right side of the figure, the complex is "opened up" by rotating the STRADα molecule about the vertical axes -90^o and MO25α +90^o with respect to the binary complex.
B) Sequence conservation (dark blue = conserved, white = not conserved) of STRADα and MO25α from *C. elegans* to *H. sapiens* (sequence alignments provided in Figs. 3.19 and 3.20). The putative LKB1 binding pocket and the Arg240 site are indicated with an arrow. STRADα and MO25α are shown in the same orientation as in panel (A) to aid visualization of conserved areas that are buried in the STRADα/MO25α complex.

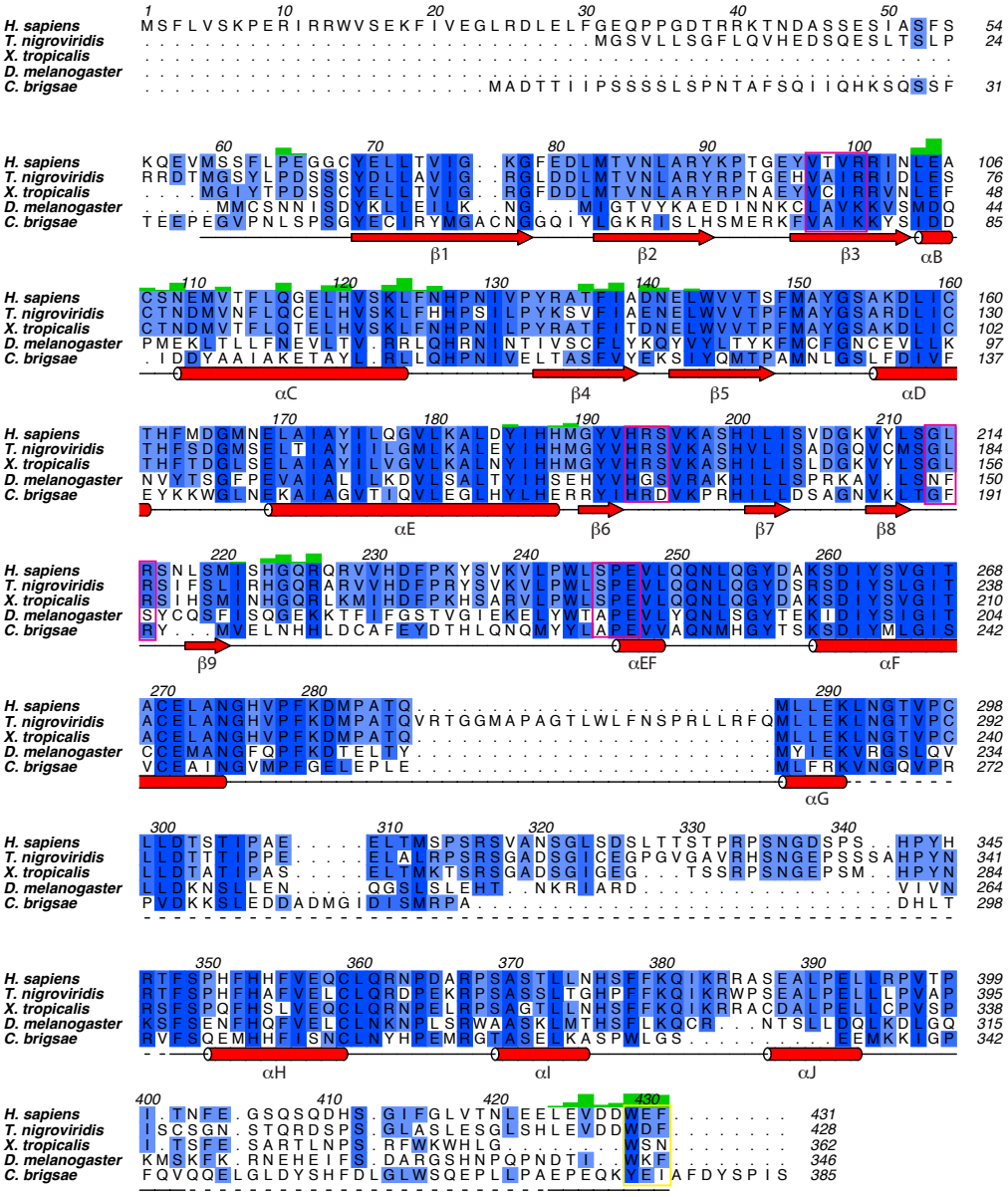

Figure 3.19: STRADα multiple sequence alignement, secondary structure and residues contributing to the interactions with MO25α

Multiple sequence alignment (dark blue = conserved, white = not conserved) of STRADα from the indicated species of the metazoan kingdom. Alignments were performed with MUSCLE (Edgar, 2004) and edited and displayed using ALINE (Bond and Schüttelkopf, 2009). A graph of residues involved in STRADα/MO25α interaction against their contact area (green bars), is displayed. Height of the bar represents the contact area (atom pairs closer than 3.9 Å, analysed by CONTACT from the CCP4 package (Collaborative Computational Project, 1994)), divided by the total surface area of the participating amino acid. Key STRADα catalytic motifs and the WEF motif are boxed. The secondary structure (analysed by DSSP (Kabsch and Sander, 1983)) is shown in red. Dotted lines represent residues missing in the structural model. The same colouring graph has been applied to the molecular surfaces shown in Fig. 3.18

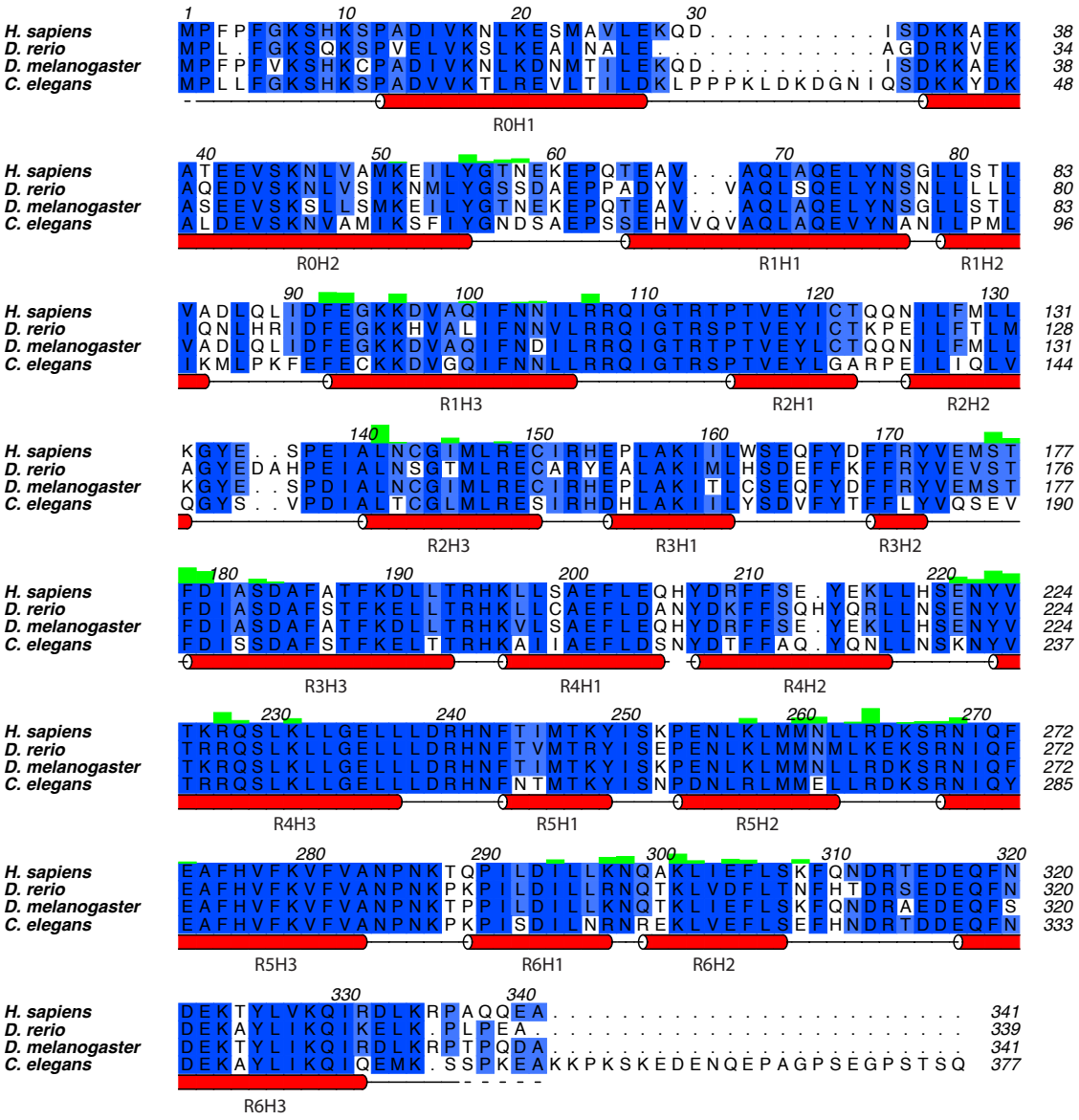

Figure 3.20: MO25α multiple sequence alignement, secondary structure and residues contributing to the interactions with STRADα

Multiple sequence alignment (dark blue = conserved, white = not conserved) of MO25α from the indicated species of the metazoan kingdom. Alignments were performed with MUSCLE (Edgar, 2004) and edited and displayed using ALINE (Bond and Schüttelkopf, 2009). A graph of residues involved in STRADα/MO25α interaction against their contact area (green bars), is displayed. Height of the bar represents the contact area (atom pairs closer than 3.9 Å, analysed by CONTACT from the CCP4 package (Collaborative Computational Project, 1994)), divided by the total surface area of the participating amino acid. Key STRADα catalytic motifs and the WEF motif are boxed. The secondary structure (analysed by DSSP (Kabsch and Sander, 1983)) is shown in red. Dotted lines represent residues missing in the structural model. The same colouring graph has been applied to the molecular surfaces shown in Fig. 3.18

β4 and β5 strands of STRADα (termed the "β4/β5 site" here, Figs. 3.17B and 3.18A). STRADα and STRADβ also possess an insertion of ten residues (221-229) in the activation loop that is not observed in the closely related TAO2 or other STE20 kinases (Fig. 1A). Within this insertion, His223, Gly224, and Arg226 show weak interactions with the R0 and R1 helical repeat of MO25α (termed the "activation loop site" here, (Fig. 3.18A). This interaction perhaps explains why the STRADα activation-loop is ordered, although a large part of the activation segment, including the p+1 loop is solvent exposed (Fig. 3.17A). All of the key STRADα/MO25α interacting residues are highly conserved between species (Figs. 3.18, 3.19 and 3.20).

3.5.3 The MO25α concave surface is required for STRADα binding

The structure of the STRADα/MO25α complex reveals that in addition to the WEF binding pocket on the convex surface of MO25α, a major interaction network between STRADα and the concave surface of MO25α exists. This involves the αB, αC, αE, β4/β5 and activation loop sites. To test the importance of these additional interactions, mutations of key interacting residues located on the MO25α concave surface were tested for their ability to interact with STRADα. MO25α residues present in the novel αB, αC, αE, β4/β5, and activation loop binding sites as well as the previously characterised WEF

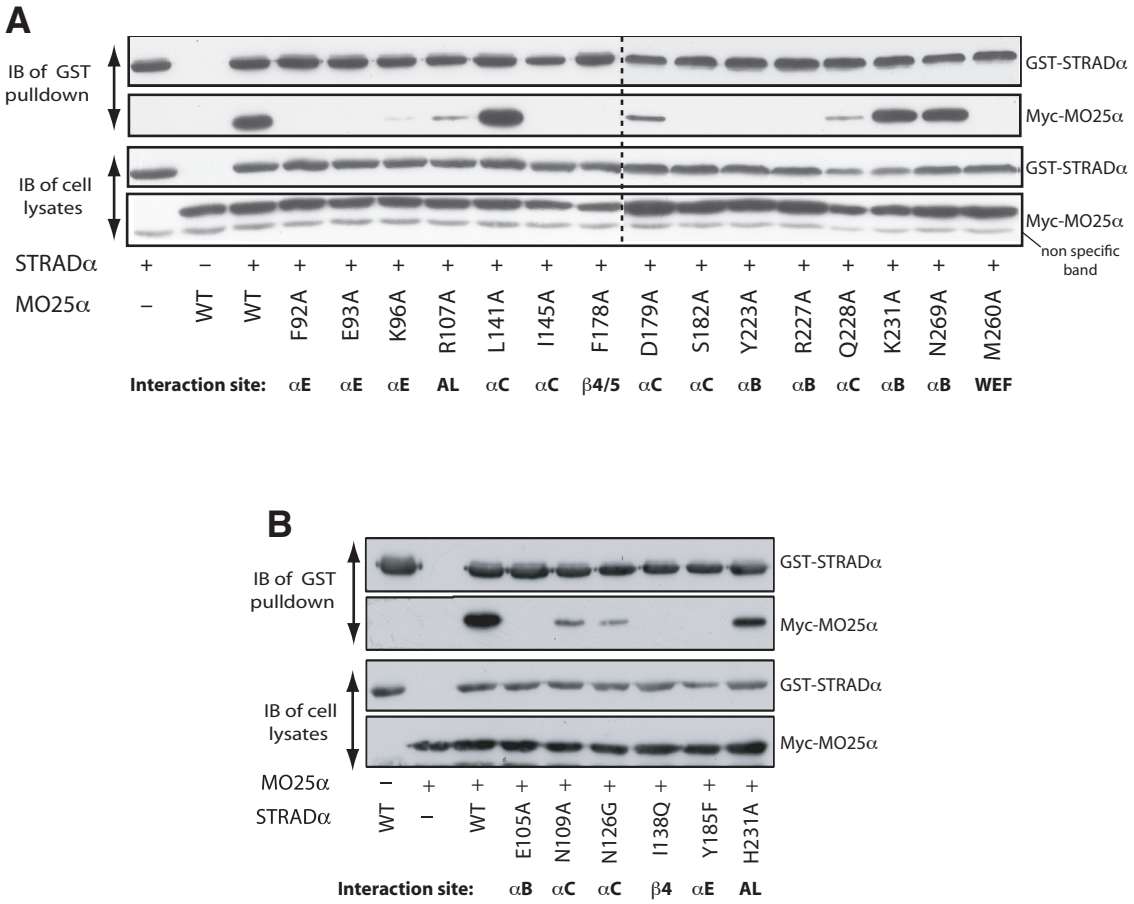

Figure 3.21: Mutation of MO25α concave surface residues abolishes STRADα binding Mutant forms of STRADα (A) and MO25α (B) were tested for their ability to form cellular complexes in a GST pulldown assay. Indicated constructs of GST-STRADα and Myc-MO25α were expressed in 293 cells. Cells 36 h after transfection were lysed and GST-STRADα was purified with glutathione-Sepharose. The purified GST-STRADα preparation (upper panels) as well as the cell extracts (lower panel) were immunoblotted with the indicated antibodies. Similar results were obtained in 3 separate experiments. Dotted line indicates the junction of two gels; AL = activation loop.

pocket were mutated (Fig. 3.21). As reported previously, mutation of Met260 in the WEF pocket of MO25α abolishes its ability to interact with STRADα in HEK293 cells (Milburn et al., 2004). However, it was also observed that mutations in the two anchor regions (Phe92, Glu93, Lys96 from the αE site and Tyr223, Arg227 from the αB site) abolished MO25α binding to STRADα (Fig. 3.21A). Similarly, mutating Phe178 in the $\beta4/\beta5$ site, Ile145 and Ser182 in the αC site or Arg107 in the activation loop site, markedly disrupted the MO25α-STRADα interaction. Mutations of Leu141, Lys231 and Asn269 in the αC site did not significantly affect binding (Fig. 3.21A). Mutation of the reciprocal interacting residues on STRADα, including Glu105, Asn109, Asn126, Ile138 and Tyr185, also abolished or markedly reduced binding to MO25α (Fig. 3.21B). These results confirm the importance of the network of interactions between the concave surface of MO25α and STRADα in enabling the stable association between these two proteins, at least in the absence of LKB1.

Previous work has shown that MO25α mutants where the WEF pocket was disrupted and that were no longer able to form a complex with STRADα, were still capable of forming a heterotrimeric complex with LKB1 and STRADα (Boudeau et al., 2003a, 2004). Similarly, MO25α mutants in which key STRADα binding residues

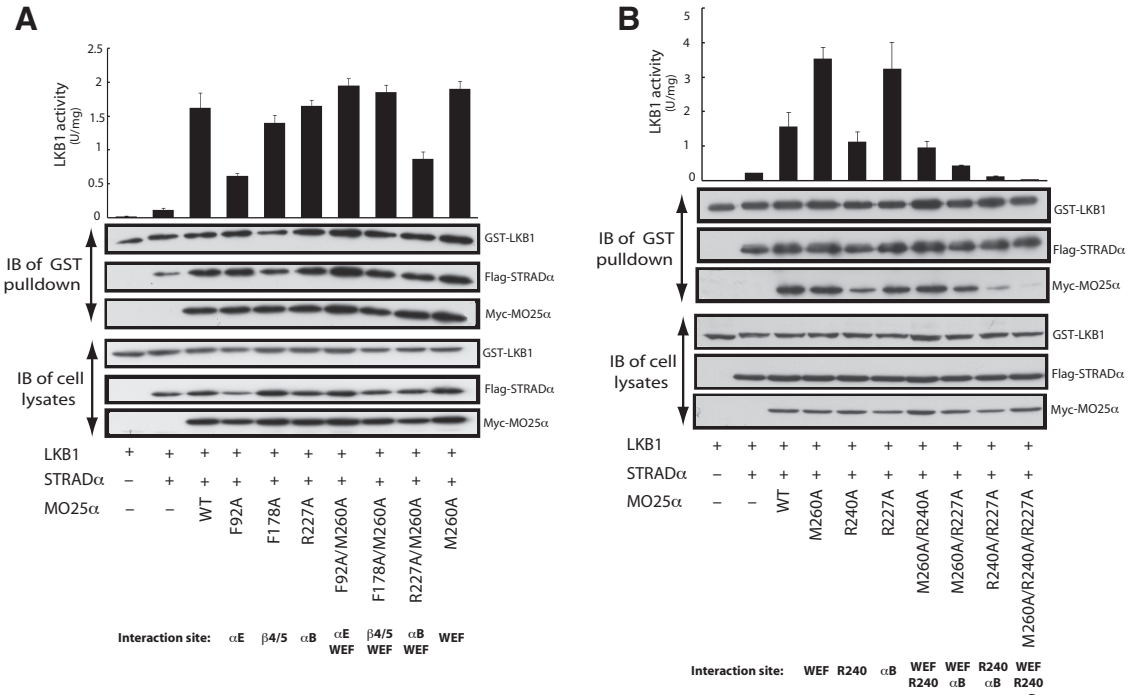

Figure 3.22: Mutation of MO25α residues abolishes LKB1/STRADα binding
293 cells were co-transfected with the indicated constructs of GST-LKB1, Flag-STRADα and Myc-MO25α. Cells 36 h after transfection were lysed and GST-LKB1 was purified and assayed for its ability to phosphorylate the LKBtide peptide. Kinase activities are representative of three independent assays carried out in triplicate (error bars represent the SD for 1 experiment). Affinity purified GST-LKB1 preparation (upper panel) as well as cell extracts (lower panel) were immunoblotted with the indicated antibodies.

located within the concave surface were mutated are still capable of interacting with the LKB1/STRADα complex (Fig. 3.22A). Even double MO25α mutants in which both the WEF pockets and the αB, αE, or $\beta 4/\beta 5$ sites were disrupted were capable of associating with the LKB1/STRADα complex (Fig. 3.22A). Moreover, the specific activity of LKB1/STRADα complexes associated with these MO25α mutants was either normal or only moderately reduced (Fig. 3.22A). This suggests the presence of additional interactions between MO25α and LKB1 in the presence of STRADα.

Earlier studies revealed that mutation of a conserved Arg240 residue

located on the concave surface of MO25α reduced interaction with LKB1 complexed to STRADα lacking the WEF motif (Boudeau et al., 2004). Arg240 might be involved in interaction with LKB1, as this residue is located on the concave surface of MO25α, distant from STRADα (Fig. 3.18). To further investigate the role of Arg240 in enabling MO25α to associate with LKB1/STRADα, Arg240 was mutated alone or in combination with residues in either the WEF pocket (Met260) or the αB STRADα binding sites (Arg227). Mutation of Arg240 alone does not prevent MO25α from interacting with LKB1/STRADα (Fig. 3.22B). However, a double MO25α mutant lacking Arg240 and a key concave surface-binding site in the αB site (Arg227), markedly impaired binding to LKB1/STRADα (Fig. 3.22B). A triple mutant of MO25α lacking Arg240, Arg227 and the WEF pocket sites, failed to associate with LKB1/STRADα and stimulate LKB1 activity (Fig. 3.22B). These observations indicate that MO25α possesses three sites with which it can interact with the LKB1/STRADα complex (Fig. 3.18), namely two STRADα binding regions (extensive concave MO25α surface and WEF pocket) as well as a putative LKB1 binding site (Arg240).

3.5.4 The STRADα/MO25α interaction is similar to the CDK/cyclin complex

Inspection of the STRADα/MO25α complex reveals an unexpected resemblance to the interaction between activated cyclin-dependent kinase 2 (CDK2) and its activating regulatory subunit Cyclin A (Fig. 3.23) (Jeffrey et al., 1995). Although MO25α/β isoforms are not related to cyclins at the primary sequence level, both proteins consist of multiple α-helical repeats. Crystal structures of CDK2/Cyclin A complex have revealed cyclin A binds to the so-called "PSTAIRE (αC) helix" of CDK2 kinase as well as the loop immediately preceding this helix (Jeffrey et al., 1995). Comparisons between free CDK2 and CDK2/cyclin A complex structures have shown that the cyclin molecule orients a conserved glutamate residue (Glu51) from the αC helix of the protein kinase to allow formation of an ion pair with a lysine residue (Lys33) from the conserved VAIK motif (Jeffrey et al., 1995), that keeps the CDK2 kinase in a closed conformation (Fig. 3.23B). Similarly, the position of MO25α in the STRADα/MO25α complex is centered on helix αC and the loop preceding this helix (αB region; Fig. 3.17B). The interaction between Glu118 from the αC helix and Arg100 from the VAIK (VTVR in STRADα) motif (analogous to the Glu51-Lys33 interaction in CDK2) is maintained, albeit via two water molecules (Fig. 3.7).

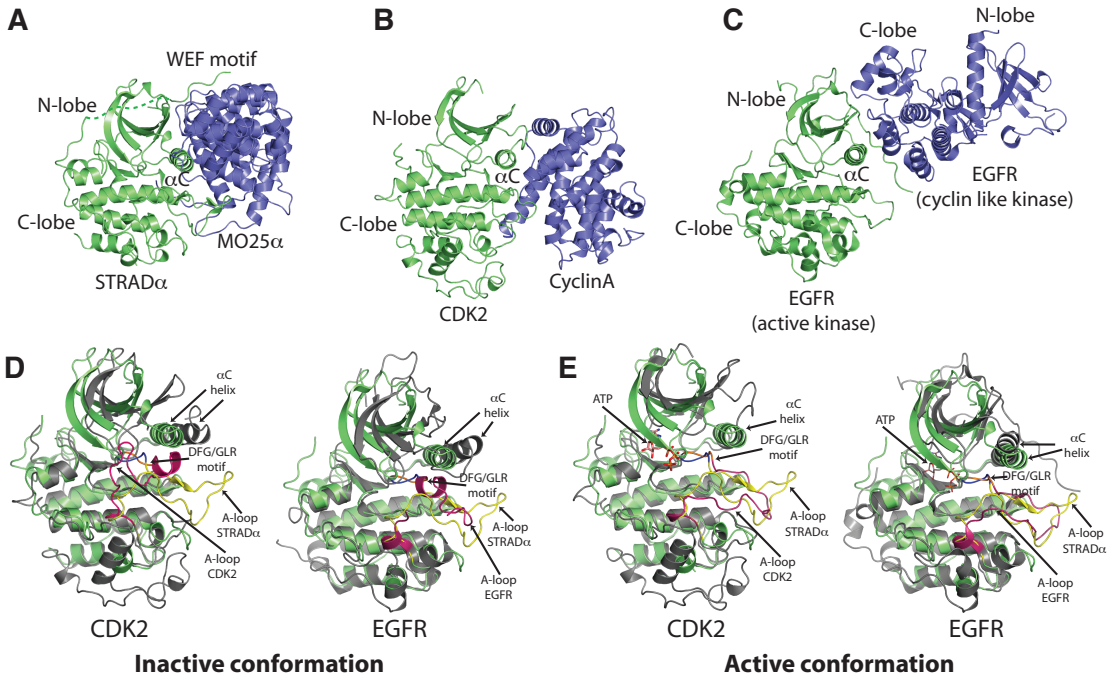

Figure 3.23: Structural comparison of the STRADα/MO25α interaction
Resemblance of (A) STRADα/MO25α complex with (B) the CDK2/cyclin A complex (PDBID 1FIN) and (C) the EGFR/EGFR kinase domain dimer (PDBID 2GS2). The kinases are shown as green ribbons, with the binding partners shown as blue ribbons. The αC helix, where binding of the "activator" is centered is labelled.
D & E) Comparison of the STRADα structure (green) to the active and inactive structures of CDK2 and EGFR (gray). Residues from the C-lobe of STRADα (152-431) were superimposed onto the structures of inactive CDK2 (PDBID 1HCK (Schulze-Gahmen et al., 1996)) and EGFR kinase (PDBID 2GS7), and active CDK2 (PDBID 1JST) and EGFR (PDBID 2GS2). The activation loop of STRADα has been coloured yellow and the activation loops of CDK2 and EGFR kinases are shown in magenta.

Another example where this type of interaction is involved in regulating the activity of protein kinases is the ligand-induced dimerisation of the EGFR family of tyrosine kinases (Fig. 3.23C). Crystal structures of EGFR kinase domain and biochemical data demonstrate the importance of a dimer formation that involves the intermolecular interaction of the EGFR αC helix on one monomer and the C-lobe on the other monomer (Fig. 3.23C) (Zhang et al., 2006b). A comparison between the structure of active, dimeric EGFR kinase with the monomeric form reveals the role of dimerisation for keeping the EGFR kinase in the closed and active conformation. Similarly, the structure of STRADα in complex with MO25α resembles the closed conformation of both CDK2 and EGFR kinase, with its activation loop and αC helix positioned in an orientation that is typical of active protein kinases (Fig. 3.23D and E). Such regulatory mechanism may also explain why some members of the EGFR family of kinases that lack kinase activity and are classified as pseudokinases (Her3) are still able to exert their function (Zhang et al., 2006b), despite their "inactivatory" substitutions, similar to what has been observed for STRADα (Fig. 3.8).

The interactions in the EGFR homodimer, the CDK2/cyclin A heterodimer and the STRADα/MO25α complex are similar only in gen-

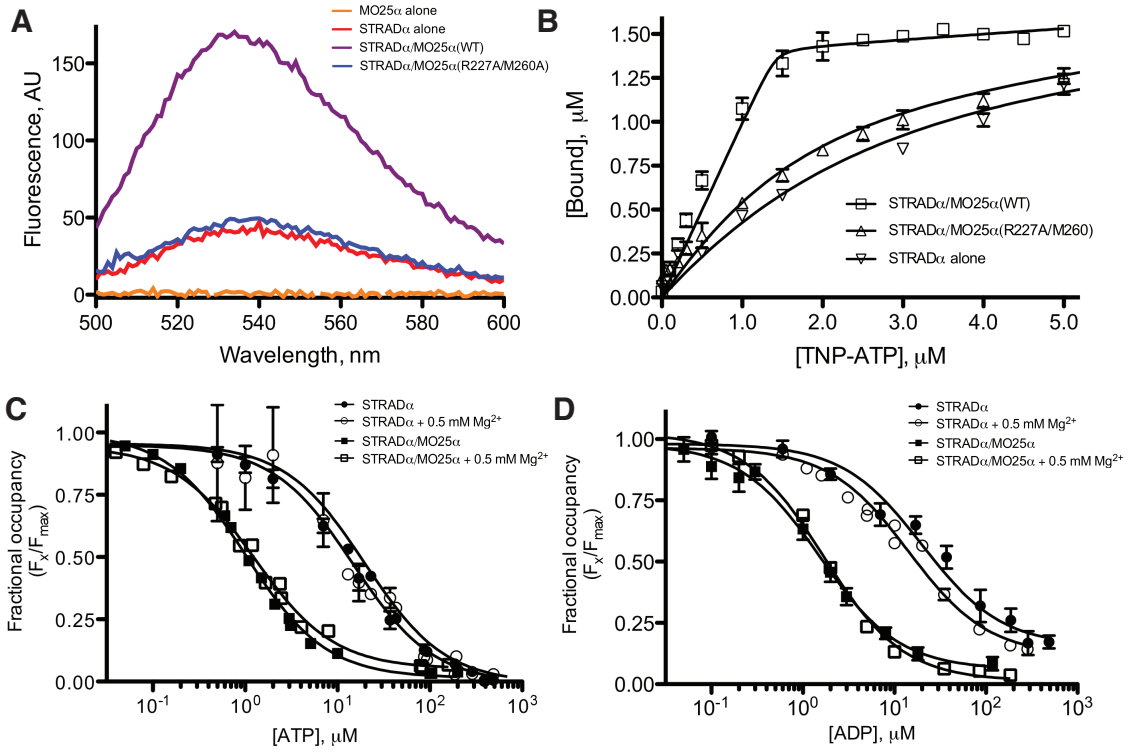

E

	$K_d^{TNP-ATP}$ (μM)		K_d^{ATP} (μM)		K_d^{ADP} (μM)	
	No Mg^{2+}	0.5 mM Mg^{2+}	No Mg^{2+}	0.5 mM Mg^{2+}	No Mg^{2+}	0.5 mM Mg^{2+}
STRADα	1.1 ± 0.2	1.3 ± 0.8	2.4 ± 0.4	3.0 ± 1.4	2.9 ± 0.5	4.1 ± 1.6
STRADα/MO25α	0.09 ± 0.03	0.23 ± 0.09	0.02 ± 0.002	0.07 ± 0.010	0.03 ± 0.004	0.07 ± 0.01

Figure 3.24: MO25α enhances the ability of STRADα to bind ATP and ADP in a Mg^{2+} independent manner

A) Fluorescence emission spectra (excitation 410 nm) of TNP-ATP (5 μM) bound to the indicated forms of STRADα (2 μM) and/or MO25α (2 μM). A reference cuvette containing TNP-ATP (5 μM) only was subtracted as background.

B) Saturation binding experiments for STRADα, STRADα complexed to MO25α (WT, wild type) and MO25α (R227A/M260A) to TNP-ATP. Bound was defined as (F_x/F_{max})[R], where (F_{max} and F_x are maximal and fractional fluorescence (recorded at 540 nm) respectively and [R] equals the binding capacity, defined by the enzyme concentration, fixed at 1.5 μM. Equilibrium binding curves were then fitted to the quadratic equation suitable for tight binding interactions with ligand depletion (Copeland, 2000, p.92) (see chapter II, section 2.12.2). Data is shown as an average from 3 independent experiments ± SEM.

C & D) Displacement of TNP-ATP by ATP and ADP in the presence and absence of 0.5 mM $MgCl_2$. Concentrations of TNP-ATP (5 μM), STRADα (2 μM) and STRADα/MO25α (2 μM) complex were fixed and either ATP or ADP was titrated (0.05-500 μM). Emission at 540 nm was recorded and the fractional occupancy (F_x/F_{max}) was plotted as a function of added nucleotide concentration. Dose response curves were fitted using GraphPad-PRISM (See chapter II, section 2.12.2). Data are shown as an average from 3 independent experiments ± SEM.

E) Equilibrium binding constants for TNP-ATP, ATP and ADP in the presence and absence of 0.5 mM $MgCl_2$. K_d values were calculated as explained in chapter II, section 2.12.2.

eral topological terms. However, it appears that the mechanism of protein kinase interaction via helix αC with their activity modulators is wider than previously thought, and not exclusive to the CDK family of kinases. Indeed, there are now many examples of how protein kinases are stabilised in an active conformation via helix αC. These include members of the MAP kinase family (White et al., 2007), the AGC family of kinases (Kannan et al., 2007b; Gold et al., 2006; Taylor et al., 2004) and several tyrosine kinases (Filippakopoulos et al., 2008)). While in these examples the αC helix is stabilised by flanking N- or C-terminal sequences/domains present in the same polypeptide chain, the mechanisms of allosteric activation are similar.

3.6 The role of ATP and MO25α binding to STRADα

3.6.1 STRADα ATP binding is markedly enhanced by MO25α

Although MO25α appears to induce a STRADα active conformation similar to CDK2/cyclin A, the effect of this "active conformation" cannot be measured through ATPase/kinase activity due to STRADα being a pseudokinase. Instead, the affinity of ATP for STRADα was measured and how this was modulated by STRADα interaction with MO25α was monitored. The fluorescent ATP analogue 2',3'-O-2,4,6-trinitrophenyl-ATP (TNP-ATP) was used, since TNP-ATP fluores-

cence emission is enhanced upon its titration with ATP-binding proteins/enzymes (Hiratsuka, 1982). This feature has previously been exploited to measure equilibrium binding constants of kinases for ATP (Mukherjee et al., 2008). Using this approach, the K_d of STRADα for TNP-ATP in the absence of MO25α was determined to be 1.1 μM (Fig. 3.24A, B and E). K_d values of STRADα for ATP and ADP were also assessed by their ability to displace bound TNP-ATP and found to be 2-3 μM (Fig. 3.24C, D and E). Strikingly, addition of an equimolar amount of MO25α to STRADα enhanced binding of TNP-ATP by an order of magnitude (Fig. 3.24A, B and E) and TNP-ATP displacement by two orders of magnitude (Fig. 3.24C, D and E) indicating significantly stronger affinity compared to the interaction of ATP as a substrate to active kinases. In contrast, the binding of STRADα to TNP-ATP was not enhanced by addition of the MO25α(R227A/M260A) mutant that is unable to bind STRADα (Fig. 3.24A and B). The lack of a Mg^{2+} binding motif on STRADα suggests that Mg^{2+} should not contribute to the STRADα-ATP interaction. Indeed, Mg^{2+} did not affect binding of STRADα to TNP-ATP or displacement of TNP-ATP by ATP or ADP (Fig. 3.24C, D, E). This contrasts to the CASK "pseudokinase" where Mg^{2+} reportedly inhibits ATP binding and hence kinase activity (Mukherjee et al., 2008).

It should be noted that although STRADα does not appear to require Mg^{2+} for binding ATP, most cellular ATP is complexed to Mg^{2+} ions. Although there is no space for Mg^{2+} to bind in the canonical protein kinase mode through the DFG motif, Mg^{2+} ions could reside in the solvent exposed region of the phosphate moiety. A candidate water molecule coordinated by negative charges of β/γ phosphates of ATP and a nearby hydroxyl group (Ser199), that could be replaced by Mg^{2+} ions is shown in Fig. 3.6. Alternatively, it is possible that conformational changes in the structure could accommodate Mg^{2+}, without affecting the ability of STRADα to bind MO25α (see section below). As mentioned previously (section 3.4.3, the canonical Mg^{2+} coordinating residues appear to have been substituted through evolution with positively charged residues (Arg215 and H200), thus making redundant the role of Mg^{2+} ions.

3.6.2 ATP stimulates binding of STRADα to MO25α

To further investigate the functional consequences of ATP binding to STRADα, quantitative Surface Plasmon Resonance (SPR) measurements were employed. The focus of these measurements was how ATP influenced affinity of STRADα for MO25α. In the absence of ATP, the binding of STRADα for MO25α was fitted to a single site binding equation (Fig. 3.25). From measuring the rate constants for asso-

ciation and dissociation (Table 3.3 and Fig. A.3), the dissociation constant (K_d) was calculated as 3.8 μM (Fig. 3.25 and Table 3.3). However, in the presence of ATP, binding could be fitted to a two site binding equation (Hill slope of 0.4, Fig. 3.25A and Table 3.3). The second binding constant (K_{d2}) was measured as 12 nM, over 2 orders of magnitude higher than K_{d1} calculated as 2.5 μM (Fig. 3.25A and Table 3.3). MgATP enhanced binding of STRADα to MO25α, to a similar extent as ATP (Fig. 3.25A). These results indicate that binding of ATP to STRADα leads to a high affinity MO25α interaction site being exposed. Mutation of Met260 in the WEF binding pocket of MO25α did not significantly affect binding of MO25α to STRADα, nor did it influence the effect of ATP at enhancing interaction (Fig. 3.25B and Table 3.3). It should be noted that this observation contrasts with the data obtained from co-expression studies in 293 cells (Fig. 3.21A) and previous studies (Milburn et al., 2004), where mutation of Met260 inhibits MO25α binding to STRADα, suggesting that the WEF pocket is required for cellular complex assembly of MO25α and STRADα. Mutation of Arg227, in the newly identified concave site of MO25α, which interacts with the αB site of STRADα, virtually abolished binding of STRADα observed by SPR in the absence of ATP (Fig. 3.25C and Table 3.3). In the presence of ATP or MgATP,

no two-site binding of MO25α(R227A) to STRADα was detected, displaying only low micromolar binding to a single site (Fig. 3.25C and Table 3.3). A double MO25α(R227A/M260A) mutant failed to interact with STRADα even in the presence of ATP (Fig. 3.25D and Table 3.3). These results indicate that the key STRADα high-affinity binding site on MO25α lies on the concave surface and is only recognized by STRADα in the presence of ATP. Together with the finding that MO25α also enhances affinity of STRADα for ATP (Fig. 3.24), this suggests that the interaction of ATP and MO25α to STRADα is cooperative. A similar synergistic mechanism is observed for the PKA catalytic subunit where a nucleotide analogue was shown to stablise a complex with the PKI inhibitory peptide (Lew et al., 1997). However, in the case of PKA/PKI interaction the γ-phosphate can not be transferred because there is no acceptor, whereas in case of STRADα it can not be transferred because of the lack of a base catalyst.

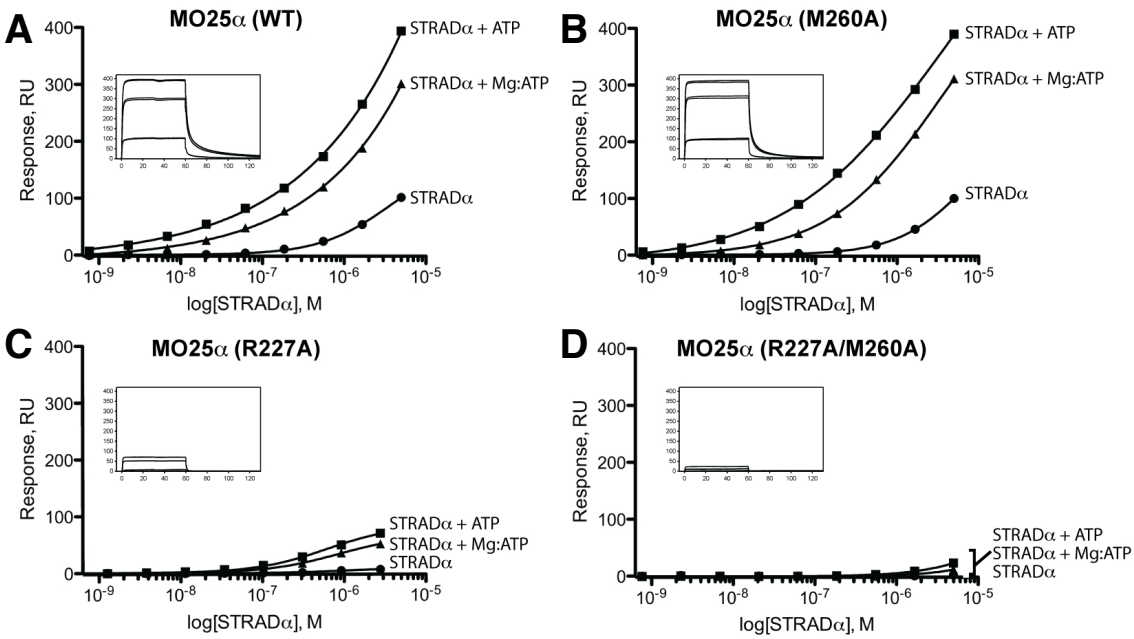

Figure 3.25: ATP enhances the ability of STRADα to bind MO25α in a Mg^{2+}-independent manner.
Binding of STRADα to MO25α was assessed in an SPR BIAcore assay by immobilising (A) MO25α (WT, wild type), (B) MO25α(M260A), (C) MO25α(R227A) and (D) MO25α(R227A/M260A) to a CM5 sensor chip and STRADα was allowed to bind over 50 s by injecting different concentrations over a range of 0.4 nM to 5 μM in the presence or absence of 0.1 mM ATP and/or 1 mM $MgCl_2$. Response levels for specific binding of STRADα to MO25α were plotted against STRADα concentration (log scale), using, where appropriate, a variable slope model to determine the Hill slope from the data. Boxed are representative BIAcore sensograms recorded in duplicate and corresponding to the highest concentration for each of the labelled STRADα curves. A complete set of primary sensograms are provided in Fig. A.3. Similar results were obtained in at least two separate experiments.

Table 3.3: STRADα interaction rate constants for wild-type MO25α and MO25α mutants (error values are in brackets). Binding constants (K_d) were calcualted as $K_d = k_d/k_a$ and are given in the last two columns

Analyte and condition	k_{a1} ($M^{-1}s^{-1}$)	k_{d1} (s^{-1})	k_{a2} ($M^{-1}s^{-1}$)	k_{d2} (s^{-1})	K_{d1} (μM)	K_{d2} (μM)
Target: MO25α (WT)						
STRADα	1.7×10^5 (7.0×10^2)	0.63 (3.0×10^{-3})	ND	ND	3.8 ± 0.08	ND
STRADα + ATP	1.6×10^5 (5.8×10^2)	0.40 (1.3×10^{-3})	2.5×10^6 (1.1×10^4)	0.03 (0.8×10^{-4})	2.5 ± 0.01	0.012 ± 0.0001
STRADα + ATP + Mg^{2+}	8.3×10^4 (3.5×10^2)	0.43 (1.4×10^{-3})	7.9×10^5 (2.9×10^3)	0.04 (8.8×10^{-5})	5.1 ± 0.02	0.051 ± 0.0002
His-STRADα + ATP + Mg^{2+}	1.9×10^5 (1.4×10^3)	0.55 (3.8×10^{-3})	1.1×10^6 (9.9×10^3)	0.08 (4.8×10^{-4})	2.9 ± 0.03	0.070 ± 0.0008
Target: MO25α (M260A)						
STRADα	1.1×10^5 (4.0×10^2)	0.92 (3.0×10^{-3})	ND	ND	8.1 ± 0.02	ND
STRADα + ATP	3.5×10^5 (1.9×10^3)	0.52 (2.9×10^{-3})	2.0×10^6 (1.2×10^4)	0.06 (2.2×10^{-4})	1.5 ± 0.01	0.030 ± 0.0002
STRADα + ATP + Mg^{2+}	1.9×10^5 (7.0×10^2)	0.43 (1.7×10^{-3})	6.1×10^5 (3.8×10^3)	0.05 (2.3×10^{-4})	2.3 ± 0.01	0.082 ± 0.0006
His-STRADα + ATP + Mg^{2+}	3.3×10^5 (2.4×10^3)	0.77 (4.6×10^{-3})	5.0×10^5 (3.6×10^3)	0.11 (5.3×10^{-4})	2.3 ± 0.02	0.220 ± 0.0019
Target: MO25α (R227A)						
STRADα	ND	ND	ND	ND	ND	ND
STRADα + ATP	1.1×10^6 (2.0×10^3)	0.66 (1.0×10^{-3})	ND	ND	0.6 ± 0.003	ND
STRADα + ATP + Mg^{2+}	9.1×10^5 (2.0×10^3)	0.72 (2.0×10^{-3})	ND	ND	0.8 ± 0.005	ND
His-STRADα + ATP + Mg^{2+}	7.0×10^5 (3.0×10^3)	1.61 (7.0×10^{-3})	ND	ND	1.5 ± 0.030	ND
Target: MO25α (R227A/M260A)						
STRADα	ND	ND	ND	ND	ND	ND
STRADα + ATP	ND	ND	ND	ND	ND	ND
STRADα + ATP + Mg^{2+}	ND	ND	ND	ND	ND	ND
His-STRADα + ATP + Mg^{2+}	ND	ND	ND	ND	ND	ND

ND = Not determined

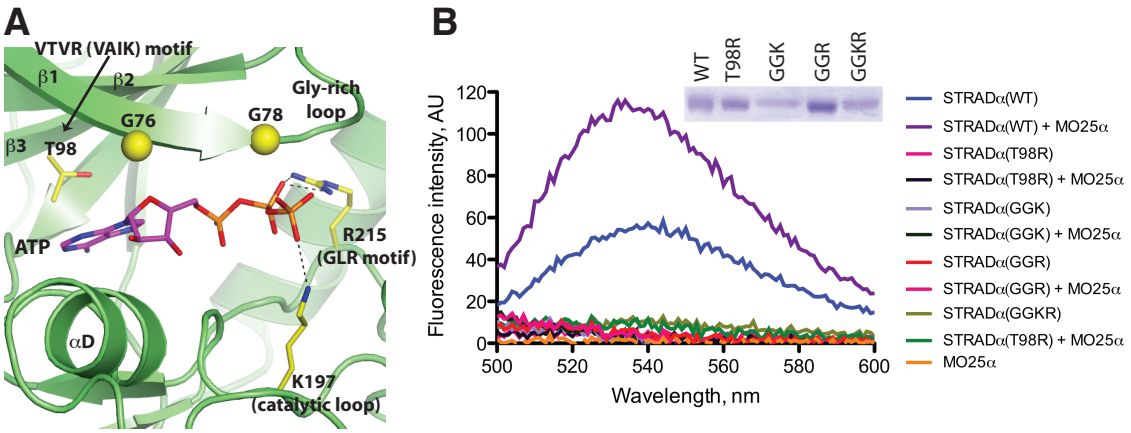

Figure 3.26: Design of STRADα mutants incapable of binding ATP
A) The structure of the ATP binding site of STRADα, in which key interacting and nearby residues, are emphasized.
B) Fluorescence emission spectra (excitation 410 nm) of TNP-ATP (5 μM) bound to wild type and mutant forms of STRADα (2 μM) and/or wild type MO25α (2 μM). A reference cuvette containing only TNP-ATP (5 μM) was subtracted as background. A Coomassie stained SDS-PAGE gel of each form of STRADα analysed is shown (GGK = G76D + G78D + K197E, GGR = G76D + G78D + R215E, GGKR = G76D + G78D + K197E + R215E).

3.6.3 ATP and MO25α are required for STRADα activation of LKB1

Having established that ATP increases the affinity of STRADα-MO25α interaction, the question whether ATP binding to STRADα also affects assembly and activity of the LKB1 heterotrimeric complex, was addressed. Using the STRADα-ATP structure, a number of STRADα mutants were designed to disrupt binding of the adenine or phosphate moieties of ATP (Fig. 3.26A). Four of these were indeed unable to interact with TNP-ATP in the presence or absence of MO25α (Fig. 3.26B). Interestingly, these mutants also affected association with LKB1 when co-expressed in 293 cells (Fig. 3.27A), suggesting that binding of ATP to STRADα, in the absence of MO25α,

enhances the ability of STRADα to interact with LKB1. However, these mutants were capable of forming complexes with LKB1 when co-expressed with LKB1 and MO25α (Fig. 3.27B), that retained catalytic activity as measured by activation of AMPK (Fig. 3.27B). It is possible that binding of MO25α to these STRADα mutants compensates for their inability to bind ATP, by inducing a closed "active-like" conformation of STRADα, capable of binding and activating LKB1. To explore this idea, mutants of STRADα incapable of binding to both ATP and MO25α were generated. Strikingly, these combined STRADα mutants lost their ability to activate LKB1, despite still being capable of forming a heterotrimeric complex (Fig. 3.28).

Taken together, these observations suggest that the closed "active-like" conformation of STRADα is maintained through binding to ATP and/or MO25α, and is required for activation of LKB1. Mutations that prevent STRADα from binding to ATP or MO25α do not affect activation of LKB1 (Figs. 3.22 and 3.27B), suggesting that ATP binding to STRADα can compensate for loss of MO25α interaction and *vice versa*. However, loss of both ATP and MO25α binding prevents STRADα from activating LKB1 (Fig. 3.28. Such mutations may leave STRADα in the open "inactive-like" conformation incapable of activating LKB1. Unfortunately, crystallisation trials of STRADα in the

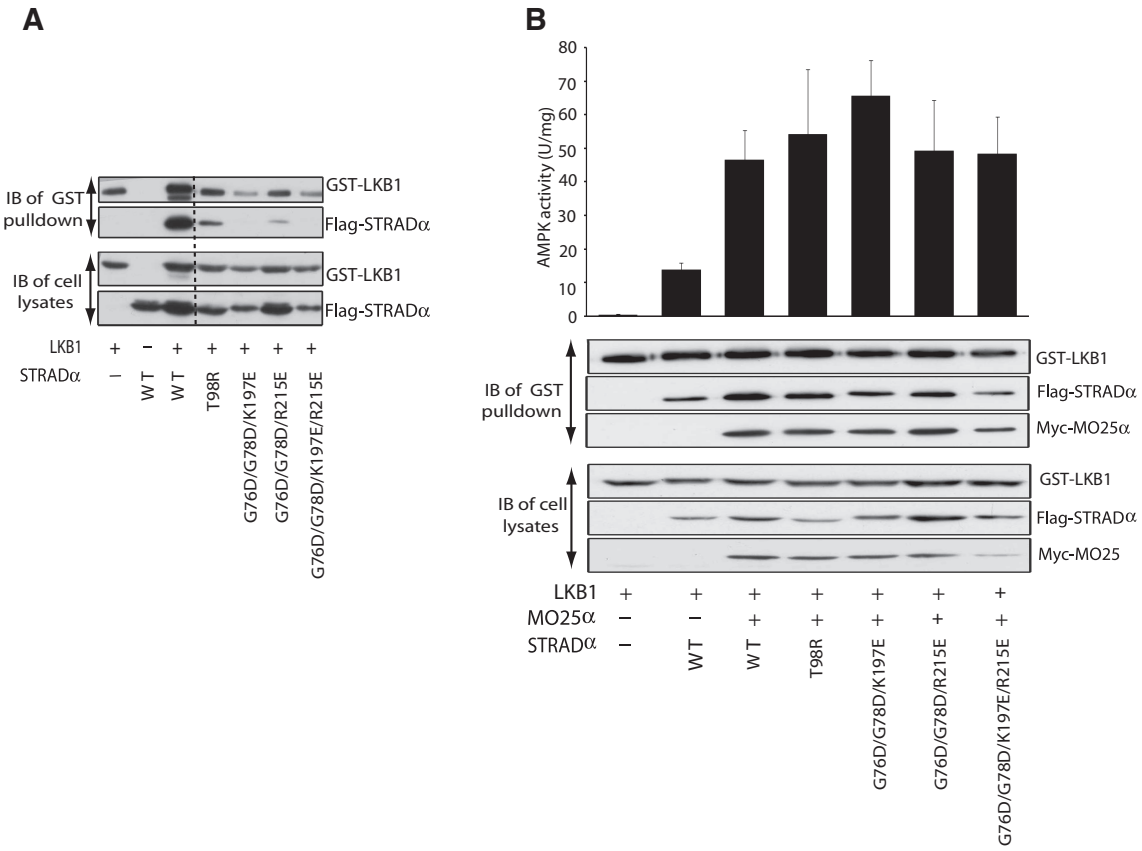

Figure 3.27: ATP binding to STRADα is required for STRADα/LKB1 interaction in the absence of MO25α

A & B) Wild type GST-LKB1 and indicated forms of Flag-STRADα were expressed in 293 cells in the absence (A) and presence (B) of Myc-MO25α. Cells at 36 h post-transfection were lysed and GST-LKB1 affinity purified on glutathione-Sepharose. Kinase activities are representative of three independent assays carried out in triplicate (error bars represent the SD for a single triplicate experiment). The purified GST-LKB1 preparation (upper panel) as well as the cell extracts (lower panel) were immunoblotted with the indicated antibodies. Similar results were obtained in three separate experiments. Dotted line indicates where the gel was cut.

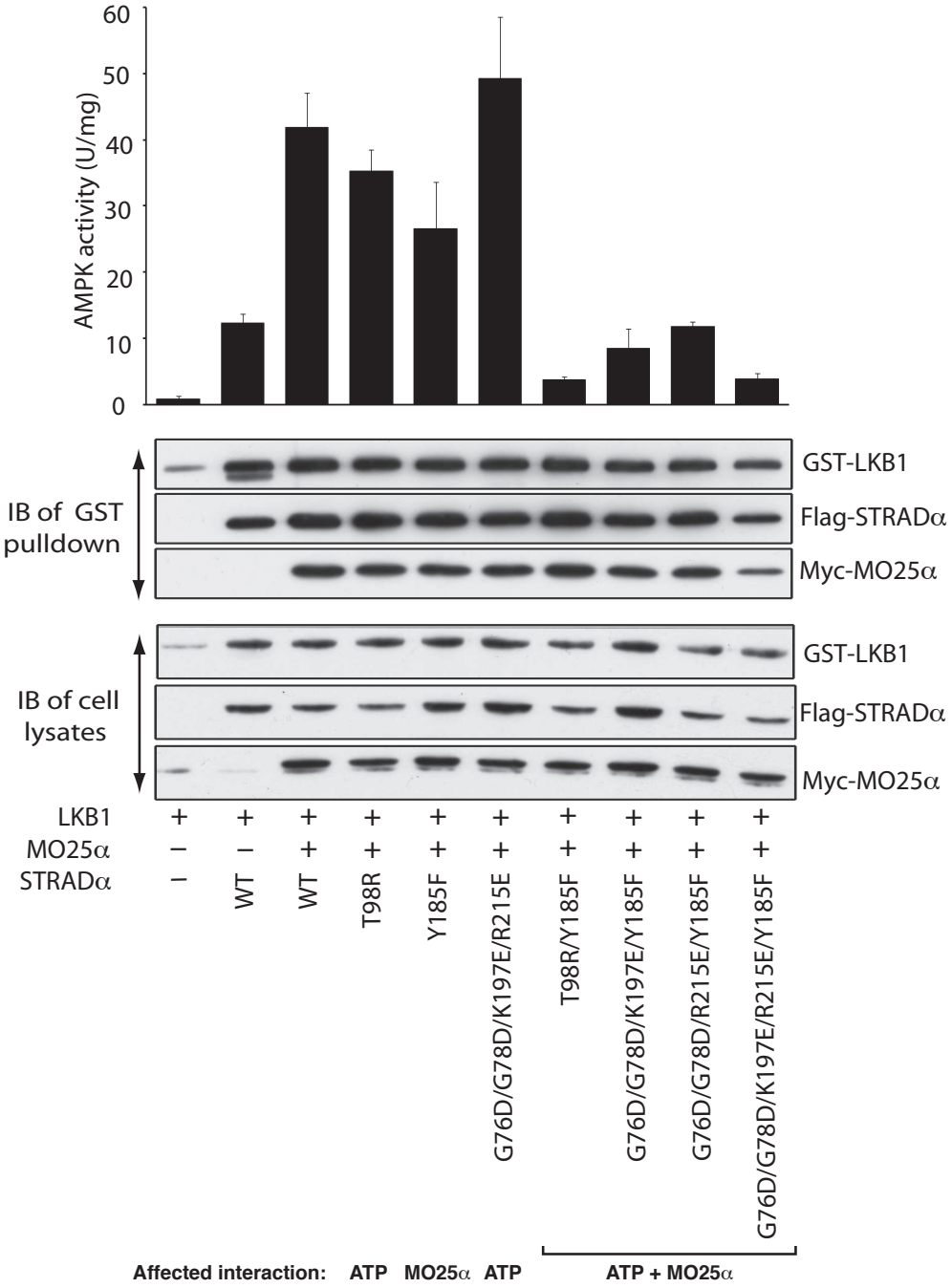

Figure 3.28: Interaction of ATP and MO25α with STRADα controls LKB1 activity
293 cells were co-transfected with the indicated constructs of GST-LKB1, Flag-STRADα and Myc-MO25α. Cells at 36 h post-transfection were lysed and GST-LKB1 affinity purified and assayed for the ability to activate heterotrimeric AMPK complex expressed in *E. coli* as described in chapter II, section 2.11.2. Kinase activities are representative of three independent assays carried out in triplicate (error bars represent the SD for a single triplicate experiment). Affinity purified GST-LKB1 preparation (upper panels) as well as cell extracts (lower panels) were immunoblotted with the indicated antibodies.

absence of MO25α that could have demonstrated this were unsuccessful. However, binding of ATP to several kinases, promotes the closed, active conformation of these enzymes. Moreover, as discussed above, binding of cyclin to CDK2 is reminiscent of the interaction of STRADα with MO25α. Interaction of cyclin A is well known to promote the closed, active, conformation of CDK2 (Jeffrey et al., 1995).

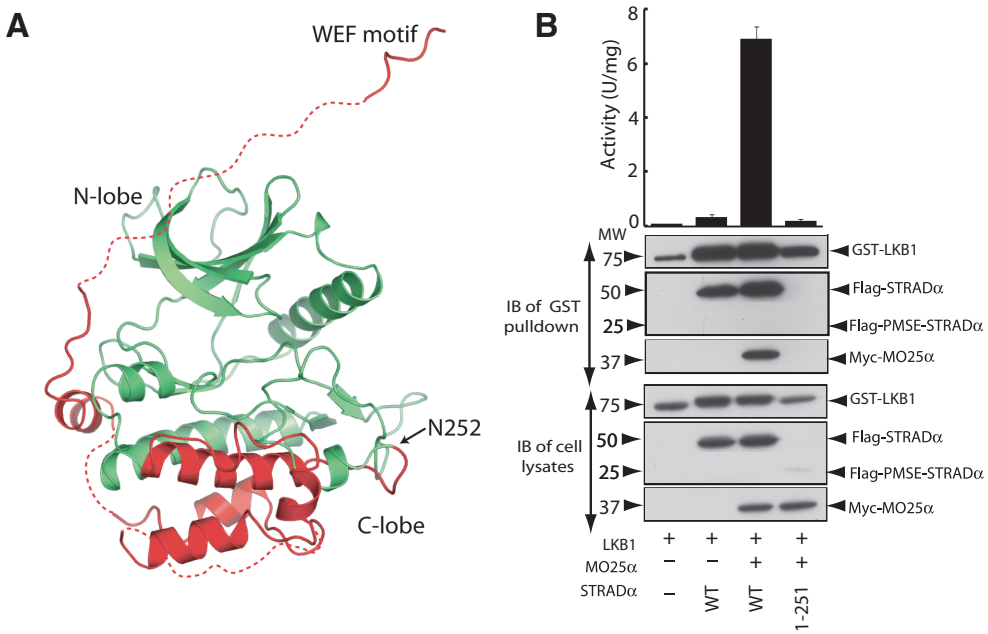

Figure 3.29: PMSE truncation and the stability of STRADα
A) Structure of STRADα in which the region beyond Asn252 that is truncated in PMSE patients is coloured in red.
B) 293 cells were co-transfected with the constructs encoding wild type GST-LKB1 and Myc-MO25α together with constructs encoding wild type or PMSE mutant Flag-STRADα. Cells at 36 h post-transfection were lysed and GST-LKB1 affinity purified and assayed for ability to phosphorylate the LKBtide peptide. Kinase activities are representative of three independent assays carried out in triplicate (error bars represent the SD for a single experiment carried out in triplicate). Affinity-purified GST-LKB1 preparation (upper panels) as well as cell extracts (lower panels) were immunoblotted with the indicated antibodies.

3.7 The PMSE mutation structurally impairs STRADα

Recently, a homozygous deletion of the *STRADA/LYK5* gene was reported to cause PMSE syndrome, a severe human developmental and epileptic syndrome (discussed in chapter I, section 1.5.3) (Puffenberger et al., 2007). The PMSE causing mutation in humans results in a STRADα truncation at residue 251, thus removing the last 180 amino acids (Puffenberger et al., 2007). Inspection of the STRADα structure reveals that this mutation would delete almost half of the C-terminal lobe of the pseudokinase domain, beginning with structurally vital components such as helix αF (Fig. 3.29A). This could destabilize the STRADα protein, as helix αF forms numerous hydrophobic interactions within the C-lobe of the pseudokinase domain, which would become solvent exposed in the PMSE mutant. Attempts to express the PMSE-STRADα (residues 1-251) mutant in 293 cells revealed this was expressed at significantly lower levels than full length STRADα (Fig. 3.29B), consistent with this fragment being unstable. Moreover, STRADα (1-251) failed to interact with or activate LKB1 (Fig. 3.29B). These results confirm that the STRADα mutation found in PMSE patients represents a loss-of-function mutation that would be unable to stimulate the LKB1 pathway. This could account for the elevated mTOR pathway activity that was observed in neuronal cells

derived from PMSE patients (Puffenberger et al., 2007). Therefore, it is possible that mTOR inhibitors that are currently in clinical trials may be beneficial in treating PMSE patients.

It is worth noting that while PMSE patients have lower LKB1 activity, no PJS-like symptoms were reported by Puffenberger et al. (2007). It is possible that polyposis and harmatomas may have gone unrecognised, considerng the young cohort (median age 16 years, range 7 months to 28 years), and the lack of colonoscopies for the patients studied (Puffenberger et al., 2007). Perhaps longer time periods occlusion of LKB1 activity in patients may be required to develop PJS syndrome. Indeed, PJS and predisposition to malignant cancers may be a later manifestation of PMSE syndrome, and it will be interesting if animal models of PMSE syndrome developed these symptoms.

3.8 Conclusions

The first structure of the STRADα pseudokinase and its interaction with MO25α, a heterodimeric interaction within the heterotrimer LKB1 tumour suppressor complex, is described in this thesis. A key discovery is the identification of an unexpected extensive interaction between STRADα and the concave surface of MO25α, previously proposed to harbour a ligand binding site (Milburn et al., 2004). Armadillo repeat proteins that are structurally related to MO25α such

as PUM1 (Wang et al., 2001), β-catenin (Graham et al., 2000) and importin-α (Conti and Kuriyan, 2000), also bind their macromolecular partners along their concave surface. In general topological terms, the STRADα/MO25α complex resembles the interaction between CDK2 and Cyclin A, and the EGFR/EGFR dimer, and provides another example of protein kinase regulatory mechanism via helix αC.

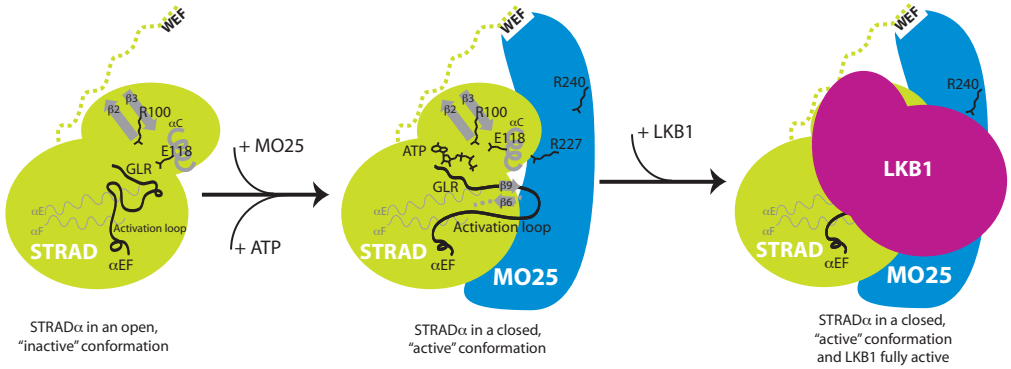

Figure 3.30: Model of how STRADα/MO25α might interact and activate LKB1
The model is based on mutagenesis and structural data discussed in this chapter. Binding of either ATP and/or MO25α to STRADα induce STRADα to adopt a closed conformation, leading to the assembly of a fully active LKB1 complex.

The data presented in this thesis show that, despite lacking most essential catalytic residues, STRADα has maintained its ability to adopt a closed "active-like" conformation, which binds ATP and possesses an ordered activation loop similar to active protein kinases. This closed conformation is stabilised through binding of ATP and/or MO25α. Moreover, binding of MO25α to STRADα markedly enhances affinity for ATP and binding of ATP to STRADα stimulates interaction with MO25α. These findings support a model in which binding of either MO25α or ATP is sufficient to enable STRADα to activate LKB1.

Consistent with this, mutant forms of STRADα that are incapable of binding both ATP and MO25α can no longer activate LKB1, whilst mutant forms of STRADα that retain the ability to bind either ATP or MO25α still activate LKB1. Thus, the closed "active-like" conformation rather than catalytic phosphoryl transfer activity, is likely to be the key to the mechanism by which STRADα activates the LKB1 tumour suppressor. A model of how STRADα/MO25α might interact and activate LKB1 based on mutagenesis and structural data is presented in Fig. 3.30. Future work may establish other examples of pseudokinases that, like STRADα, regulate signal transduction networks through their conformational state alone.

Chapter IV

Structure of the LKB1/STRADα/MO25α heterotrimeric complex

4 Structure of the LKB1/STRADα/MO25α heterotrimeric complex

4.1 Foreword

In the work described below, mutagenesis studies involving expression of LKB1, STRADα and MO25α in HEK293 cells, pulldown and LKB1 activity assays were a collaborative effort involving Dr Beatrice Maria Filippi, University of Dundee, who helped with these experiments. Details of the experimental work are provided in chapter II, Materials and Methods section of this thesis.

4.2 Project overview and aims

4.2.1 LKB1 is activated by STRADα/β and MO25α/β

In cells, LKB1 is found in a 1:1:1 heterotrimeric complex with the pseudokinase STRAD (Baas et al., 2003) and the scaffolding protein MO25 (Boudeau et al., 2003a). Unlike the majority of protein kinases that are regulated by phosphorylation, binding to STRAD and MO25 (Hawley et al., 2003; Boudeau et al., 2004) activates LKB1 through an unknown molecular mechanism. As described in chapter III of this thesis, the structure of STRADα complexed with MO25α, revealed additional interactions between the concave surface of MO25α and the regulatory αC helix of STRADα. STRADα, despite being a cat-

alytically inactive pseudokinase, adopts a closed conformation typical of fully active protein kinases. The closed conformation of STRADα is maintained through its cooperative binding to ATP and MO25α. Mutations that inhibit binding to ATP and MO25α, prevent LKB1 activation, suggesting the active conformational state of STRADα is required for activation of LKB1 (discussed in chapter III).

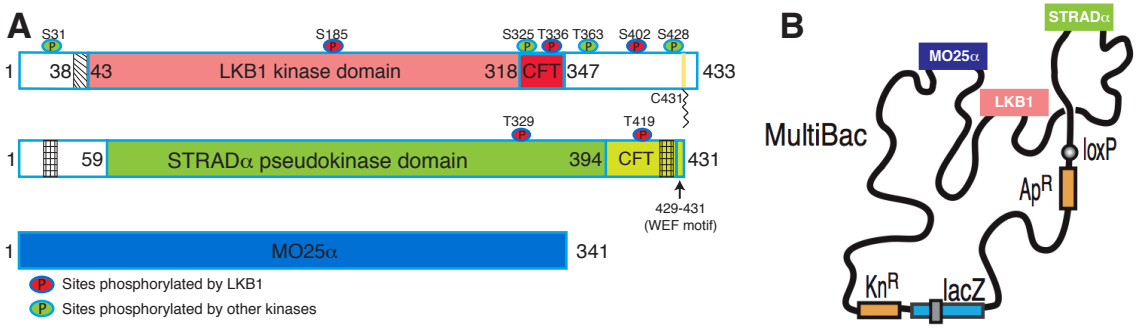

Figure 4.1: Domain architecture of LKB1/STRADα/MO25α and boundaries for co-expression and crystallisation
A) Overview of the domain architecture of LKB1, STRADα and MO25α. Sequence motifs, phosphorylation, and prenylation sites are labelled (adopted and redrawn from Alessi et al. (2006)).The LKB1 nuclear localisation sequence (residues 38-42) is shown as a hatched rectangle. Nuclear export signal sequences of STRADα (residues 21-29 and 417-426 (Dorfman and Macara, 2008)) are shown as grids. Coloured regions were used for crystallisation and the same colouring scheme is adopted throughout this chapter, unless specified otherwise.
B) Architecture of the MultiBac bacmid (adapted and modified from Berger et al. (2004)), used to recombinantly co-express the *LKB1/STRADA/MO25A* genes.

4.2.2 Aims

The aim of this work was to understand the mechanism by which the tomour suppressor kinase LKB1 is activated. To do this I sought to determine the 3-dimensional structure of the LKB1/STRADα/MO25α heterotrimer. While there are many examples whereby pseudokinases contribute to the activation of active kinases, no detailed molecu-

lar mechanisms have been described. Thus, particularly interesting was the study of mechanisms by which STRADα, a pseudokinase and MO25α, a scaffolding protein could activate LKB1. Another aim of this work was to understand the structure-function relationship of disease-causing mutations of LKB1, by studying their location on the LKB1 3-dimensional structure.

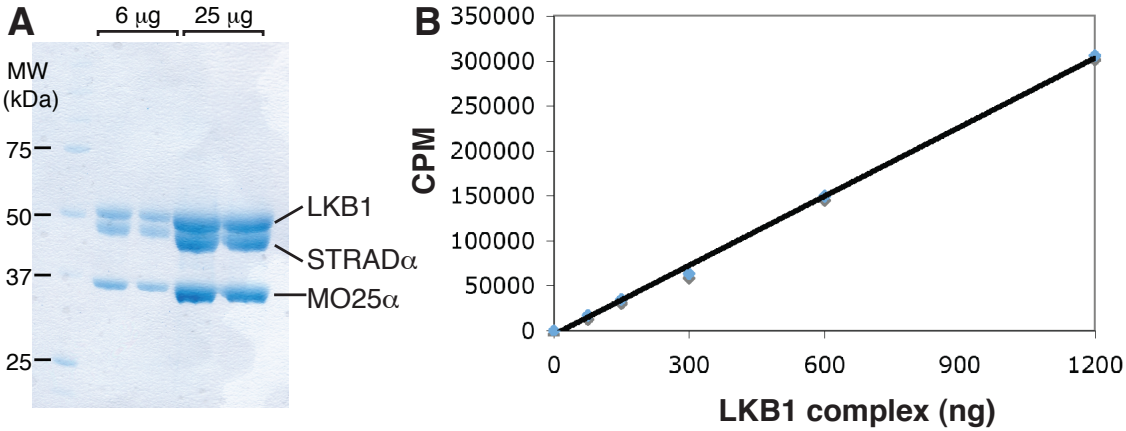

Figure 4.2: Purification of the full length LKB1/STRADα/MO25α complex
A) SDS-PAGE analysis of the purified full length LKB1/STRADα/MO25α heterotrimeric complex.
B) Activity assay using the LKBtide peptide substrate. The specific activity for the preparation was calculated as 23 U/mg.

4.3 Overview of experimental procedures

4.3.1 Expression and purification of LKB1/STRADα/MO25α complex

Following the successful co-expression of the STRADα/MO25α complex in *E. coli* (chapter II), the same approach was used for the co-expression of the LKB1/STRADα/ MO25α complex. The LKB1 gene (residues 43–347, preceded by a 6-His purification tag) was inserted in one of the remaining gene expression cassettes of the pOPCH vector

(Tan, 2001), together with full length STRADα and MO25α genes (Fig. A.4A). However, attempts to express and purify the LKB1 heterotrimeric complex using this system were unsuccessful (see Fig. A.4B in the appendix chapter VI). All of the three LKB1 complex components could be detected and confirmed by peptide mass spectrometry, however, the yield and purity of the LKB1 heterotrimer purified from *E. coli* were unsuitable for crystallography work. Instead, the attention was shifted to an eukaryotic cell expression system, using the *Spodoptera frugiperda* (Sf) cells as expression hosts, that were infected with baculoviruses genetically engineered to contain any of the subunits of the LKB1 heterotrimeric complex. This involved infecting Sf21 cells with three different viruses at once. Although it was possible to express and purify the LKB1 heterotrimer, the success rate was very low and the method difficult to reproduce, presumably because not all three viruses have the same efficiency at expressing each of the components at similar levels. This may have lead to an overall lower complex yield given that the three components are thought to be present at similar stoichiometry ((Neumann et al., 2007) and discussed below).

At this stage, it became clear that a system that ensures co-infection of all three subunits at once was necessary, and a similar system called

MultiBac had been developed in 2004 by Imre Berger, Daniel Fitzgerald and Tim Richmond at ETH Zürich (Berger et al., 2004). Therefore, the LKB1/STRADα/MO25α heterotrimeric complex was successfully co-expressed in Sf21 cells, using the MultiBac (Berger et al., 2004) expression system (Fig. 4.1). At first the full length and active LKB1 co-expressed with full length STRADα and MO25α, were co-purified at reasonable yield (5-6 mg/l of culture) and good purity (Fig. 4.2).

4.3.2 Identification of construct boundaries for crystallisation

Crystallisation trials, using the full length preparations did not result in any crystals. It is possible that the non-kinase domains of LKB1 and STRADα, predicted not to contain any well-folded domains, contribute to flexible regions that interfere with the crystallisation process. In addition, LKB1 N- and C-terminal regulatory regions contain multiple phosphorylation/auto-phosphorylation sites and a prenylation site (Fig. 4.1A), that could also contribute to sample heterogeneity and reduce the probability of crystal formation.

Previous work has suggested that the catalytic domain of LKB1 is sufficient to form active complexes with STRADα (Baas et al., 2003). Biochemical analysis to identify the shortest LKB1 fragment capable of forming active complexes with STRADα/MO25α were carried out by Dr Jerome Boudeau in the Alessi laboratory. LKB1

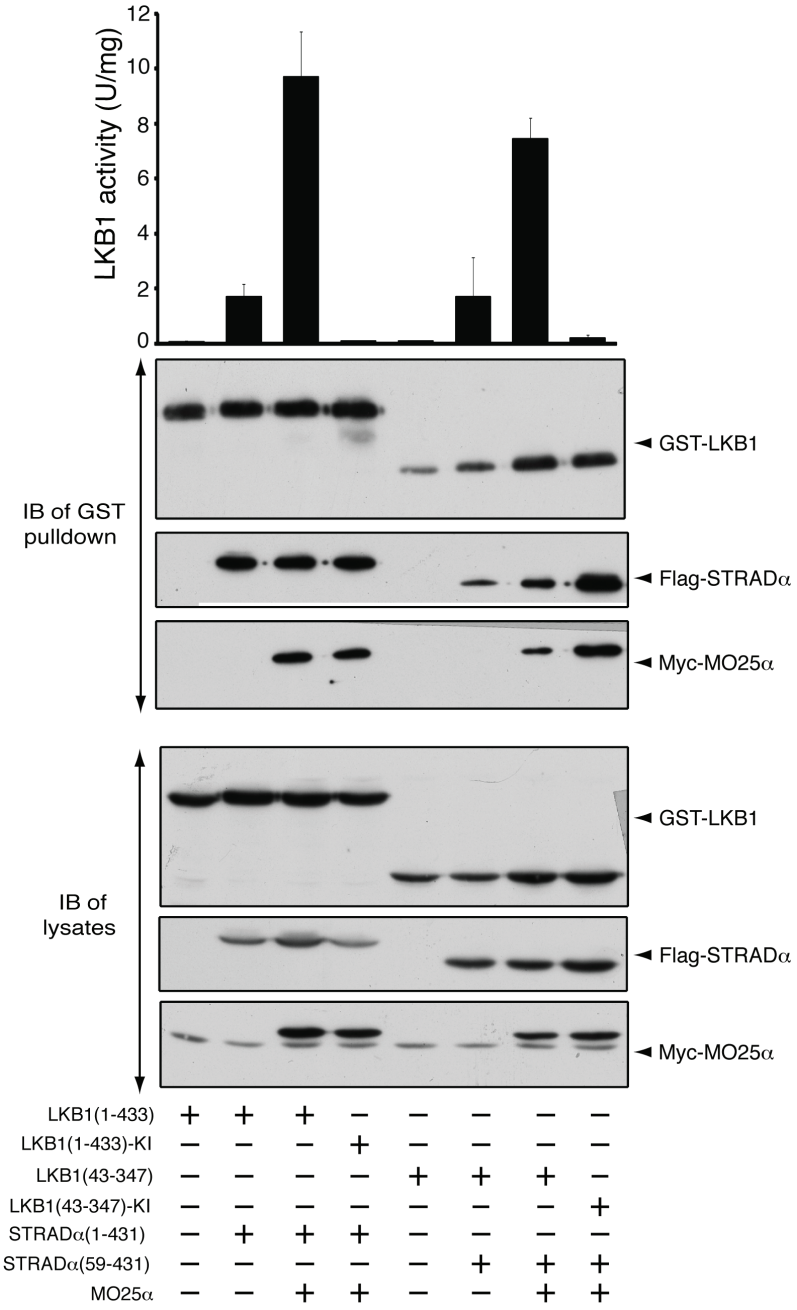

Figure 4.3: Activation of LKB1 by STRADα and MO25α
293 cells were co-transfected with the indicated constructs of GST-LKB1, Flag-STRADα and Myc-MO25α. Cells at 36 h post-transfection were lysed and GST-LKB1 affinity purified and assayed for the ability to phosphorylate LKBtide as described in section 2.11.1. (KI, kinase inactive (D174A) mutant).

residues 43–347 (containing the kinase domain) when co-expressed with full length STRADα and MO25α and purified from HEK 293 cells, retained the activity of that of full length LKB1 (Dr Jerome Boudeau, unpublished data). The construct boundaries of STRADα

and MO25α were identical to the constructs used for crystallisation studies of STRADα/MO25α complex discussed in chapter III of this thesis. Therefore, LKB1 (residues 43–347), STRADα (58–431) and full length MO25α were cloned into the pFBDM (MultiBac) vector (Berger et al., 2004) for expression and crystallisation studies (Fig. 4.1). Complex assembly and activity of LKB1 with these boundaries were assayed using a HEK 293 co-expression system and the abilty of LKB1 to phosphoryalte the LKB1tide substrate was assayed as described in chapter II, sections 2.8.9 and 2.11.1. The activity of LKB1 (residues 43–347) complex was comparable to the wild type LKB1 complex, and the truncated form of STRADα and full length MO25α were able to activate LKB1 to the same extent as wild type STRADα/MO25α (Fig. 4.3). In previous overexpression studies using HEK 293 cells, LKB1 has been reported to autophosphorylate in three sites Ser185, Thr336 and Ser402, as well as STRADα at residues Thr329 and Thr419 (Fig. 4.1A) (Sapkota et al., 2002a). Therefore, to avoid a heterogeneously phosphorylated sample, the catalytically inactive mutant of LKB1 (Asp194Ala) was used for crystallisation studies. This prevents LKB1 binding to Mg^{2+} ions required for phosphoryl transfer, but not its ability to interact with STRADα and MO25α (Fig. 4.3). The heterotrimeric complex with the catalytically inactive

mutant of LKB1 was expressed in Sf21 cells giving a good yield (6 mg/l of culture) and was crystallography-grade purified using metal-affinity, anion exchange and size exclusion chromatography (see chapter II section 2.8.7 for details). LKB1/STRADα/MO25α eluted as a heterotrimer from a size exclusion chromatography column at the expected size of a heterotrimer monomer (Fig. 4.4A and B). The sample purity and dispersity were analysed using SDS-PAGE and dynamic light scattering (DLS) respectively, revealing >97% purity and low (13.6%) polydispersity (4.4C and D).

4.3.3 Crystallisation and structure solution of LKB1 heterotrimeric complex

LKB1/STRADα/MO25α crystallised in the presence of the non- hydrolysable ATP analogue (AMP-PNP), producing diffraction to 3.0 Å. This was improved to 2.65 Å by chemical lysine methylation (Fig. 4.5A, B and Table 4.1). The presence of LKB1, STRADα and MO25α was confirmed by SDS-PAGE analysis of crystals after sequential washes in mother liquor (Fig. 4.5C). The structure was solved by molecular replacement using the already known MO25α structure (Milburn et al., 2004) and the STRADα structure described in chapter III of this thesis. Non-crystallographic symmetry averaging and manual model building revealed two heterotrimeric complexes in the asymmetric unit, displaying similar structures with an RMSD = 0.5 Å on 791

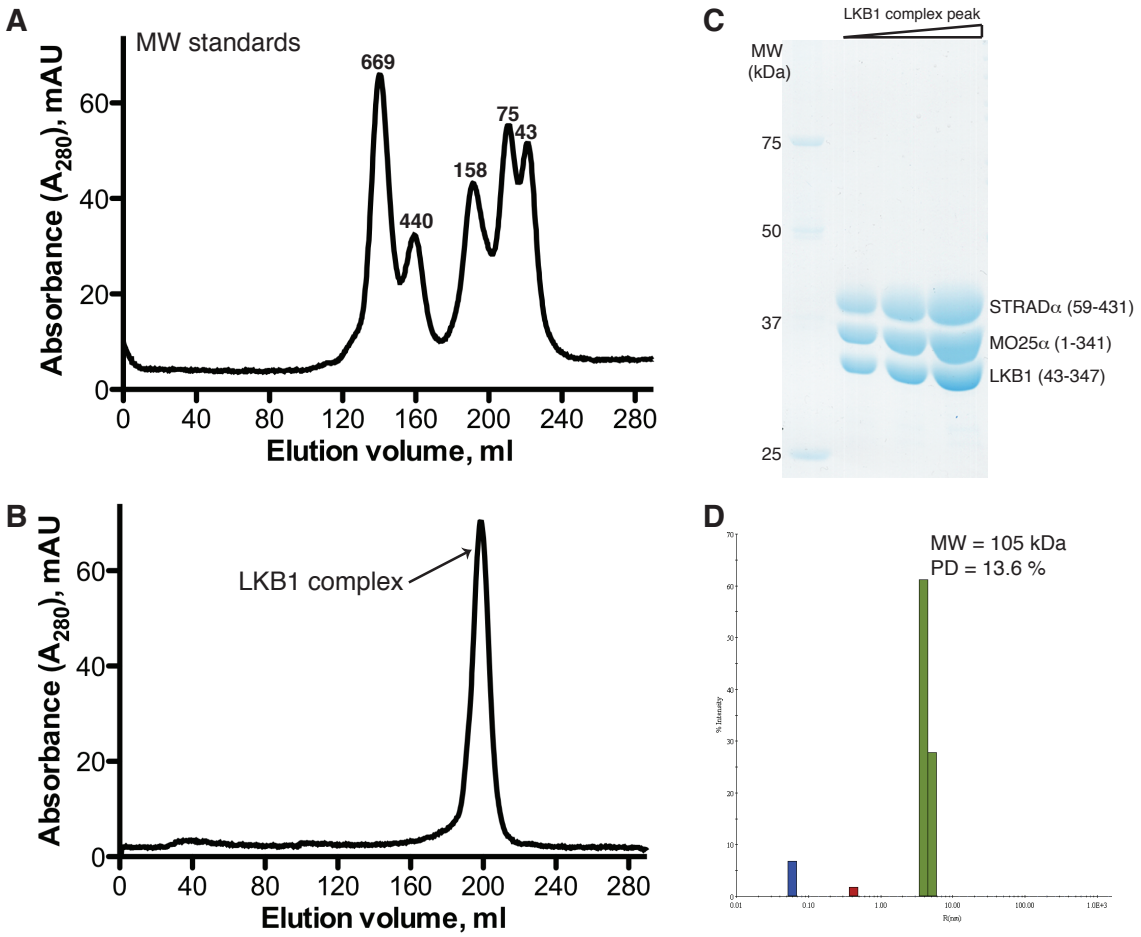

Figure 4.4: Isolation of the heterotrimeric LKB1/STRADα/MO25α complex
A) Elution profile of the molecular mass standards, Thyroglobulin (669 kDa), Ferritin (440 kDa), Aldolase (158 kDa), Conalbumin (75 kDa) and Ovalbumin (43 kDa).
B) Gel filtration profiles of LKB1/STRADα/MO25α co-expressed in Sf21 cells and crystallised in this thesis.
C) Fractions in which LKB1/STRADα/MO25α heterotrimer eluted, were pulled together, analysed by SDS-PAGE and stained with Coomassie blue dye.
D) Dynamic light scattering analysis of the LKB1 complex sample. The theoretical molecular weight (MW) = 115.8 kDa; PD = polydispersity.

Cα atoms (Fig. 4.6). Both STRADα and LKB1 are in complex with AMP-PNP displaying binding modes typical of other protein kinases (Knighton et al., 1991b), with the two hydrogen bonds between atoms N1 and N6 from the adenine ring and backbone atoms of residues from the hinge region of the kinase domain (Fig. 4.7). The γ-phosphate for AMP-PNP bound to LKB1 was not defined by electron density and therefore it is not included in the final model (Fig. 4.7A). It is possible

that the Asp194Ala mutation in the LKB1 DFG motif, that impairs the coordination of Mg^{2+} ions by the Mg^{2+} binding loop, accounts for the disorder of the γ-phosphate of the bound AMP-PNP. Ordered electron density was also observed for the STRADα C-terminal WEF motif interacting with a pocket on MO25α as shown previously by (Milburn et al., 2004) and discussed in chapter III. The connectivity of the WEF motif with the rest of STRADα is not clear, since the closest (straight line distance) and possible donating monomers belong to different LKB1 heterotrimers (Fig. 4.6). This is likely to be due to the crystal packing since there was no evidence of heterotrimer dimers in sedimentation equilibrium experiments using analytical centrifugation in the presence and absence of MgATP (Fig. A.5).

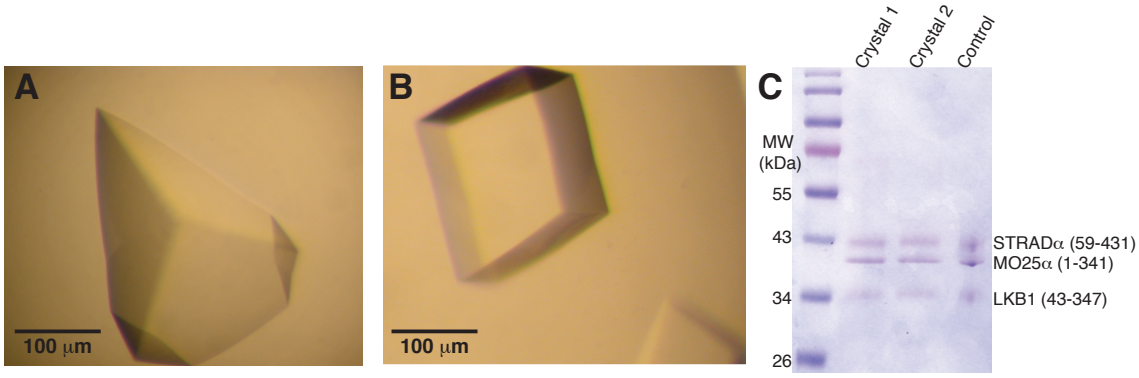

Figure 4.5: Crystals of the LKB1/STRADα/MO25α complex
Crystals of the native LKB1/STRADα/MO25α complex (A), and methylated LKB1/STRADα/MO25α complex (B).
C) SDS-PAGE gel (Coomassie stained) of LKB1 complex crystals electrophorised after three subsequent washes in mother liquor.

Table 4.1: Summary of data collection, structure refinement and analysis. Values for the highest resolution shell are given in brackets.

	Native	Methylated
Space Group	$P3_121$	$P3_121$
Unit cell (Å)		
a	118.7	118.4
b	118.7	118.4
c	390.0	390.0
Molecules/asu		
LKB1	2	2
STRADα	2	2
MO25α	2	2
Resolution (Å)	29.0-3.0 (3.1-3.0)	20.0-2.65 (2.75-2.65)
Observed reflections	284269	400006
Unique reflections	61869 (6033)	91884 (9144)
Redundancy	4.6 (4.6)	4.4 (4.4)
$I/\sigma I$	13.6 (1.6)	14.8 (2.6)
Completeness (%)	95.2 (94.6)	99.2 (99.8)
R_{merge}	0.079 (0.743)	0.063 (0.648)
R_{work}, R_{free}	-	0.240, 0.291
RMSD from ideal geometry		
bonds (Å)	-	0.011
angles (^{o})	-	1.343
B-factor RMSD (Å^2)		
(backbone bonds)	-	1.03
B (Å^2)		
protein	-	75.47
ligands (AMP-PNP)	-	78.63
water	-	26.26
Ramachandran plot statistics (%)		
Favoured region	-	93.9
Allowed region	-	5.2
Outlier region	-	0.9

4.4 General features of the LKB1 heterotrimer

4.4.1 Overall structure of the LKB1/STRADα/MO25α heterotrimer

The LKB1 heterotrimer has an overall compact globular shape with significant interactions between all of the three subunits (Figs. 4.8 and 4.9). The pseudokinase domain of STRADα binds to the kinase domain of LKB1. The horseshoe-shaped MO25α acts as a scaffold for assembly of the heterotrimer, by binding both LKB1 and STRADα through highly conserved residues on the concave face of its helical repeats (Figs. 4.8, 4.9 and 4.10). MO25α binds to STRADα through a large interface (2100 Å^2 buried surface area) centred around the regulatory helix αC of STRADα (Fig. 4.8 and 4.9). This is similar to the interaction observed in the structure of the STRADα/MO25α binary complex discussed in chapter III of this thesis (RMSD = 0.5 Å on 529 Cα atoms and Fig. 4.13). The WEF motif interacting with a pocket on MO25α, for which connectivity can not be unambiguously identified contributes to an additional 825 Å^2 buried surface area.

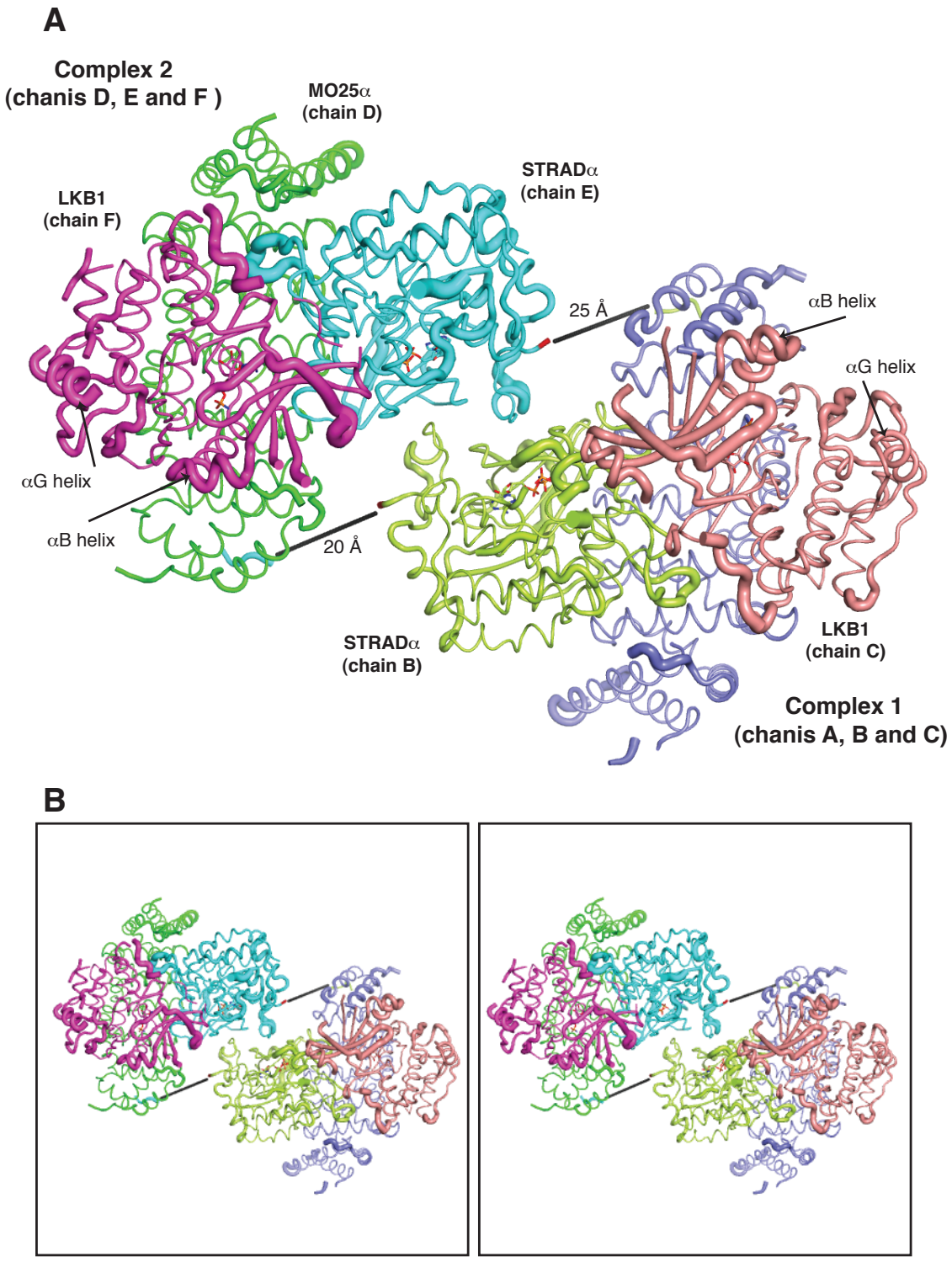

Figure 4.6: Contents of the asymmetric unit in crystals of the LKB1 heterotrimer
A) LKB1/STRADα/MO25α heterotrimers that make up the asymmetric unit. Protein structures are represented as cartoons and thickness of the cartoons is proportional to the B-factor value. AMP-PNP molecules bound to STRADα and LKB1 are shown as sticks. The shortest straight line distance between the last visible residue of STRADα pseudokinase domain (coloured red) and the first visible residue of the WEF motif is labelled.
B) Stereo view of the contents of the asymmetric unit shown in the same orientation as in (A).

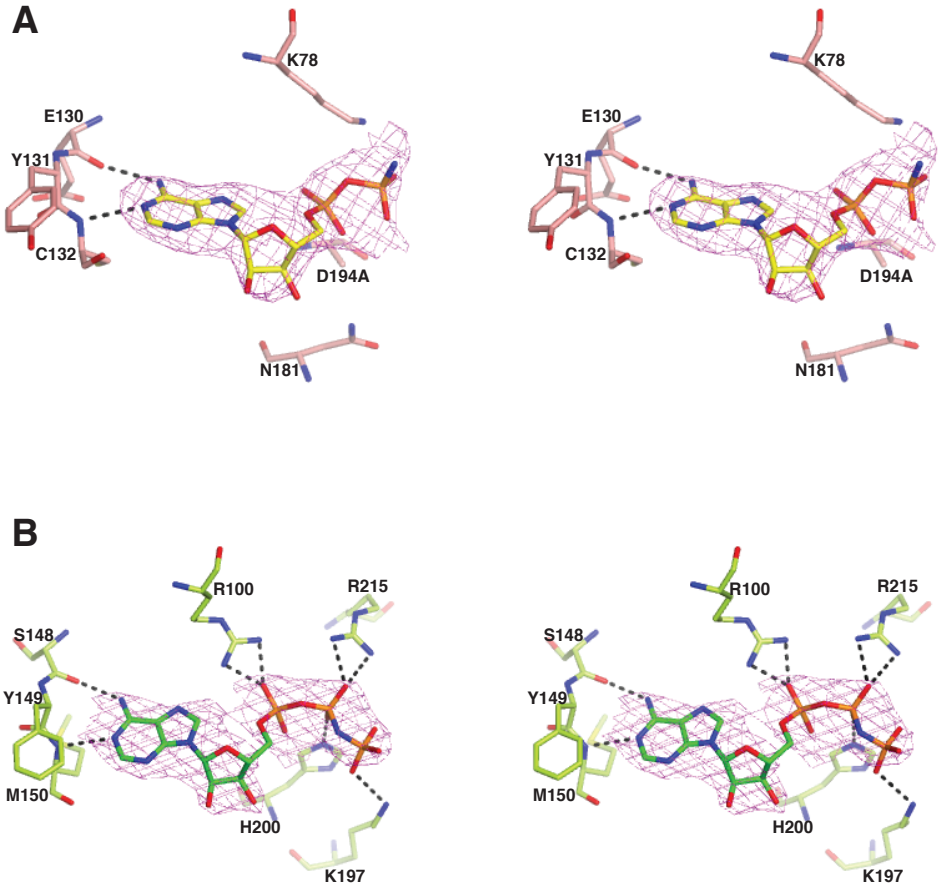

Figure 4.7: AMP-PNP binding to LKB1 and STRADα
A) Stereo figure of AMP-PNP (modelled as sticks with yellow carbons) and LKB1 residues that contribute to AMP-PNP binding. Unbiased F_o-F_c electron density map for the ATP molecule is coloured magenta and contoured at 2.4σ. Dashed lines represent hydrogen bonds between AMP-PNP and residues from LKB1 hinge region. The mutated Mg^{2+} binding residue from the DFG motif (D194A) is also labelled. The presence of this mutation may explain the absence of clear electron density for the γ-P of AMP-PNP. Hence the positioning of the phosphate groups is not optimal for hydrogen bonding with the indicated nearby residues.
B) Stereo figure of AMP-PNP (modelled as sticks with green carbons) and STRADα residues that contribute to AMP-PNP binding. Unbiased F_o-F_c electron density map for the AMP-PNP molecule is coloured magenta and contoured at 2.4σ. Dashed lines represent hydrogen bonds.

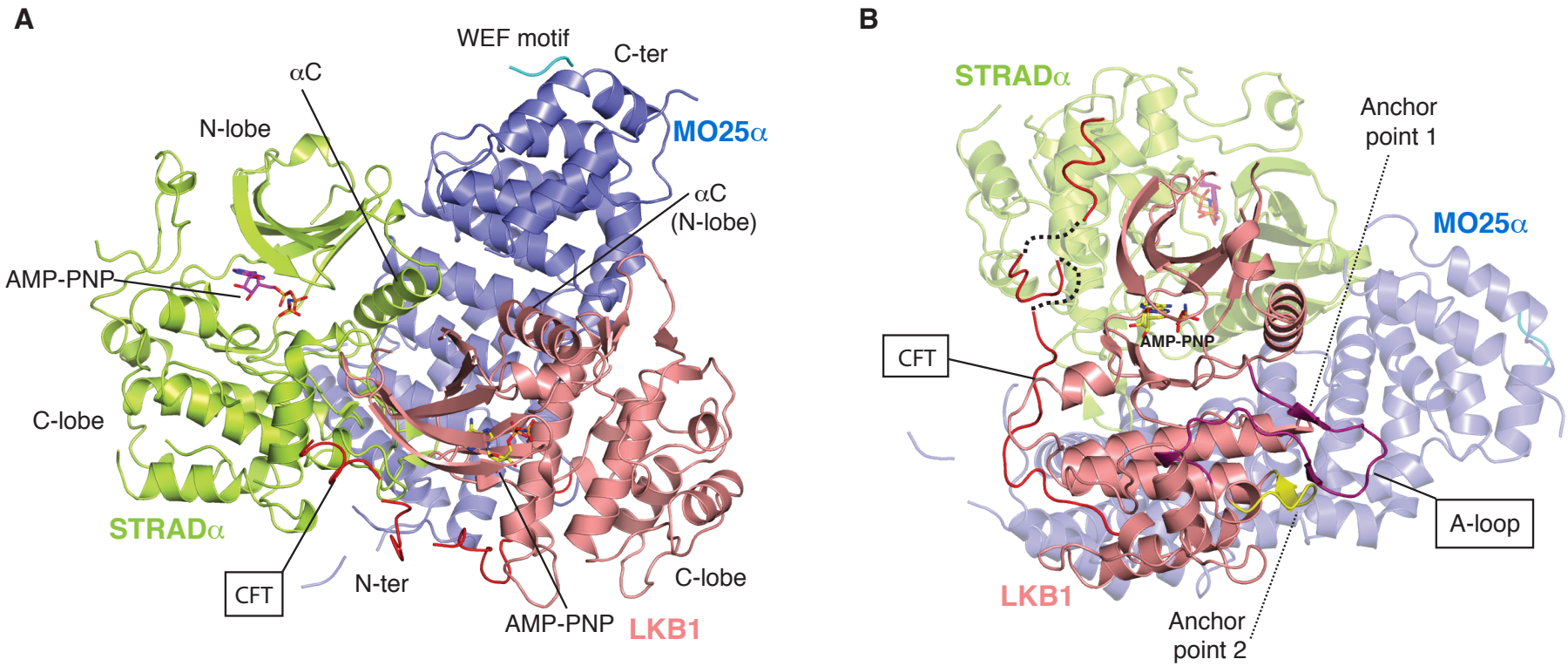

Figure 4.8: Overall structure of the LKB1/STRADα/MO25α heterotrimer

A) Cartoon representation of the LKB1/STRADα/MO25α heterotrimeric complex and two bound AMP-PNP molecules are shown in sticks representations (LKB1, yellow carbons; STRADα, magenta carbons). The γ-P for AMP-PNP bound to LKB1 was not visible due to disorder. The WEF motif at the C-terminus of STRADα, for which connectivity could not be unambiguously identified due to disorder of the linkers, is shown in cyan.

B) Alternate view centred on LKB1. The C-terminal flanking tail (CFT) and activation loop (A-loop) of LKB1 are coloured red and magenta respectively. Two anchor points within the activation segment of LKB1, consisting of β6/β9 and β9'/β9" are labelled as 1 and 2 respectively. The LKB1 αEF/αF loop is coloured yellow. Dashed lines represent areas that were not well-defined by electron density.

The remaining MO25α concave surface is engaged in contacts with the LKB1 activation loop and the C-terminus of LKB1 helix αC, burying a total of 1580 Å^2 surface area (Figs. 4.8 and 4.9). The interface between LKB1 and STRADα mainly involves the C-lobe of STRADα and both N- and C-lobes of LKB1 (burying a total of 1840 Å^2 surface area, (Fig. 4.8 and 4.9), comparable in size to the LKB1/MO25α interaction.

4.5 Analysis of the LKB1/STRADα/MO25α heterotrimer

4.5.1 LKB1 adopts an active conformation in a phospho-independent manner

LKB1, unlike most protein kinases, does not require phosphorylation of its activation loop to achieve an active conformation (Boudeau et al., 2004). Instead, activation of LKB1 is thought to be mediated through a conformational change triggered by binding to STRAD and MO25 isoforms (Baas et al., 2003; Boudeau et al., 2003a, 2004). The structure of the LKB1 heterotrimer is consistent with this, as LKB1 lacks phosphorylation of the activation loop, yet the activation loop is ordered (fully defined by electron density, Fig. 4.14A), a feature normally seen in structures of protein kinases that crystallise in the active conformation. In most protein kinases the function of this phosphorylation event is to anchor the catalytic H(R/K)D motif via

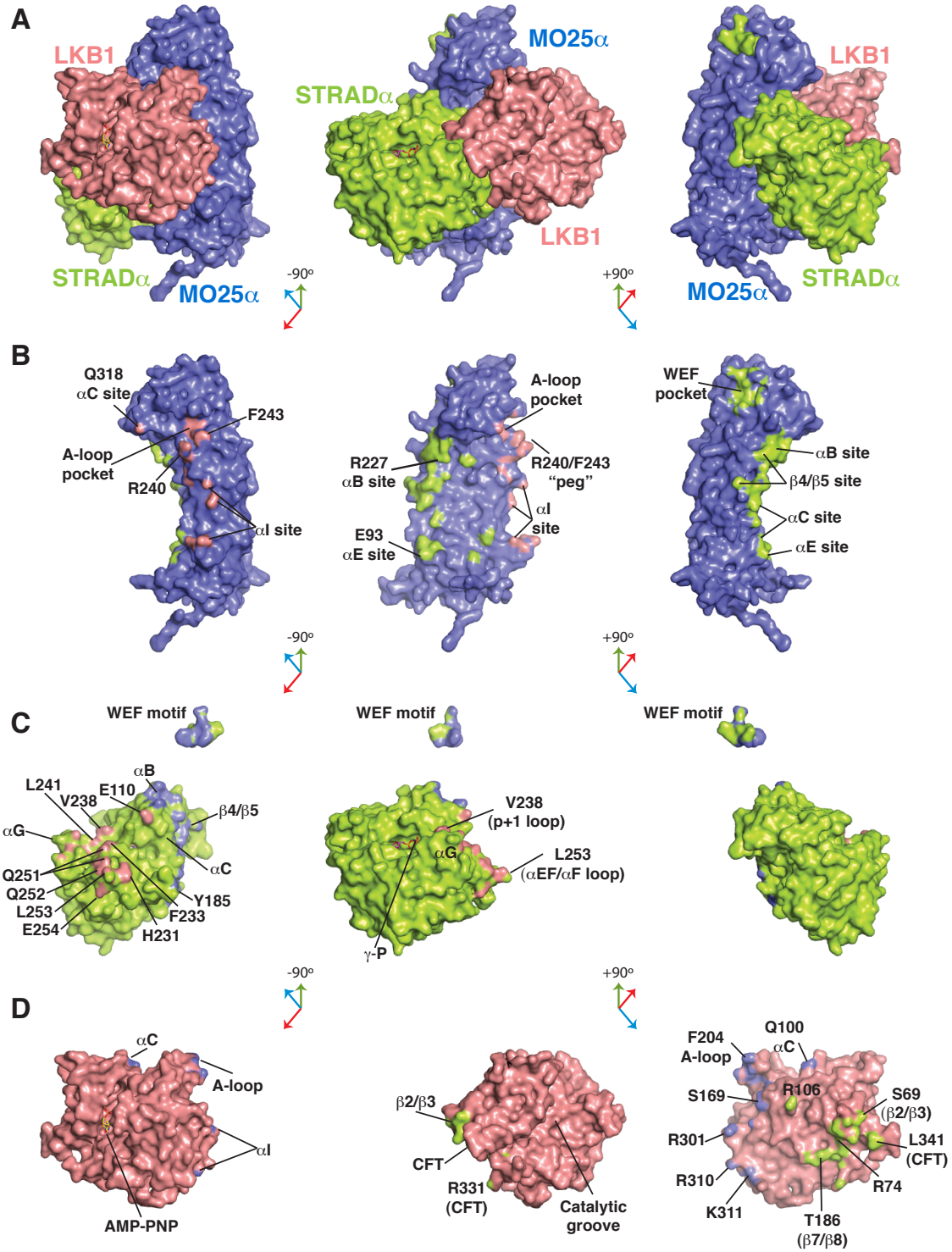

Figure 4.9: Sites of the LKB1/STRADα/MO25α interaction
A) Surface representation of the LKB1/STRADα/MO25α heterotrimer is shown at three alternative views: centre, rotated by -90 and 90^o in the left and right panels respectively.
B, C & D) MO25α (blue), STRADα (green) and LKB1 (pink) are shown in the same orientations as in panel (A). A map of interaction surfaces as defined by the program CONTACT (atom pairs closer than 3.9 Å) is coloured correspondingly. Residues that are discussed further in the text are labelled to aid orientation and visualisation. For a full list of interacting residues and their evolutionary conservation, see sequence alignments in Figs. 4.10, 4.11 and 4.12.

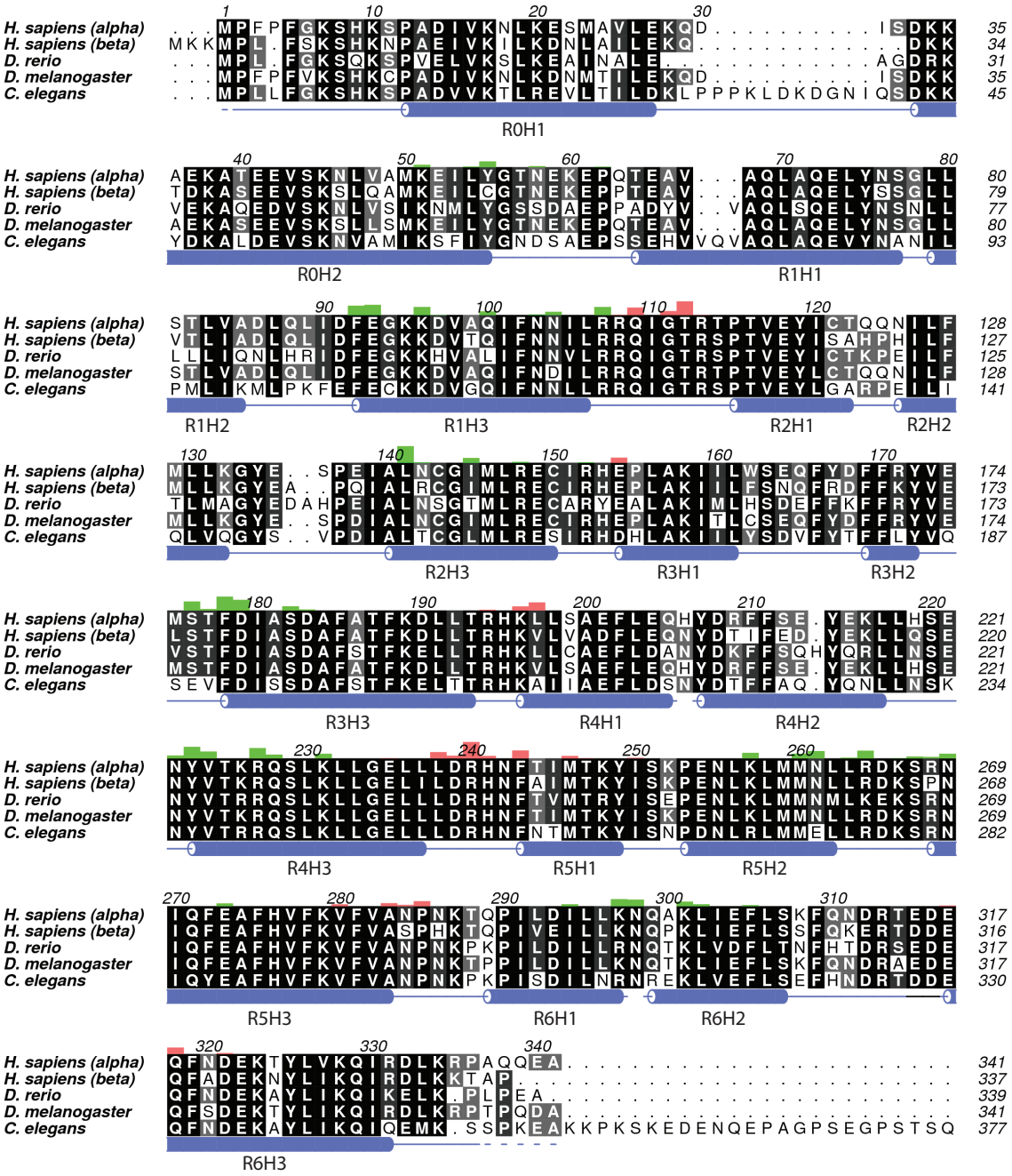

Figure 4.10: MO25α multiple sequence alignment, secondary structure and residues contributing to the interactions with LKB1/STRADα

Multiple sequence alignment (black = conserved, white = not conserved) of MO25α from the indicated species of the metazoan kingdom. Alignments were performed with MUSCLE (Edgar, 2004) and edited and displayed using ALINE (Bond and Schüttelkopf, 2009). A graph of residues involved in LKB1/STRADα interaction against their contact area (green bars = STRADα, pink bars = LKB1) is displayed. Height of the bar represents the contact area (atom pairs closer than 3.9 Å, analysed by CONTACT from the CCP4 package (Collaborative Computational Project, 1994)), divided by the total surface area of the participating amino acid. The secondary structure (analysed by DSSP (Kabsch and Sander, 1983)) is shown in red.

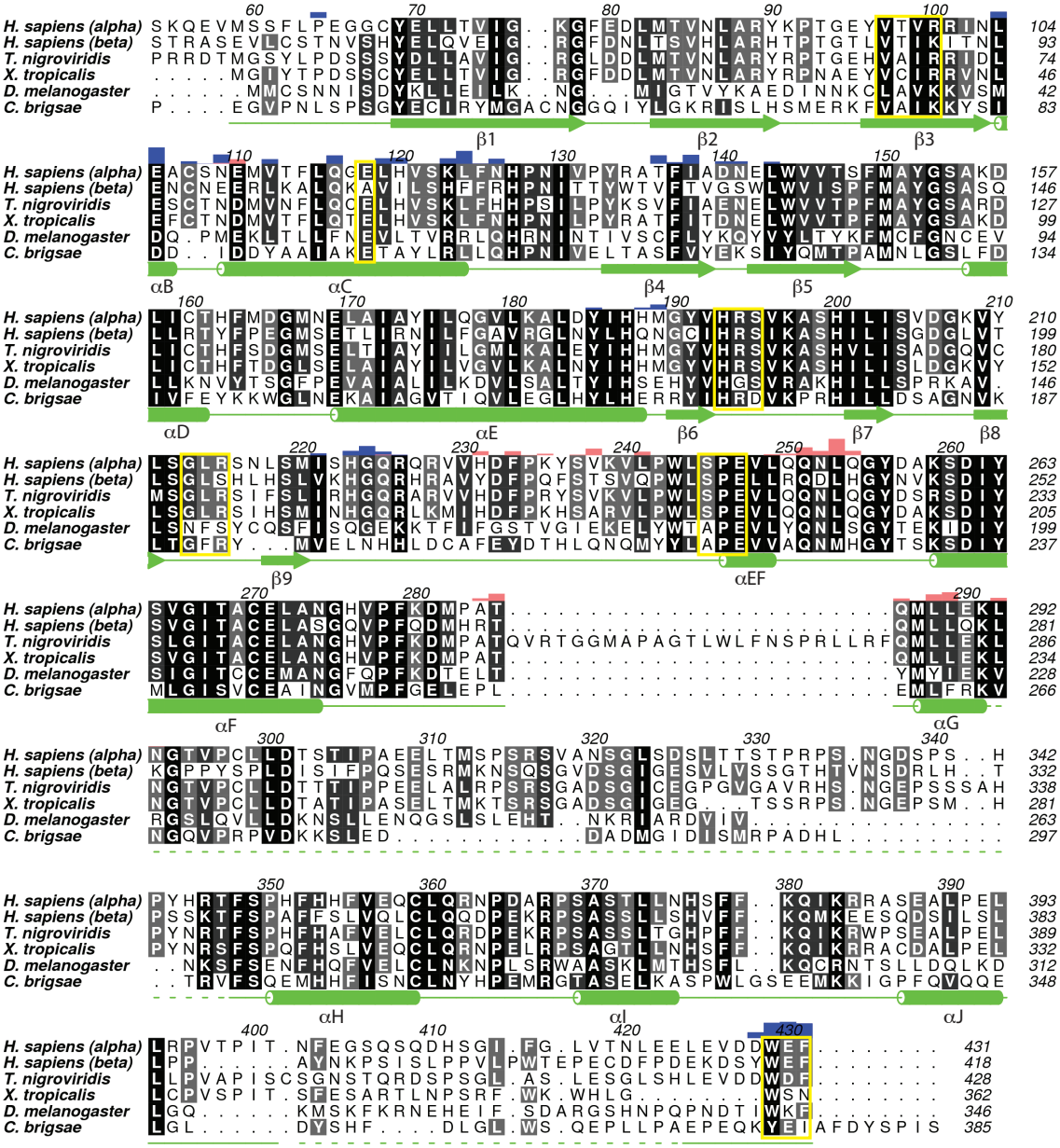

Figure 4.11: STRADα multiple sequence alignment, secondary structure and residues contributing to the interactions with LKB1/MO25α

Multiple sequence alignment (black = conserved, white = not conserved) of STRADα from the indicated species of the metazoan kingdom. Alignments were performed with MUSCLE (Edgar, 2004) and edited and displayed using ALINE (Bond and Schüttelkopf, 2009). A graph of residues involved in LKB1/MO25α interaction against their contact area (blue bars = MO25α, pink bars = LKB1), is displayed. Height of the bar represents the contact area (atom pairs closer than 3.9 Å, analysed by CONTACT from the CCP4 package (Collaborative Computational Project, 1994)), divided by the total surface area of the participating amino acid. Key STRADα "catalytic" motifs and the WEF motif are boxed. The secondary structure (analysed by DSSP (Kabsch and Sander, 1983)) is shown in green.

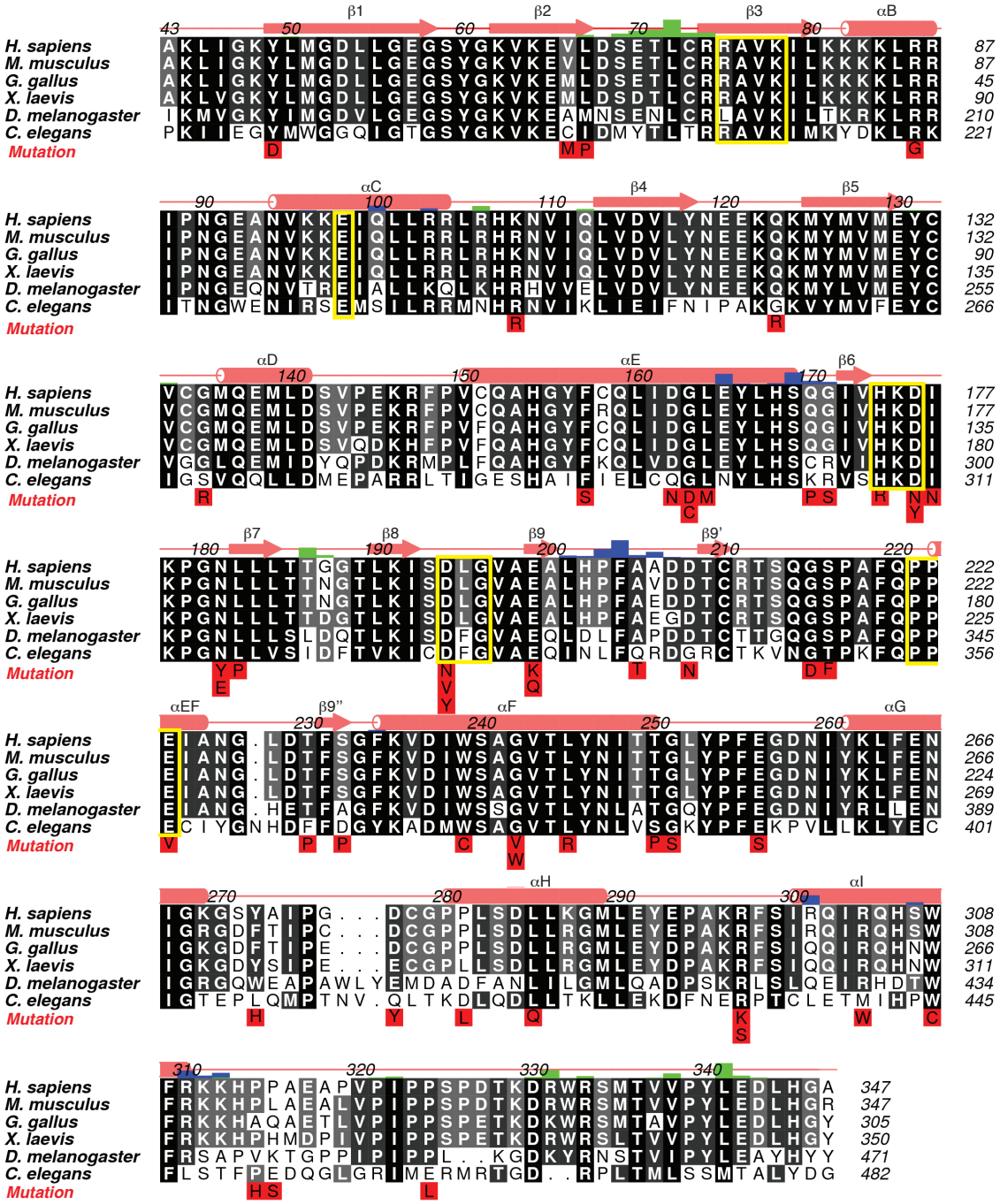

Figure 4.12: LKB1 multiple sequence alignment, secondary structure and residues contributing to the interactions with STRADα/MO25α

Multiple sequence alignment (black = conserved, white = not conserved) of LKB1 from the indicated species of the metazoan kingdom. Alignments were performed with MUSCLE (Edgar, 2004) and edited and displayed using ALINE (Bond and Schüttelkopf, 2009). A graph of residues involved in STRADα/MO25α interaction against their contact area (green bars = STRADα, blue bars = MO25α), is displayed. Height of the bar represents the contact area (atom pairs closer than 3.9 Å, analysed by CONTACT from the CCP4 package (Collaborative Computational Project, 1994)), divided by the total surface area of the participating amino acid. Key LKB1 catalytic motifs are boxed. The secondary structure (analysed by DSSP (Kabsch and Sander, 1983)) is shown in pink. Disease-causing mutations are displayed at the corresponding amino acid position and have been coloured red.

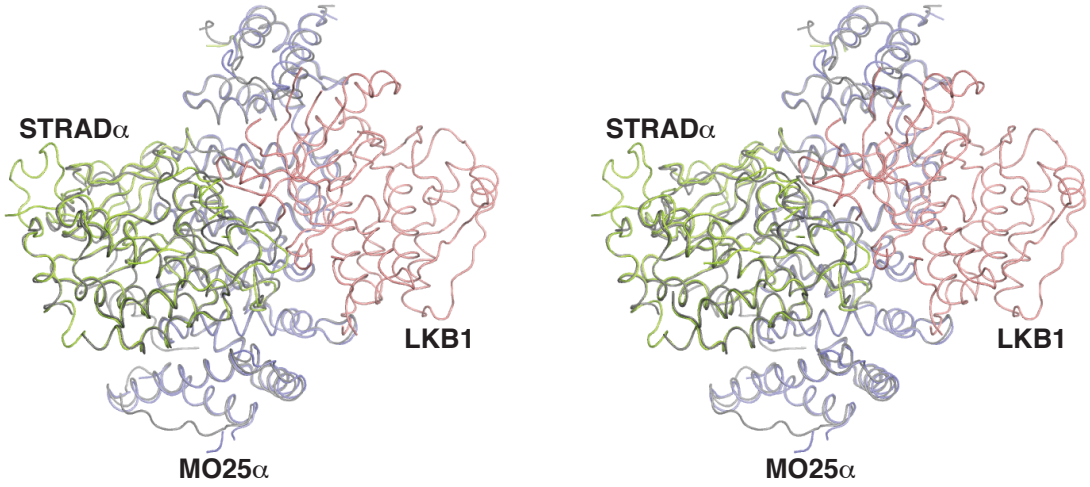

Figure 4.13: Superposition of the STRADα/MO25α dimer with the LKB1 heterotrimer
Stereo view of a superposed STRADα/MO25α complex (coloured gray; discussed in chapter III) and the LKB1/STRADα/MO25α heterotrimer. RMSD = 0.5 Å on 529 Cα atoms.

hydrogen bonding with the R/K residues as well as contribute to an overall closed conformation of the kinase domain by interacting with basic residues from helix αC (Johnson et al., 1996; Huse and Kuriyan, 2002). Interestingly, the position of Thr212 is very similar to that of the phospho-threonine of other protein kinases (such as PKA) that require an activatory phospho-residue in the activation loop (Fig. 4.15). However, the negative charge that would otherwise be provided by the phosphate group is now replaced by Glu199 from β9, that is in hydrogen bonding distance with Lys175 (Fig. 4.15). Interestingly, the majority of eukaryotic protein kinases have preference for a positively charged residue at this position (usually a lysine residue, (Kannan et al., 2007b); see also Fig. 3.8, PKA position 168), presumably to counteract the negative charge from a phosphorylated residue.

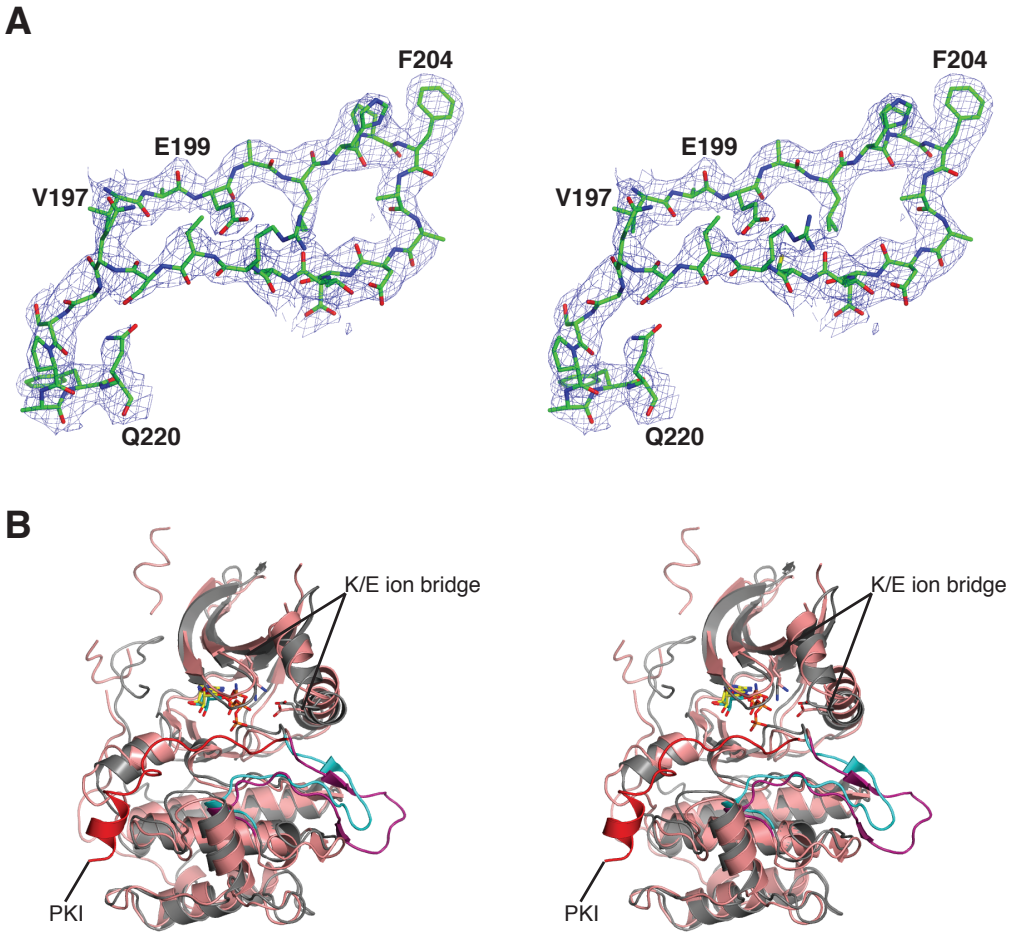

Figure 4.14: LKB1 adopts an active conformation
A) Stereo figure of the final $2F_o$-F_c electron density map, (coloured blue and contoured at 1σ level), for the LKB1 activation segment (residues 197–220). Residues are shown as sticks with green coloured carbons and those discussed in the text are labelled.
B) Stereo view of LKB1 structure (pink cartoons with activation segment coloured magenta) superimposed onto the structure of PKA (PDBID 1ATP; gray cartoons with activation segment coloured cyan). The conserved ion bridge between the glutamine (αC helix) and lysine (VAIK motif, β3 sheet) is labelled. The PKA inhibitor peptide (PKI) bound to the PKA substrate binding site (Knighton et al., 1991b) is coloured red.

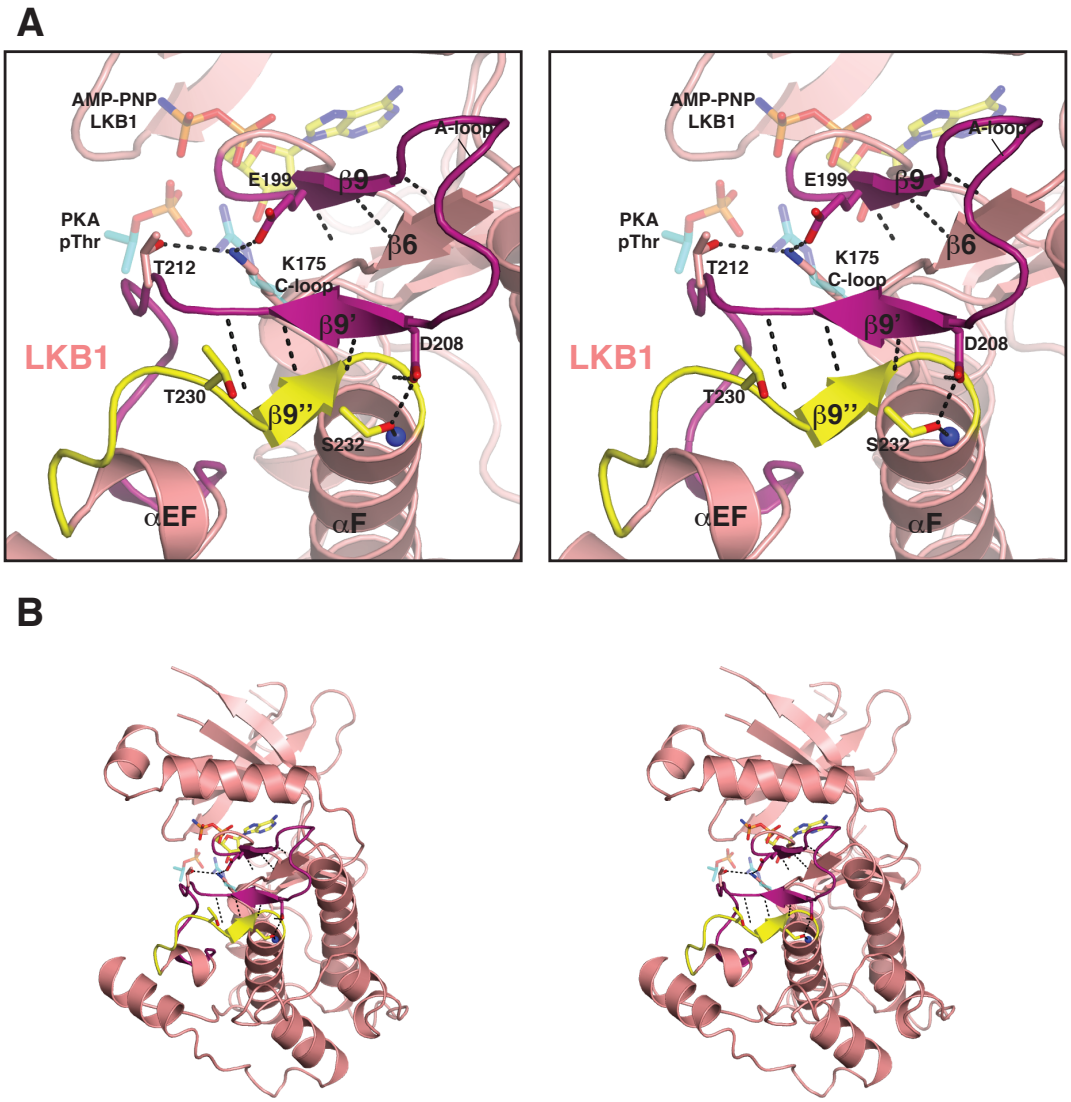

Figure 4.15: LKB1 activation loop requires no phosphorylation
A) Detailed stereo view of anchor points 1 (β6/β9) and 2 (β9'/β9''). Backbone atoms of residues 208–210 and 230–234 are shown, whereas residues Asp208, Thr230 and Ser232 mutated in PJS are labelled and their side chains displayed. A salt bridge between Glu199 and Lys175 depicted as dashed lines, represent the interaction of LKB1 activation segment with its catalytic loop (C-loop). The corresponding interaction found in PKA (PDBID 1ATP) between the phospho-threonine 197 (pThr) and Arg165 is also shown, with PKA residues represented as transparent sticks (carbon atoms coloured cyan). The typical "activatory" threonine (Thr202) present in LKB1 A-loop is labelled. Secondary structure elements are labelled according to the structure of PKA (Knighton et al., 1991b). Dashed lines represent hydrogen bonding interactions
B) Stereo view of the LKB1 kinase domain shown in the same orientation as in (A).

Furthermore, the LKB1 structure displays many similarities with other protein kinases that have been crystallised in the active conformation. The formation of a short $\beta 6/\beta 9$ sheet between catalytic and activation loops—one of the hallmarks of active conformations of protein kinases (Nolen et al., 2004),—provides the first anchoring point for the activation segment and is present in LKB1. Anchor point 1 (AP1) is found near the N-terminus of the activation segment of LKB1, beginning with three residues C-terminal of the Mg^{2+} binding motif (Figs. 4.8B and 4.15). Towards the N-terminus of the activation segment of LKB1, a second anchoring point (AP2) is also present (Fig. 4.8B). Residues 208–210 (activation loop) and residues 231–233 (αEF/αF loop) make backbone interactions in the form of a short antiparallel β-sheet, here referred to as $\beta 9'/\beta 9''$ sheet (Fig. 4.15). The side chain of Asp208 also contributes to the strength of this anchoring point by hydrogen bonding with Ser232 and Tyr234 backbone atoms. The presence of AP2 is a structurally conserved feature of tyrosine protein kinases envisaged to contribute to the stability of substrate binding (Levinson et al., 2008), since this contributes to the positioning of the p+1 loop through its interactions with the αEF/αF loops. Furthermore, the LKB1 αC helix is rotated into the canonical closed conformation (Johnson et al., 1996; Huse and Kuriyan, 2002), with the

conserved ion pair between Lys78 (the so-called VAIK motif in subdomain II) and Glu100 (αC helix in subdomain III, Fig. 4.14B). The structure suggests that this active conformation of LKB1 is achieved through contributions of both STRADα and MO25α.

4.5.2 STRADα binds both N- and C-terminal lobes of LKB1

As shown in chapter III of this thesis, the STRADα/MO25α complex structure have revealed that the STRADα N-lobe is extensively engaged in MO25α binding (chapter III, Fig. 3.18). Moreover, ATP and MO25α binding to STRADα promote an active conformation of the pseudokinase, required for LKB1 activity (discussed in chapter III, section 3.6.3). Together, these results suggest that structural components typical of an active conformational state such as the activation segment will be involved in LKB1 binding and/or activation. Consistent with these observations, in the structure of LKB1/STRADα/MO25α heterotrimer, two residues from STRADα activation loop, Phe233 and His231, bind to the β2/β3 (N-lobe) and β7/β8 (C-lobe) of LKB1 respectively (Fig. 4.16). Additional key contacts between Gln251 from the αEF/αF loop and LKB1 backbone atoms (residues Cys73–Arg74, β2/β3 loop) are also present (Fig. 4.16). The p+1 loop of STRADα also contributes to interactions with LKB1 β2/β3 loop mainly via hydrophobic contacts between Leu241 (STRADα) and Leu72 (LKB1).

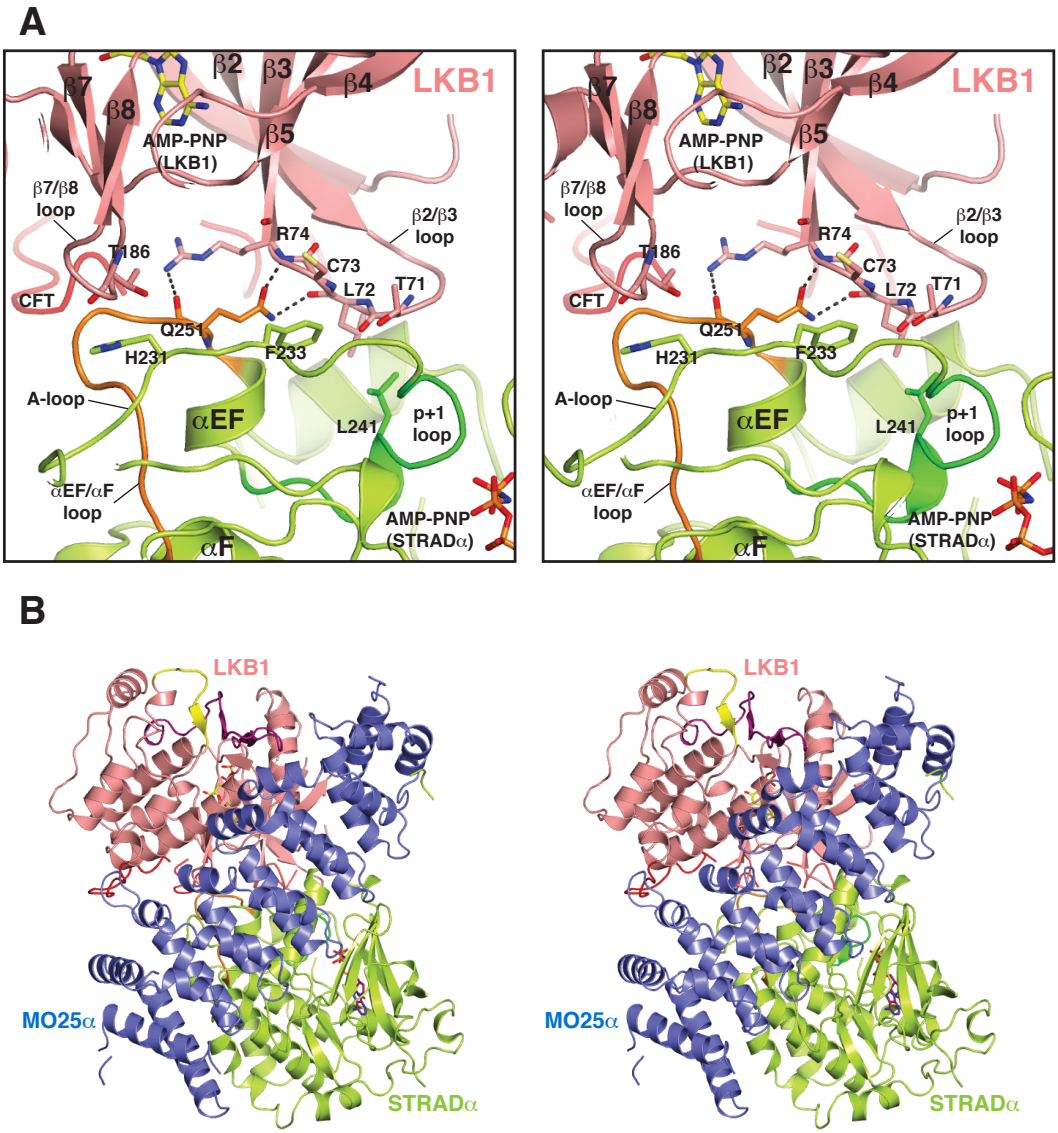

Figure 4.16: Details of the LKB1/STRADα interaction
A) Detailed view of LKB1/STRADα interaction. STRADα p+1 and αEF/αF loops are coloured green and orange respectively. The MO25α structure was removed to aid visualisation.
B) Stereo view of the LKB1 heterotrimeric complex shown in the same orientation as in (A).

Another site of LKB1/STRADα interaction is between the CFT region of LKB1 and the αG helix of STRADα. Thus, it appears that structural elements on the STRADα C-terminal lobe that normally make up the substrate binding site in active protein kinases (i.e. αG helix (Dar et al., 2005; Komander et al., 2008), p+1 loop (Knighton et al., 1991b)), interact with LKB1 (Fig. 4.17).

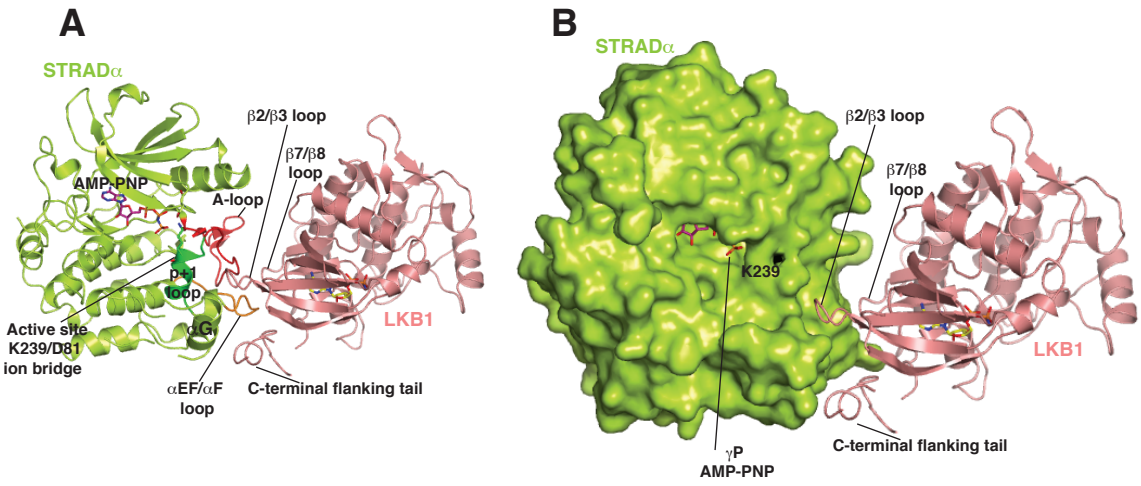

Figure 4.17: LKB1/STRADα interaction and STRADα "active site"
Sites of STRADα/LKB1 interaction are labelled and STRADα is displayed as cartoon (A) and surface models (B). The activation loop of STRADα is coloured red and αEF/αF loop is coloured orange. STRADα K239 from the p+1 loop and D81 from β1/β2 loop that appear to interfere with accessibility of the γ-P are displayed as green sticks and surface.

4.5.3 STRADα is an allosteric activator of LKB1

To understand the role of STRADα binding to LKB1, alanine mutations of interacting residues were made and the effects that these had on LKB1 complex formation and activity were studied. Mutation of residues in the substrate-binding region of STRADα (Leu241 in the p+1 loop and Gln251 in the αEF/αF loop) markedly inhibited interaction with LKB1, whilst mutation of Gln286 (αG helix)

had a moderate effect (Fig. 4.18A). Combining the Gln251 (αEF/αF loop) mutation with an additional mutation on STRADα that has been shown to disrupt the MO25α-STRADα interaction (Tyr185Phe; chapter III, Fig. 3.21A), suppressed LKB1 activation without affecting complex assembly (Fig. 4.18B). Residues on the STRADα activation loop (His231/Phe233), that bind to β7/β8 (C-lobe) and the β2/β3 (N-lobe) of LKB1, respectively (Fig. 4.16), were also mutated. In the absence of MO25α, mutation of His231 and/or Phe233 prevented STRADα from binding to LKB1 (Fig. 4.18A). However, in the presence of MO25α, only the His231/Phe233 double mutant significantly reduced LKB1 activation and complex assembly (Fig. 4.18B). Combining the His231/Phe233 double mutant with the Tyr185 mutation that disrupts interaction with MO25α, resulted in a mutant STRADα that is unable to form a complex with LKB1 and MO25α (Fig. 4.18B). These experiments define the regions on STRADα that interact with LKB1 and MO25α and contribute to the assembly of an active LKB1 complex. Because His231 and Phe233 interact on either lobe of the kinase domain, and their contribution is required for LKB1 activity, it is possible that this interaction "wedges" the LKB1 kinase domain into an active conformation. Moreover, anchoring of these two particular β-sheets (β2/β3 and β7/β8) is of significant importance, as two

catalytically indispensable motifs are found in $\beta 3$ (VAIK motif) and preceding the $\beta 7$ strand (HRD motif).

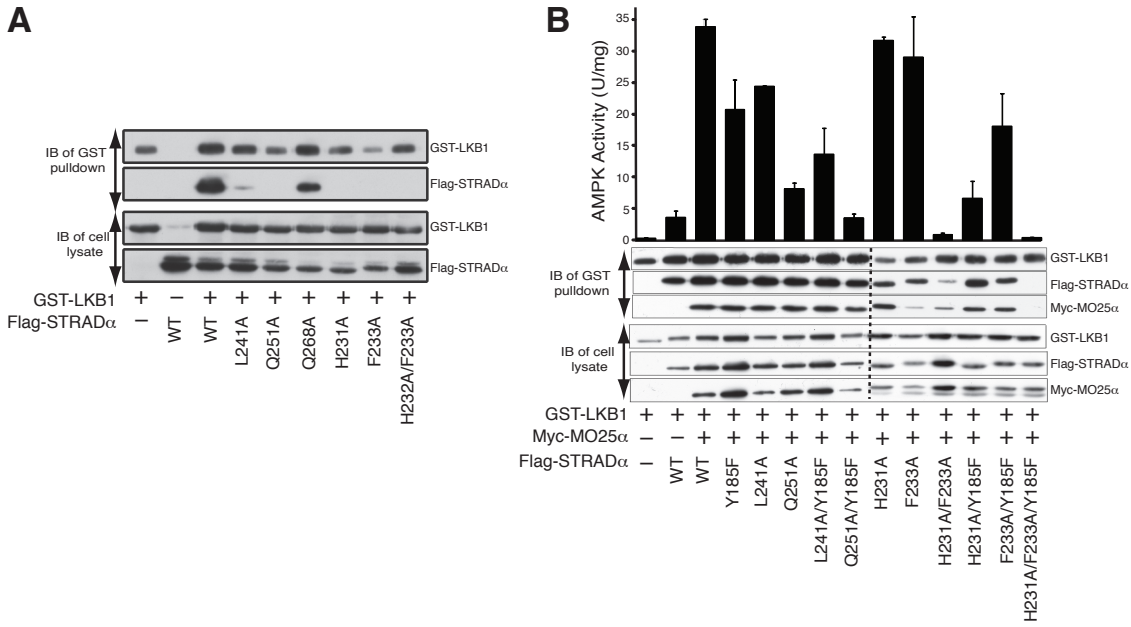

Figure 4.18: Characterisation of the LKB1/STRADα interactions
A) The indicated constructs of GST-LKB1 and Flag-STRADα were expressed in 293 cells in the absence of MO25α. Cells at 36 h post-transfection were lysed and GST-LKB1 affinity purified on glutathione-Sepharose. The purified GST-LKB1 preparation (upper panel) as well as the cell extracts (lower panel) were immunoblotted with the indicated antibodies. Similar results were obtained in three separate experiments.
B) 293 cells were co-transfected with the indicated constructs of GST-LKB1, Flag-STRADα and Myc-MO25α. Cells at 36 h post-transfection were lysed and GST-LKB1 affinity purified and assayed for the ability to activate the heterotrimeric AMPK complex expressed in *E. coli* as described in section 2.11.2. Kinase activities are representative of three independent assays carried out in triplicate (error bars represent the SD for a single triplicate experiment). Affinity purified GST-LKB1 preparation (upper panel) as well as cell extracts (lower panel) were immunoblotted with the indicated antibodies.

4.5.4 The C-terminal flanking tail of LKB1 is essential for formation of an active complex

A common feature of many protein kinase folds (e.g. the AGC kinases) is a C-terminal flanking tail (CFT) that interacts with the N-terminal lobe of the kinase (Kannan et al., 2007a). This tail either serves directly as an auto-activatory mechanism or provides a docking site for

regulatory interacting partners (Kannan et al., 2007a). The structure reveals that LKB1 possesses a proline-rich CFT (residues 311–347) running along the STRADα/LKB1 interface, interacting with the STRADα helix αG as well as the LKB1 N-terminal lobe (Fig. 4.19). An LKB1 mutant (residues 1–318), lacking part of the CFT motif (ΔCFT) failed to interact with STRADα in the absence of MO25α (Fig. 4.20A). Mutation of individual residues in/interacting with the CFT (Trp332/Tyr340/Arg74) did not affect assembly of the LKB1 complex, however LKB1(ΔCFT) formed a complex with markedly reduced catalytic activity when co-expressed with STRADα and MO25α (Fig. 4.20B). Furthermore, mutation of Arg74 (that interacts with the CFT, but also with STRADα, (Figs. 4.16 and 4.19) on LKB1 abolished interaction with STRADα in the absence of MO25α (Fig. 4.20A) and also resulted in a heterotrimeric complex possessing reduced catalytic activity (Fig. 4.20B).

The CFT region present in LKB1 also contains two characterised phosphorylation sites—Ser325 (Sapkota et al., 2002a), which may be phosphorylated by ERK MAPK kinase (Zheng et al., 2009; Esteve-Puig et al., 2009) and Thr336, an autophosphorylation site (Sapkota et al., 2002a). The LKB1 complex structure suggest that these are surface exposed and phosphorylation of these sites would not be pre-

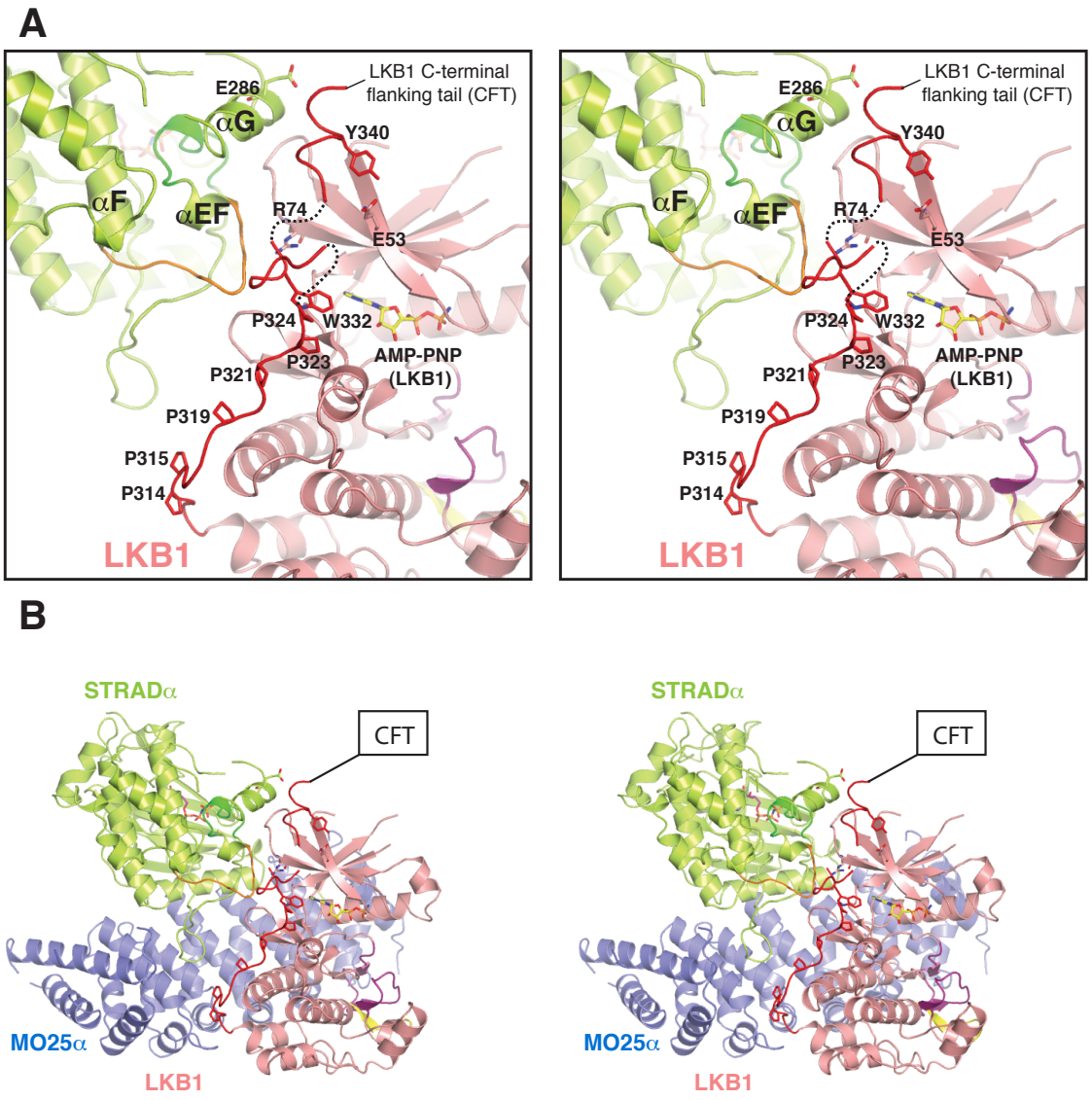

Figure 4.19: LKB1 CFT region runs through the LKB1/STRADα interface
A) Stereo view of the LKB1 CFT interacting with STRADα and LKB1 N- and C-lobes. The proline-rich CFT is coloured red.
B) Stereo view of the LKB1 heterotrimeric complex shown in the same orientation as in (A).

dicted to influence association of the CFT with the LKB1 kinase domain. This is consistent with previous work suggesting that these sites do not directly affect LKB1 catalytic activity (Sapkota et al., 2002a) or complex assembly (Boudeau et al., 2004), but could affect association of LKB1 with substrates or regulators.

These results reveal an important role for CFT in LKB1/STRADα interactions and LKB1 activity and are suggestive of a potential role for other, as yet unidentified, LKB1 regulators that may utilise this region.

4.5.5 LKB1/STRADα interaction and evolution of pseudokinases

As already mentioned in the introduction (chapter I) and chapter III of this thesis, a significant number of human genes code for protein kinases that lack essential residues in their catalytic machinery and have been termed pseudokinases (Manning et al., 2002; Boudeau et al., 2006). Although some predicted pseudokinases have recently been shown to be in fact catalytically competent (Min et al., 2004; Mukherjee et al., 2008; Kawagoe et al., 2008), others remain "true" pseudokinases and are either incapable of binding ATP (Labesse et al., 2009; Scheeff et al., 2009) or catalysing phosphoryltransfer (e.g. STRADα). This raises a number of intriguing possibilities concerning their function and evolutionary origins. It is possible that STRADα evolved

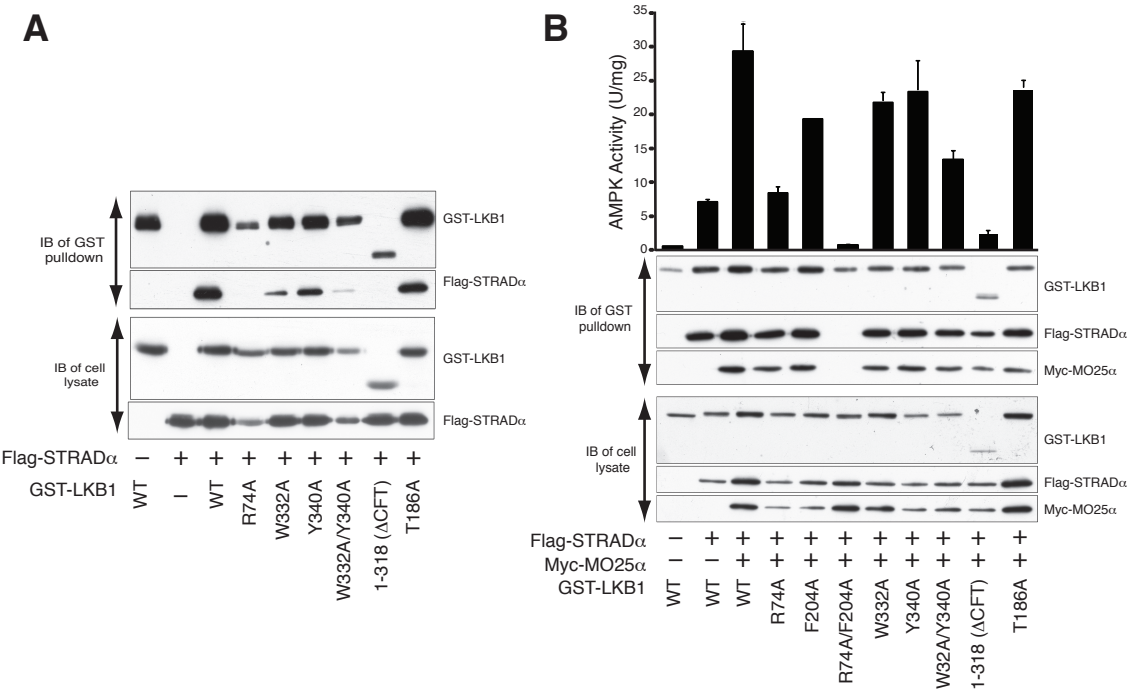

Figure 4.20: Characterisation of LKB1 interacting residues
A) The indicated constructs of GST-LKB1 and Flag-STRADα were expressed in 293 cells in the absence of MO25α. Cells at 36 h post-transfection were lysed and GST-LKB1 affinity purified on glutathione-Sepharose. The purified GST-LKB1 preparation (upper panel) as well as the cell extracts (lower panel) were immunoblotted with the indicated antibodies. Similar results were obtained in three separate experiments.
B) 293 cells were co-transfected with the indicated constructs of GST-LKB1, Flag-STRADα and Myc-MO25α. Cells at 36 h post-transfection were lysed and GST-LKB1 affinity purified and assayed for the ability to activate heterotrimeric AMPK complex expressed in *E. coli* as described in section 2.11.2. Kinase activities are representative of three independent assays carried out in triplicate (error bars represent the SD for a single triplicate experiment). Affinity purified GST-LKB1 preparation (upper panel) as well as cell extracts (lower panel) were immunoblotted with the indicated antibodies.

from a catalytically competent protein kinase, capable of phosphorylating and activating LKB1. During evolution, the mechanism by which STRADα stimulated LKB1 activity may have changed to favour regulation through direct interaction, rather than phosphorylation. This notion is supported by the observation that STRADα interacts with LKB1 using structural elements in its C-lobe that are normally utilised by active protein kinases to bind their substrates (e.g. the p+1 loop/αG helix). Protein kinases generally need to be in their

active conformation to bind their substrates. As it has already been described in chapter III of this thesis, STRADα has to adopt an "active" conformation, stabilised through ATP and MO25 in order to activate LKB1. The finding that LKB1 interacts with STRADα as a "pseudosubstrate" accounts for this requirement of the active conformation of STRADα. This allosteric mechanism of activation may have resulted in loss of evolutionary pressure to retain STRADα catalytic activity, thus explaining the loss of at least six essential catalytic residues on STRADα. It is possible that other pseudokinases that lack critical catalytic residues evolved in a similar way.

In order for LKB1 to phosphorylate AMPK substrates, the active site cleft of LKB1 has to be accessible. Indeed, the structure of the heterotrimer shows that the C-terminal lobe of LKB1 is not engaged in interactions with STRADα or MO25α that would impair substrate interaction (Figs. 4.8 and 4.14B). Moreover, the region around the γ-phosphate (disordered in our structure) of ATP is solvent exposed in LKB1—this contrasts with the equivalent region on STRADα, which is inaccessible due to interactions with LKB1, with the γ-phosphate being shielded by Lys239 of STRADα (Fig. 4.17).

4.5.6 MO25α stabilises the LKB1 activation loop

Most protein kinases are activated by phosphorylation of their activation loop, producing a conformation competent for substrate binding, with the formation of short β6/β9 and β9'/β9" sheets between catalytic and activation loops (Nolen et al., 2004; Levinson et al., 2008). Despite the lack of activatory phosphorylation, the LKB1 activation loop is well-ordered (fully defined by electron density) and adopts a conformation typical of active protein kinases (Fig. 4.14). Key to this is the interaction of the LKB1 activation loop (residues 204–206) with residues from the concave surface of MO25α (Fig. 4.21). Residues Met246, Ile250, Val280 and Pro285 form a hydrophobic pocket on MO25α, accommodating Phe204 on the LKB1 activation loop (Fig. 4.21). Individual mutation of these residues did not affect LKB1 complex formation or activity (Fig. A.6). However, mutation of Phe204 together with Arg74, a residue required for LKB1/STRADα interaction (Fig. 4.16 and 4.20A), resulted in LKB1 species that were incapable of forming a heterotrimeric complex (Fig. 4.20B).

Additional interactions occur between Arg240/Phe243 on MO25α with the backbone of Ala205/Ala206 of LKB1 that act as a molecular "peg", to orient the activation loop of LKB1 and stabilise its active conformation (Fig. 4.21). Although mutation of both Arg240 and

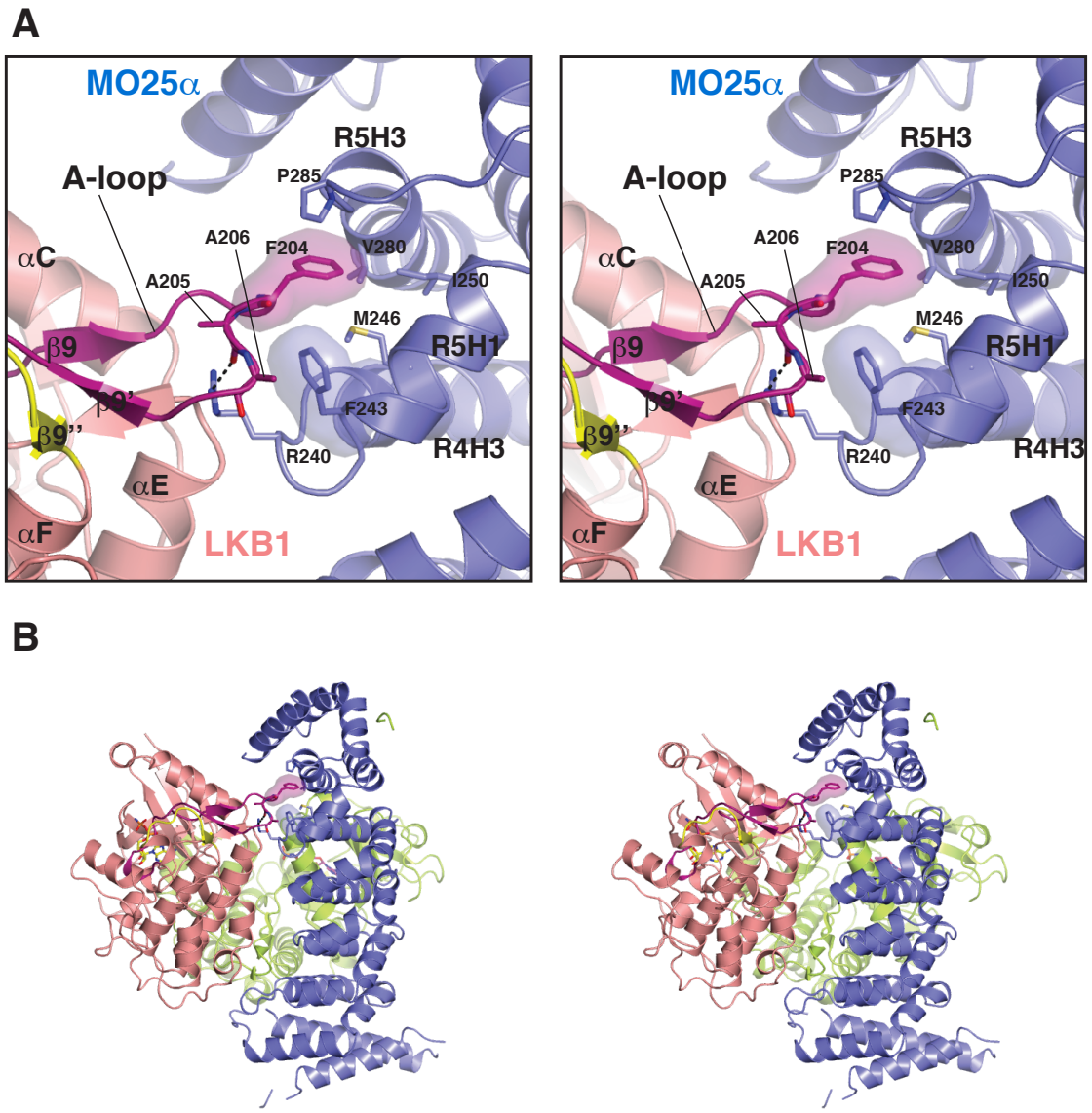

Figure 4.21: Details of the LKB1 activation loop and MO25α concave surface interaction

A) Stereo view of LKB1/MO25α interaction. The LKB1 activation loop is coloured magenta and the αEF/αF loop is coloured yellow. For clarity, STRADα is not shown.

B) Stereo view of the LKB1 heterotrimeric complex shown in the same orientation as in (A).

Phe243 did not affect the ability of MO25α to interact with STRADα and LKB1, the resulting complex is inactive, establishing the importance of this interaction in stimulating LKB1 (Fig. 4.22).

Taken together, these data suggest that MO25α stabilises the activation loop of LKB1 in an optimal conformation required for phosphorylation of substrates such as AMPK.

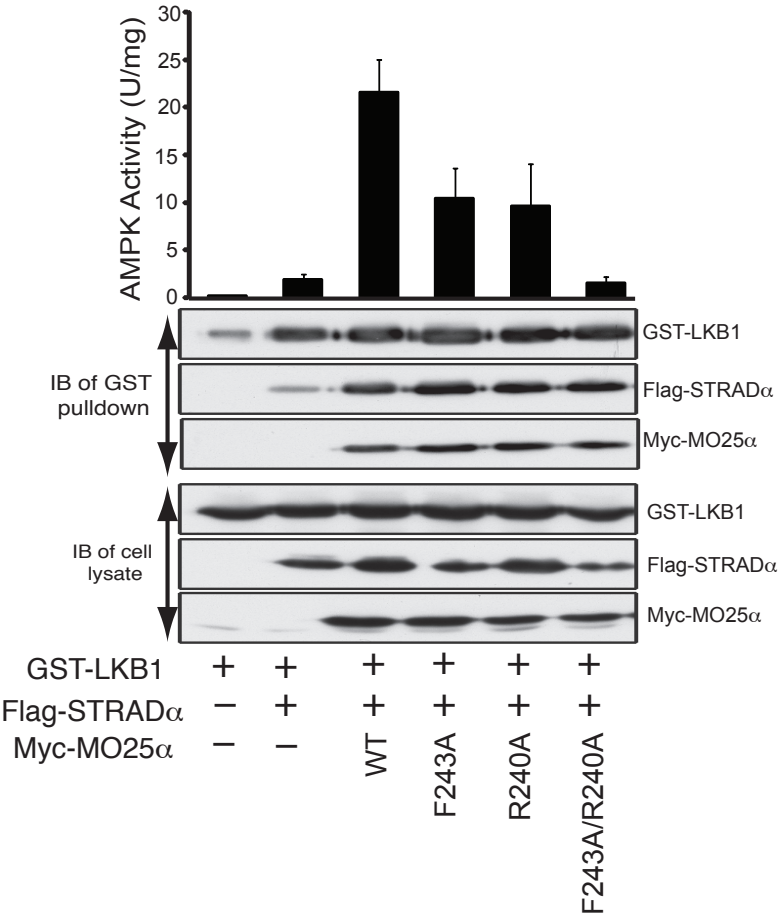

Figure 4.22: Characterisation of the LKB1/MO25α interactions
293 cells were co-transfected with the indicated constructs of GST-LKB1, Flag-STRADα and Myc-MO25α. Cells at 36 h post-transfection were lysed and GST-LKB1 affinity purified and assayed for the ability to activate heterotrimeric AMPK complex expressed in *E. coli* as described in section 2.11.2. Kinase activities are representative of three independent assays carried out in triplicate (error bars represent the SD for a single triplicate experiment). Affinity purified GST-LKB1 preparation (upper panel) as well as cell extracts (lower panel) were immunoblotted with the indicated antibodies.

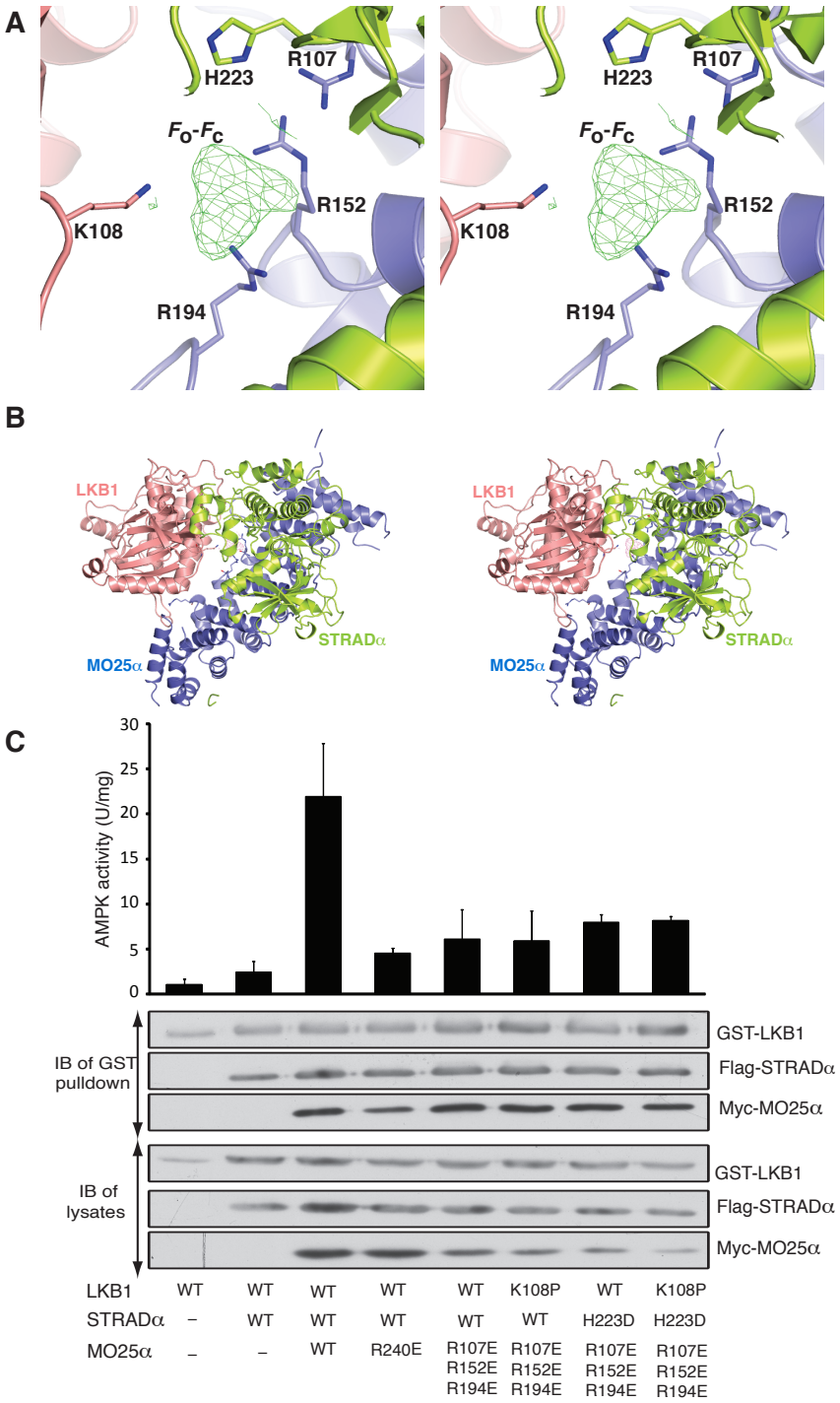

Figure 4.23: Possible ligand coordination by LKB1, STRADα and MO25α
A) Stereo view of unbiased F_o-F_c electron density map (contoured at 2.5σ) indicating a possible small molecule/ligand that is coordinated by positively charged residues from LKB1, STRADα and MO25α.
B) Stereo view of the LKB1 heterotrimeric complex shown in the same orientation as in (A).
C) 293 cells were co-transfected with the indicated constructs of GST-LKB1, Flag-STRADα and Myc-MO25α. Cells at 36 h post-transfection were lysed and GST-LKB1 affinity purified and assayed for the ability to activate the AMPK complex. Kinase activities are representative of three independent assays carried out in triplicate (error bars represent the SD for a single triplicate experiment). Affinity purified GST-LKB1 preparation (upper panel) as well as cell extracts (lower panel) were immunoblotted with the indicated antibodies.

4.6 A possible ligand coordination by LKB1, STRADα and MO25α

Inspection of the electron density for the LKB1 complex revealed clear positive density at an unexpected region of the asymmetric unit that excludes disordered protein residues (Fig. 4.23). Attempts at assigning the occupancy to small molecules that were part of buffer components were unsuccessful, leaving open the possibility that a small molecule/metabolite present in the expression host cells was carried along during the LKB1 complex purification. This unidentified small molecule appears to be coordinated by positively charged LKB1 (Lys108 from the HPN loop), STRADα (His223) and MO25α (Arg107, Arg152 and Arg195) residues (Fig. 4.23A and B). Interestingly, a Lys108Arg mutation is found in PJS patients (Olschwang et al., 2001) suggesting a change in the chemical environment around this putative ligand could affect LKB1 signalling. Furthermore, reverse charge mutations of MO25α contributing residues, either alone or in combination with His232Asp (STRADα) and Lys108Pro (LKB1) reduced the ability of LKB1 to activate AMPK (Fig. 4.23C). However, it remains unclear whether an as yet unidentified negatively charged small molecule/metabolite, is involved in regulating LKB1 activity and more data are needed to support this observation.

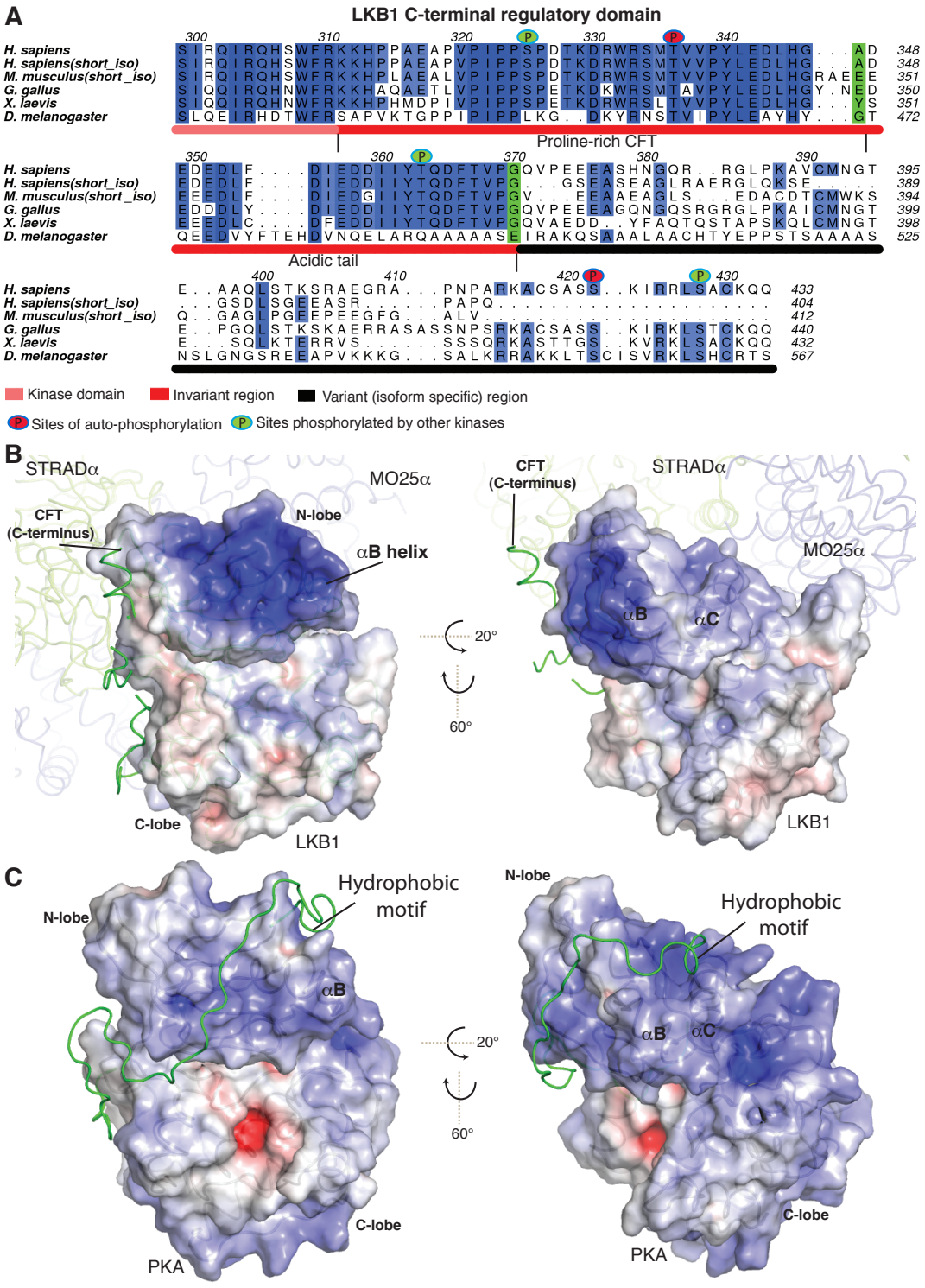

Figure 4.24: LKB1 acidic C-terminal tail and positively charged N-terminal pocket
A) Multiple sequence alignment (dark blue = conserved, white = not conserved) of the LKB1 C-terminal regulatory domain (CRD; residues 311-433) from the indicated species.
B) Electrostatic potential of the LKB1 kinase domain (semi-transparent) surface, analysed by APBS (N.A. Baker and McCammon, 2001). Blue areas (+10 kT) represent positively charged surfaces and red areas (−10 kT) represent negatively charged surfaces. The CFT is shown as a green cartoon. STRADα and MO25α are shown as semi-transparent cartoons.
C) Interaction of the AGC kinase PKA (PDBID 1ATP (Knighton et al., 1991b)) C-terminal tail and hydrophobic motif with the N-lobe and hydrophobic pocket. The PKA surface is shown as in (B) and the C-terminal tail as a green cartoon.

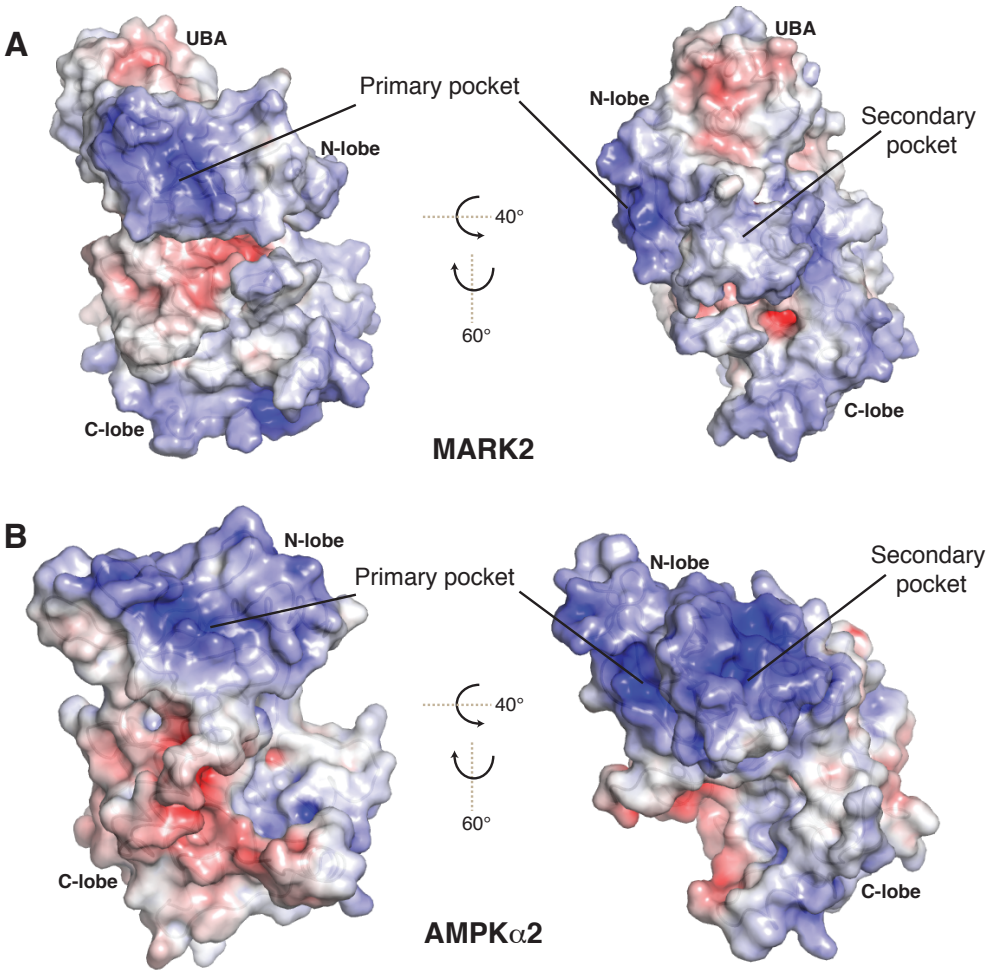

Figure 4.25: LKB1 contains an acidic C-terminal tail and a positively charged N-terminal pocket

Electrostatic potential of (A) MARK2 (PDBID 2R0I (Panneerselvam et al., 2006)) and (B) human AMPKα2 kinase domain (PDBID 2H6D (Littler et al., 2006)), analysed by APBS (N.A. Baker and McCammon, 2001) and shown as transparent surfaces. Blue areas (+10 kT) represent positively charged surfaces and red areas (−10 kT) represent negatively charged surfaces.

4.7 The LKB1 N-lobe contains a positively charged pocket

Inspection of sequence conservation among different species and between the different spliced isoform (LKB1 short; found predominantly in testis (Towler et al., 2008; Denison et al., 2009)), reveals some interesting features of the C-terminal regulatory domain (Fig 4.24A). The CRD comprises the C-terminal non-kinase domain (residues 311-433) of LKB1 (Fig 4.24A). Residues 311-370 are identical between the LKB1 short and long isoforms (Towler et al., 2008; Denison et al., 2009), and this is referred to here as the invariable region of CRD. Residues beyond 370 differ between the short and long isoforms and this region is referred to here as the variable region of CRD. The CRD invariant region can be further subdivided into a proline-rich tail (residues 311-347, referred here as the proline-rich CFT and discussed in section 4.5.4 of this chapter) and an acidic tail (residues 348-370), that contains stretches of aspartic and glutamic acids (Fig. 4.24A), three large hydrophobic residues (Phe354, Tyr362 and Phe366) and a mapped phosphorylation site (Thr363) Sapkota et al. (2002a). Interestingly, the proline-rich CFT immediately preceding the acidic tail (not present in the crystallised construct) is found close to the N-lobe of the kinase domain, nearby a highly positively charged area of LKB1 (Fig. 4.24B). This basic "barrel" is formed by charge contributions

from clusters of Lys/Arg residues present in the αB helix (residues 81–84 and 85–87) and lysine residues from β2 (Lys62, Lys64) and β5 (Lys124) strands, that are part of the N-terminal β-barrel of the kinase domain (Fig. 4.12). It is plausible to hypothesise that the acidic tail of LKB1 will be binding to this positively charged region in an analogous manner that AGC kinases such as PKB (Yang et al., 2002), PKCι (Messerschmidt et al., 2005) and PKA (illustrated in Fig. 4.24C). These kinases use their C-terminal tail to bind to the N-lobe and regulate their activity. However, AGC kinases typically have (so-called) turn and hydrophobic motifs (reviewed by Komander et al., 2006) that bind to corresponding pockets and are also regulated by phosphorylation (Hauge et al., 2007). While the functions and molecular mechanisms for the hydrophobic and turn motif binding/phosphorylation have been well studied for the AGC kinases, no analogy to this system has been described for other groups of protein kinases. However, the mechanism of action is well conserved throughout the human kinome, since the binding of the hydrophobic motif to the hydrophobic pocket, regulates the rotation of the αC helix, a feature first described for CDK2 activation by cyclins (Jeffrey et al., 1995) and later for AGC kinases (Bayliss et al., 2003), tyrosine kinases (Filippakopoulos et al., 2008) and even pseudokinases such as

STRADα (described in chapter III of this thesis). Therefore, it is possible the acidic tail, also containing a phosphorylation site (Thr363), interacts with positively charged/hydrophobic pockets in the LKB1 N-lobe, analogous to the turn and hydrophobic motifs of AGC kinases. However, the function of this binding is unclear, since LKB1 (43-347) lacking the acidic tail forms complexes with STRADα/MO25α and phosphorylates a peptide substrate to the same extent as the WT-LKB1 (Fig. 4.3). Thus, LKB1 is unlikely to use the acidic tail/basic "barrel" to regulate its activation. Instead LKB1 may be using its acidic tail, and/or its basic "barrel", for docking with/to interacting partners, similar to the upstream AGC activating master kinase, PDK1 that binds to the hydrophobic motif of its downstream targets using it N-lobe hydrophobic pocket (Biondi et al., 2002).

Intriguingly, downstream targets of LKB1, for which structures are known, MARK2 and AMPK, possess similar positively charged pockets in their N-lobe (Fig. 4.25). Interestingly, the AMPKα2 kinase domain (Littler et al., 2006) contains two such highly positively charged pockets, a primary pocket present in the β barrel, and a secondary pocket present between the αB–αC helices (Fig.4.25B).

Further work is required to establish the role of the acidic tail of LKB1. A crystal structure of the LKB1 kinase containing this region

will be useful to understand the interactions between the acidic tail and the N-lobe of the kinase domain, that could also reveal the possible role of the LKB1 basic "barrel". In addition, investigating the ability of LKB1 that lacks the acidic tail, to interact with, and activate AMPK and the AMPK related kinases, could provide more insights into the molecular mechanism of LKB1 activation of these kinases.

4.8 Structural basis of Peutz-Jeghers syndrome

Following the key discovery of mutations in the LKB1 gene as the main cause of Peutz-Jeghers syndrome (Hemminki et al., 1998) a decade ago, at least 50 missense mutations derived from PJS patients and sporadic cancers have been mapped to the LKB1 kinase domain and the CFT loop (see chapter I, section 1.4.2). The study carried out by Boudeau et al., (2004), characterised the effects that 32 of these mutations have on the ability of LKB1 to form active heterotrimeric complexes with STRADα and MO25α (Boudeau et al., 2004). The remaining 18 mutations were characterised in this thesis, together with 6 of the previously tested mutations (Boudeau et al., 2004), to ensure reproducibility of the assay. The location of these mutations, how they may affect LKB1 structure or function, and the experimental data on LKB1 complex assembly and activity are summarised in Table 4.2, Figs. 4.26 and 4.27. The structural map reveals that the majority of

mutations are located in the C-lobe of the LKB1 kinase domain and are residues important for structural integrity of LKB1 (Fig. 4.26A). From these, there are two hydrophobic clusters, named hydrophobic cluster 1 (Phe157, Leu242, Leu285, Trp308) and hydrophobic cluster 2 (L164, I177 and L182) (Fig. 4.26A). Many of these mutations resulted in low LKB1 expression levels, suggestive of generating unstable protein species, and all LKB1 mutants were incapable of forming active complexes with STRADα and MO25α (Fig. 4.27 and Table 4.2). In addition, at least 10 mutations involve residues required for catalysis or substrate binding (Fig. 4.26). While these mutants properly assembled into complexes with STRADα and MO25α, these were devoid of catalytic activity (Fig. 4.27 and Table 4.2).

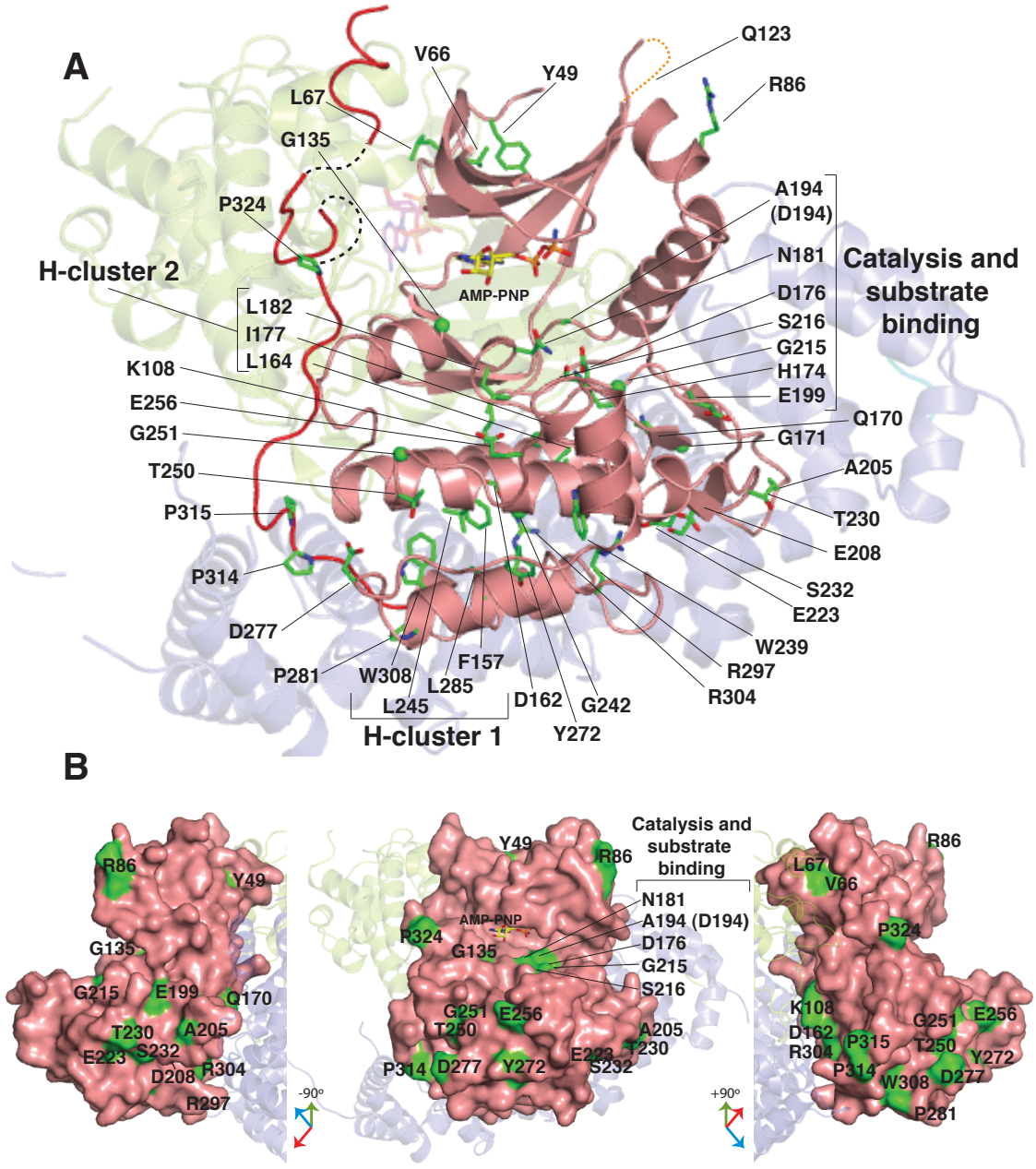

Figure 4.26: Map of oncogenic mutations on the LKB1 kinase domain
A) Location of LKB1 residues that are mutated in PJS and other types of cancer. The CFT region is coloured red and dashed lines represent areas that were not well-defined by electron density.
B) Surface exposed residues mutated in PJS and other types of cancer.

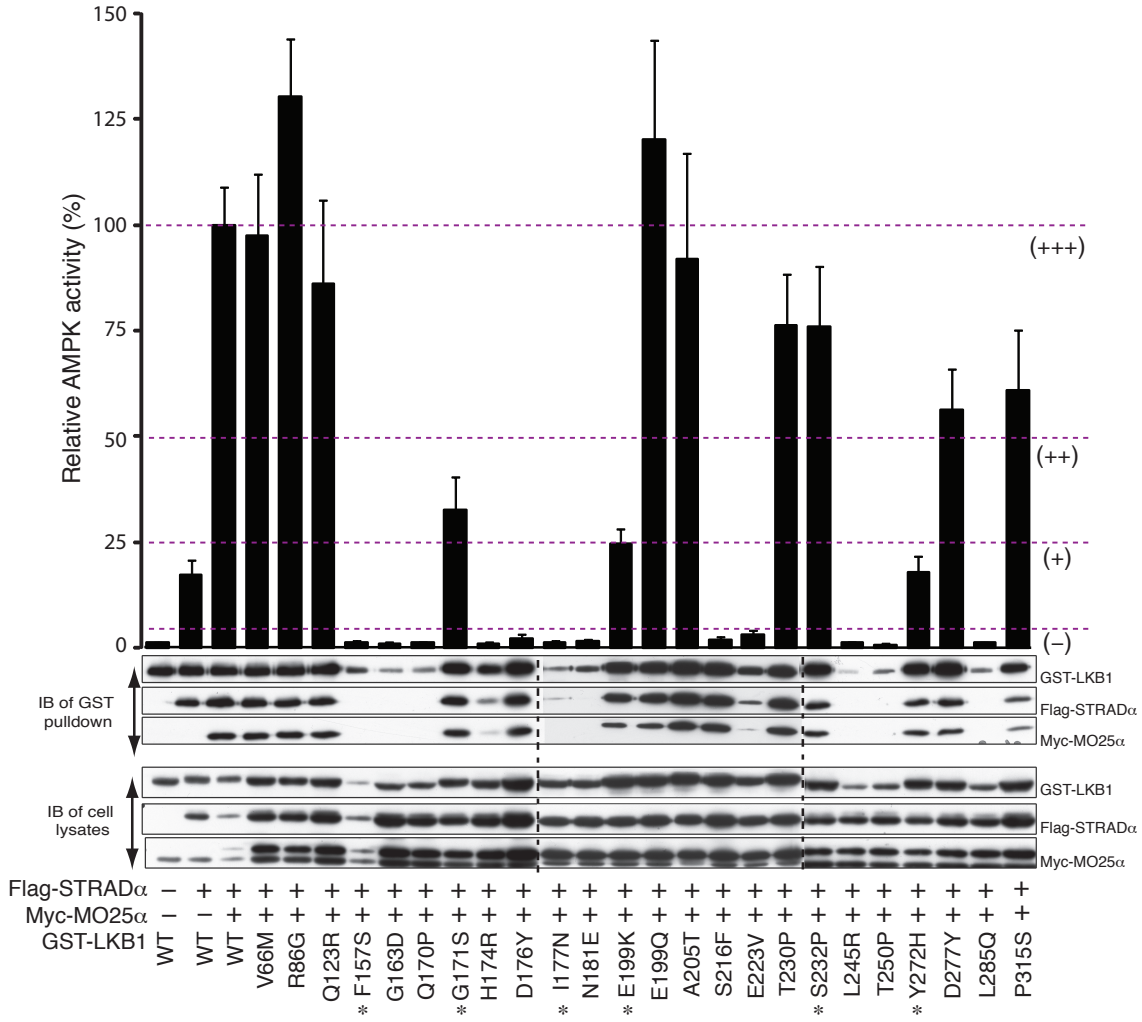

Figure 4.27: Effect of the oncogenic mutations on LKB1 activity
293 cells were co-transfected with the indicated constructs of GST-LKB1, Flag-STRADα and Myc-MO25α. Cells at 36 h post-transfection were lysed and GST-LKB1 affinity purified and assayed for the ability to activate rat heterotrimeric AMPK complex expressed in *E. coli* as described in the Materials and Methods. Kinase activities are standardised relative to the activity of the wild type LKB1/STRADα/MO25α complex ($-$, <5%; $+$, 5-25%; $++$, 25-50%; $+++$, >50%) and represent the average of six independently purified complexes, assayed in duplicate (error bars represent the SEM). Representative Western blots of affinity purified GST-LKB1 preparations (upper panel) as well as cell extracts (lower panels), probed with the indicated antibodies are also shown. Asterisk indicate mutation was previously investigated by Boudeau et al., (2009).

Table 4.2: Cancer causing mutations found in the LKB1 tumour suppressor kinase domain and the C-terminal flanking tail

Mutation	Disease	Location and functional significance	Comp.	Act.	Reference
Y49D	PJS	β1, possible destabilisation of the N-lobe	Yes	+	(Rowan et al., 1999)
V66M*	PJS, Cervix	β2, possible destabilisation of the N-lobe	Yes	+++	(Kuragaki et al., 2003)
L67P	PJS	β2, possible destabilisation of the N-lobe	No	−	(Hemminki et al., 1998)
R86G*	PJS, NSCLC	αB, basic (Arg-rich) region; solvent exposed	Yes	+++	(Strazisar et al., 2009)
K108R	PJS	HKN loop	Yes	+++	(Olschwang et al., 2001)
Q123R*	NCLS	β4-β5 loop; solvent exposed	Yes	+++	(Ji et al., 2007)
G135R	PJS	Hinge region, ATP binding	Yes	−	(Rowan et al., 1999)
F157S**	PJS	Part of hydrophobic cluster 1: L245, M289, I303, F309, L285	No	−	(Ylikorkala et al., 1999)
D162N	PJS	Structural role; forms ion pair with R304	Yes	+++	(Westerman et al., 1999a)
G163D*	PJS, NSCLC	Presence of side chain may distort the LKB1 catalytic loop	No	−	(Westerman et al., 1999a)
L164M	PJS	Mutation may misposition the catalytic HRD motif	Yes	+++	(Westerman et al., 1999a)
Q170P*	PJS	Structural role, possible distortion of helix αE	No	−	(Forbes et al., 2008)
G171S**	PJS	May interfere with the correct positioning of R240	Yes	++	(Dong et al., 1998)
H174R*	NSCLC	Part of the catalytic HKD motif	Yes	−	(Blons et al., 2008)
D176N	PJS	Catalytic residue, HKD motif	Yes	−	(Mehenni et al., 1998)
D176Y*	PJS	Catalytic residue, HKD motif	Yes	−	(Koivunen et al., 2008)
I177N**	PJS	Part of hydrophobic cluster 2: L160, L164, L182	No	−	(Resta et al., 2002)
N181Y	PJS	Hydrogen bonding with catalytic residue D176 and ATP	Yes	−	(Ylikorkala et al., 1999)
N181E*	PJS	Hydrogen bonding with catalytic residue D176 and ATP	No	−	(Ylikorkala et al., 1999)
L182P	PJS	Part of hydrophobic cluster 2; possible disruption of β6-β9 sheet	No	−	(Olschwang et al., 2001)
D194N/V/Y	PJS, NSCLC	Mg^{2+} binding residue, catalysis	Yes	−	(Westerman et al., 1999a; Avizienyte et al., 1999; Guldberg et al., 1999)
E199K**	PJS	Interacts with backbone atoms from LKB1 A-loop	Yes	+	(Dong et al., 1998)
E199Q*	PJS	Interacts with backbone atoms from LKB1 A-loop	Yes	+++	(Blons et al., 2008)
A205T*	HNSCC	Possible distortion of LKB1 activation loop	Yes	+++	(Qiu et al., 2006)
D208N	PJS	Activation segment, interacts with the αEF-αF loop	Yes	+++	(Dong et al., 1998)
G215D	PJS	p+1 loop, substrate binding	Yes	−	(Dong et al., 1998)

Continued on next page...

Table 4.2 - Continued

Mutation	Disease	Location and functional significance	Comp.	Act.	Reference
S216F*	PJS, NSCLC	p+1 loop, substrate binding	Yes	−	(Ji et al., 2007)
E223V*	NSCLC	Part of the PPE motif; forms ion pair with R297	Yes	−	(Matsumoto et al., 2007)
T230P*	PJS	Short β-strand with A-loop	Yes	+++	(Forbes et al., 2008)
S232P**	PJS	Short β-strand with A-loop; interacts with D208	Yes	+++	(Yoon et al., 2000)
W239C	PJS	Structural role; interacts with L290 and the PPE motif	No	−	(Scott et al., 2002)
G242W/V	PJS	Structural role; αH	No	−	(Olschwang et al., 2001)
L245R*	PJS	Structural role; Possible clashes with W308, L282	No	−	(Forbes et al., 2008)
T250P*	NSCLC	Structural role; C-terminal of helix αF	No	−	(Matsumoto et al., 2007)
G251S	PJS	Possible distortion of the hinge region	Yes	+++	(Resta et al., 1998)
E256S	PJS, NSCLC	Solvent exposed. Binding of possible interactors/substrates	Yes	+++	(Yoon et al., 2000)
Y272H**	PJS	αG-αH loop. Solvent exposed	Yes	+	(Boardman et al., 2000)
D277Y*	PJS, NSCLC	αG-αH loop. Solvent exposed	Yes	+++	(Koivunen et al., 2008)
P281L	PJS	Provides turn between αG-αH loop into αH helix	Yes	+++	(Nishioka et al., 1999; Wang et al., 1999)
L285Q*	NSCLC	Part of hydrophobic cluster 1	No	−	(Forbes et al., 2008)
R297S	PJS	Ion pair with E223 from the PPE motif (helix αEF)	No	−	(Westerman et al., 1999a)
R297K	PJS	Ion pair with E223 from the PPE motif (helix αEF)	No	−	(Boardman et al., 2000)
R304W	PJS	Structural role; hydrogen bonds with D162, E165	No	+	(Resta et al., 1998)
W308C	PJS	Part of hydrophobic cluster 1	No	−	(Mehenni et al., 1998; Onozato et al., 2007)
P314H	PJS	C-terminal flanking tail; binding of possible interactors/substrates	Yes	+++	(Resta et al., 1998)
P315S*	PJS	C-terminal flanking tail; binding of possible interactors/substrates	Yes	+++	(Scott et al., 2002)
P324L	PJS	C-terminal flanking tail; binding of possible interactors/substrates	Yes	+++	(Park et al., 1998; Westerman et al., 1999b)

*Mutants tested in this study; **Mutants tested in this study and by Boudeau et al. (2004)

Comp., Complex formation

Act., LKB1 activity (−, <5%; +, 5-25%; ++, 25-50%; +++, >50%)

PJS, Peutz-Jeghers syndrome

NSCLC, non-small cell lung carcinoma

HNSCC, head and neck non-small cell carcinoma

Other mutations present in the activation loop (Ala205Thr and Asp208Asn), the αEF/αF loop (Thr230Pro, Ser232Pro) and CFT region (Pro314His, Pro315Ser and Pro324Leu) did not markedly affect the ability of LKB1 to assemble into an active complex (Table 4.2). There are also a number of oncogenic mutations in solvent-exposed residues (Arg86Gly, Gln123Arg, Pro315Ser, Tyr272His, Asp277Tyr) that do not affect complex assembly or activity (Fig. 4.27 and Table 4.2). Thus, out of 50 mutations analysed, 18 are still capable of forming a complex with STRADα and MO25α that possesses significant LKB1 activity (Table 4.2). Assuming these are cancer driving rather than passenger mutations, some of these mutations may be involved in interacting with other regulators or substrates of the LKB1 pathway.

Although the data described in this chapter show that STRADα and MO25α are required for activation of LKB1 using a novel allosteric mechanism of activation, it is worth noting that none of the LKB1 oncogenic mutations identified to date, lie on the direct interfaces between LKB1 and STRADα/MO25α. However, this is in agreement with our site directed mutagenesis data (Figs. 4.18, 4.20, 4.22, A.6 and A.7), showing that single mutations that disrupt any of the dimeric interfaces are not sufficient to disrupt formation of an active heterotrimeric complex. While we have shown that it is possible

to engineer an inactive double mutant of LKB1 that disrupts the interfaces with both STRADα and MO25α, this is unlikely to occur spontaneously. Similarly, redundancy of the *MO25A/B* and *STRADA/B* genes may also explain why no oncogenic mutations have been identified in these genes to date (Alhopuro et al., 2005).

4.9 Concluding remarks

The structure of the LKB1 complex has revealed how LKB1 is activated through a phosphorylation-independent mechanism, involving direct interaction with STRADα and MO25α. The active conformation of LKB1 is induced by binding to the C-lobe and activation loop of STRADα. MO25α binding to the activation loop of LKB1 further stabilises this active conformation. MO25α and ATP binding play an important role in stabilising STRADα active conformation, that is crucial for interaction with LKB1 (chapter III of this thesis). Thus, MO25α plays a central role in stabilising association of STRADα and LKB1, as well as controlling their active conformations. A cartoon figure summarising key interactions within the LKB1 heterotrimeric complex is provided in Fig. 4.28

The results discussed in this chapter provide insights into how a subset of protein kinases may have evolved as pseudokinases, incapable of phosphoryltransfer. Instead, pseudokinases such as STRADα have

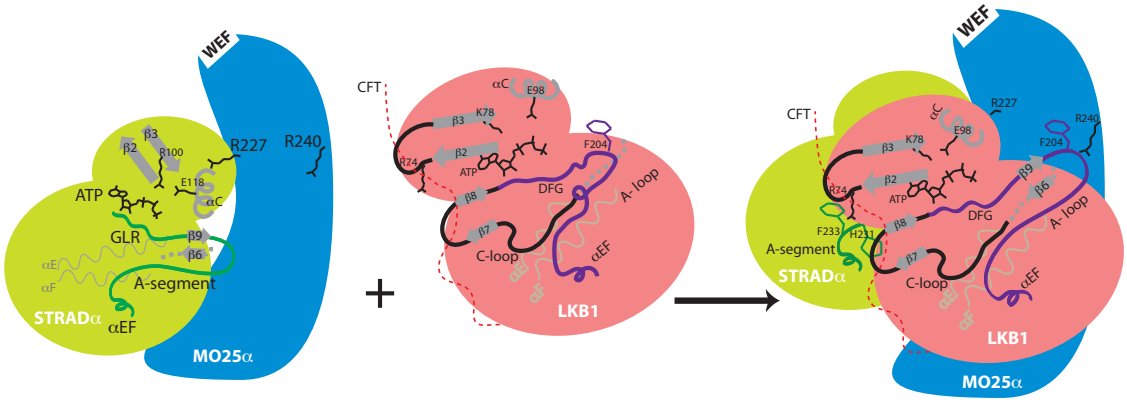

Figure 4.28: Summary of LKB1/STRADα/MO25α interactions and LKB1 activation The model is based on structural and mutagenesis data discussed in this chapter. STRADα interacts via its activation loop residues H231 and Phe233 with either lobe of LKB1, "wedging" them apart and promoting an active kinase conformation. This is stabilised by MO25α interacting mainly via residues Arg240 and Phe243 with the activation loop of LKB1. Two key interacting residues from LKB1 are shown, Arg74 and Phe204 located in the STRADα and MO25α interaction sites respectively.

retained an active conformation required to interact with regulators in a similar manner by which active kinases bind their substrates. The mechanism by which LKB1 is activated, represents a novel way in which kinases can be regulated allosterically and independently of activation loop phosphorylation. Finally, the data provide insights into how cancer mutations affect LKB1 function by impairing complex assembly, catalytic activity and potential interactions with substrates or regulators.

Chapter V

Discussion and future perspectives

5 Discussion and future perspectives

5.1 Pseudokinases

5.1.1 Origin of pseudokinases

A large number of protein kinases in metazoan organisms are predicted to be inactive (Manning et al., 2002; Boudeau et al., 2006). However no comprehensive phylogenetic studies for the pseudokinase family have been conducted thus far. The recent publication of the genome sequence of the choanoflagellate *Monosiga brevicollis* (King et al., 2008)—a protist believed to be the closest relative to metazoans—could help in shedding light to the evolution of these enigmatic proteins. The *M. brevicollis* tyrosine kinome has provided interesting insights in tyrosine signalling by revealing an unexpected expansion of genes containing tyrosine kinase domains (Manning et al., 2008). Analysis of the available sequences (128 in total) of the *M. brevicollis* tyrosine kinome (Manning et al., 2008) reveal eight tyrosine kinases with degenerate HRD and DFG motifs, strongly suggesting inactivity for these kinases (Fig. 5.1). This represents 6% of the total tyrosine kinome and considering the number of human pseudokinases (∼10%) is an overestimate, the 6% approximation could be a ratio similar to the human pseudokinase fraction.

In an attempt to answer the question of whether clear examples

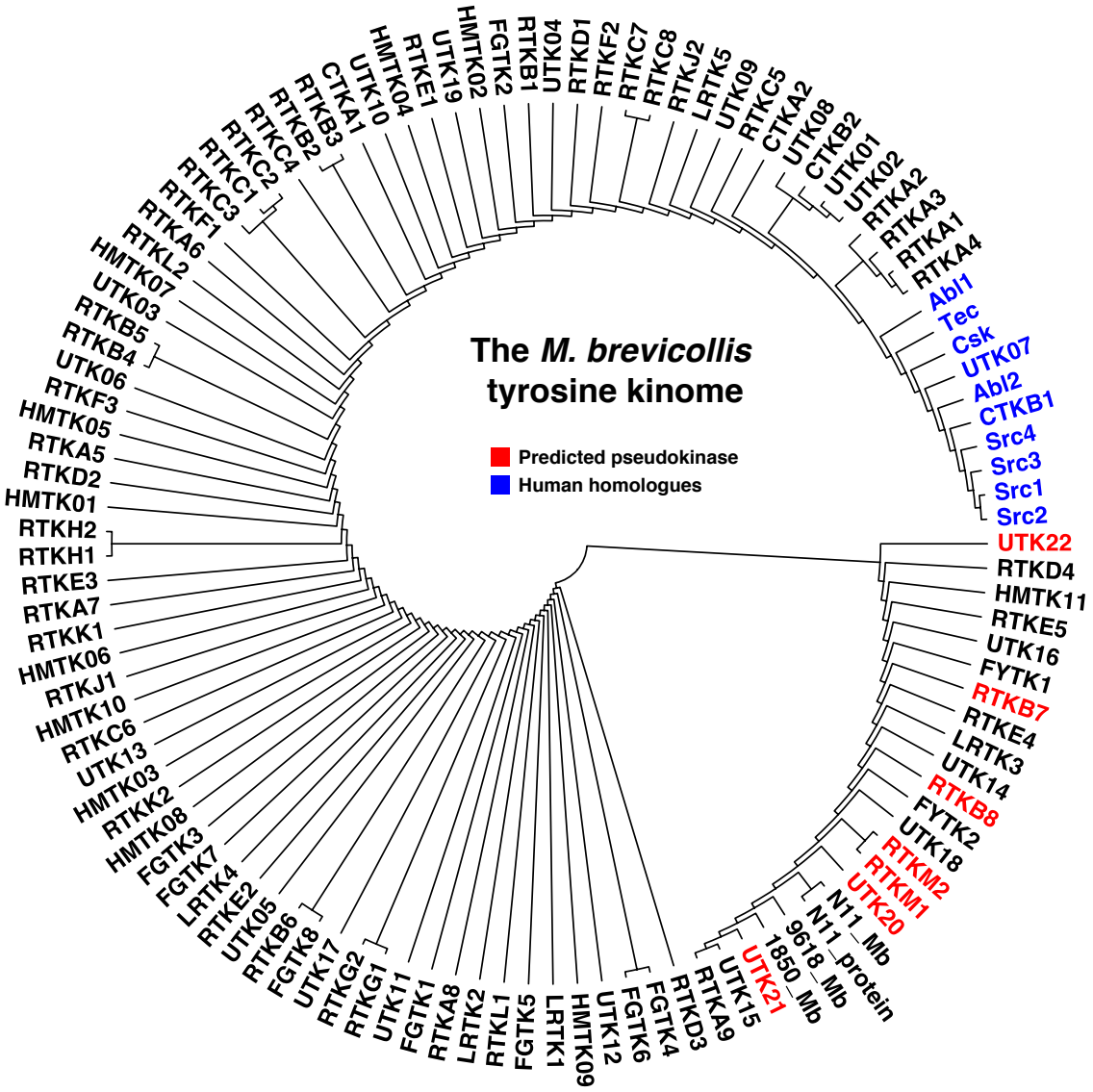

Figure 5.1: The *M. brevicollis* tyrosine kinome
Neighbour-joining distance tree of protein tyrosine kinases from *M. brevicollis*. Predicted pseudokinases are coloured red. Tyrosine kinases conserved in humans (Manning et al., 2008) are coloured blue. Sequences were downloaded from The Salk Institute for Biological Studies website (http://kinase.com/), and aligned using MUSCLE (Edgar, 2004). The tree (calculated using MUSCLE) was displayed using FIGTREE downloaded from URL: http://tree.bio.ed.ac.uk/software/figtree/

of pseudokinases exist in species lower than protozoans, the yeast kinome (Hunter and Plowman, 1997) was analysed (Fig. 5.2). Inspection of the sequences of 126 kinase domains revealed 13 members (10%) of the yeast kinome, have at least one degraded conserved motif (Fig. 5.2 and Table 5.1). A similar study of the *Dictyostelium*

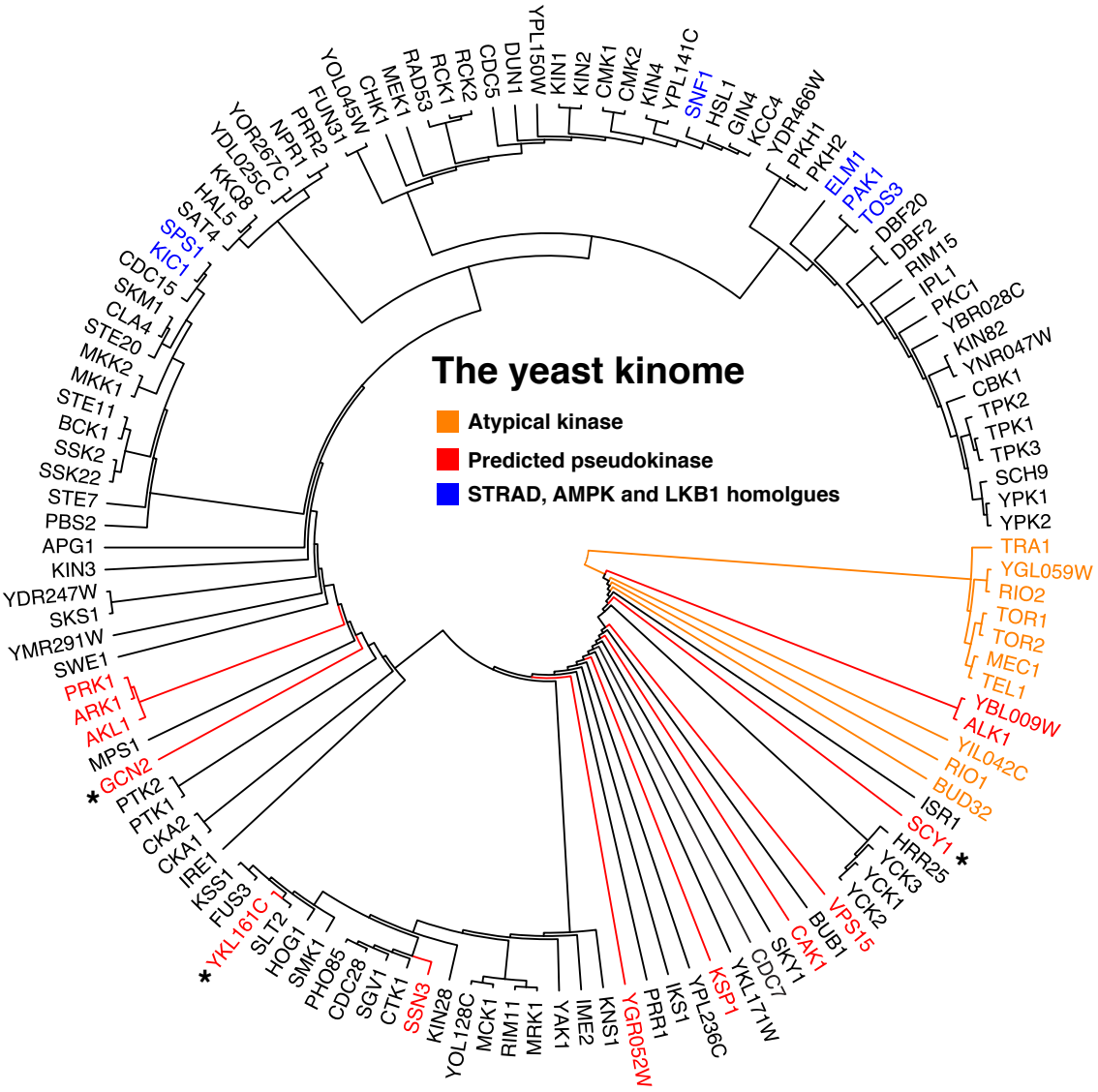

Figure 5.2: The yeast kinome
Neighbour-joining distance tree of protein kinases from *S. cerevisiae*. Predicted pseudokinases are coloured red and those with clear homologues in humans (SCY1, GCN2) are indicated with an asterisk. YKL161C (Mpl1) has been shown to function as a pseudokinase in yeast (Kim et al., 2008) and is similarly indicated with an asterisk. Sequences were downloaded from the KINOMER server, http://www.compbio.dundee.ac.uk/kinomer/index.html (Martin et al., 2009a), and aligned using MUSCLE (Edgar, 2004). The tree (calculated using MUSCLE) was displayed using FIGTREE downloaded from URL: http://tree.bio.ed.ac.uk/software/figtree/. For further information on individual groups of *S. cerevisea* kinases, please refer to the yeast kinome publication by Hunter and Plowman, 1997.

discoideum kinome found 29 of the total 285 (11%) predicted genes containing kinase domains, were classified as pseudokinases (Goldberg et al., 2006). These fractions are similar to the 10% approximate fraction of predicted pseudokinases in humans (Manning et al., 2002).

Interestingly two of the predicted pseudokinases in yeast (SCY1 and GCN2) have several substitutions in multiple catalytic and ATP binding motif, and both SCY1 and GCN2 have clear homologues in humans (Table 5.1), suggesting important conserved functional roles as pseudokinases. In humans there are three SCY1 homologues (SCYL1-3). SCYL1 binding, via a short C-terminal sequence to the membrane trafficking coatomer (COPI) is required for COPI-dependent vesicle trafficking from Golgi to the ER interface (Burman et al., 2008). It is argued these SCYL1 functions explain the phenotypic characteristics of SCYL1 mutations in "muscle deficient" *mdf* mice models of a human neuromuscular disease, characterised by spinocerebellar and neurodegeneration (Schmidt et al., 2007; Burman et al., 2008). Intriguingly, SCYL1-3 isoforms have multiple (1-4) heat repeats (distantly related to MO25 repeats) fused to their pseudokinase domains. Interestingly, ULK4 is another pseudokinase in the human kinome with a detectable heat repeat. It remains unknown if association of these helical repeats regulate SCYL(1-3)/ULK4 conformation in an analogous manner to the regulation of STRAD by MO25. It is worth mentioning a previous study carried out by Conner and Schmid show SCYL1 (referred to by these authors as CVAK104) is involved in clathrin coated vesicle trafficking and can associate and phosphorylate the clathrin adaptor

protein 2 (AP2) *in vitro* (Conner and Schmid, 2005). Thus, there are still questions of whether the SCYL family of pseudokinases possess intrinsic catalytic activity or whether their role is mainly of interacting nature.

Table 5.1: Degradation of conserved motifs in the *S. cerevisiae* kinome. Pseudokinases discussed in text are highlighted.

Kinases	GxG	VAIK/R	HxDxK*	N	DFG	Human homolog
YBL009W (ALK2)	GxS	YVVP	HxNxT	H	DMK	Haspin (Active)
ALK1	SxG	LSLQ	HxNxK	N	DFK	Haspin (Active)
SCY1	–	VLIG	HxNxQ	A	GLG	SCYL1-3 (Inactive)
VPS15	–	IVIK	HxDxK	N	DFA	PI3R4 (?)
CAK1	RxD	FEVS	HxDxK	N	DFG	CDK7 (Active)
KSP1	SxK	ICLE	HxDxK	N	DWG	AGC group
YGR052W	QxG	VALK	HRDxK	N	DWG	STK36 (Active)
SSN3 (CDK8)	ExL	–	HxDxK	N	DLG	CDK8 (Active)
YKL161C (Mpl1)	GxG	VAIR	HRDxK	N	NFG	ERK5 (Active)
GCN2 (N-ter)	PxS	YLLS	HxCxN	T	DFG	GCN2 (C-ter; Inactive)
AKL1	KxG	ACLK	HRDxK	N	DWG	BMP2K (Active)
ARK1	TxG	ACLK	HRDxK	N	DWG	BMP2K (Active)
PRK1	TxG	ACLK	HRDxK	N	DWG	AAK1 (Active)

*Lysine position is conserved for all Ser/Thr kinases

5.1.2 The "non-catalytic" activity of pseudokinases

A third member of yeast pseudokinases *YKL161C* (Table 5.1) also known as Mpk1 like (Mpl1) kinase because of its close homology to the yeast MAP kinase Mpk1 (SLT2; Fig. 5.2), is thought to influence gene transcription by a non-catalytic mechanism (Kim et al., 2008). Interestingly, Kim et al., demonstrate that both Mpk1 and Mpl1 form complexes with the transcription factors Swi4/Swi6 respdependentec-

tively. The formation of these complexes (detected at the *FKS2* (Glucan synthase 2) promoter) drive *FKS2* gene expression (Kim et al., 2008). The authors show that a Lys54Arg mutation in the VAIK motif of Mpk1—a naturally occurring mutation in Mpl1 (Table 5.1) that is devoid of Mpk1 catalytic activity (Martin et al., 1993; Zarzov et al., 1996; Madden et al., 1997), is still able to induce *FKS2* gene expression (Kim et al., 2008). By contrast a double mutant that changes phosphorylation site residues present in the activation loops of both Mpk1/Mpl1, was unable to associate with Swi4/Swi6 and drive *FKS2* gene expression (Kim et al., 2008). This suggests that the active "closed" conformation normally induced by phosphorylation of the activation loop is important, instead of the catalytic activity. Mpk1 and Mpl1 are homologues of the human extracellular signal-regulated kinase 5 (ERK5), known to be catalytically active (Table 5.1). Remarkably the authors were able to demonstrate the same behaviour with human ERK5 overexpressed in a yeast *mpk1*Δ*/mpl1*Δ strain, suggestive of similar non-catalytic functions for the ERK5 MAP kinase (Kim et al., 2008). Altogether, these results are in agreement with the findings and conclusions presented in chapter III of this thesis, that pseudokinases can exert their functions through their conformational state alone. Moreover, the correct positioning of the activation loop

either through phosphorylation/ATP binding and/or activity modulators appears to be a common regulatory mechanism for pseudokinases.

5.1.3 Pseudokinases regulated by nucleotide binding

Nucleotide pocket occupancy of a kinase/pseudokinase domain has not been fully appreciated in terms of regulating their conformational states, despite its obvious implications and already known examples in other classes of enzymes that bind nucleotides (e.g. G-proteins are regulated by guanine nucleotide-induced conformational changes). In chapter III of this thesis, structural, biophysical and mutagenesis data demonstrate the importance of nucleotide binding to STRADα in influencing STRADα ability to interact with its biological partners, as well as the ability of STRADα to activate the LKB1 tumour suppressor kinase.

Recently, conformational regulation of a kinase domain through nucleotide pocket occupancy has been described for catalytically active kinases. For instance in the case of IRE1, its phosphoryl transfer activity is functionally dispensable (Lee et al., 2008). Indeed, Lee et al., could demonstrate that ATP and ADP were both able to induce dimerisation of IRE1 kinase domains thus bringing together two Kinase Extension Nuclease (KEN) domains that together function as a nuclease (Lee et al., 2008). The kinase domain dimerisation oc-

curs mainly through the N-lobe, including helix αC, and does not involve the activation loop (Lee et al., 2008). The authors suggest, the pseudokinase RNaseL that lacks its activation segment, could be regulated by occupation of the nucleotide pocket despite its catalytic inactivity (Lee et al., 2008). In addition, very recent reports, show binding of ATP and ATP-competitive inhibitors control the conformation of active AGC kinases such as PKB and PKCϵ (Okuzumi et al., 2009; Cameron et al., 2009). This makes them better substrates for upstream kinases (Okuzumi et al., 2009; Cameron et al., 2009) and explains observations of so-called "activating" inhibitors.

An example of a pseudokinase influenced by ATP binding is the family of receptor guanylyl cyclases (RGC), an important cell surface receptor family that produces the second messenger cGMP in response to the binding of several natriuretic factors (reviewed in (Sharma, 2002)). These lack the HRD motif that provides the catalytic base residue, although ANP-RGC receptors are able to bind ATP leading to further amplification of receptor activity. It is thought that both activity of the guanyl cyclase domain, C-terminal to the pseudokinase domain, as well as receptor ligand affinity are influenced by ATP binding (Joubert et al., 2005). The ATP-dependent activity of the receptor is not affected when non-hydrolysable forms of ATP (e.g. ATP-γ-S)

are used and is sensitive to point mutations in the glycine-rich loop and VAIK motifs that affects ATP interaction with the pseudokinase domain (Bhandari et al., 2001; Sharma, 2002). Moreover, Jaleel at al., 2006 raised a monoclonal antibody that recognises the pseudokinase domain of guanylyl cyclase receptor 2C (GC-C) and showed that the immunoreactivity was compromised upon ATP binding, suggesting large conformational shifts between the ATP bound/unbound forms of this domain (Jaleel et al., 2006). Fine epitope mapping revealed the site of antibody recognition was Lys516 (VAIK) motif and nearby residues C-terminal to the VAIK motif. In the absence of structural data, it is difficult to envisage the exact conformational changes that would occur due to ATP binding, although in the majority of kinases the VAIK motif (β3) is followed by the αC helix, a well known region that undergoes large conformational changes upon formation of the conserved Lys(β3)/Glu(αC) ion bridge. Future studies in this area may demonstrate that the active/inactive conformations of the pseudokinase domain are indeed required for RGC activity via a regulatory mechanism similar to the one described in this thesis for STRADα.

5.1.4 Pseudokinases interacting with active kinases

Interestingly, there are a number of membrane receptors that contain a cytoplasmic pseudokinase domain, including members of the ephrin

receptor EphB6 and EphB10 as well as members of the epidermal growth factor receptor family ErbB3/Her3. As already discussed in Chapter III section 3.5.4 the four members of the EGF receptor kinases (ErbB1-4) are envisaged to trans-activate by forming so-called asymmetric heterodimers, upon ligand binding rather than phosphorylation (Zhang et al., 2006a; Jura et al., 2009). This lack of evolutionary pressure to conserve phosphoryl transfer activity may also be responsible for the loss of catalytic activity by ErbB3.

Another example where a pseudokinase forms complexes with active kinases are members of the kinase suppressor of Ras 1 and 2 (KSR1/2), that are essential for Ras induced activation of the RAF-MEK-ERK module in MAP kinase signalling. The pseudokinases act as scaffolds bringing together the three components of the MAP kinase pathway (MAPKKK, MAPKK and MAPK), thus regulating signalling output and potentiation (Kolch, 2005; McKay et al., 2009; Dougherty et al., 2009). The role of scaffold proteins in MAP signalling is well studied in budding yeast and the importance of Ste5p scaffold for bringing together the MAPK components module is well established (Elion, 2001; Bhattacharyya et al., 2006a; Good et al., 2009). It appears the Ste5p scaffolding roles for MAP kinases in higher organisms have been substituted by KSR1 and KSR2 (Morrison and Davis, 2003; Kolch, 2005).

The pseudokinase domain of KSR1 binds MEK and RAF, whereas ERK is recruited to the signalling complex via a conserved domain N-terminal to the pseudokinase domain (Kolch, 2005). In addition, recent work that established KSR2 as an important scaffold (similar to KSR1) of MAP kinase signalling, reveals KSR2 can be regulated by dephosphorylation by calcineurin in response to changing Ca^{2+} levels (Dougherty et al., 2009). The lack of structural information makes it difficult to precisely understand the mechanism by which KSR1/2 contribute to these scaffolding complexes. In light of the findings presented here for the STRAD pseudokinase, it will be interesting to investigate ligand (ATP) binding capabilities of KSR1/2 and see if this is required for MAP kinase signalling.

Perhaps the most studied pseudokinase domain belongs to the members of Janus tyrosine kinase (JAK) family. The JAK isoforms include JAK1, JAK2, JAK3 and TYK2 all of which contain an N-terminal pseudokinase domain (JH2) followed by a kinase domain (JH1). This characteristic feature of containing two kinase domain gives JAKs their name, referring to the two-faced Roman God Janus. JAKs respond upon receptor binding to cytokines and phosphorylate the cytoplasmic region of these cytokine receptors, thus creating sites of interaction for downstream signalling molecules. The pseudokinase domain is re-

quired for JAK2 auto-inhibition and is essential for JAK2 cytokine activation (Saharinen and Silvennoinen, 2002; Saharinen et al., 2003). Strikingly, a gain-of-function mutation (Val617Phe) in the JAK2 JH2 domain is a cause of myeloproliferative disorders in humans (Baxter et al., 2005; James et al., 2005; Levine et al., 2005). Structural modelling and biochemical data suggest the N-lobe of JH2 domain where Val617 resides, is in close proximity to the JH1 domain (Saharinen et al., 2003). Recently gain-of-function somatic mutations of another residue present in the JH2 domain (Arg683Gly/Ser/Lys) were found in 18% of patients suffering with Down's syndrome-associated acute lymphoblastic leukaemia (Malinge et al., 2007; Bercovich et al., 2008; Kearney et al., 2009). The exact location of these disease causing mutations and how their position relates to the JH1 domain are not known. It will be interesting to see if structural studies of JH1/JH2 domains will reveal the molecular mechanism of action of these mutations, and whether these resemble any of the STRAD/LKB1 interactions.

5.1.5 Pseudokinases as elastic scaffolds

Structural studies of predicted pseudokinases have shed light to the mechanisms of protein kinase inactivity. Recently, the structure of VRK3 was published by Scheeff et al., explaining how non-conservative

substitutions of catalytic motifs compromised VRK3 catalytic competence (Scheeff et al., 2009). The VRK3 structure is similar to the closely related active kinase VRK2 structure. However, VRK3 lacks catalytic activity (Scheeff et al., 2009). Similar to the STRADα pseudokinase discussed in this thesis, VRK3 appears to attain a "closed" conformation that resembles active protein kinases (Fig. 5.3A and B). Interestingly, this is achieved in the absence of ATP, and the so-called hydrophobic spine is completed by nearby hydrophobic residues that compensate for the loss of the ATP adenine ring (Scheeff et al., 2009). Scheeff et al., studied the surface conservation of the VRK3 catalytic domain and identified a conserved area, away from the active site, that could be important for binding macromolecular partners (Scheeff et al., 2009), thus suggesting that VRK3 may have a scaffolding role, rather than functioning as a protein kinase.

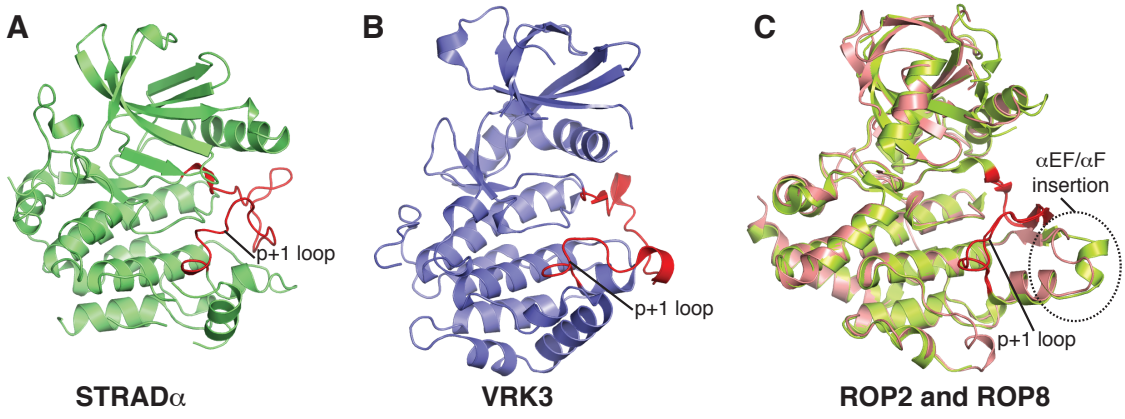

Figure 5.3: Structures of pseudokinases
Carton representations of (A) STRADα from the LKB1/STRADα/MO25α complex (chapter III), (B) VRK3 (PDBID 2V62; (Scheeff et al., 2009)) and (C) superposed ROP2 (PDBID 3BYV) and ROP8 (PDBID 3DZO) pseudokinases (Labesse et al., 2009; Qiu et al., 2009). The activation segments are coloured red and the p+1 loops are labelled. A short (αEF/αF) insertion present in ROP2 and ROP8 is circled.

Two other pseudokinase structures, members of the Rhotropy (ROP) family, ROP2 and ROP8 from the intracellular parasite *Toxoplasma gondii* (Labesse et al., 2009; Qiu et al., 2009), appeared in print during the last year of this study. Of the eight members of the ROP family, five are predicted to be pseudokinases, namely ROP2, ROP4, ROP5, ROP7 and ROP8. Both structures of ROP2 and ROP8 attain similar conformations, with activation and p+1 loops in the canonical conformation typical of active protein kinases (Fig. 5.3C). One noticeable difference is the presence of a short insert within the αEF/αF loop, that may also account for specific binding of macromolecular partners. This insertion blocks the active site of ROP2/8, by sitting on the top of the p+1 loop (Fig. 5.3). Interestingly, this is analogous to the blocking of the active site of STRADα by LKB1 (discussed in chapter IV of this thesis), which may also explain why these kinases are inactive. Unlike VRK3, the ATP pocket is empty in ROP2 and ROP8 structures, although Labesse et al., reported ROP2 could not interact with ATP (Labesse et al., 2009). It is unclear if the nucleotide pocket harbours a true ligand binding site and whether the ROP pseudokinases are regulated by ATP binding.

Overall, the structures of VRK3, ROP2/8 and those presented in this thesis support the notion put forward by Boudeau et al., 2006,

that pseudokinases function as scaffolds, bringing together components of a signalling pathway (e.g. KSR1/2 (McKay et al., 2009; Dougherty et al., 2009)), and/or activity modulators (e.g. STRADα/β, chapter III, IV of this thesis and ErB3/Her3 (Zhang et al., 2006a)). In addition, data presented in chapter III of this thesis suggest a regulatory mechanism for pseudokinase function, modulated by ligand (ATP) binding as well as macromolecular binding partners, that together impinge on activation loop conformation. The importance of this conformational state regulation is supported in chapter IV, by the structure of the LKB1 complex and mutagenesis data, demonstrating a key role for residues present in the STRADα activation loop in binding and activating LKB1. Thus, it is possible to envisage pseudokinases as "elastic" scaffolds, the function of which can be regulated by post translational modification, as well as allosterically through binding of micromolecular/macromolecular ligand binding.

5.1.6 Phylogenetic studies of the STRAD pseudokinase

STRAD appears to be conserved throughout evolution with clear homologues present in primitive species such as budding yeast (Fig. 5.4). Phylogenetic analysis of the STRADα gene reveals two important features. Firstly, STRAD evolved as a pseudokinase in the early metazoan evolution since orthologous genes with degraded catalytic motifs

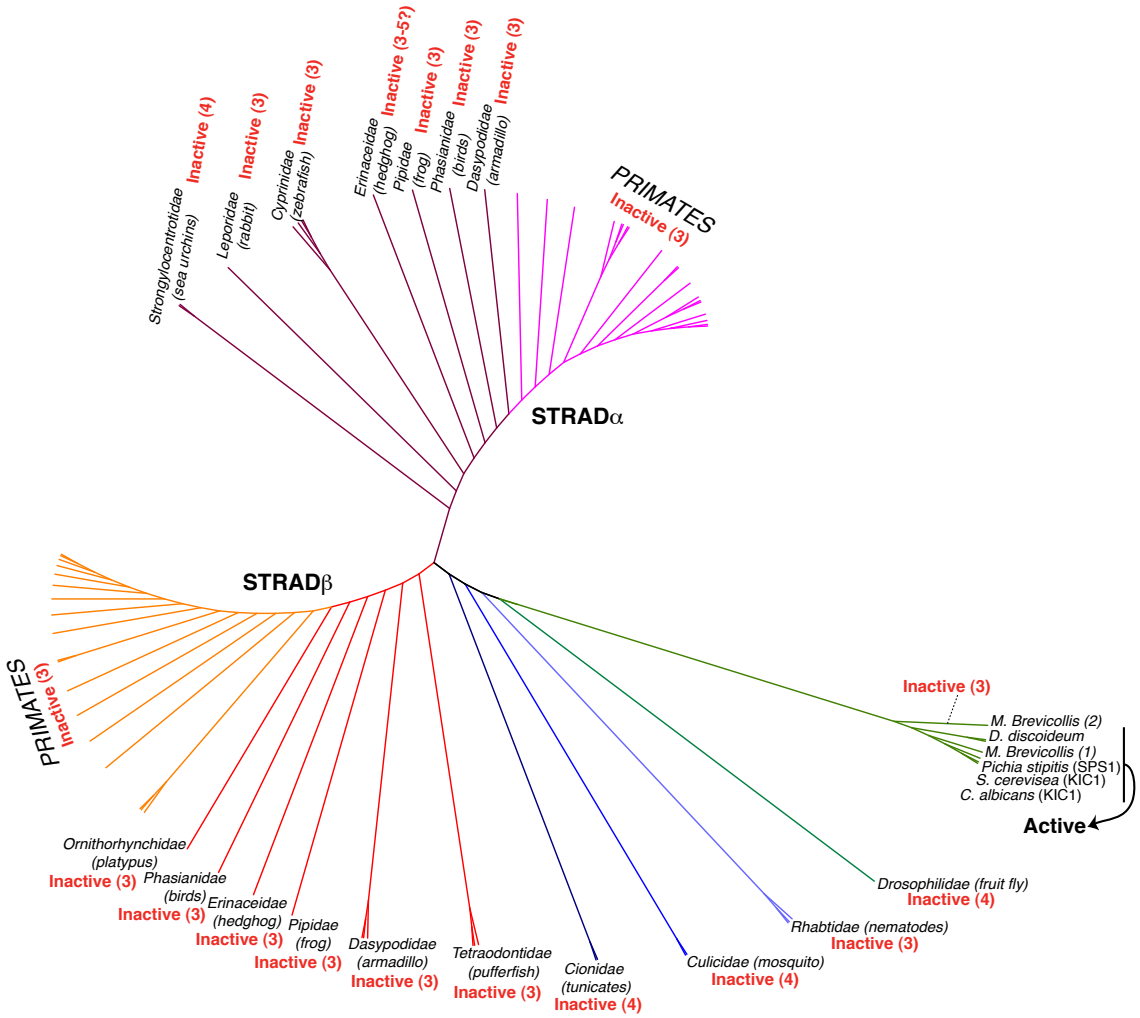

Figure 5.4: Evolution of the STRAD pseudokinase
Neighbour-joining distance tree of STRAD gene family from eukaryotic species. The general family name for the species belonging to each clade is labelled and a common name is given in brackets. The number of degraded catalytic motifs is shown in red. Sequences were downloaded from TREEFAM (http://www.treefam.org/) and UNIPROT (http://www.uniprot.org/) databases and aligned using MUSCLE (Edgar, 2004). The tree (calculated using MUSCLE) was displayed using FIGTREE downloaded from URL: http://tree.bio.ed.ac.uk/software/figtree/

were also identified in the choanoflagelate *M. brevicollis* (Table. 5.2), that as mentioned above is believed to be the closest unicellular organism to animals. Secondly, STRADα and STRADβ diverged as two separate genes much later in metazoan evolution, possibly due to a gene duplication event (Fig. 5.4). Interestingly, changes in catalytic motifs of the STRADα pseudokinase, unlike STRADβ, are strictly

conserved among species (Table 5.2), possibly reflecting a central biological role for this gene. Surprisingly, STRAD emerged as a pseudokinase with three degraded motifs (out of the five conserved motifs) in *M. brevicollis* and similar changes are present throughout evolution (Fig. 5.4). Interestingly, this organism has two candidate genes that may be STRAD precursors. MbSTRAD1 is inactive and resembles STRADα3 and STRADβ2 splice isoforms, lacking the WEF motif. MbSTRAD2 contains a conserved WEF motif and is predicted to be active.

STRAD orthologues, predicted to be active are present in *D. discoideum* and yeast species (Fig. 5.4 and Table 5.2)—these all contain a WEF motif, suggestive they may interact with MO25. Indeed clear genetic interaction for STRAD with MO25 has been demonstrated in yeast between the active Kic1 and Hym1 (Jorgensen et al., 2002; Nelson et al., 2003). The STRADα pseudokinase homologues have been shown to interact with LKB1 and function upstream of AMPK kinase in *C. elegans* (Narbonne and Roy, 2009).

5.1.7 Evolution of pseudokinases

The ultimate question is how did pseudokinases evolve? In general it is plausible to believe that kinases evolved from ATP binding enzymes, since nucleotide binding must have preceded catalytic function.

Table 5.2: Catalytic motif degradation of the STRADα pseudokinase

	ATP binding		Catalytic loop		Mg^{2+} loop	
Species	GxG	VAIK/R	HRDxK	N	DFG	Altered motifs
S. cerevisiae	GxG	YAIK	HRDxK	N	DFG	0
D. discoideum	GxG	VAIK	HRDxK	N	DFG	0
M. brevicollis	GxG	VAIR	HNRxG	S	NFH	3
D. melanogaster	KxG	LAVK	HGSxR	H	NFS	4
C. elegans	GxC	VAIK	HRDxK	H	GFR	3
A. gambiae	AxC	VAVK	HRSxR	H	GFR	4
C. intestinalis	GxC	LAVK	HRGxK	H	GHR	4
STRADβ						
T. nigroviridis	GxG	VAIK	HRSxK	H	GLH	3
D. novemcinctus	GxG	VTIK	HRSxK	L	GLS	3
X. tropicalis	GxG	VTVR	HRNxK	H	GLS	3
E. europaeus	GxR	VTIK	HRSxK	H	GLS	4
G. gallus	GxG	VAVR	HRNxK	H	GLN	3
O. anatinus	GxG	VAVR	HRSxK	S	GFS	3
B. taurus	GxG	VTIK	HRSxK	H	GLF	3
M. musculus	GxG	VTVK	HRSxK	H	GLS	3
H. Sapiens	GxG	VTVK	HRSxK	H	GLS	3
STRADα						
S. purpuratus	GxN	VAVR	HRSxK	H	GLR	4
O. cuniculus	GxG	VTVR	HRSxK	H	GLR	3
D. rerio	GxG	VAIR	HRSxK	H	GLR	3
E. europaeus	?	?	HRSxK	H	GLR	3-5?
X. tropicalis	GxG	VCIR	HRSxK	H	GLR	3
G. gallus	GxG	VTVR	HRSxK	H	GLR	3
D. novemcinctus	GxG	VTVR	HRSxK	H	GLR	3
B. taurus	GxG	VTVR	HRSxK	H	GLR	3
M. musculus	GxG	VTVR	HRSxK	H	GLR	3
H. Sapiens	GxG	VTVR	HRSxK	H	GLR	3

Therefore it is not surprising that ligand (ATP) binding plays a key regulatory component for pseudokinase/kinase function. As a consequence there are two possibilities—either pseudokinases represent "would-be" active kinases, or they represent kinases that have lost their catalytic activity.

The first scenario could be true for proteins that are well con-

served as pseudokinases throughout eukaryotic kinase evolution such as SCYL1-3 and GCN2 (discussed in section 5.1.1). For instance, ATP-binding precursors of yeast SCY1 and GCN2 may have failed to "mature" as active protein kinases capable of phosphoryl transfer. Instead, important non-catalytic functions were conserved throughout evolution for these pseudokinases. In GCN2 this could have been aided by loss of evolutionary pressure for kinase maturation, since another kinase domain is present in the same polypeptide chain. In the case of SCY1, gene duplication events leading to SCYL1-3 in higher organisms may have fulfilled the same purpose.

However, the reasoning above can not account for the larger group of pseudokinases that do not have clear pseudokinase homologues in primitive species (e.g. STRADα, KSR1/2, Erb3 etc...). Therefore these may have evolved via a different route. One possibility is that pseudokinases have evolved from active kinases once capable of phosphorylating and activating their substrates. These may have lost their activity during evolution. The process of using previously catalytically competent domains as scaffolds is plausible from an evolutionary perspective—active enzymes know how to bind their substrates—and also observed in other classes of enzymes such as pseudophosphotases (Conner et al., 2006; Moorhead et al., 2009). The structures

of STRADα and VRK3 show that despite being inactive, these pseudokinases are able to assume an active conformation with a highly organised active site poised for phosphoryl transfer. This suggests that pseudokinases like STRAD were able to phosphorylate substrates at some stage during evolution. In addition, the structure of the LKB1 heterotrimer reveals that LKB1 can bind STRAD as a substrate, by utilising regions of the activation segment and αG helix, both of which are commonly used by active kinases to interact with substrates. It is tempting to suggest that LKB1 binding to STRAD as a pseudosubstrate blocking the STRAD active site, resulted in the degradation of catalytic motifs seen in STRAD. If this was the case, the number of degraded catalytic motifs in STRAD should increase from lower species such as *M. brevicollis* to more complex organisms such as primates. However, this is not observed in the phylogenetic analysis in Fig. 5.4 and Table 5.2 Instead, it is more likely that STRAD may have been an upstream kinase for LKB1 and (by becoming a pseudokinase through gene duplication events and spontaneous mutations) evolved as an allosteric activator of LKB1 rather than an activator by phosphorylation. This would ensure the indispensable functions of LKB1-AMPK axis remained unaltered.

To support this theory, kinase active STRAD homologues in organ-

isms like *D. discoideum* (FRAY2), *S. cerevisiae* (Kic1) could be tested for the ability of phosphorylating and activating LKB1 homologues in these species. Additional, interesting candidates are the *M. brevicollis* MbSTRAD1 and MbSTRAD2 isoforms. Perhaps this organism has an active STRAD (MbSTRAD1) capable of activating MbLKB1 by phosphorylation and an inactive STRAD (MbSTRAD2) that activates LKB1 via interaction. Future studies may generate more data in support of the idea that pseudokinases evolved from active protein kinases.

5.2 The STRADα WEF motif—is it crystal clear?

5.2.1 The STRADα WEF motif could be a "recruiting/docking" motif

At the start of this work, the most well known interaction within the LKB1 heterotrimer, was that of the STRADα WEF motif with the convex surface of MO25α (Boudeau et al., 2003a, 2004; Milburn et al., 2004). The crystal structures presented in Chapters III and IV of this thesis, are in agreement with these initial observations. Clear electron density for the WEF motif binding in the same manner as previously reported by Milburn et al., (2004) was observed (Figs. 3.11 and 4.9). However, the connectivity of the WEF motif with the rest of the STRAD molecule in the structure of STRADα/MO25α

complex is uncertain (Fig. 3.13) whereas in the structure of the LKB1 complex, is most probably swapped between the heterotrimers (Fig. 4.6). This could be due to crystallographic packing, since the WEF motif, located in a mobile loop, is free to bind the nearest MO25 molecule available. This raises the question of whether this is also the case *in vivo*. Thus far, work carried out in this thesis does not suggest the possibility of an LKB1 heterotrimer dimer, maintained via the WEF motif (See figures 4.4 and A.5). Similarly, work of others with purified LKB1/STRADα/MO25α complex from *E. coli* has suggested the presence of an LKB1 heterotrimer monomer (Neumann et al., 2007).

The structures discussed in this thesis have uncovered an additional area, 2.5 times larger than that of the WEF motif (2100 Å^2 vs. 825 Å^2 of buried surface area) participates in STRADα/MO25α interaction. Moreover, extensive mutagenesis work carried out in this thesis as well as in other studies (Boudeau et al., 2003a, 2004) does not suggest the binding of the WEF motif to MO25 is absolutely required for LKB1 activity. These findings, together with the fact that STRADα3 and STRADβ2 isoforms do not contain a WEF motif (Fig. 1.12), leads to a number of possibilities for future exploration in the study of LKB1 regulation.

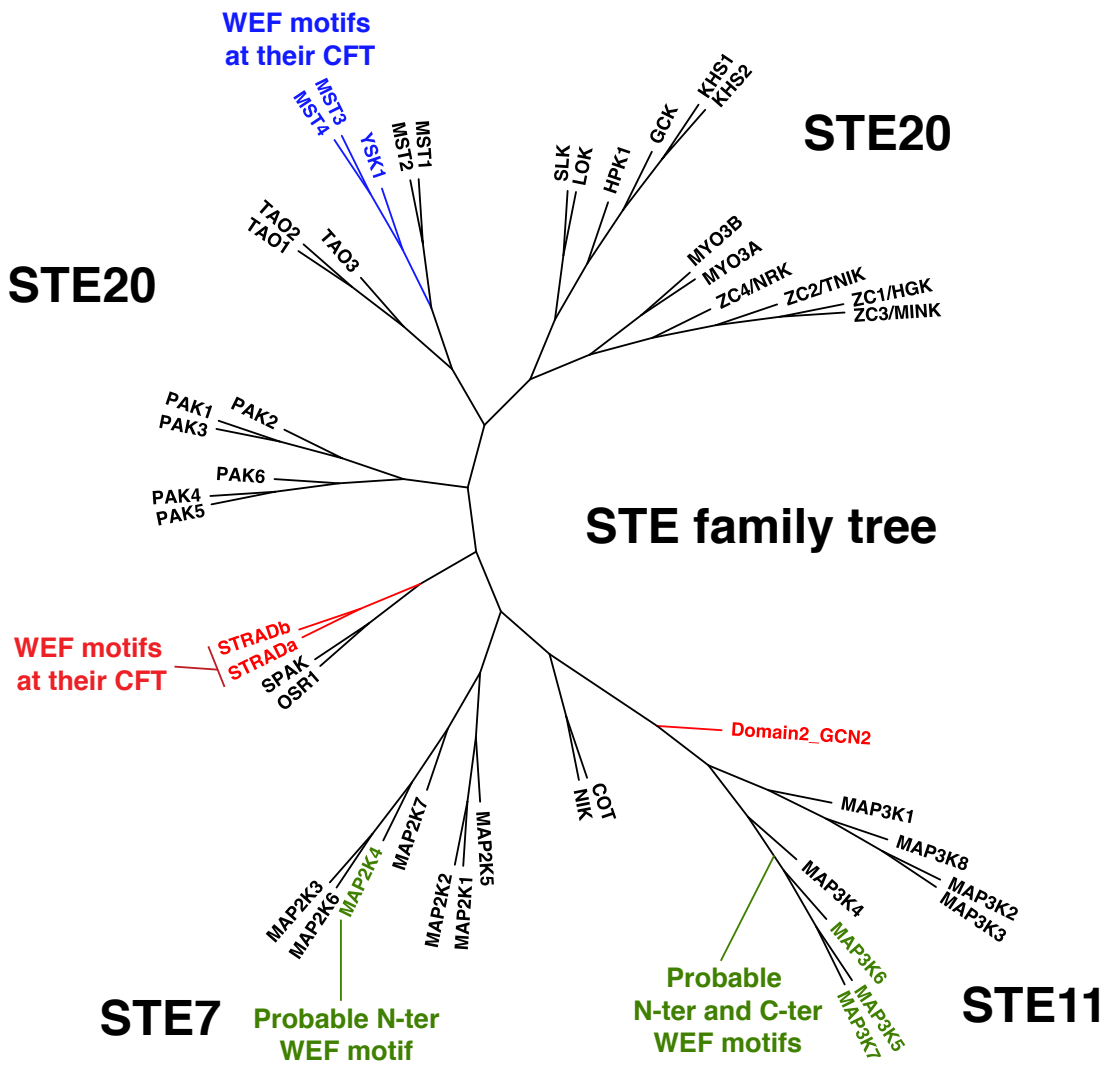

Figure 5.5: The human STE kinase family
Neighbour-joining distance tree of the human STE family of kinases. pseudokinases are coloured red. Kinases with possible WEF motifs are coloured green, whereas kinases with WEF motifs at their CFT similar to the STRAD isoforms are coloured blue. Sequences were downloaded from The Salk Institute for Biological Studies (http://kinase.com/), and aligned using MUSCLE (Edgar, 2004). The tree (calculated using MUSCLE) was displayed using FIGTREE downloaded from URL: http://tree.bio.ed.ac.uk/software/figtree/

For instance, a complex formed with the STRADΔWEF isoforms results in an unoccupied WEF pocket on the MO25 surface. This free pocket can be used by other protein kinases that contain a WEF motif at their CFT to bind MO25. Analysis of the STE group of kinases, most similar to STRAD, reveals one STE7 and three STE11 protein kinases contain probable WEF motifs at their N- and C-terminal re-

gions (Fig. 5.5). Furthermore, three members of the STE20 germinal centre group of kinases contain WEF motifs at their CFT that are very similar to STRAD (Fig. 5.5). These are MST3, MST4 and YSK. Interestingly, MO25 was shown to bind MST4 resulting in MST4 translocation from Golgi vesicles to apical membranes, that leads to Ezrin phosphorylation and brush border formation (ten Klooster et al., 2009) (Fig. 5.6). The sites of MST4/MO25 interaction remain unknown, although it is possible that conserved residues between STRAD and MST4, including the WEF motif could be involved in MO25 interaction. Similarly, the involvement of LKB1 in Ezrin phosphorylation (ten Klooster et al., 2009) remains unexplained.

Another possibility is that the STRAD WEF motif can be a recruiting or docking motif for other proteins. STRAD is involved in interactions with E-cadherin, postulated to regulate LKB1 complex localisation and AMPK phosphorylation at adherens junctions (Sebbagh et al., 2009). The mode of interactions between E-cadherin and STRAD are unclear however, considering the STRAD N-lobe and activation sites are engaged in interactions with MO25 and LKB1 respectively, it is possible, the C-lobe and the STRAD CFT, including the WEF motif, interact with E-cadherin (Fig. 5.6).

Finally, STRADα interacts with Exportin-7 and CRM1 leading to

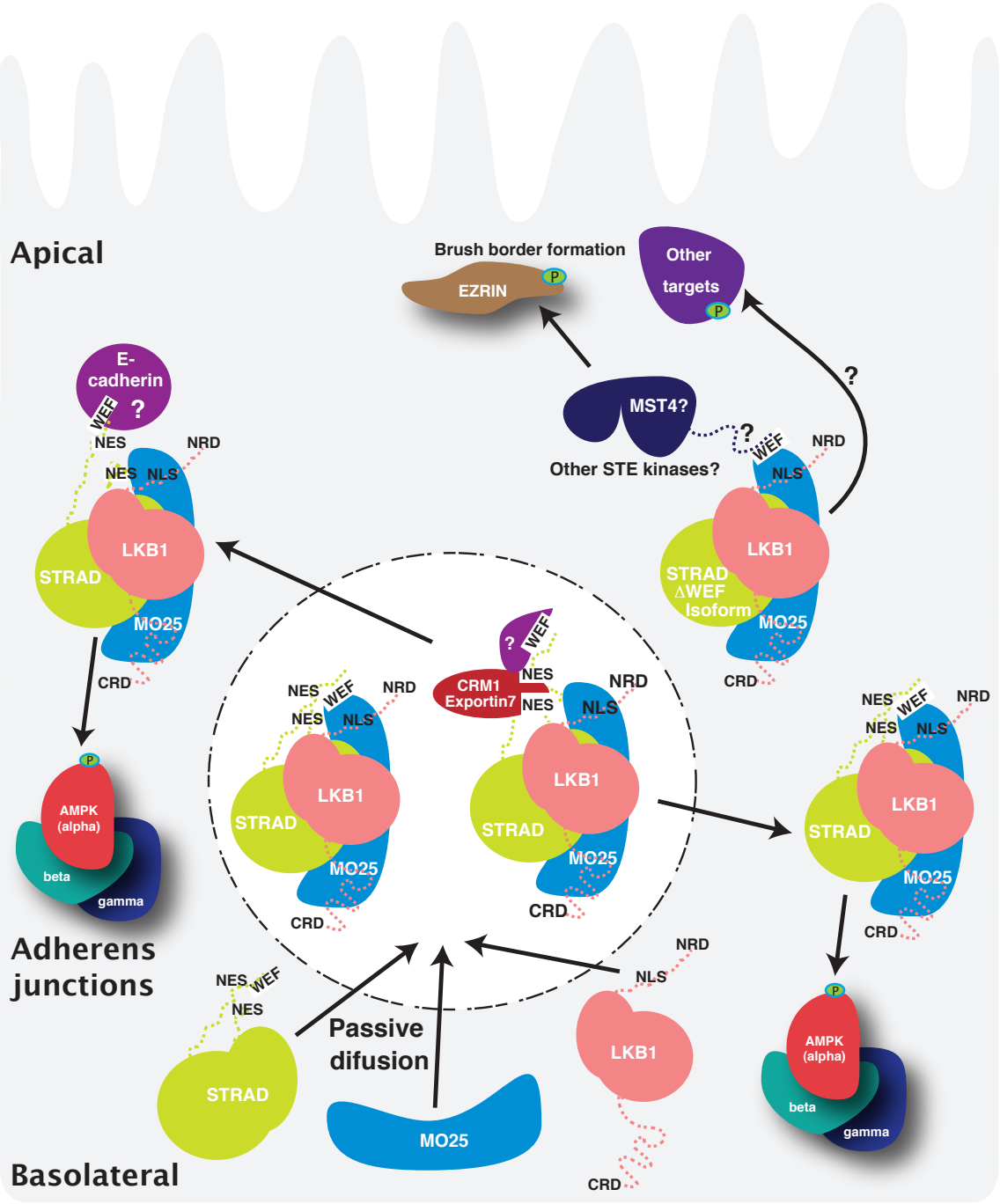

Figure 5.6: Possible interactions of the WEF motif
LKB1 relocalises to the cytoplasm via STRAD interactions with the karyopherins Exportin-7 and CRM1 (Dorfman and Macara, 2008). Possible interactions of the STRADα WEF motif with known STRAD interactors are shown and marked with a question mark. Similarly, MST4 known to interact with MO25 (ten Klooster et al., 2009) and contain a WEF motif at its CFT is shown. NLS = nuclear localisation signal, NES = nuclear export signal, NRD = N-terminal regulatory domain and CRD = C-terminal regulatory domain.

LKB1 transport from the nucleus to the cytoplasm (Dorfman and Macara, 2008). Exportin-7 and CRM1 bind nuclear export signals that are present in the STRAD N- and C-terminal flanking tails (Fig.

5.6). One of these NES signals is located two amino acids N-terminal to the WEF motif. Again, it remains unclear if the WEF motif is involved in interactions with Exportin-7 and CRM1.

5.3 MO25—a bridging scaffold within the LKB1 complex

The importance of MO25 functions as a scaffolding protein are made evident by its high degree of conservation (discussed in section 1.5.4). Its role in activating LKB1 is clear from various studies (Boudeau et al., 2003a, 2004) including the results presented here. MO25α serves as a bridge for both STRADα and LKB1 (see for instance the interaction footprint on the MO25α concave surface in Fig. 4.9). Through allosteric binding, MO25 stabilises the active conformations of both STRADα and LKB1 (discussed in chapters III and IV). However, until now the role of MO25 in activating LKB1 has been overshadowed by the activatory role of STRAD, since in the absence of STRAD, LKB1/MO25 interaction is undetectable in co-expression assays (Boudeau et al., 2003a, 2004). Therefore, it is plausible to assume, the STRAD/MO25 complex binds and activate LKB1. The role of STRAD in this case is to bring MO25 into close proximity of LKB1, and/or by interacting with LKB1, STRAD indirectly induces a conformational change (for instance exposing the LKB1 activation loop) that is better suited for LKB1/MO25 interaction. To understand this

fully, a structure of LKB1 alone, STRAD alone and LKB1/STRAD complex may be necessary. Obtaining the structures of LKB1 and STRAD alone has been hindered by the lack of recombinant expression of LKB1, and inability to crystallise STRAD in the absence of LKB1 and MO25 (section 3.3.3). These are suggestive of unstable conformations of these two proteins when MO25 is not present. Therefore, it is likely that MO25 binds STRAD and LKB1 through a mixture of concerted and cooperative mechanisms, ultimately "fixing" both STRAD and LKB1 in their active conformations.

5.4 Interaction of LKB1 with its substrates

A challenge in the field of LKB1 signalling is how LKB1 recognises AMPK and the AMPK related kinases. Attempts to co-crystallise an AMPK peptide derived from the AMPKα2 activation loop resulted in no crystals (data not shown). Similarly, crystal soaking experiments, designed to obtain a structure of the LKB1 complex with a substrate peptide did not result in a kinase/substrate complex structure, despite several attempts and collection of multiple datasets (data not shown). The failure of the latter experiments could be a result of the high salt concentration of $(NH_4)_2SO_4$ present in the crystallisation condition, reducing the solubility of the peptide as well as the affinity of kinase/substrate interaction.

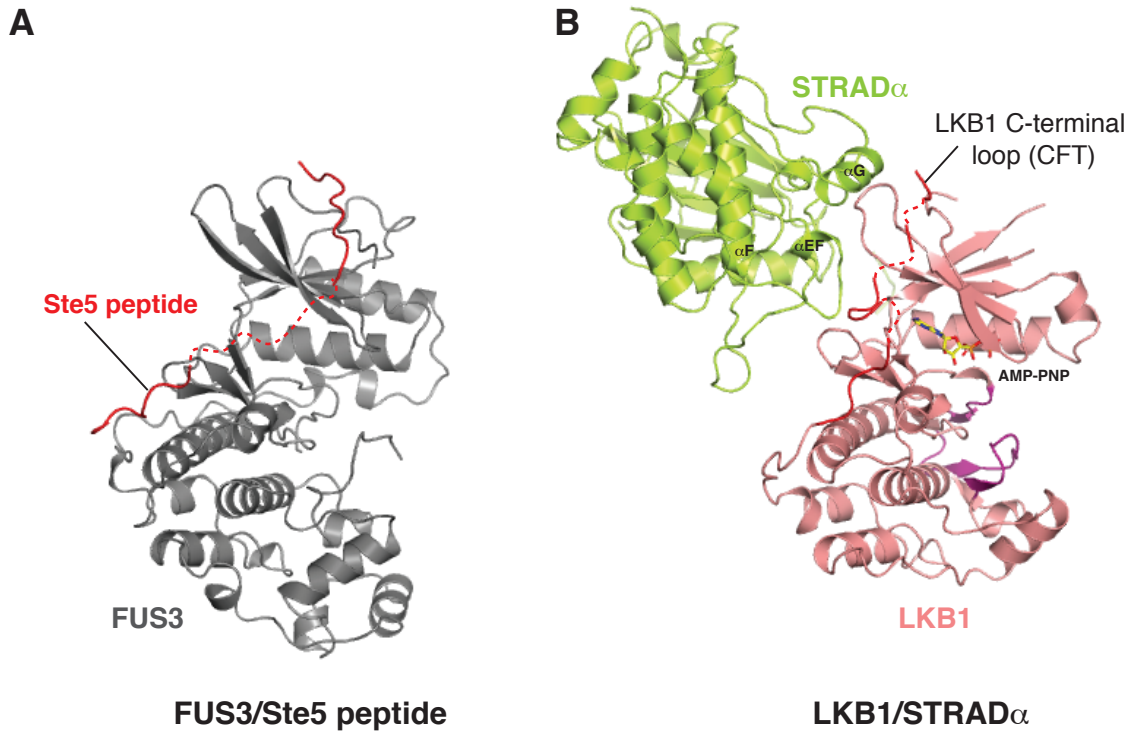

Figure 5.7: Comparisons of the STRADα/LKB1 with Ste5/Fus3 interactions
A) The structure of Fus3 MAP kinase complexed to a peptide from the Ste5 scaffold (PDBID 2F49; (Bhattacharyya et al., 2006b)).
B) STRADα/LKB1 interaction within the LKB1 heterotrimer. The LKB1 activation loop is coloured magenta.

A key feature of the LKB1 complex structure is the LKB1 active site, which as expected for an active complex, is fully exposed. The binding of STRAD to the back of the kinase domain ensures there is no steric hindrance of the LKB1 catalytic and substrate binding sites. This may be one of the reasons why STRAD has evolved this unique activation mechanism, regulating interlobe dynamics by interacting with both lobes of the LKB1 kinase domain. The only example distantly resembling this type of interaction is between the scaffold protein Ste5 and the MAP kinase Fus3, that are components of the yeast mating pathway (Fig. 5.7 (Bhattacharyya et al., 2006b)). Therefore,

it is unlikely that STRADα will contribute directly to interactions with the AMPK kinase family, although this can not be categorically ruled out. Interestingly, MO25α binding to the LKB1 activation loop, brings MO25α in close proximity to the LKB1 substrate binding site. Some of these features are similar to the CDK2/Cyclin A complex (Fig. 5.8). CDK2 like most kinases interacts with the substrate peptide via the p+1 loop (Fig. 5.8A). It is reasonable to assume that LKB1 can interact with the activation loop of AMPK-related kinases in a similar way (Fig. 5.8B). However, in the case of CDK2/cyclin A, a second recruiting site is also present on the surface of the Cyclin molecule (Fig. 5.8A). The MO25α surface may indeed provide a docking site for the downstream targets of LKB1 similar to cyclins that participate in this type of interaction. However, data are needed to support this idea. A structure of the LKB1 complex with either AMPK or an AMPK-related kinase would be the ultimate proof, although a structure of the LKB1/STRAD/MO25 complex with substrate peptides could help shed some light to the mechanism of LKB1 substrate recognition.

As mentioned in section 1.5.6, LKB1 contains N- and C-terminal regulatory regions with multiple phosphorylation sites. These are not present in the crystallised fragment of LKB1 described in this the-

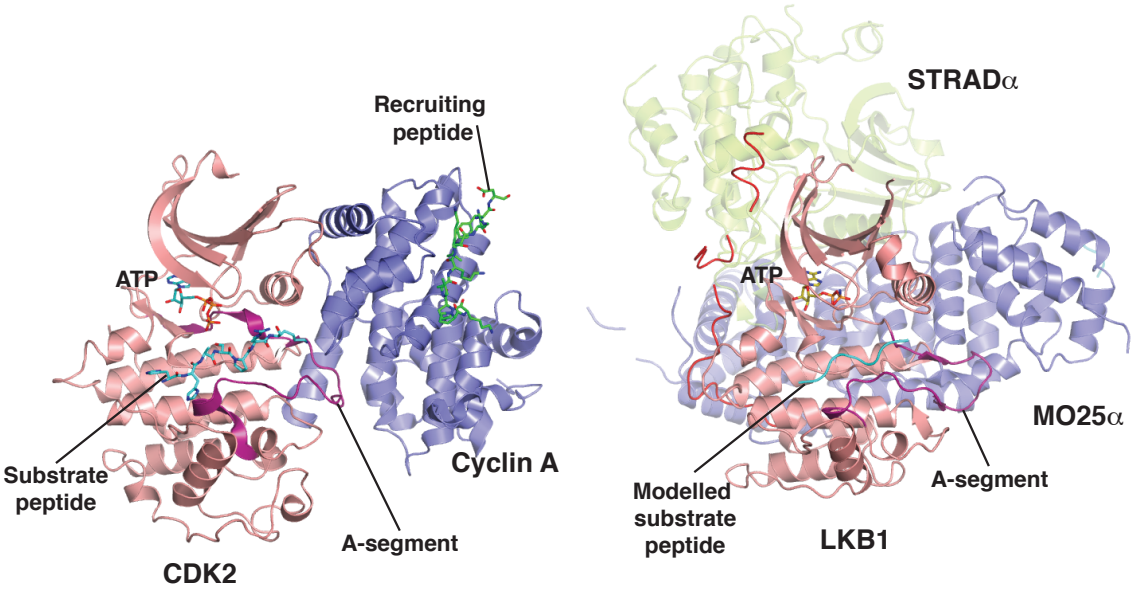

Figure 5.8: Substrate binding to CDK2 and LKB1
A) Structure of CDK2/cyclin A bound to an 11 residue recruitment peptide (green sticks) derived from the retinoblastoma associated protein (PDBID 1H25; (Lowe et al., 2002)). A substrate peptide bound to the p+1 loop (PDBID 1QMZ (Brown et al., 1999)) is also shown in sticks and coloured cyan. The activation segment is coloured magenta.
B) Structure of the LKB1 complex. LKB1 is shown in the same orientation as CDK2 and the same substrate peptide (A) is modelled on the LKB1 p+1 loop. LKB1 activation segment is coloured magenta.

sis, thus their relative position to the LKB1 kinase domain and/or STRADα and MO25α remain unknown. Although recent reports (Zheng et al., 2009; Esteve-Puig et al., 2009) have claimed part of the LKB1 CFT could interact with AMPK, this requires further investigation.

Recently, concentration-dependent dimerisation of AMPK via helix αG was described by Sholz et al., (Scholz et al., 2009). The authors report that LKB1 helix αG (residues Ile260 and Phe264) and AMPK helix αG (residues Val219 and Phe223) are involved in LKB1/AMPK interactions. In the LKB1 structure Ile260 and Phe264 are facing the p+1 loop of LKB1 and Phe260 in particular, makes important contri-

butions to ensure the right conformation of the p+1 loop. The authors claim that the AMPK αG helix interacts with residues Ile260 and Phe264 of LKB1 (Scholz et al., 2009). Since by definition the activation loop of AMPK should bind to the p+1 loop of LKB1, it is unclear how helix αG of AMPK as well as the activation loop could be accommodated, without significant changes of the LKB1 active/substrate binding sites.

5.5 Final conclusions and remarks

The structures of the 82 kDa STRADα/MO25α complex and the 116 kDa LKB1/ STRADα/MO25α complex have been determined at 2.35 and 2.65 Å resolution respectively. This represents the first structural analysis of the LKB1 tumour suppressor and the pseudokinase STRAD. The work described in this thesis reveals for the first time how the conformation of a pseudokinase can be regulated by ligand (ATP) binding as well as via activity modulators such as the scaffold protein MO25, in an analogous fashion to the CDK/Cyclin complexes. Moreover, this work reveals that pseudokinases serve as elastic scaffolds bringing together regulatory components of signalling pathways. Unlike the conventional scaffolding proteins, pseudokinases may have an advantageous feature, as their conformation can be modulated between the active and inactive states similar to catalytically competent

protein kinases. Central to this regulation is the movement of helix αC and the conformation of the activation loop. Thus, the STRADα pseudokinase may serve as an example for other pseudokinases that are also involved in regulating important signalling pathways.

The structure of the LKB1 heterotrimeric complex reveals for the first time, a novel molecular mechanism by which a protein kinase is activated independently of activation loop phosphorylation. This is achieved by a concerted action of the scaffolding protein MO25, that mediates the active conformations of both STRAD and LKB1. An "active" STRAD serves two main functions: it brings MO25 in close proximity to LKB1 and possibly induces a conformational change on LKB1, thus making LKB1 more likely to interact with MO25. Importantly, MO25 stabilises the active conformation of the LKB1 activation loop, leading to a fully active LKB1, capable of phosphorylating its downstream targets.

Despite the numerous phosphorylation events between kinase domains in a cell, crystal structures of a kinase domain bound to another substrate kinase domain are not available. The structure of LKB1 bound to STRADα using typical active site elements of the later, may represent the closest example to date. Intriguingly, this may also represent an ancient kinase/substrate interaction, that could

also be significant in explaining the evolution of pseudokinases.

Because of the intrinsically transient nature of kinase/substrate interaction, data are lacking into the exact mechanism of how LKB1 recognises its substrates (e.g. AMPK). Similarly, the functions for the N- and C-terminal regulatory regions of LKB1, not present in the structure described here, are unclear. The ultimate goal will be to crystallise the LKB1 complex with a kinase substrate, like AMPK or a member of the AMPK family of kinases.

Finally, the LKB1 structure provides insights into the molecular mechanisms of how oncogenic mutations that occur in patients with PJS and more aggressive types of cancers affect LKB1 structure and function.

References

Adams, P. D., Grosse-Kunstleve, R. W., Hung, L. W., Ioerger, T. R., McCoy, A. J., Moriarty, N. W., Read, R. J., Sacchettini, J. C., Sauter, N. K., Terwilliger, T. C., 2002. PHENIX: building new software for automated crystallographic structure determination. Acta Crystallogr D Biol Crystallogr 58 (Pt 11), 1948–54.

Alessi, D., Zeqiraj, E., 2007. Protein phosphorylation. The Biochemist 29, 23–23.

Alessi, D. R., Cohen, P., Ashworth, A., Cowley, S., Leevers, S. J., Marshall, C. J., 1995. Assay and expression of mitogen-activated protein kinase, MAP kinase kinase, and Raf. Methods Enzymol 255, 279–90.

Alessi, D. R., Sakamoto, K., Bayascas, J. R., 2006. Lkb1-dependent signaling pathways. Annu. Rev. Biochem. 75, 137–163.

Alhopuro, P., Katajisto, P., Lehtonen, R., Ylisaukko-Oja, S. K., Naatsaari, L., Karhu, A., Westerman, A. M., Wilson, J. H. P., de Rooij, F. W. M., Vogel, T., Moeslein, G., Tomlinson, I. P., Aaltonen, L. A., Makela, T. P., Launonen, V., 2005. Mutation analysis of three genes encoding novel LKB1-interacting proteins, BRG1, STRADalpha, and MO25alpha, in Peutz-Jeghers syndrome. Br J Cancer 92 (6), 1126–9.

Alhopuro, P., Phichith, D., Tuupanen, S., Sammalkorpi, H., Nybondas, M., Saharinen, J., Robinson, J. P., Yang, Z., Chen, L.-Q., Orntoft, T., Mecklin, J.-P., Jarvinen, H., Eng, C., Moeslein, G., Shibata, D., Houlston, R. S., Lucassen, A., Tomlinson, I. P. M., Launonen, V., Ristimaki, A., Arango, D., Karhu, A., Sweeney, H. L., Aaltonen, L. A., 2008. Unregulated smooth-muscle myosin in human intestinal neoplasia. Proc Natl Acad Sci U S A 105 (14), 5513–8.

Amodeo, G. A., Rudolph, M. J., Tong, L., 2007. Crystal structure of the heterotrimer core of Saccharomyces cerevisiae AMPK homologue SNF1. Nature 449 (7161), 492–5.

Amos, C. I., Bali, D., Thiel, T. J., Anderson, J. P., Gourley, I., Frazier, M. L., Lynch, P. M., Luchtefeld, M. A., Young, A., McGarrity, T. J., Seldin, M. F., 1997. Fine mapping of a genetic locus for Peutz-Jeghers syndrome on chromosome 19p. Cancer Res 57 (17), 3653–6.

Avizienyte, E., Loukola, A., Roth, S., Hemminki, A., Tarkkanen, M., Salovaara, R., Arola, J., Butzow, R., Husgafvel-Pursiainen, K., Kokkola, A., Jarvinen, H., Aaltonen, L. A., 1999. LKB1 somatic mutations in sporadic tumors. Am J Pathol 154 (3), 677–81.

Baas, A. F., Boudeau, J., Sapkota, G. P., Smit, L., Morrice, N. A., Alessi, D. R., Clevers, H. C., 2003. Activation of the tumour suppressor kinase LKB1 by the STE20-like pseudokinase. EMBO J. 22, 3062–3072.

Baas, A. F., Kuipers, J., van der Wel, N. N., Batlle, E., Koerten, H. K., Peters, P. J., Clevers, H. C., 2004a. Complete polarization of single intestinal epithelial cells upon activation of lkb1 by strad. Cell 116, 457–466.

Baas, A. F., Smit, L., Clevers, H., 2004b. LKB1 tumor suppressor protein: PARtaker in cell polarity. Trends Cell Biol. 14, 312–319.

Bardeesy, N., Sinha, M., Hezel, A. F., Signoretti, S., Hathaway, N. A., Sharpless, N. E., Loda, M., Carrasco, D. R., DePinho, R. A., 2002. Loss of the LKB1 tumour suppressor provokes intestinal polyposis but resistance to transformation. Nature 419, 162–167.

Barker, W. C., Dayhoff, M. O., 1982. Viral src gene-products are related to the catalytic chain of mammalian camp-dependent protein-kinase. Proc Nat Acad Sci Us-Biol Sci 79, 2836–2839.

Barnes, A. P., Lilley, B. N., Pan, Y. A., Plummer, L. J., Powell, A. W., Raines, A. N., Sanes, J. R., Polleux, F., 2007. LKB1 and SAD kinases define a pathway required for the polarization of cortical neurons. Cell 129, 549–563.

Baxter, E. J., Scott, L. M., Campbell, P. J., East, C., Fourouclas, N., Swanton, S., Vassiliou, G. S., Bench, A. J., Boyd, E. M., Curtin, N., Scott, M. A., Erber, W. N., Green, A. R., 2005. Acquired mutation of the tyrosine kinase JAK2 in human myeloproliferative disorders. Lancet 365 (9464), 1054–61.

Bayliss, R., Sardon, T., Vernos, I., Conti, E., 2003. Structural basis of Aurora-A activation by TPX2 at the mitotic spindle. Mol Cell 12 (4), 851–62.

Bercovich, D., Ganmore, I., Scott, L. M., Wainreb, G., Birger, Y., Elimelech, A., Shochat, C., Cazzaniga, G., Biondi, A., Basso, G., Cario, G., Schrappe, M., Stanulla, M., Strehl, S., Haas, O. A., Mann, G., Binder, V., Borkhardt, A., Kempski, H., Trka, J., Bielorei, B., Avigad, S., Stark, B., Smith, O., Dastugue, N., Bourquin, J.-P., Tal, N. B., Green, A. R., Izraeli, S., 2008. Mutations of JAK2 in acute lymphoblastic leukaemias associated with Down's syndrome. Lancet 372 (9648), 1484–92.

Berger, I., Fitzgerald, D. J., Richmond, T. J., 2004. Baculovirus expression system for heterologous multiprotein complexes. Nat Biotechnol 22 (12), 1583–7.

Bhandari, R., Srinivasan, N., Mahaboobi, M., Ghanekar, Y., Suguna, K., Visweswariah, S. S., 2001. Functional inactivation of the human guanylyl cyclase C receptor: modeling and mutation of the protein kinase-like domain. Biochemistry 40 (31), 9196–206.

Bhattacharyya, R. P., Remenyi, A., Good, M. C., Bashor, C. J., Falick, A. M., Lim, W. A., 2006a. The Ste5 scaffold allosterically modulates signaling output of the yeast mating pathway. Science 311 (5762), 822–6.

Bhattacharyya, R. P., Reményi, A., Good, M. C., Bashor, C. J., Falick, A. M., Lim, W. A., 2006b. The ste5 scaffold allosterically modulates signaling output of the yeast mating pathway. Science 311, 822–826.

Bidlingmaier, S., Weiss, E. L., Seidel, C., Drubin, D. G., Snyder, M., 2001. The Cbk1p pathway is important for polarized cell growth and cell separation in Saccharomyces cerevisiae. Mol Cell Biol 21 (7), 2449–62.

Biernat, J., Wu, Y.-Z., Timm, T., Zheng-Fischhofer, Q., Mandelkow, E., Meijer, L., Mandelkow, E.-M., 2002. Protein kinase MARK/PAR-1 is required for neurite outgrowth and establishment of neuronal polarity. Mol Biol Cell 13 (11), 4013–28.

Biondi, R. M., Komander, D., Thomas, C. C., Lizcano, J. M., Deak, M., Alessi, D. R., van Aalten, D. M. F., 2002. High resolution crystal structure of the human PDK1 catalytic domain defines the regulatory phosphopeptide docking site. EMBO J. 21, 4219–4228.

Blons, H., Pallier, K., Corre, D. L., Danel, C., Tremblay-Gravel, M., Houdayer, C., Fabre-Guillevin, E., Riquet, M., Dessen, P., Laurent-Puig, P., 2008. Genome wide SNP comparative analysis between EGFR and KRAS mutated NSCLC and characterization of two models of oncogenic cooperation in non-small cell lung carcinoma. BMC Med Genomics 1 (NIL), 25.

Boardman, L. A., Couch, F. J., Burgart, L. J., Schwartz, D., Berry, R., McDonnell, S. K., Schaid, D. J., Hartmann, L. C., Schroeder, J. J., Stratakis, C. A., Thibodeau, S. N., 2000. Genetic heterogeneity in Peutz-Jeghers syndrome. Hum Mutat 16 (1), 23–30.

Bond, C. S., Schüttelkopf, A. W., 2009. ALINE: a WYSIWYG protein-sequence alignment editor for publication-quality alignments. Acta Crystallogr D Biol Crystallogr 65 (Pt 5), 510–2.

Boudeau, J., Baas, A. F., Deak, M., Morrice, N. A., Kieloch, A., Schutowski, M., Prescott, A. R., Clevers, H. C., Alessi, D. R., 2003a. MO25 isoforms interact with STRADα/β enhancing their ability to bind, activate and localise LKB1. EMBO J. 22, 5102–5114.

Boudeau, J., Miranda-Saavedra, D., Barton, G. J., Alessi, D. R., 2006. Emerging roles of pseudokinases. Trends Cell Biol. 16, 443–452.

Boudeau, J., Sapkota, G., Alessi, D. R., 2003b. LKB1, a protein kinase regulating cell proliferation and polarity. FEBS Lett. 546, 159–165.

Boudeau, J., Scott, J. W., Resta, N., Deak, M., Kieloch, A., Komander, D., Hardie, D. G., Prescott, A. R., van Aalten, D. M. F., Alessi, D. R., 2004. Analysis of the LKB1-STRAD-MO25 complex. J. Cell Sci. 117, 6365–6375.

Brown, N. R., Noble, M. E., Endicott, J. A., Johnson, L. N., 1999. The structural basis for specificity of substrate and recruitment peptides for cyclin-dependent kinases. Nat Cell Biol 1 (7), 438–43.

Buck, J. L., Harned, R. K., Lichtenstein, J. E., Sobin, L. H., 1992. Peutz-Jeghers syndrome. Radiographics 12 (2), 365–78.

Burman, J. L., Bourbonniere, L., Philie, J., Stroh, T., Dejgaard, S. Y., Presley, J. F., McPherson, P. S., 2008. Scyl1, mutated in a recessive form of spinocerebellar neurodegeneration, regulates COPI-mediated retrograde traffic. J Biol Chem 283 (33), 22774–86.

Cameron, A. J. M., Escribano, C., Saurin, A. T., Kostelecky, B., Parker, P. J., 2009. PKC maturation is promoted by nucleotide pocket occupation independently of intrinsic kinase activity. Nat Struct Mol Biol 16 (6), 624–30.

Carling, D., Clarke, P. R., Zammit, V. A., Hardie, D. G., 1989. Purification and characterization of the AMP-activated protein kinase. Copurification of acetyl-CoA carboxylase kinase and 3-hydroxy-3-methylglutaryl-CoA reductase kinase activities. Eur J Biochem 186 (1-2), 129–36.

Chen, L., Jiao, Z.-H., Zheng, L.-S., Zhang, Y.-Y., Xie, S.-T., Wang, Z.-X., Wu, J.-W., 2009. Structural insight into the autoinhibition mechanism of AMP-activated protein kinase. Nature 459 (7250), 1146–9.

Cheng, Y., Prusoff, W. H., 1973. Relationship between the inhibition constant (K1) and the concentration of inhibitor which causes 50 per cent inhibition (I50) of an enzymatic reaction. Biochem Pharmacol 22 (23), 3099–108.

Cohen, D., Brennwald, P. J., Rodriguez-Boulan, E., Musch, A., 2004. Mammalian PAR-1 determines epithelial lumen polarity by organizing the microtubule cytoskeleton. J Cell Biol 164 (5), 717–27.

Cohen, P., 2002a. The origins of protein phosphorylation. Nat Cell Biol 4 (5), E127–30.

Cohen, P., 2002b. Protein kinases–the major drug targets of the twenty-first century? Nat Rev Drug Discov 1 (4), 309–15.

Collaborative Computational Project, N. ., 1994. The ccp4 suite: programs for protein crystallography. Acta Cryst. D50, 760–763.

Collins, S. P., Reoma, J. L., Gamm, D. M., Uhler, M. D., 2000. LKB1, a novel serine/threonine protein kinase and potential tumour suppressor, is phosphorylated by camp-dependent protein kinase (pka) and prenylated in vivo. Biochem. J. 345, 673–680.

Conner, S. D., Schmid, S. L., 2005. CVAK104 is a novel poly-L-lysine-stimulated kinase that targets the beta2-subunit of AP2. J Biol Chem 280 (22), 21539–44.

Conner, S. H., Kular, G., Peggie, M., Shepherd, S., Schuttelkopf, A. W., Cohen, P., Aalten, D. M. F. V., 2006. TAK1-binding protein 1 is a pseudophosphatase. Biochem J 399 (3), 427–34.

Conti, E., Kuriyan, J., 2000. Crystallographic analysis of the specific yet versatile recognition of distinct nuclear localization signals by karyopherin alpha. Structure 8 (3), 329–338.

Contreras, C. M., Gurumurthy, S., Haynie, J. M., Shirley, L. J., Akbay, E. A., Wingo, S. N., Schorge, J. O., Broaddus, R. R., Wong, K.-K., Bardeesy, N., Castrillon, D. H., 2008. Loss of Lkb1 provokes highly invasive endometrial adenocarcinomas. Cancer Res 68 (3), 759–66.

Cook, A., Lowe, E. D., Chrysina, E. D., Skamnaki, V. T., Oikonomakos, N. G., Johnson, L. N., 2002. Structural studies on phospho-CDK2/cyclin A bound to nitrate, a transition state analogue: implications for the protein kinase mechanism. Biochemistry 41 (23), 7301–11.

Copeland, R. A., 2000. Enzymes: A Practical Introduction to Structure, Mechanism, and Data Analysis. Wiley-VCH, New York, NY.

Cowtan, K., 1998. Modified phased translation functions and their application to molecular fragment location. Acta Cryst. D54, 750–756.

Dale, S., Wilson, W. A., Edelman, A. M., Hardie, D. G., 1995. Similar substrate recognition motifs for mammalian AMP-activated protein kinase, higher plant HMG-CoA reductase kinase-A, yeast SNF1, and mammalian calmodulin-dependent protein kinase I. FEBS Lett 361 (2-3), 191–5.

Dar, A. C., Dever, T. E., Sicheri, F., 2005. Higher-order substrate recognition of eIF2alpha by the RNA-dependent protein kinase PKR. Cell 122 (6), 887–900.

Davies, H., Hunter, C., Smith, R., Stephens, P., Greenman, C., Bignell, G., Teague, J., Butler, A., Edkins, S., Stevens, C., Parker, A., O'Meara, S., Avis, T., Barthorpe, S., Brackenbury, L., Buck, G., Clements, J., Cole, J., Dicks, E., Edwards, K., Forbes, S., Gorton, M., Gray, K., Halliday, K., Harrison, R., Hills, K., Hinton, J., Jones, D., Kosmidou, V., Laman, R., Lugg, R., Menzies, A., Perry, J., Petty, R., Raine, K., Shepherd, R., Small, A., Solomon, H., Stephens, Y., Tofts, C., Varian, J., Webb, A., West, S., Widaa, S., Yates, A., Brasseur, F., Cooper, C. S., Flanagan, A. M., Green, A., Knowles, M., Leung, S. Y., Looijenga, L. H. J., Malkowicz, B., Pierotti, M. A., Teh, B. T., Yuen, S. T., Lakhani, S. R., Easton, D. F., Weber, B. L., Goldstraw, P., Nicholson, A. G., Wooster, R., Stratton, M. R., Futreal, P. A., 2005. Somatic mutations of the protein kinase gene family in human lung cancer. Cancer Res 65 (17), 7591–5.

De Bondt, H. L., Rosenblatt, J., Jancarik, J., Jones, H. D., Morgan, D. O., Kim, S. H., 1993. Crystal structure of cyclin-dependent kinase 2. Nature 363, 595–602.

DeLano, W. L., 2004. Use of pymol as a communications tool for molecular science. Abstr.Pap.Am.Chem.Soc. 228, 030–CHED.

Denison, F. C., Hiscock, N. J., Carling, D., Woods, A., 2009. Characterization of an alternative splice variant of LKB1. J Biol Chem 284 (1), 67–76.

Dong, S. M., Kim, K. M., Kim, S. Y., Shin, M. S., Na, E. Y., Lee, S. H., Park, W. S., Yoo, N. J., Jang, J. J., Yoon, C. Y., Kim, J. W., Kim, S. Y., Yang, Y. M., Kim, S. H., Kim, C. S., Lee, J. Y., 1998. Frequent somatic mutations in serine/threonine kinase 11/Peutz-Jeghers syndrome gene in left-sided colon cancer. Cancer Res 58 (17), 3787–90.

Dorfman, J., Macara, I. G., 2008. STRADalpha Regulates LKB1 Localization by Blocking Access to Importin-alpha, and by Association with Crm1 and Exportin-7. Mol Biol Cell 19 (4), 1614–26.

Dougherty, M. K., Ritt, D. A., Zhou, M., Specht, S. I., Monson, D. M., Veenstra, T. D., Morrison, D. K., 2009. KSR2 is a calcineurin substrate that promotes ERK cascade activation in response to calcium signals. Mol Cell 34 (6), 652–62.

Ducruix, A., Giegé, R., (eds), 1999. Crystallization of Nucleic Acids and Proteins: A Practical Approach. Oxford University Press, Oxford, UK.

Edgar, R. C., 2004. MUSCLE: multiple sequence alignment with high accuracy and high throughput. Nucleic Acids Res 32 (5), 1792–7.

Elion, E. A., 2001. The Ste5p scaffold. J Cell Sci 114 (Pt 22), 3967–78.

Emsley, P., Cowtan, K., 2004. Coot: model-building tools for molecular graphics. Acta Cryst. D60, 2126–2132.

Esteve-Puig, R., Canals, F., Colome, N., Merlino, G., Recio, J. A., 2009. Uncoupling of the LKB1-AMPKalpha energy sensor pathway by growth factors and oncogenic BRAF. PLoS One 4 (3), e4771.

Filippakopoulos, P., Kofler, M., Hantschel, O., Gish, G. D., Grebien, F., Salah, E., Neudecker, P., Kay, L. E., Turk, B. E., Superti-Furga, G., Pawson, T., Knapp, S., 2008. Structural coupling of SH2-kinase domains links Fes and Abl substrate recognition and kinase activation. Cell 134 (5), 793–803.

Fischer, E. H., Graves, D. J., Crittenden, E. R. S., Krebs, E. G., 1959. Structure of the site phosphorylated in the phosphorylase b to a reaction. J Biol Chem 234 (7), 1698–704.

Fischer, E. H., Krebs, E. G., 1955. Conversion of phosphorylase b to phosphorylase a in muscle extracts. J Biol Chem 216 (1), 121–32.

Fogarty, S., Hardie, D. G., 2009. C-terminal phosphorylation of LKB1 is not required for regulation of AMP-activated protein kinase, BRSK1, BRSK2, or cell cycle arrest. J Biol Chem 284 (1), 77–84.

Forbes, S. A., Bhamra, G., Bamford, S., Dawson, E., Kok, C., Clements, J., Menzies, A., Teague, J. W., Futreal, P. A., Stratton, M. R., 2008. The Catalogue of Somatic Mutations in Cancer (COSMIC). Curr Protoc Hum Genet Chapter 10, Unit 10.11.

Giacovazzo, C., Monaco, H., Artioli, G., Viterbo, D., Ferraris, G., Gilli, G., Zanotti, G., Catti, M., 2002. Fundamentals of Crystallography, 2nd Edition. Oxford University Press, Oxford, UK.

Gold, M. G., Barford, D., Komander, D., 2006. Lining the pockets of kinases and phosphatases. Curr. Opin. Struct. Biol. 16, 693–701.

Goldberg, J. M., Manning, G., Liu, A., Fey, P., Pilcher, K. E., Xu, Y., Smith, J. L., 2006. The dictyostelium kinome–analysis of the protein kinases from a simple model organism. PLoS Genet 2 (3), e38.

Good, M., Tang, G., Singleton, J., Remenyi, A., Lim, W. A., 2009. The Ste5 scaffold directs mating signaling by catalytically unlocking the Fus3 MAP kinase for activation. Cell 136 (6), 1085–97.

Graham, T. A., Weaver, C., Mao, F., Kimelman, D., Xu, W. Q., 2000. Crystal structure of a beta-catenin/tcf complex. Cell 103, 885–896.

Guldberg, P., thor Straten, P., Ahrenkiel, V., Seremet, T., Kirkin, A. F., Zeuthen, J., 1999. Somatic mutation of the Peutz-Jeghers syndrome gene, LKB1/STK11, in malignant melanoma. Oncogene 18 (9), 1777–80.

Gurumurthy, S., Hezel, A. F., Berger, J. H., Bosenberg, M. W., Bardeesy, N., 2008. LKB1 deficiency sensitizes mice to carcinogen-induced tumorigenesis. Cancer Res. 68, 55–63.

Gwinn, D. M., Shackelford, D. B., Egan, D. F., Mihaylova, M. M., Mery, A., Vasquez, D. S., Turk, B. E., Shaw, R. J., 2008. AMPK phosphorylation of raptor mediates a metabolic checkpoint. Mol Cell 30 (2), 214–26.

Hanks, S. K., Quinn, A. M., Hunter, T., 1988. The protein-kinase family - conserved features and deduced phylogeny of the catalytic domains. Science 241, 42–52.

Hardie, D. G., 2007a. AMP-activated protein kinase as a drug target. Annu Rev Pharmacol Toxicol 47, 185–210.

Hardie, D. G., 2007b. AMP-activated/SNF1 protein kinases: conserved guardians of cellular energy. Nat Rev Mol Cell Biol 8 (10), 774–85.

Hardie, D. G., Sakamoto, K., 2006. AMPK: a key sensor of fuel and energy status in skeletal muscle. Physiol. (Bethesda). 21, 48–60.

Harned, R. K., Buck, J. L., Sobin, L. H., 1995. The hamartomatous polyposis syndromes: clinical and radiologic features. AJR Am J Roentgenol 164 (3), 565–71.

Hauge, C., Antal, T. L., Hirschberg, D., Doehn, U., Thorup, K., Idrissova, L., Hansen, K., Jensen, O. N., Jorgensen, T. J., Biondi, R. M., Frodin, M., 2007. Mechanism for activation of the growth factor-activated AGC kinases by turn motif phosphorylation. EMBO J 26 (9), 2251–61.

Hawley, S. A., Boudeau, J., L., R. J., Udd, L., Makela, T., Alessi, D., Hardie, D., 2003. Complexes between the LKB1 tumour suppressor, STRADα/β and MO25α/β are upstream kinases in the amp-activated protein kinase cascade. Journal of Biology 2, 28.

Hawley, S. A., Davison, M., Woods, A., Davies, S. P., Beri, R. K., Carling, D., Hardie, D. G., 1996. Characterization of the AMP-activated protein kinase kinase from rat

liver and identification of threonine 172 as the major site at which it phosphorylates AMP-activated protein kinase. J Biol Chem 271 (44), 27879–87.

Hawley, S. A., Pan, D. A., Mustard, K. J., Ross, L., Bain, J., Edelman, A. M., Frenguelli, B. G., Hardie, D. G., 2005. Calmodulin-dependent protein kinase kinase-beta is an alternative upstream kinase for AMP-activated protein kinase. Cell Metab 2 (1), 9–19.

Hearle, N., Schumacher, V., Menko, F. H., Olschwang, S., Boardman, L. A., Gille, J. J. P., Keller, J. J., Westerman, A. M., Scott, R. J., Lim, W., Trimbath, J. D., Giardiello, F. M., Gruber, S. B., Offerhaus, G. J. A., de Rooij, F. W. M., Wilson, J. H. P., Hansmann, A., Möslein, G., Royer-Pokora, B., Vogel, T., Phillips, R. K. S., Spigelman, A. D., Houlston, R. S., 2006. Frequency and spectrum of cancers in the peutz-jeghers syndrome. Clin. Cancer Res. 12, 3209–3215.

Hemminki, A., 1999. The molecular basis and clinical aspects of Peutz-Jeghers syndrome. Cell. Mol. Life Sci. 55, 735–750.

Hemminki, A., Markie, D., Tomlinson, I., Avizienyte, E., Roth, S., Loukola, A., Bignell, G., Warren, W., Aminoff, M., Hoglund, P., Jarvinen, H., Kristo, P., Pelin, K., Ridanpaa, M., Salovaara, R., Toro, T., Bodmer, W., Olschwang, S., Olsen, A. S., Stratton, M. R., de la Chapelle, A., Aaltonen, L. A., 1998. A serine/threonine kinase gene defective in Peutz-Jeghers syndrome. Nature 391, 184–187.

Hemminki, A., Tomlinson, I., Markie, D., Jarvinen, H., Sistonen, P., Bjorkqvist, A. M., Knuutila, S., Salovaara, R., Bodmer, W., Shibata, D., de la Chapelle, A., Aaltonen, L. A., 1997. Localization of a susceptibility locus for Peutz-Jeghers syndrome to 19p using comparative genomic hybridization and targeted linkage analysis. Nat Genet 15 (1), 87–90.

Hezel, A. F., Gurumurthy, S., Granot, Z., Swisa, A., Chu, G. C., Bailey, G., Dor, Y., Bardeesy, N., Depinho, R. A., 2008. Pancreatic LKB1 deletion leads to acinar polarity defects and cystic neoplasms. Mol Cell Biol 28 (7), 2414–25.

Hiratsuka, T., 1982. Biological activities and spectroscopic properties of chromophoric and fluorescent analogs of adenine nucleoside and nucleotides, 2',3'-O-(2,4,6-trinitrocyclohexadienylidene) adenosine derivatives. Biochim Biophys Acta 719 (3), 509–17.

Hong, S.-P., Leiper, F. C., Woods, A., Carling, D., Carlson, M., 2003. Activation of yeast Snf1 and mammalian AMP-activated protein kinase by upstream kinases. Proc Natl Acad Sci U S A 100 (15), 8839–43.

Huang, X., Wullschleger, S., Shpiro, N., McGuire, V. A., Sakamoto, K., Woods, Y. L., McBurnie, W., Fleming, S., Alessi, D. R., 2008. Important role of the LKB1-AMPK pathway in suppressing tumorigenesis in PTEN-deficient mice. Biochem J 412 (2), 211–21.

Hunter, T., Plowman, G. D., 1997. The protein kinases of budding yeast: six score and more. Trends Biochem Sci 22 (1), 18–22.

Hunter, T., Sefton, B. M., 1980. Transforming gene product of Rous sarcoma virus phosphorylates tyrosine. Proc Natl Acad Sci U S A 77 (3), 1311–5.

Huse, M., Kuriyan, J., 2002. The conformational plasticity of protein kinases. Cell 109 (275-282).

Ingebritsen, T. S., Cohen, P., 1983. Protein phosphatases: properties and role in cellular regulation. Science 221 (4608), 331–8.

International Human Genome Sequencing Consortium, 2004. Finishing the euchromatic sequence of the human genome. Nature 431 (7011), 931–45.

Jaleel, M., McBride, A., Lizcano, J. M., Deak, M., Toth, R., Morrice, N. A., Alessi, D. R., 2005. Identification of the sucrose non-fermenting related kinase SNRK, as a novel LKB1 substrate. FEBS Lett 579 (6), 1417–23.

Jaleel, M., Villa, F., Deak, M., Toth, R., Prescott, A. R., Van Aalten, D. M. F., Alessi, D. R., 2006. The ubiquitin-associated domain of AMPK-related kinases regulates conformation and LKB1-mediated phosphorylation and activation. Biochem. J. 394, 545–555.

James, C., Ugo, V., Couedic, J.-P. L., Staerk, J., Delhommeau, F., Lacout, C., Garcon, L., Raslova, H., Berger, R., Bennaceur-Griscelli, A., Villeval, J. L., Constantinescu, S. N., Casadevall, N., Vainchenker, W., 2005. A unique clonal JAK2 mutation leading to constitutive signalling causes polycythaemia vera. Nature 434 (7037), 1144–8.

Jancarik, J., Kim, S. H., 1991. Sparse matrix sampling: a screening method for crystallization of proteins. Journal of Applied Crystallography 24, 409–411.

Jansen, M., Klooster, J. P. T., Offerhaus, G. J., Clevers, H., 2009. LKB1 and AMPK family signaling: the intimate link between cell polarity and energy metabolism. Physiol Rev 89 (3), 777–98.

Jeffrey, P. D., Russo, A. A., Polyak, K., Gibbs, E., Hurwitz, J., Massagué, J., Pavletich, N. P., 1995. Mechanism of CDK activation revealed by the structure of a cyclinA-CDK2 complex. Nature 376, 313–320.

Jeghers, H., McKusick, V. A., Katz, K. H., 1949. Generalized intestinal polyposis and melanin spots of the oral mucosa, lips and digits; a syndrome of diagnostic significance. N Engl J Med 241 (26), 1031–6.

Jenne, D. E., Reimann, H., Nezu, J., Friedel, W., Loff, S., Jeschke, R., Muller, D., Back, W., Zimmer, M., 1998. Peutz-Jeghers syndrome is caused by mutations in a novel serine threonine kinase. Nature Genet. 18, 38–44.

Ji, H., Ramsey, M. R., Hayes, D. N., Fan, C., McNamara, K., Kozlowski, P., Torrice, C., Wu, M. C., Shimamura, T., Perera, S. A., Liang, M.-C., Cai, D., Naumov, G. N., Bao, L., Contreras, C. M., Li, D., Chen, L., Krishnamurthy, J., Koivunen, J., Chirieac, L. R., Padera, R. F., Bronson, R. T., Lindeman, N. I., Christiani, D. C., Lin, X., Shapiro, G. I., Jänne, P. A., Johnson, B. E., Meyerson, M., Kwiatkowski, D. J., Castrillon, D. H., Bardeesy, N., Sharpless, N. E., Wong, K.-K., 2007. LKB1 modulates lung cancer differentiation and metastasis. Nature 448, 807–810.

Johnson, D. A., Akamine, P., Radzio-Andzelm, E., Madhusudan, Taylor, S. S., 2001. Dynamics of camp-dependent protein kinase. Chem. Rev. 101, 2243–2270.

Johnson, L. N., Noble, M. E. M., Owen, D. J., 1996. Active and inactive protein kinases: Structural basis for regulation. Cell 85, 149–158.

Jorgensen, P., Nelson, B., Robinson, M. D., Chen, Y., Andrews, B., Tyers, M., Boone, C., 2002. High-resolution genetic mapping with ordered arrays of Saccharomyces cerevisiae deletion mutants. Genetics 162 (3), 1091–9.

Joubert, S., Jossart, C., McNicoll, N., Lean, A. D., 2005. Atrial natriuretic peptide-dependent photolabeling of a regulatory ATP-binding site on the natriuretic peptide receptor-A. FEBS J 272 (21), 5572–83.

Jura, N., Endres, N. F., Engel, K., Deindl, S., Das, R., Lamers, M. H., Wemmer, D. E., Zhang, X., Kuriyan, J., 2009. Mechanism for activation of the EGF receptor catalytic domain by the juxtamembrane segment. Cell 137 (7), 1293–307.

Kabsch, W., Sander, C., 1983. Dictionary of protein secondary structure: pattern recognition of hydrogen-bonded and geometrical features. Biopolymers 22, 2577–2637.

Kanai, M., Kume, K., Miyahara, K., Sakai, K., Nakamura, K., Leonhard, K., Wiley, D. J., Verde, F., Toda, T., Hirata, D., 2005. Fission yeast MO25 protein is localized at SPB and septum and is essential for cell morphogenesis. EMBO J 24 (17), 3012–25.

Kannan, N., Haste, N., Taylor, S. S., Neuwald, A. F., 2007a. The hallmark of AGC kinase functional divergence is its C-terminal tail, a cis-acting regulatory module. Proc Natl Acad Sci U S A 104 (4), 1272–7.

Kannan, N., Taylor, S. S., Zhai, Y., Venter, J. C., Manning, G., 2007b. Structural and functional diversity of the microbial kinome. PLoS Biol. 5, e17.

Karos, M., Fischer, R., 1996. hymA (hypha-like metulae), a new developmental mutant of Aspergillus nidulans. Microbiology 142 (Pt 11) (NIL), 3211–8.

Karos, M., Fischer, R., 1999. Molecular characterization of HymA, an evolutionarily highly conserved and highly expressed protein of Aspergillus nidulans. Mol Gen Genet 260 (6), 510–21.

Katajisto, P., Vallenius, T., Vaahtomeri, K., Ekman, N., Udd, L., Tiainen, M., Mäkelä, T. P., 2007. The LKB1 tumor suppressor kinase in human disease. Biochim. Biophys. Acta 1775, 63–75.

Kawagoe, T., Sato, S., Matsushita, K., Kato, H., Matsui, K., Kumagai, Y., Saitoh, T., Kawai, T., Takeuchi, O., Akira, S., 2008. Sequential control of Toll-like receptor-dependent responses by IRAK1 and IRAK2. Nat Immunol 9 (6), 684–91.

Kearney, L., Castro, D. G. D., Yeung, J., Procter, J., Horsley, S. W., Eguchi-Ishimae, M., Bateman, C. M., Anderson, K., Chaplin, T., Young, B. D., Harrison, C. J., Kempski, H., So, C. W. E., Ford, A. M., Greaves, M., 2009. Specific JAK2 mutation (JAK2R683) and multiple gene deletions in Down syndrome acute lymphoblastic leukemia. Blood 113 (3), 646–8.

Kemphues, K. J., Priess, J. R., Morton, D. G., Cheng, N. S., 1988. Identification of genes required for cytoplasmic localization in early C. elegans embryos. Cell 52 (3), 311–20.

Kennedy, E. P., Burnett, G., 1954. The enzymatic phosphorylation of proteins. J Biol Chem 211 (2), 969–80.

Kim, K.-Y., Truman, A. W., Levin, D. E., 2008. Yeast Mpk1 mitogen-activated protein kinase activates transcription through Swi4/Swi6 by a noncatalytic mechanism that requires upstream signal. Mol Cell Biol 28 (8), 2579–89.

King, N., Westbrook, M. J., Young, S. L., Kuo, A., Abedin, M., Chapman, J., Fairclough, S., Hellsten, U., Isogai, Y., Letunic, I., Marr, M., Pincus, D., Putnam, N., Rokas, A., Wright, K. J., Zuzow, R., Dirks, W., Good, M., Goodstein, D., Lemons, D., Li, W., Lyons, J. B., Morris, A., Nichols, S., Richter, D. J., Salamov, A., Sequencing, J. G. I., Bork, P., Lim, W. A., Manning, G., Miller, W. T., McGinnis, W., Shapiro, H., Tjian, R., Grigoriev, I. V., Rokhsar, D., 2008. The genome of the choanoflagellate Monosiga brevicollis and the origin of metazoans. Nature 451 (7180), 783–8.

Knighton, D. R., Zheng, J. H., Ten Eyck, L. F., Xuong, N. H., Taylor, S. S., Sowadski, J. M., 1991a. Structure of a peptide inhibitor bound to the catalytic subunit of cyclic adenosine monophosphate-dependent protein kinase. Science 253, 414–420.

Knighton, D. R., Zheng, J. H., Teneyck, L. F., Ashford, V. A., Xuong, N. H., Taylor, S. S., Sowadski, J. M., 1991b. Crystal-structure of the catalytic subunit of cyclic adenosinemonophosphate dependent protein-kinase. Science 253, 407–414.

Koivunen, J. P., Kim, J., Lee, J., Rogers, A. M., Park, J. O., Zhao, X., Naoki, K., Okamoto, I., Nakagawa, K., Yeap, B. Y., Meyerson, M., Wong, K.-K., Richards, W. G., Sugarbaker, D. J., Johnson, B. E., Janne, P. A., 2008. Mutations in the LKB1 tumour suppressor are frequently detected in tumours from Caucasian but not Asian lung cancer patients. Br J Cancer 99 (2), 245–52.

Kolch, W., 2005. Coordinating ERK/MAPK signalling through scaffolds and inhibitors. Nat Rev Mol Cell Biol 6 (11), 827–37.

Komander, D., Garg, R., Wan, P. T. C., Ridley, A. J., Barford, D., 2008. Mechanism of multi-site phosphorylation from a ROCK-I:RhoE complex structure. EMBO J 27 (23), 3175–85.

Komander, D., Kular, G. S., Bain, J., Elliott, M., Alessi, D. R., Van Aalten, D. M. F., 2003. Structural basis for UCN-01 (7-hydroxystaurosporine) specificity and PDK1 (3-phosphoinositide-dependent protein kinase-1) inhibition. Biochem. J. 375, 255–262.

Komander, D., Kular, G. S., Schüttelkopf, A. W., Deak, M., Prakash, K. R. C., Bain, J., Elliott, M., Garrido-Franco, M., Kozikowski, A. P., Alessi, D. R., van Aalten, D. M. F., 2004. Interactions of LY333531 and other bisindolyl maleimide inhibitors with PDK1. Structure (Camb). 12, 215–226.

Kornev, A. P., Haste, N. M., Taylor, S. S., Eyck, L. F. T., 2006. Surface comparison of active and inactive protein kinases identifies a conserved activation mechanism. Proc. Natl. Acad. Sci. USA 103, 17783–17788.

Krissinel, E., Henrick, K., 2007. Inference of macromolecular assemblies from crystalline state. J Mol Biol 372 (3), 774–97.

Kuragaki, C., Enomoto, T., Ueno, Y., Sun, H., Fujita, M., Nakashima, R., Ueda, Y., Wada, H., Murata, Y., Toki, T., Konishi, I., Fujii, S., 2003. Mutations in the STK11 gene characterize minimal deviation adenocarcinoma of the uterine cervix. Lab Invest 83 (1), 35–45.

Labesse, G., Gelin, M., Bessin, Y., Lebrun, M., Papoin, J., Cerdan, R., Arold, S. T., Dubremetz, J.-F., 2009. ROP2 from Toxoplasma gondii: a virulence factor with a protein-kinase fold and no enzymatic activity. Structure 17 (1), 139–46.

Lander, E. S., Linton, L. M., Birren, B., Nusbaum, C., Zody, M. C., Baldwin, J., Devon, K., Dewar, K., Doyle, M., FitzHugh, W., Funke, R., Gage, D., Harris, K., Heaford, A., Howland, J., Kann, L., Lehoczky, J., LeVine, R., McEwan, P., McKernan, K., Meldrim, J., Mesirov, J. P., Miranda, C., Morris, W., Naylor, J., Raymond, C., Rosetti, M., Santos, R., Sheridan, A., Sougnez, C., Stange-Thomann, N., Stojanovic, N., Subramanian, A., Wyman, D., Rogers, J., Sulston, J., Ainscough, R., Beck, S., Bentley, D., Burton, J., Clee, C., Carter, N., Coulson, A., Deadman, R., Deloukas, P., Dunham, A., Dunham, I., Durbin, R., French, L., Grafham, D., Gregory, S., Hubbard, T., Humphray, S., Hunt, A., Jones, M., Lloyd, C., McMurray, A., Matthews, L., Mercer, S., Milne, S., Mullikin, J. C., Mungall, A., Plumb, R., Ross, M., Shownkeen, R., Sims, S., Waterston, R. H., Wilson, R. K., Hillier, L. W., McPherson, J. D., Marra, M. A., Mardis, E. R., Fulton, L. A., Chinwalla, A. T., Pepin, K. H., Gish, W. R., Chissoe, S. L., Wendl, M. C., Delehaunty, K. D., Miner, T. L., Delehaunty, A., Kramer, J. B., Cook, L. L., Fulton, R. S., Johnson, D. L., Minx, P. J., Clifton, S. W., Hawkins, T., Branscomb, E., Predki, P., Richardson, P., Wenning, S., Slezak, T., Doggett, N., Cheng, J. F., Olsen, A., Lucas, S., Elkin, C., Uberbacher, E., Frazier, M., Gibbs, R. A., Muzny, D. M., Scherer, S. E., Bouck, J. B., Sodergren, E. J., Worley, K. C., Rives, C. M., Gorrell, J. H., Metzker,

M. L., Naylor, S. L., Kucherlapati, R. S., Nelson, D. L., Weinstock, G. M., Sakaki, Y., Fujiyama, A., Hattori, M., Yada, T., Toyoda, A., Itoh, T., Kawagoe, C., Watanabe, H., Totoki, Y., Taylor, T., Weissenbach, J., Heilig, R., Saurin, W., Artiguenave, F., Brottier, P., Bruls, T., Pelletier, E., Robert, C., Wincker, P., Smith, D. R., Doucette-Stamm, L., Rubenfield, M., Weinstock, K., Lee, H. M., Dubois, J., Rosenthal, A., Platzer, M., Nyakatura, G., Taudien, S., Rump, A., Yang, H., Yu, J., Wang, J., Huang, G., Gu, J., Hood, L., Rowen, L., Madan, A., Qin, S., Davis, R. W., Federspiel, N. A., Abola, A. P., Proctor, M. J., Myers, R. M., Schmutz, J., Dickson, M., Grimwood, J., Cox, D. R., Olson, M. V., Kaul, R., Raymond, C., Shimizu, N., Kawasaki, K., Minoshima, S., Evans, G. A., Athanasiou, M., Schultz, R., Roe, B. A., Chen, F., Pan, H., Ramser, J., Lehrach, H., Reinhardt, R., McCombie, W. R., de la Bastide, M., Dedhia, N., Blocker, H., Hornischer, K., Nordsiek, G., Agarwala, R., Aravind, L., Bailey, J. A., Bateman, A., Batzoglou, S., Birney, E., Bork, P., Brown, D. G., Burge, C. B., Cerutti, L., Chen, H. C., Church, D., Clamp, M., Copley, R. R., Doerks, T., Eddy, S. R., Eichler, E. E., Furey, T. S., Galagan, J., Gilbert, J. G., Harmon, C., Hayashizaki, Y., Haussler, D., Hermjakob, H., Hokamp, K., Jang, W., Johnson, L. S., Jones, T. A., Kasif, S., Kaspryzk, A., Kennedy, S., Kent, W. J., Kitts, P., Koonin, E. V., Korf, I., Kulp, D., Lancet, D., Lowe, T. M., McLysaght, A., Mikkelsen, T., Moran, J. V., Mulder, N., Pollara, V. J., Ponting, C. P., Schuler, G., Schultz, J., Slater, G., Smit, A. F., Stupka, E., Szustakowski, J., Thierry-Mieg, D., Thierry-Mieg, J., Wagner, L., Wallis, J., Wheeler, R., Williams, A., Wolf, Y. I., Wolfe, K. H., Yang, S. P., Yeh, R. F., Collins, F., Guyer, M. S., Peterson, J., Felsenfeld, A., Wetterstrand, K. A., Patrinos, A., Morgan, M. J., de Jong, P., Catanese, J. J., Osoegawa, K., Shizuya, H., Choi, S., Chen, Y. J., 2001. Initial sequencing and analysis of the human genome. Nature 409 (6822), 860–921.

Laskowski, R. A., McArthur, M. W., Moss, D. S., Thornton, J. M., 1993. PROCHECK: a program to check the stereochemical quality of protein structures. J.Appl.Cryst. 26, 283–291.

Lee, K. P. K., Dey, M., Neculai, D., Cao, C., Dever, T. E., Sicheri, F., 2008. Structure of the dual enzyme ire1 reveals the basis for catalysis and regulation in nonconventional RNA splicing. Cell 132, 89–100.

Levine, R. L., Wadleigh, M., Cools, J., Ebert, B. L., Wernig, G., Huntly, B. J. P., Boggon, T. J., Wlodarska, I., Clark, J. J., Moore, S., Adelsperger, J., Koo, S., Lee, J. C., Gabriel, S., Mercher, T., D'Andrea, A., Frohling, S., Dohner, K., Marynen, P., Vandenberghe, P., Mesa, R. A., Tefferi, A., Griffin, J. D., Eck, M. J., Sellers, W. R., Meyerson, M., Golub, T. R., Lee, S. J., Gilliland, D. G., 2005. Activating mutation in the tyrosine kinase JAK2 in polycythemia vera, essential thrombocythemia, and myeloid metaplasia with myelofibrosis. Cancer Cell 7 (4), 387–97.

Levinson, N. M., Seeliger, M. A., Cole, P. A., Kuriyan, J., 2008. Structural basis for the recognition of c-Src by its inactivator Csk. Cell 134 (1), 124–34.

Lew, J., Coruh, N., Tsigelny, I., Garrod, S., Taylor, S. S., 1997. Synergistic binding of

nucleotides and inhibitors to cAMP-dependent protein kinase examined by acrylodan fluorescence spectroscopy. J Biol Chem 272 (3), 1507–13.

Littler, D., Walker, J., Wybenga-Groot, L., Newman, E., Butler-Cole, C., Mackenzie, F., Finerty, P., Weigelt, J., Sundstrom, M., Arrowsmith, C., Edwards, A., Bochkarev, A., Dhe-Paganon, S., 2006. Structure of the protein kinase domain of the human 5'-amp-activated protein kinase catalytic subunit alpha-2 (ampk alpha-2 chain). Structural Genomics Consortium (SGC) To be published (PDBID 2H6D).

Liu, Y., Gray, N. S., 2006. Rational design of inhibitors that bind to inactive kinase conformations. Nat Chem Biol 2 (7), 358–64.

Lizcano, J. M., Goransson, O., Toth, R., Deak, M., Morrice, N. A., Boudeau, J., Hawley, S. A., Udd, L., Makela, T. P., Hardie, D. G., Alessi, D. R., 2004. LKB1 is a master kinase that activates 13 kinases of the AMPK subfamily, including MARK/PAR-1. EMBO J 23 (4), 833–43.

Lovell, S. C., Davis, I. W., 3rd Arendall, W. B., de Bakker, P. I. W., Word, J. M., Prisant, M. G., Richardson, J. S., Richardson, D. C., 2003. Structure validation by Calpha geometry: phi,psi and Cbeta deviation. Proteins 50 (3), 437–50.

Lowe, E. D., Tews, I., Cheng, K. Y., Brown, N. R., Gul, S., Noble, M. E. M., Gamblin, S. J., Johnson, L. N., 2002. Specificity determinants of recruitment peptides bound to phospho-CDK2/cyclin A. Biochemistry 41 (52), 15625–34.

Madden, K., Sheu, Y. J., Baetz, K., Andrews, B., Snyder, M., 1997. SBF cell cycle regulator as a target of the yeast PKC-MAP kinase pathway. Science 275 (5307), 1781–4.

Madhusudan, u. n. k. n. o. w. n., Akamine, P., Xuong, N. H., Taylor, S. S., 2002. Crystal structure of a transition state mimic of the catalytic subunit of camp-dependent protein kinase. Nat. Struct. Biol. 9, 273–277.

Malinge, S., Ben-Abdelali, R., Settegrana, C., Radford-Weiss, I., Debre, M., Beldjord, K., Macintyre, E. A., Villeval, J.-L., Vainchenker, W., Berger, R., Bernard, O. A., Delabesse, E., Penard-Lacronique, V., 2007. Novel activating JAK2 mutation in a patient with Down syndrome and B-cell precursor acute lymphoblastic leukemia. Blood 109 (5), 2202–4.

Mandelkow, E.-M., Thies, E., Trinczek, B., Biernat, J., Mandelkow, E., 2004. MARK/PAR1 kinase is a regulator of microtubule-dependent transport in axons. J Cell Biol 167 (1), 99–110.

Manning, G., Whyte, D. B., Martinez, R., Hunter, T., Sudarsanam, S., 2002. The protein kinase complement of the human genome. Science 298, 1912–1934.

Manning, G., Young, S. L., Miller, W. T., Zhai, Y., 2008. The protist, Monosiga brevicollis, has a tyrosine kinase signaling network more elaborate and diverse than found in any known metazoan. Proc Natl Acad Sci U S A 105 (28), 9674–9.

Marignani, P. A., Scott, K. D., Bagnulo, R., Cannone, D., Ferrari, E., Stella, A., Guanti, G., Simone, C., Resta, N., 2007. Novel splice isoforms of STRADalpha differentially affect LKB1 activity, complex assembly and subcellular localization. Cancer Biol Ther 6 (10), 1627–31.

Martin, D. M. A., Miranda-Saavedra, D., Barton, G. J., 2009a. Kinomer v. 1.0: a database of systematically classified eukaryotic protein kinases. Nucleic Acids Res 37 (Database issue), D244–50.

Martin, H., Arroyo, J., Sanchez, M., Molina, M., Nombela, C., 1993. Activity of the yeast MAP kinase homologue Slt2 is critically required for cell integrity at 37 degrees C. Mol Gen Genet 241 (1-2), 177–84.

Martin, M. J., Carling, D., Marais, R., 2009b. Taking the stress out of melanoma. Cancer Cell 15 (3), 163–4.

Martin, S. G., St Johnston, D., 2003. A role for *drosophila* LKB1 in anterior-posterior axis formation and epithelial polarity. Nature 421, 379–384.

Matsumoto, S., Iwakawa, R., Takahashi, K., Kohno, T., Nakanishi, Y., Matsuno, Y., Suzuki, K., Nakamoto, M., Shimizu, E., Minna, J. D., Yokota, J., 2007. Prevalence and specificity of LKB1 genetic alterations in lung cancers. Oncogene 26 (40), 5911–8.

McBride, A., Ghilagaber, S., Nikolaev, A., Hardie, D. G., 2009. The glycogen-binding domain on the AMPK beta subunit allows the kinase to act as a glycogen sensor. Cell Metab 9 (1), 23–34.

McCarthy, A., Lord, C. J., Savage, K., Grigoriadis, A., Smith, D. P., Weigelt, B., Reis-Filho, J. S., Ashworth, A., 2009. Conditional deletion of the Lkb1 gene in the mouse mammary gland induces tumour formation. J Pathol (In press).

McCoy, A. J., 2007. Solving structures of protein complexes by molecular replacement with Phaser. Acta Crystallogr D Biol Crystallogr 63 (Pt 1), 32–41.

McKay, M. M., Ritt, D. A., Morrison, D. K., 2009. Signaling dynamics of the KSR1 scaffold complex. Proc Natl Acad Sci U S A 106 (27), 11022–7.

McKusick, V. A., 2007. Mendelian Inheritance in Man and its online version, OMIM. Am J Hum Genet 80 (4), 588–604.

McPherson, A., 1999. Crystallization of Biological Macromolecules. Cold Spring Harbor Laboratory Press, New York, NY.

Mehenni, H., Blouin, J. L., Radhakrishna, U., Bhardwaj, S. S., Bhardwaj, K., Dixit, V. B., Richards, K. F., Bermejo-Fenoll, A., Leal, A. S., Raval, R. C., Antonarakis, S. E., 1997. Peutz-Jeghers syndrome: confirmation of linkage to chromosome 19p13.3 and identification of a potential second locus, on 19q13.4. Am J Hum Genet 61 (6), 1327–34.

Mehenni, H., Gehrig, C., Nezu, J., Oku, A., Shimane, M., Rossier, C., Guex, N., Blouin, J. L., Scott, H. S., Antonarakis, S. E., 1998. Loss of LKB1 kinase activity in Peutz-Jeghers syndrome, and evidence for allelic and locus heterogeneity. Am. J. Hum. Genet. 63, 1641–1650.

Messerschmidt, A., Macieira, S., Velarde, M., Badeker, M., Benda, C., Jestel, A., Brandstetter, H., Neuefeind, T., Blaesse, M., 2005. Crystal structure of the catalytic domain of human atypical protein kinase C-iota reveals interaction mode of phosphorylation site in turn motif. J Mol Biol 352 (4), 918–31.

Milburn, C. C., Boudeau, J., Deak, M., Alessi, D. R., van Aalten, D. M. F., 2004. Crystal structure of MO25 alpha in complex with the c terminus of the pseudo kinase STE20-related adaptor. Nat. Struct. Mol. Biol. 11, 193–200.

Min, X., Lee, B.-H., Cobb, M. H., Goldsmith, E. J., 2004. Crystal structure of the kinase domain of WNK1, a kinase that causes a hereditary form of hypertension. Structure 12 (7), 1303–11.

Miyamoto, H., Matsushiro, A., Nozaki, M., 1993. Molecular cloning of a novel mRNA sequence expressed in cleavage stage mouse embryos. Mol Reprod Dev 34 (1), 1–7.

Momcilovic, M., Hong, S.-P., Carlson, M., 2006. Mammalian TAK1 activates Snf1 protein kinase in yeast and phosphorylates AMP-activated protein kinase in vitro. J Biol Chem 281 (35), 25336–43.

Moorhead, G. B. G., Wever, V. D., Templeton, G., Kerk, D., 2009. Evolution of protein phosphatases in plants and animals. Biochem J 417 (2), 401–9.

Morrison, D. K., Davis, R. J., 2003. Regulation of MAP kinase signaling modules by scaffold proteins in mammals. Annu Rev Cell Dev Biol 19 (NIL), 91–118.

Mukherjee, K., Sharma, M., Urlaub, H., Bourenkov, G. P., Jahn, R., Sudhof, T. C., Wahl, M. C., 2008. CASK Functions as a Mg2+-independent neurexin kinase. Cell 133 (2), 328–39.

Munday, M. R., Campbell, D. G., Carling, D., Hardie, D. G., 1988. Identification by amino acid sequencing of three major regulatory phosphorylation sites on rat acetyl-CoA carboxylase. Eur J Biochem 175 (2), 331–8.

Murshudov, G. N., Vagin, A. A., Dodson, E. J., 1997. Refinement of macromolecular structures by the maximum-likelihood method. Acta Cryst. D53, 240–255.

Myszka, D. G., Morton, T. A., 1998. CLAMP: a biosensor kinetic data analysis program. Trends Biochem Sci 23 (4), 149–50.

N.A. Baker, D. Sept, S. J. M. J. H., McCammon, J. A., 2001. Electrostatics of nanosystems: application to microtubules and the ribosome. Proc.Natl.Acad.Sci. USA 98, 10037–10041.

Narbonne, P., Roy, R., 2009. Caenorhabditis elegans dauers need LKB1/AMPK to ration lipid reserves and ensure long-term survival. Nature 457 (7226), 210–4.

Nelson, B., Kurischko, C., Horecka, J., Mody, M., Nair, P., Pratt, L., Zougman, A., McBroom, L. D. B., Hughes, T. R., Boone, C., Luca, F. C., 2003. RAM: a conserved signaling network that regulates Ace2p transcriptional activity and polarized morphogenesis. Mol Biol Cell 14 (9), 3782–803.

Neumann, D., Suter, M., Tuerk, R., Riek, U., Wallimann, T., 2007. Co-expression of LKB1, MO25alpha and STRADalpha in bacteria yield the functional and active heterotrimeric complex. Mol Biotechnol 36 (3), 220–31.

Neumann, D., Woods, A., Carling, D., Wallimann, T., Schlattner, U., 2003. Mammalian AMP-activated protein kinase: functional, heterotrimeric complexes by co-expression of subunits in Escherichia coli. Protein Expr Purif 30 (2), 230–7.

Nishioka, Y., Kobayashi, K., Sagae, S., Sugimura, M., Ishioka, S., Nagata, M., Terasawa, K., Tokino, T., Kudo, R., 1999. Mutational analysis of STK11 gene in ovarian carcinomas. Jpn J Cancer Res 90 (6), 629–32.

Nolen, B., Taylor, S., Ghosh, G., 2004. Regulation of protein kinases; controlling activity through activation segment conformation. Mol. Cell 15, 661–675.

Nooren, I. M. A., Thornton, J. M., 2003. Structural characterisation and functional significance of transient protein-protein interactions. J Mol Biol 325 (5), 991–1018.

Nozaki, M., Onishi, Y., Togashi, S., Miyamoto, H., 1996. Molecular characterization of the Drosophila Mo25 gene, which is conserved among Drosophila, mouse, and yeast. DNA Cell Biol 15 (6), 505–9.

Okuzumi, T., Fiedler, D., Zhang, C., Gray, D. C., Aizenstein, B., Hoffman, R., Shokat, K. M., 2009. Inhibitor hijacking of Akt activation. Nat Chem Biol 5 (7), 484–493.

Olschwang, S., Boisson, C., Thomas, G., 2001. Peutz-Jeghers families unlinked to stk11/LKB1 gene mutations are highly predisposed to primitive biliary adenocarcinoma. J. Med. Genet. 38, 356–360.

Onozato, R., Kosaka, T., Achiwa, H., Kuwano, H., Takahashi, T., Yatabe, Y., Mitsudomi, T., 2007. LKB1 gene mutations in Japanese lung cancer patients. Cancer Sci 98 (11), 1747–51.

Otwinowski, Z., Minor, W., 1997. Processing of X-ray diffraction data collected in oscillation mode. Methods in Enzymology 276, 307–326.

Owen, D. J., Noble, M. E. M., Garman, E. F., Papageorgiou, A. C., Johnson, L. N., 1995. Two structures of the catalytic domain of phosphorylase-kinase - an active protein-kinase complexed with substrate-analog and product. Structure 3, 467–482.

Panneerselvam, S., Marx, A., Mandelkow, E.-M., Mandelkow, E., 2006. Structure of the catalytic and ubiquitin-associated domains of the protein kinase MARK/Par-1. Structure 14 (2), 173–83.

Park, W. S., Moon, Y. W., Yang, Y. M., Kim, Y. S., Kim, Y. D., Fuller, B. G., Vortmeyer, A. O., Fogt, F., Lubensky, I. A., Zhuang, Z., 1998. Mutations of the STK11 gene in sporadic gastric carcinoma. Int J Oncol 13 (3), 601–4.

Pearson, H. B., McCarthy, A., Collins, C. M. P., Ashworth, A., Clarke, A. R., 2008. Lkb1 deficiency causes prostate neoplasia in the mouse. Cancer Res 68 (7), 2223–32.

Peutz, J., 1921. Over een zeer merkwaardige, gecombineerde familiaire polyposis van de slijmliezen van den tractus intestinalis met die van de neuskeelholte en gepaard met eigenaardige pigmentaties van huid-en slijmvliezen. Ned Maandschr v Gen 10, 134–46.

Popov, A. N., Bourenkov, G. P., Jul 2003. Choice of data-collection parameters based on statistic modelling. Acta Crystallographica Section D 59 (7), 1145–1153.

Prade, L., Engh, R. A., Girod, A., Kinzel, V., Huber, R., Bossemeyer, D., 1997. Staurosporine-induced conformational changes of camp-dependent protein kinase catalytic subunit explain inhibitory potential. Structure 5, 1627–1637.

Puffenberger, E. G., Strauss, K. A., Ramsey, K. E., Craig, D. W., Stephan, D. A., Robinson, D. L., Hendrickson, C. L., Gottlieb, S., Ramsay, D. A., Siu, V. M., Heuer, G. G., Crino, P. B., Morton, D. H., 2007. Polyhydramnios, megalencephaly and symptomatic epilepsy caused by a homozygous 7-kilobase deletion in LYK5. Brain. 130, 1929–1941.

Qiu, W., Schönleben, F., Thaker, H. M., Goggins, M., Su, G. H., 2006. A novel mutation of STK11/LKB1 gene leads to the loss of cell growth inhibition in head and neck squamous cell carcinoma. Oncogene. 25, 2937–2942.

Qiu, W., Wernimont, A., Tang, K., Taylor, S., Lunin, V., Schapira, M., Fentress, S., Hui, R., Sibley, L. D., 2009. Novel structural and regulatory features of rhoptry secretory kinases in Toxoplasma gondii. EMBO J 28 (7), 969–79.

Radaev, S., Sun, P. D., Dec 2002. Crystallization of protein–protein complexes. Journal of Applied Crystallography 35 (6), 674–676.

Resta, N., Simone, C., Mareni, C., Montera, M., Gentile, M., Susca, F., Gristina, R., Pozzi, S., Bertario, L., Bufo, P., Carlomagno, N., Ingrosso, M., Rossini, F. P., Tenconi, R., Guanti, G., 1998. STK11 mutations in Peutz-Jeghers syndrome and sporadic colon cancer. Cancer Res 58 (21), 4799–801.

Resta, N., Stella, A., Susca, F. C., Giacomo, M. D., Forleo, G., Miccolis, I., Rossini, F. P., Genuardi, M., Piepoli, A., Grammatico, P., Guanti, G., 2002. Two novel mutations and a new STK11/LKB1 gene isoform in Peutz-Jeghers patients. Hum Mutat 20 (1), 78–9.

Rhodes, G., 2006. Crystallography Made Crystal Clear: A Guide for Users of Macromolecular Models, 3rd Edition. Academic Press, San Diego, CA.

Richardson, C., Alessi, D. R., 2008. The regulation of salt transport and blood pressure by the WNK-SPAK/OSR1 signalling pathway. J Cell Sci 121 (Pt 20), 3293–304.

Robinson, J., Lai, C., Martin, A., Nye, E., Tomlinson, I., Silver, A., 2009. Oral rapamycin reduces tumour burden and vascularization in Lkb1(+/-) mice. J Pathol 219 (1), 35–40.

Rossi, D. J., Ylikorkala, A., Korsisaari, N., Salovaara, R., Luukko, K., Launonen, V., Henkemeyer, M., Ristimaki, A., Aaltonen, L. A., Makela, T. P., 2002. Induction of cyclooxygenase-2 in a mouse model of Peutz-Jeghers polyposis. Proc Natl Acad Sci U S A 99 (19), 12327–32.

Rowan, A., Bataille, V., MacKie, R., Healy, E., Bicknell, D., Bodmer, W., Tomlinson, I., 1999. Somatic mutations in the Peutz-Jeghers (LKB1/STKII) gene in sporadic malignant melanomas. J Invest Dermatol 112 (4), 509–11.

Russo, A. A., Jeffrey, P. D., Pavletich, N. P., 1996. Structural basis of cyclin-dependent kinase activation by phosphorylation. Nat. Struct. Biol. 3, 696–700.

Saharinen, P., Silvennoinen, O., 2002. The pseudokinase domain is required for suppression of basal activity of Jak2 and Jak3 tyrosine kinases and for cytokine-inducible activation of signal transduction. J Biol Chem 277 (49), 47954–63.

Saharinen, P., Vihinen, M., Silvennoinen, O., 2003. Autoinhibition of Jak2 tyrosine kinase is dependent on specific regions in its pseudokinase domain. Mol Biol Cell 14 (4), 1448–59.

Sakamoto, K., McCarthy, A., Smith, D., Green, K. A., Hardie, D. G., Ashworth, A., Alessi, D. R., 2005. Deficiency of LKB1 in skeletal muscle prevents AMPK activation and glucose uptake during contraction. EMBO J 24 (10), 1810–20.

Sanchez-Cespedes, M., 2007. A role for LKB1 gene in human cancer beyond the Peutz-Jeghers syndrome. Oncogene. 26, 7825–7832.

Sanchez-Cespedes, M., Parrella, P., Esteller, M., Nomoto, S., Trink, B., Engles, J. M., Westra, W. H., Herman, J. G., Sidransky, D., 2002. Inactivation of LKB1/STK11 is a common event in adenocarcinomas of the lung. Cancer Res. 62, 3659–3662.

Sanders, M. J., Grondin, P. O., Hegarty, B. D., Snowden, M. A., Carling, D., 2007. Investigating the mechanism for AMP activation of the AMP-activated protein kinase cascade. Biochem J 403 (1), 139–48.

Sapkota, G. P., Boudeau, J., Deak, M., Kieloch, A., Morrice, N., Alessi, D. R., 2002a. Identification and characterization of four novel phosphorylation sites (ser(31), ser(325), thr(336) and thr(366)) on LKB1/stk11, the protein kinase mutated in peutzjeghers cancer syndrome. Biochem. J. 362, 481–490.

Sapkota, G. P., Deak, M., Kieloch, A., Morrice, N., Goodarzi, A. A., Smythe, C., Shiloh, Y., Lees-Miller, S. P., Alessi, D. R., 2002b. Ionizing radiation induces ataxia telangiectasia mutated kinase (atm)-mediated phosphorylation of LKB1/stk11 at thr-366. Biochem. J. 368, 507–516.

Sapkota, G. P., Kieloch, A., Lizcano, J. M., Lain, S., Arthur, J. S. C., Williams, M. R., Morrice, N., Deak, M., Alessi, D. R., 2001. Phosphorylation of the protein kinase mutated in Peutz-Jeghers cancer syndrome, LKB1/stk11, at ser(431) by p90(rsk) and campdependent protein kinase, but not its farnesylation at cys(433), is essential for LKB1 to suppress cell growth. J. Biol. Chem. 276, 19469–19482.

Scheeff, E. D., Eswaran, J., Bunkoczi, G., Knapp, S., Manning, G., 2009. Structure of the pseudokinase VRK3 reveals a degraded catalytic site, a highly conserved kinase fold, and a putative regulatory binding site. Structure 17 (1), 128–38.

Schmidt, W. M., Kraus, C., Hoger, H., Hochmeister, S., Oberndorfer, F., Branka, M., Bingemann, S., Lassmann, H., Muller, M., Macedo-Souza, L. I., Vainzof, M., Zatz, M., Reis, A., Bittner, R. E., 2007. Mutation in the Scyl1 gene encoding amino-terminal kinase-like protein causes a recessive form of spinocerebellar neurodegeneration. EMBO Rep 8 (7), 691–7.

Scholz, R., Suter, M., Weimann, T., Polge, C., Konarev, P., Thali, R., Tuerk, R., Viollet, B., Wallimann, T., Schlattner, U., Neumann, D., 2009. Homooligomerization and activation of AMP-activated protein kinase is mediated by the kinase domain alphaG-helix. J Biol Chem (In press).

Schuck, P., 2000. Size-distribution analysis of macromolecules by sedimentation velocity ultracentrifugation and lamm equation modeling. Biophys J 78 (3), 1606–19.

Schulze-Gahmen, U., Bondt, H. L. D., Kim, S. H., 1996. High-resolution crystal structures of human cyclin-dependent kinase 2 with and without ATP: bound waters and natural ligand as guides for inhibitor design. J Med Chem 39 (23), 4540–6.

Scott, R. J., Crooks, R., Meldrum, C. J., Thomas, L., Smith, C. J. A., Mowat, D., McPhillips, M., Spigelman, A. D., 2002. Mutation analysis of the STK11/LKB1 gene and clinical characteristics of an Australian series of Peutz-Jeghers syndrome patients. Clin Genet 62 (4), 282–7.

Sebbagh, M., Santoni, M.-J., Hall, B., Borg, J.-P., Schwartz, M. A., 2009. Regulation of LKB1/STRAD localization and function by E-cadherin. Curr Biol 19 (1), 37–42.

Sessa, F., Mapelli, M., Ciferri, C., Tarricone, C., Areces, L. B., Schneider, T. R., Stukenberg, P. T., Musacchio, A., 2005. Mechanism of Aurora B activation by INCENP and inhibition by hesperadin. Mol Cell 18 (3), 379–91.

Shackelford, D. B., Shaw, R. J., 2009. The LKB1-AMPK pathway: metabolism and growth control in tumour suppression. Nat Rev Cancer 9 (8), 563–75.

Shackelford, D. B., Vasquez, D. S., Corbeil, J., Wu, S., Leblanc, M., Wu, C.-L., Vera, D. R., Shaw, R. J., 2009. mTOR and HIF-1alpha-mediated tumor metabolism in an LKB1 mouse model of Peutz-Jeghers syndrome. Proc Natl Acad Sci U S A 106 (27), 11137–42.

Sharma, R. K., 2002. Evolution of the membrane guanylate cyclase transduction system. Mol Cell Biochem 230 (1-2), 3–30.

Shaw, R. J., 2009. LKB1 and AMP-activated protein kinase control of mTOR signalling and growth. Acta Physiol (Oxf) 196 (1), 65–80.

Shaw, R. J., Kosmatka, M., Bardeesy, N., Hurley, R. L., Witters, L. A., DePinho, R. A., Cantley, L. C., 2004. The tumor suppressor LKB1 kinase directly activates AMP-activated kinase and regulates apoptosis in response to energy stress. Proc Natl Acad Sci U S A 101 (10), 3329–35.

Shaw, R. J., Lamia, K. A., Vasquez, D., Koo, S.-H., Bardeesy, N., Depinho, R. A., Montminy, M., Cantley, L. C., 2005. The kinase LKB1 mediates glucose homeostasis in liver and therapeutic effects of metformin. Science 310, 1642–1646.

Shelly, M., Cancedda, L., Heilshorn, S., Sumbre, G., Poo, M.-M., 2007. LKB1/STRAD promotes axon initiation during neuronal polarization. Cell 129, 565–577.

Shoji, S., Parmelee, D. C., Wade, R. D., Kumar, S., Ericsson, L. H., Walsh, K. A., Neurath, H., Long, G. L., Demaille, J. G., Fischer, E. H., Titani, K., 1981. Complete amino acid sequence of the catalytic subunit of bovine cardiac muscle cyclic AMP-dependent protein kinase. Proc Natl Acad Sci U S A 78 (2), 848–51.

Shulman, J. M., Benton, R., St Johnston, D., 2000. The drosophila homolog of c-elegans par-1 organizes the oocyte cytoskeleton and directs oskar mrna localization to the posterior pole. Cell 101, 377–388.

Sicheri, F., Kuriyan, J., 1997. Structures of Src-family tyrosine kinases. Curr Opin Struct Biol 7 (6), 777–85.

Steinberg, G. R., Kemp, B. E., 2009. AMPK in Health and Disease. Physiol Rev 89 (3), 1025–78.

Strazisar, M., Mlakar, V., Rott, T., Glavac, D., 2009. Somatic alterations of the serine/threonine kinase LKB1 gene in squamous cell (SCC) and large cell (LCC) lung carcinoma. Cancer Invest 27 (4), 407–16.

Stryer, L., Berg, J. M., Tymoczko, J. L., 2002. Biochemistry, 5th Edition. W.H.Freeman & Co Ltd, New York, NY.

Sutherland, C. M., Hawley, S. A., McCartney, R. R., Leech, A., Stark, M. J. R., Schmidt, M. C., Hardie, D. G., 2003. Elm1p is one of three upstream kinases for the saccharomyces cerevisiae SNF1 complex. Curr. Biol. 13, 1299–1305.

Sutherland, E. W. J., Wosilait, W. D., 1955. Inactivation and activation of liver phosphorylase. Nature 175 (4447), 169–70.

Takeda, H., Miyoshi, H., Kojima, Y., Oshima, M., Taketo, M. M., 2006. Accelerated onsets of gastric hamartomas and hepatic adenomas/carcinomas in Lkb1+/-p53-/- compound mutant mice. Oncogene 25 (12), 1816–20.

Tan, S., 2001. A modular polycistronic expression system for overexpressing protein complexes in escherichia coli. Protein Exp. Purif. 21, 224–234.

Taylor, S. S., Radzio-Andzelm, E., 1994. Three protein-kinase structures define a common motif. Structure 2, 345–355.

Taylor, S. S., Yang, J., Wu, J., Haste, N. M., Radzio-Andzelm, E., Anand, G., 2004. PKA: a portrait of protein kinase dynamics. Biochim Biophys Acta 1697 (1-2), 259–69.

ten Klooster, J. P., Jansen, M., Yuan, J., Oorschot, V., Begthel, H., Giacomo, V. D., Colland, F., de Koning, J., Maurice, M. M., Hornbeck, P., Clevers, H., 2009. Mst4 and Ezrin induce brush borders downstream of the Lkb1/Strad/Mo25 polarization complex. Dev Cell 16 (4), 551–62.

Terwilliger, T. C., 2003. Solve and resolve: Automated structure solution and density modification. Methods Enzymol. 374, 22–37.

Tiainen, M., Ylikorkala, A., Makela, T. P., 1999. Growth suppression by LKB1 is mediated by a g(1) cell cycle arrest. Proc.Natl.Acad.Sci.USA. 96, 9248–9251.

Tomlinson, I. P., Houlston, R. S., 1997. Peutz-Jeghers syndrome. J Med Genet 34 (12), 1007–11.

Towler, M. C., Fogarty, S., Hawley, S. A., Pan, D. A., Martin, D. M. A., Morrice, N. A., McCarthy, A., Galardo, M. N., Meroni, S. B., Cigorraga, S. B., Ashworth, A., Sakamoto, K., Hardie, D. G., 2008. A novel short splice variant of the tumour suppressor LKB1 is required for spermiogenesis. Biochem J 416 (1), 1–14.

Townley, R., Shapiro, L., 2007. Crystal structures of the adenylate sensor from fission yeast AMP-activated protein kinase. Science 315 (5819), 1726–9.

Vagin, A., Teplyakov, A., 1997. Molrep: an automated program for molecular replacement. J.Appl.Cryst. 30, 1022–1025.

Venter, J. C., Adams, M. D., Myers, E. W., Li, P. W., Mural, R. J., Sutton, G. G., Smith, H. O., Yandell, M., Evans, C. A., Holt, R. A., Gocayne, J. D., Amanatides, P., Ballew, R. M., Huson, D. H., Wortman, J. R., Zhang, Q., Kodira, C. D., Zheng, X. H., Chen, L., Skupski, M., Subramanian, G., Thomas, P. D., Zhang, J., Miklos, G. L. G., Nelson, C., Broder, S., Clark, A. G., Nadeau, J., McKusick, V. A., Zinder, N., Levine, A. J., Roberts, R. J., Simon, M., Slayman, C., Hunkapiller, M., Bolanos, R., Delcher, A., Dew, I., Fasulo, D., Flanigan, M., Florea, L., Halpern, A., Hannenhalli, S., Kravitz, S., Levy, S., Mobarry, C., Reinert, K., Remington, K., Abu-Threideh, J., Beasley, E., Biddick, K., Bonazzi, V., Brandon, R., Cargill, M., Chandramouliswaran, I., Charlab, R., Chaturvedi, K., Deng, Z., Francesco, V. D., Dunn, P., Eilbeck, K., Evangelista, C., Gabrielian, A. E., Gan, W., Ge, W., Gong, F., Gu, Z., Guan, P., Heiman, T. J., Higgins, M. E., Ji, R. R., Ke, Z., Ketchum, K. A., Lai, Z., Lei, Y., Li, Z., Li, J., Liang, Y., Lin, X., Lu, F., Merkulov, G. V., Milshina, N., Moore, H. M., Naik, A. K., Narayan, V. A., Neelam, B., Nusskern, D., Rusch, D. B., Salzberg, S., Shao, W., Shue, B., Sun, J., Wang, Z., Wang, A., Wang, X., Wang, J., Wei, M., Wides, R., Xiao, C., Yan, C., Yao, A., Ye, J., Zhan, M., Zhang, W., Zhang, H., Zhao, Q., Zheng, L., Zhong, F., Zhong, W., Zhu, S., Zhao, S., Gilbert, D., Baumhueter, S., Spier, G., Carter, C., Cravchik, A., Woodage, T., Ali, F., An, H., Awe, A., Baldwin, D., Baden, H., Barnstead, M., Barrow, I., Beeson, K., Busam, D., Carver, A., Center, A., Cheng, M. L., Curry, L., Danaher, S., Davenport, L., Desilets, R., Dietz, S., Dodson, K., Doup, L., Ferriera, S., Garg, N., Gluecksmann, A., Hart, B., Haynes, J., Haynes, C., Heiner, C., Hladun, S., Hostin, D., Houck, J., Howland, T., Ibegwam, C., Johnson, J., Kalush, F., Kline, L., Koduru, S., Love, A., Mann, F., May, D., McCawley, S., McIntosh, T., McMullen, I., Moy, M., Moy, L., Murphy, B., Nelson, K., Pfannkoch, C., Pratts, E., Puri, V., Qureshi, H., Reardon, M., Rodriguez, R., Rogers, Y. H., Romblad, D., Ruhfel, B., Scott, R., Sitter, C., Smallwood, M., Stewart, E., Strong, R., Suh, E., Thomas, R., Tint, N. N., Tse, S., Vech, C., Wang, G., Wetter, J., Williams, S., Williams, M., Windsor, S., Winn-Deen, E., Wolfe, K., Zaveri, J., Zaveri, K., Abril, J. F., Guigo, R., Campbell, M. J., Sjolander, K. V., Karlak, B., Kejariwal, A., Mi, H., Lazareva, B., Hatton, T., Narechania, A., Diemer, K., Muruganujan, A., Guo, N., Sato, S., Bafna, V., Istrail, S., Lippert, R., Schwartz, R., Walenz, B., Yooseph, S., Allen, D., Basu, A., Baxendale, J., Blick, L., Caminha, M., Carnes-Stine, J., Caulk, P., Chiang, Y. H., Coyne, M., Dahlke, C., Mays, A., Dombroski, M., Donnelly, M., Ely, D., Esparham, S., Fosler, C., Gire, H., Glanowski, S., Glasser, K., Glodek, A., Gorokhov, M., Graham, K., Gropman, B., Harris, M., Heil, J., Henderson, S., Hoover, J., Jennings, D., Jordan, C., Jordan, J., Kasha, J., Kagan, L., Kraft, C., Levitsky, A., Lewis, M., Liu, X., Lopez, J., Ma, D., Majoros, W., McDaniel, J., Murphy, S., Newman, M., Nguyen, T., Nguyen, N., Nodell, M., Pan, S., Peck, J., Peterson, M., Rowe, W., Sanders, R., Scott, J., Simpson, M., Smith, T., Sprague, A., Stockwell, T., Turner, R., Venter, E., Wang, M., Wen, M., Wu, D., Wu, M., Xia, A., Zandieh, A., Zhu, X., 2001. The sequence of the human genome. Science 291 (5507), 1304–51.

Vitari, A. C., Deak, M., Morrice, N. A., Alessi, D. R., 2005. The WNK1 and WNK4

protein kinases that are mutated in gordon's hypertension syndrome phosphorylate and activate SPAK and OSR1 protein kinases. Biochem. J. 391, 17–24.

Volikos, E., Robinson, J., Aittomäki, K., Mecklin, J., Järvinen, H., Westerman, A. M., de Rooji, F. W. M., Vogel, T., Moeslein, G., Launonen, V., Tomlinson, I. P. M., Silver, A. R. J., Aaltonen, L. A., 2006. LKB1 exonic and whole gene deletions are a common cause of peutz-jeghers syndrome. J. Med. Genet. 43, e18.

Wallace, K. N., Dolan, A. C., Seiler, C., Smith, E. M., Yusuff, S., Chaille-Arnold, L., Judson, B., Sierk, R., Yengo, C., Sweeney, H. L., Pack, M., 2005. Mutation of smooth muscle myosin causes epithelial invasion and cystic expansion of the zebrafish intestine. Dev Cell 8 (5), 717–26.

Walsh, D. A., Perkins, J. P., Krebs, E. G., 1968. An adenosine 3',5'-monophosphate-dependant protein kinase from rabbit skeletal muscle. J Biol Chem 243 (13), 3763–5.

Walter, T. S., Meier, C., Assenberg, R., Au, K.-F., Ren, J., Verma, A., Nettleship, J. E., Owens, R. J., Stuart, D. I., Grimes, J. M., 2006. Lysine methylation as a routine rescue strategy for protein crystallization. Structure 14, 1617–1622.

Wang, X. Q., Zamore, P. D., Hall, T. M. T., 2001. Crystal structure of a pumilio homology domain. Mol. Cell 7, 855–865.

Wang, Z. J., Churchman, M., Avizienyte, E., McKeown, C., Davies, S., Evans, D. G., Ferguson, A., Ellis, I., Xu, W. H., Yan, Z. Y., Aaltonen, L. A., Tomlinson, I. P., 1999. Germline mutations of the LKB1 (STK11) gene in Peutz-Jeghers patients. J Med Genet 36 (5), 365–8.

Wei, C., Amos, C. I., Stephens, L. C., Campos, I., Deng, J. M., Behringer, R. R., Rashid, A., Frazier, M. L., 2005. Mutation of Lkb1 and p53 genes exert a cooperative effect on tumorigenesis. Cancer Res 65 (24), 11297–303.

Wei, C., Amos, C. I., Zhang, N., Wang, X., Rashid, A., Walker, C. L., Behringer, R. R., Frazier, M. L., 2008. Suppression of Peutz-Jeghers polyposis by targeting mammalian target of rapamycin signaling. Clin Cancer Res 14 (4), 1167–71.

Wei, C., Amos, C. I., Zhang, N., Zhu, J., Wang, X., Frazier, M. L., 2009. Chemopreventive efficacy of rapamycin on Peutz-Jeghers syndrome in a mouse model. Cancer Lett 277 (2), 149–54.

Westerman, A. M., Entius, M. M., Boor, P. P. C., Koole, R., de Baar, E., Offerhaus, G. J. A., Lubinski, J., Lindhout, D., Halley, D. J. J., de Rooij, F. W. M., Wilson, J. H. P., 1999a. Novel mutations in the LKB1/stk11 gene in dutch Peutz-Jeghers families. Hum. Mutat. 13, 476–481.

Westerman, A. M., Entius, M. M., de Baar, E., Boor, P. P. C., Koole, R., van Velthuysen, M. L. F., Offerhaus, G. J. A., Lindhout, D., de Rooij, F. W. M., Wilson, J. H. P.,

1999b. Peutz-Jeghers syndrome: 78-year follow-up of the original family. Lancet 353, 1211–1215.

White, A., Pargellis, C. A., Studts, J. M., Werneburg, B. G., 2nd Farmer, B. T., 2007. Molecular basis of MAPK-activated protein kinase 2:p38 assembly. Proc Natl Acad Sci U S A 104 (15), 6353–8.

Winn, M. D., Isupov, M. N., Murshudov, G. N., 2001. Use of tls parameters to model anisotropic displacements in macromolecular refinement. Acta Cryst. D57, 122–133.

Woods, A., Dickerson, K., Heath, R., Hong, S.-P., Momcilovic, M., Johnstone, S. R., Carlson, M., Carling, D., 2005. Ca2+/calmodulin-dependent protein kinase kinase-beta acts upstream of AMP-activated protein kinase in mammalian cells. Cell Metab 2 (1), 21–33.

Woods, A., Johnstone, S. R., Dickerson, K., Leiper, F. C., Fryer, L. G. D., Neumann, D., Schlattner, U., Wallimann, T., Carlson, M., Carling, D., 2003. LKB1 is the upstream kinase in the AMP-activated protein kinase cascade. Curr Biol 13 (22), 2004–8.

Xiao, B., Heath, R., Saiu, P., Leiper, F. C., Leone, P., Jing, C., Walker, P. A., Haire, L., Eccleston, J. F., Davis, C. T., Martin, S. R., Carling, D., Gamblin, S. J., 2007. Structural basis for AMP binding to mammalian AMP-activated protein kinase. Nature 449, 496–500.

Xie, M., Zhang, D., Dyck, J. R. B., Li, Y., Zhang, H., Morishima, M., Mann, D. L., Taffet, G. E., Baldini, A., Khoury, D. S., Schneider, M. D., 2006. A pivotal role for endogenous TGF-beta-activated kinase-1 in the LKB1/AMP-activated protein kinase energy-sensor pathway. Proc Natl Acad Sci U S A 103 (46), 17378–83.

Xie, Z., Dong, Y., Zhang, J., Scholz, R., Neumann, D., Zou, M.-H., 2009. Identification of the serine 307 of LKB1 as a novel phosphorylation site essential for its nucleocytoplasmic transport and endothelial cell angiogenesis. Mol Cell Biol 29 (13), 3582–96.

Yamamoto, Y., Izumi, Y., Matsuzaki, F., 2008. The GC kinase fray and mo25 regulate drosophila asymmetric divisions. Biochem. Biophys. Res. Commun. 366, 212–218.

Yang, J., Cron, P., Thompson, V., Good, V. M., Hess, D., Hemmings, B. A., Barford, D., 2002. Molecular mechanism for the regulation of protein kinase b/akt by hydrophobic motif phosphorylation. Mol.Cell 9, 1227–1240.

Yang, J., Kennedy, E. J., Wu, J., Deal, M. S., Pennypacker, J., Ghosh, G., Taylor, S. S., 2009. Contribution of non-catalytic core residues to activity and regulation in protein kinase A. J Biol Chem 284 (10), 6241–8.

Yeh, L. A., Lee, K. H., Kim, K. H., 1980. Regulation of rat liver acetyl-CoA carboxylase. Regulation of phosphorylation and inactivation of acetyl-CoA carboxylase by the adenylate energy charge. J Biol Chem 255 (6), 2308–14.

Ylikorkala, A., Avizienyte, E., Tomlinson, I. P., Tiainen, M., Roth, S., Loukola, A., Hemminki, A., Johansson, M., Sistonen, P., Markie, D., Neale, K., Phillips, R., Zauber, P., Twama, T., Sampson, J., Jarvinen, H., Makela, T. P., Aaltonen, L. A., 1999. Mutations and impaired function of LKB1 in familial and non-familial Peutz-Jeghers syndrome and a sporadic testicular cancer. Hum Mol Genet 8 (1), 45–51.

Yoon, K. A., Ku, J. L., Choi, H. S., Heo, S. C., Jeong, S. Y., Park, Y. J., Kim, N. K., Kim, J. C., Jung, P. M., Park, J. G., 2000. Germline mutations of the STK11 gene in Korean Peutz-Jeghers syndrome patients. Br J Cancer 82 (8), 1403–6.

Zarzov, P., Mazzoni, C., Mann, C., 1996. The SLT2(MPK1) MAP kinase is activated during periods of polarized cell growth in yeast. EMBO J 15 (1), 83–91.

Zhang, B. B., Zhou, G., Li, C., 2009. AMPK: an emerging drug target for diabetes and the metabolic syndrome. Cell Metab 9 (5), 407–16.

Zhang, G., Kashimshetty, R., Ng, K. E., Tan, H. B., Yeong, F. M., 2006a. Exit from mitosis triggers chs2p transport from the endoplasmic reticulum to mother-daughter neck via the secretory pathway in budding yeast. J. Cell Biol. 174, 207–220.

Zhang, X., Gureasko, J., Shen, K., Cole, P. A., Kuriyan, J., 2006b. An allosteric mechanism for activation of the kinase domain of epidermal growth factor receptor. Cell 125, 1137–1149.

Zheng, B., Cantley, L. C., 2007. Regulation of epithelial tight junction assembly and disassembly by AMP-activated protein kinase. Proc Natl Acad Sci U S A 104 (3), 819–22.

Zheng, B., Jeong, J. H., Asara, J. M., Yuan, Y.-Y., Granter, S. R., Chin, L., Cantley, L. C., 2009. Oncogenic B-RAF negatively regulates the tumor suppressor LKB1 to promote melanoma cell proliferation. Mol Cell 33 (2), 237–47.

Zheng, J. H., Knighton, D. R., Xuong, N. H., Taylor, S. S., Sowadski, J. M., Teneyck, L. F., 1993. Crystal-structures of the myristylated catalytic subunit of camp-dependent protein-kinase reveal open and closed conformations. Protein Sci. 2, 1559–1573.

Zhou, T., Raman, M., Gao, Y., Earnest, S., Chen, Z., Machius, M., Cobb, M. H., Goldsmith, E. J., 2004. Crystal structure of the TAO2 kinase domain: activation and specificity of a ste20p MAP3K. Structure 12, 1891–1900.

Chapter VI

Appendix

6 Appendix—List of supporting figures

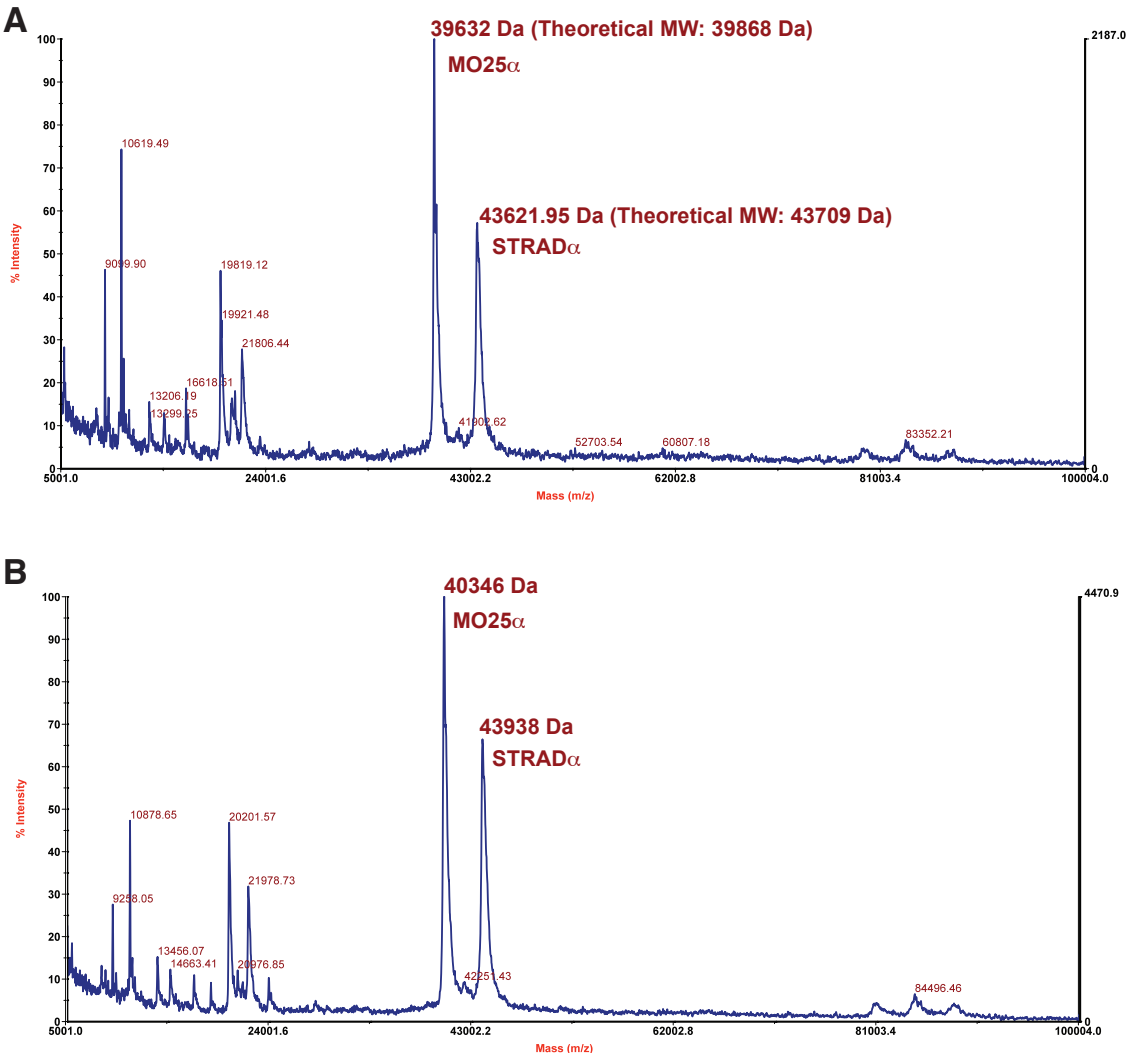

Figure A.1: MALDI-TOF analysis of His-STRADα/MO25α complex before and after lysine methylation

Mass over charge spectra for the (A) unmethylated and (B) methylated His-STRADα/MO25α complex. The His-STRADα and MO25α peaks and their corresponding measured molecular weights are labelled. The theoretical molecular weights (MW) are given in brackets.

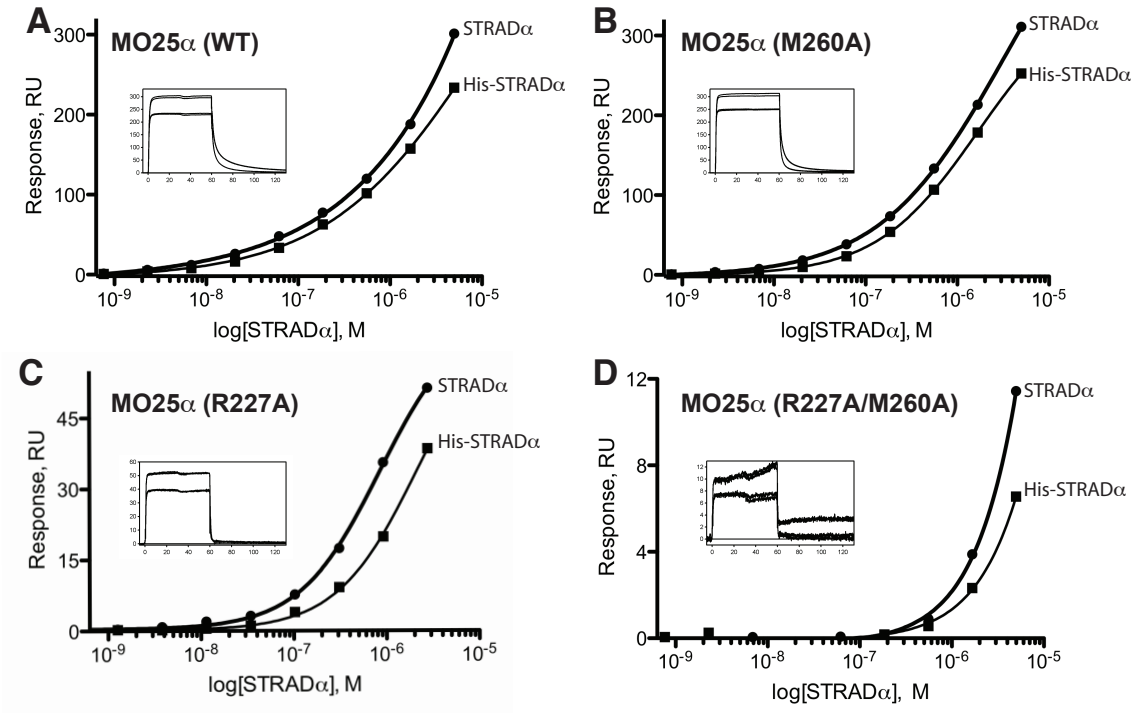

Figure A.2: His tagged STRADα and untagged STRADα bind MO25α with similar affinity

Binding of STRADα to immobilised (A) MO25α(WT, wild type), (B) MO25α(M260A), (C) MO25α(R227A) and (D) MO25α(R227A/M260A) was assessed by SPR analyses. Equivalent concentrations of His-STRADα or untagged STRADα, were allowed to bind over 50 s by injecting different concentrations over a range of 0.4 nM to 5 μM, in the presence of 0.1 mM ATP and 1 mM $MgCl_2$. Response levels for specific binding of STRADα to MO25α was plotted against STRADα concentration (log scale). Boxed are representative BIAcore sensograms recorded in duplicate and corresponding to the highest concentration for each of the labelled STRADα curves. A complete set of primary sensograms are provided in Fig. A.3. Similar results were obtained in at least two separate experiments.

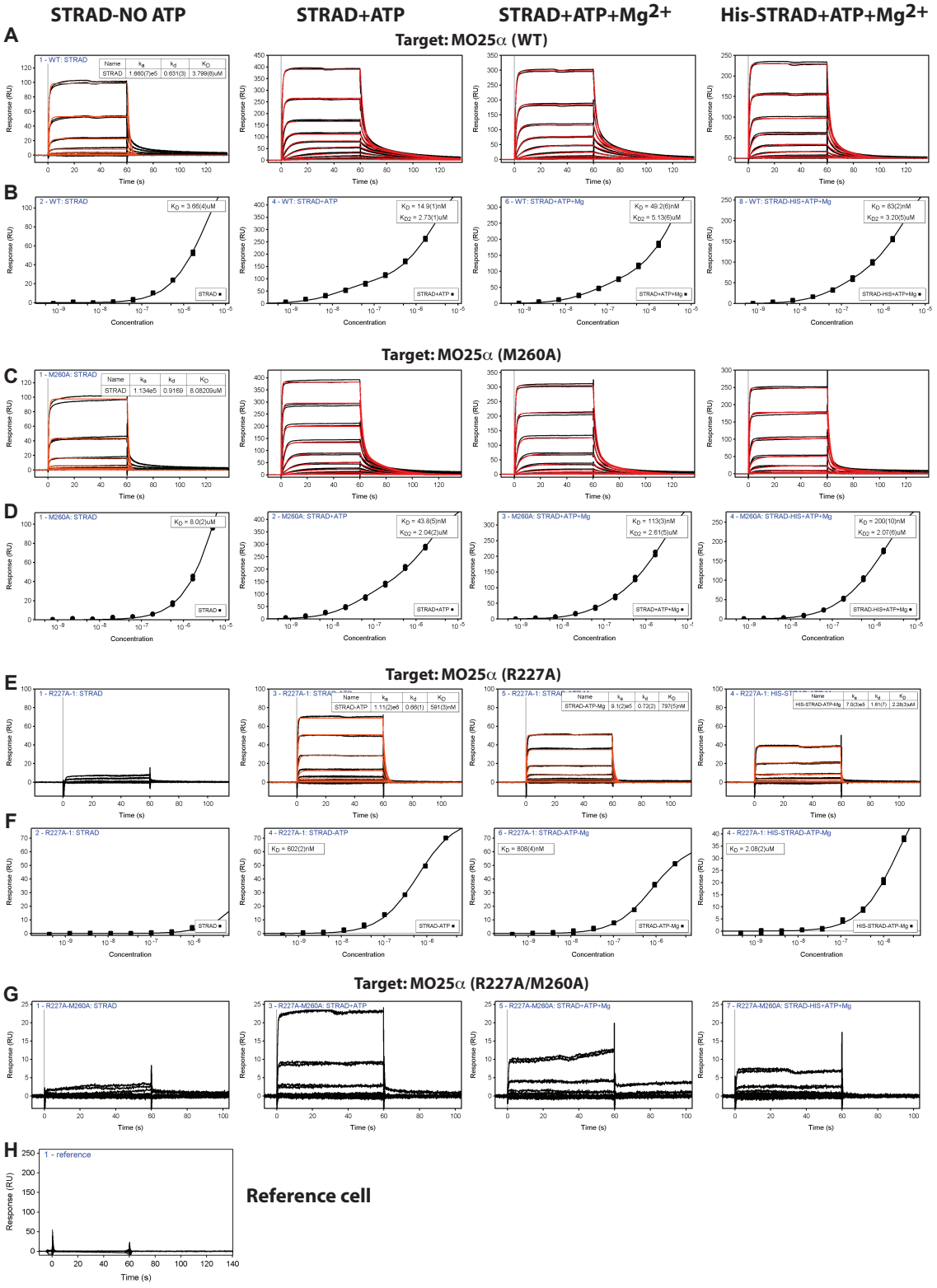

Figure A.3: Primary BIAcore sensograms from SPR analysis of the STRADα/MO25α interaction

Association/dissociation curves from the STRADα/MO25α interaction measurements and analysis. The experimantal procedure is described in chapter II, section 2.13 and data were analysed as described in section 2.13.2. Similar results were obtained in two separate experiments carried out in duplicate. Kinetic fits in panels A, C and E correlate well with equilibrium fits in panels B, D and F respectively, as it is expected for specific binding that follows law of mass action. The SPR measurments were carried out by Dr Iva Navratilova, University of Dundee.

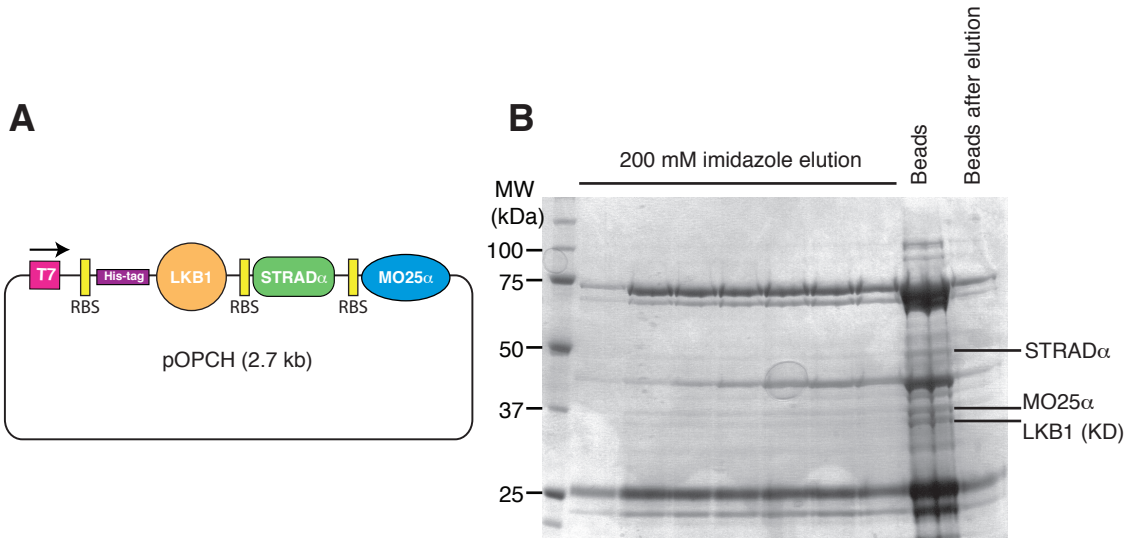

Figure A.4: Attempts for the expression and purification of the LKB1/STRADα/MO25α complex in *E. coli*

A) Architecture of the pOPCH vector (Tan, 2001) used to recombinantly co-express the $LKB1$, $STRADA$ *and* $MO25A$ genes. RBS = Ribosomal binding site.

B) SDS-PAGE analysis of the NiNTA purification of the LKB1 complex. Eluted fractions, and NiNTA beads before and after elution are labelled. The indicated bands were analysed by tryptic peptide-mass spectrometry (MS/MS) and positively identified as LKB1, STRADα and MO25α.

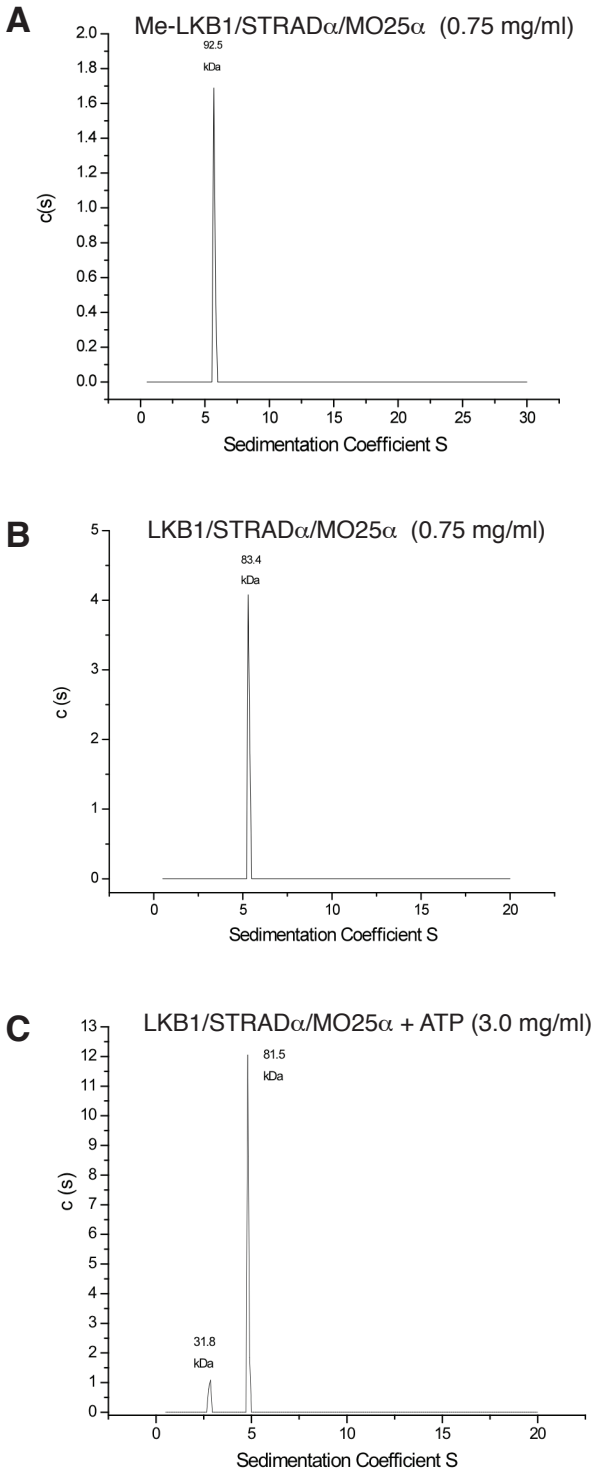

Figure A.5: Sedimentation experiments of the LKB1/STRADα/MO25α complex
A & B) Analytical ultracentrifugation experiments for the methylated (A) and unmethylated (B) forms of the LKB1 heterotrimeric complex (0.75 mg/ml; theoretical MW = 115.8 kDa) that was used for crystallisation studies in this thesis. A peak corresponding to 92.5 kDa (unmethylated) and 83.4 kDa (methylated), both indicative of a monomeric form of the heterotrimer is labelled.
C) Analytical ultracentrifugation experiments for the unmethylated form of the LKB1 heterotrimeric complex (3.0 mg/ml; theoretical MW = 115.8 kDa) in the presence of 0.1 mM ATP and 1 mM MgCl. A peak corresponding to 81.5 kDa and indicative of a monomeric form of the heterotrimer is labelled. The experiment was carried out by Dr Mark Agacan, University of Dundee.

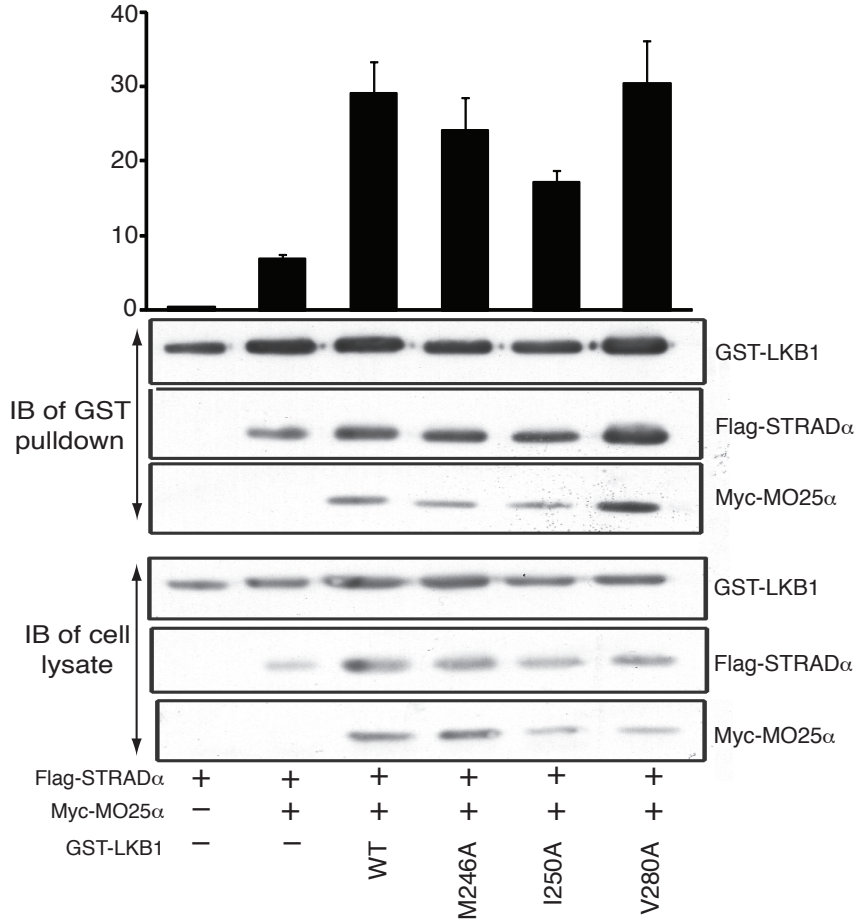

Figure A.6: Mutation of MO25α hydrophobic pocket that interact with LKB1 activation loop (Phe204) do not affect LKB1 activity

293 cells were co-transfected with the indicated constructs of GST-LKB1, Flag-STRADα and Myc-MO25α. Cells at 36 h post-transfection were lysed and GST-LKB1 affinity purified and assayed for the ability to activate heterotrimeric AMPK complex expressed in $E.\ coli$. Kinase activities are representative of three independent assays carried out in triplicate (error bars represent the SD for a single triplicate experiment). Affinity purified GST-LKB1 preparation (upper panel) as well as cell extracts (lower panel) were immunoblotted with the indicated antibodies.

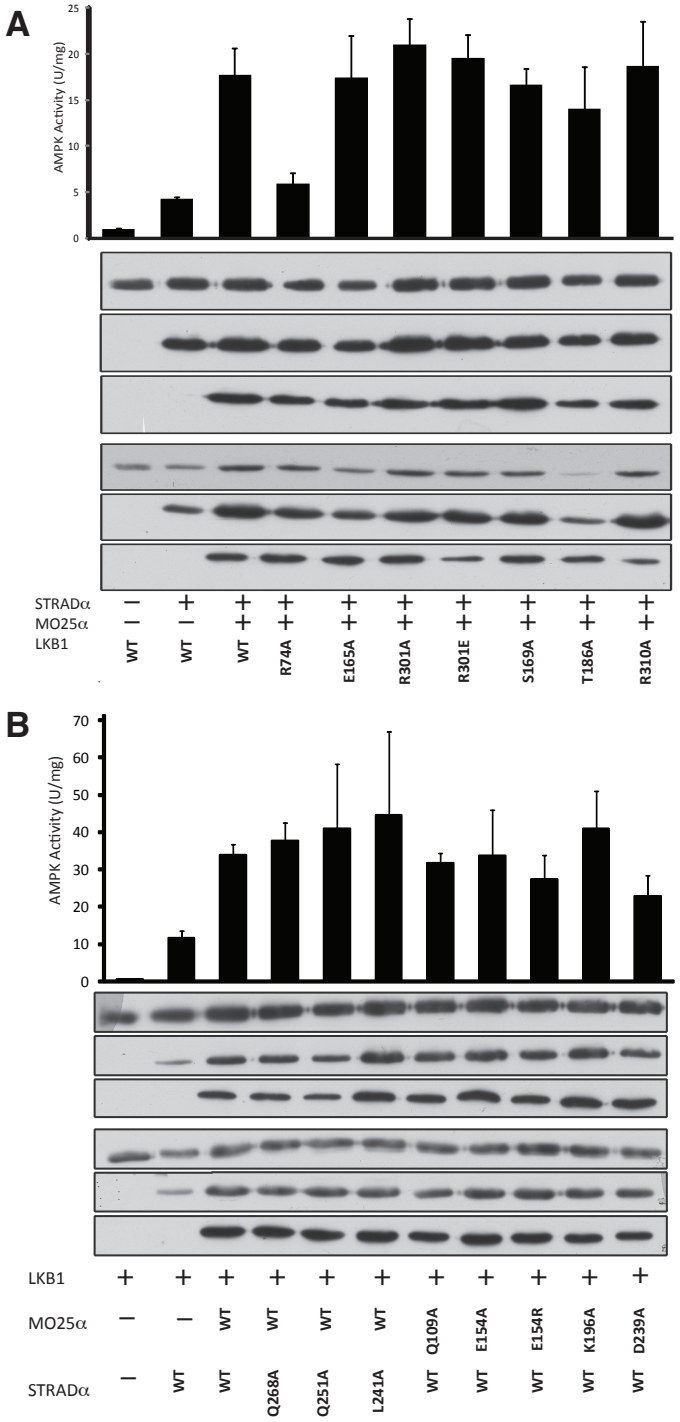

Figure A.7: Mutation of the LKB1/STRADα/MO25α interfaces
A & B) 293 cells were co-transfected with the indicated constructs of GST-LKB1, Flag-STRADα and Myc-MO25α. Cells at 36 h post-transfection were lysed and GST-LKB1 affinity purified and assayed for the ability to activate heterotrimeric AMPK complex expressed in *E. coli*. Kinase activities are representative of three independent assays carried out in triplicate (error bars represent the SD for a single triplicate experiment). Affinity purified GST-LKB1 preparation (upper panel) as well as cell extracts (lower panel) were immunoblotted with the indicated antibodies.